

Assessing the effects of cryoturbation on indicator minerals in till from the Amaruq gold deposit (Nunavut, Canada)

Mémoire

Juan David Bello Rodríguez

Sous la direction de :

Georges Beaudoin, directeur de recherche
Isabelle McMartin, codirectrice de recherche

Résumé

Les minéraux indicateurs (MI) fournissent des informations cruciales pour l'exploration minérale dans les terrains glaciaires. Dans les régions de pergélisol, les ostioles sont l'une des structures de cryoturbation les plus courantes dans les sédiments glaciaires et sont donc utilisés couramment pour les études de MI. Nous avons étudié si la dynamique du mouvement interne dans les ostioles peut générer une classification des MI dans la couche active. Dans cette étude réalisée près du gisement d'or orogénique Amaruq, au Nunavut, dans le nord du Canada, plusieurs profils verticaux jusqu'à ~1,3 m de profondeur ont été échantillonnés dans deux tranchées à ~1,5 km en aval glaciaire du gisement, y compris deux profils dans la partie centrale de deux ostioles clairement identifiés en surface (un profil atteignait le pergélisol à 1,30 m de profondeur). La fraction du concentré de minéraux lourds (<2 mm) dans tous les profils contient de l'or et de la scheelite. Les abondances de ces MI présentent une variation verticale qui n'est pas uniforme entre tous les profils. De même, la taille et la morphologie des grains d'or n'ont aucune tendance cohérente. Le till présent dans le pergélisol démontre une plus grande abondance de minéraux indicateurs par rapport au till dans la partie supérieure de la couche active. La variation latérale des MI dans un ostiole à 30 cm de profondeur montre que la plus grande quantité de grains d'or et de scheelite se trouve dans la partie centrale de l'ostiole. La composition chimique de l'or (<400 µm), de la scheelite, et de la chalcopirite (0.25-2.00 mm) a été déterminée par EPMA et LA-ICP-MS. La composition chimique des MI indique que la plupart des grains sont dérivés du gisement d'Amaruq. Aucun des minéraux ne présente de tendance verticale basée sur sa composition chimique. En résumé, les ostioles ne présentent pas de variations systématiques dans les propriétés des MI (abondance, morphologie, taille et composition chimique) à différentes profondeurs. Cette étude suggère que les processus de cryoturbation ne génèrent pas un fractionnement des minéraux indicateurs dans les ostioles en raison de multiples variables liées aux processus de gel et de dégel (différences de densité, d'humidité, de profondeur maximale de dégel, de durée d'activité, de front de gel, etc.).

Abstract

Indicator minerals (IM) provide valuable information for mineral exploration in glaciated terrains. In permafrost regions, mudboils (frost boils) are one of the most common cryoturbation features in glacial sediments and are therefore critical for IMs studies. We investigate if the inner motion dynamics in mudboils could generate a vertical sorting of IMs in the active layer. In this study, located at the Amaruq orogenic gold deposit in Nunavut, northern Canada, we sampled several vertical profiles down to ~1.3 m depth in two trenches ~1.5 km down-ice of the deposit, including two profiles in the central part of well-identified mudboils on surface (one reaching the permafrost table at 1.30m depth). The heavy mineral concentrate fraction (<2 mm) of all profile samples contains gold and scheelite. The abundance of these IMs shows vertical variations that are not uniform between all profiles. Likewise, the size and morphology of gold grains do not exhibit any consistent trend. Till in permafrost exhibits the highest IMs abundance compared to that in the overlying active layer. The IMs lateral variation examined in one mudboil at ~30cm depth indicates that the highest grain count of gold and scheelite is in the central part of the mudboil. The chemical composition of gold (<400 μm), scheelite and chalcopyrite (0.25-2.00 mm) was determined by EPMA and LA-ICP-MS. Chemical analysis of the IMs indicates that most of these minerals are derived from the Amaruq gold deposit. None of them present systematic vertical trends in chemical composition. In summary, mudboils show no systematic variations in the IM properties (mineral abundance, morphology, size and mineral chemistry) at different depths. The study suggests that cryoturbation processes do not generate a uniform fractionation of indicator minerals in mudboils due to the multiple variables involved in the freeze-thawing process (bulk density differences, moisture, maximum thaw depth, activity time, and freezing front).

Table of contents

Résumé.....	ii
Abstract.....	iii
Table of contents	iv
List of figures	vii
List of tables	x
Acknowledgments	xi
Foreword.....	xii
Introduction	1
Research background.....	1
Drift prospecting	1
Cryoturbation in glaciated terrains	3
Problem Statement	7
Objective	7
Methodology.....	8
Presentation of the article.....	14
Chapter 1.....	15
ASSESSING THE EFFECTS OF CRYOTURBATION ON INDICATOR MINERALS FROM THE AMARUQ GOLD DEPOSIT (NUNAVUT, CANADA)	15
1.1 Résumé.....	15
1.2 Abstract.....	16
1.3 INTRODUCTION.....	17
1.4 GEOLOGICAL SETTING	19
1.4.1 Bedrock geology	19
1.4.2 Quaternary geology	20
1.5 METHODOLOGY	26
1.5.1 Sampling and QA/QC	26
1.5.2 Till geochemistry	26
1.5.3 Grain size analysis, total C, organic carbon and LOI	29
1.5.4 Clast analysis	30
1.5.5 Indicator Minerals.....	30
1.5.6 Statistical analysis.....	33
1.6 RESULTS	34
1.6.1 Description of the till.....	34

1.6.2 Cryoturbation.....	36
1.6.3 Pebble counts.....	41
1.6.4 Grain-size analysis.....	42
1.6.5 Total carbon and LOI.....	43
1.6.6 Till geochemistry.....	44
1.6.7 Indicator Minerals.....	49
1.7 DISCUSSION.....	69
1.7.1 Heterogeneity of composition, texture and IM in till units.....	69
1.7.2 Evidence for cryoturbation, and weathering.....	71
1.7.3 Vertical fractionation of composition and IM.....	75
1.7.5 Mineral exploration implications.....	80
References.....	82
Conclusion.....	90
Bibliography.....	92
Appendix A - Field data.....	102
A.1 Location of trenches and the two mudboils (MB3 and MB4), coordinates in NAD83 YTM 14N.....	102
A.2 Till sample list and description.....	103
Appendix B – Laboratory data.....	105
B.1 Pebble counting percentage of the 5-9.5mm fraction.....	105
B.2 Till geochemistry (<0.063mm fraction).....	107
B.2.1 Detection Limit of the ICP-ES Analyses and lithium borate fusion digestion method..	107
B.2.2 ICP-ES and lithium borate fusion digestion method.....	109
B.2.3 Detection Limit of the ICP-MS Analyses and aqua-regia digestion method.....	112
B.2.4 ICP-MS and aqua-regia digestion method results.....	114
B.2.5 Detection Limit of the ICP-ES/MS Analyses and multi-acid digestion method.....	119
B.2.6 ICP-ES/MS and multi-acid digestion method results.....	121
B.3 Indicator minerals counting.....	125
B.3.1 Gold grains counting by ODM (non-normalized).....	125
B.3.1 Scheelite grains counting (non-normalized).....	127
B.3.1 Sulfide grains counting (non-normalized).....	128
B.4 Mineral chemistry of indicator minerals.....	129
B.4.1 Gold analysis.....	129
B.4.2 Scheelite analysis.....	144

B.4.2 Chalcopyrite analysis.....	157
----------------------------------	-----

List of figures

Figure 1.1. Internal long-term circular soil motion within mudboil. Modified from Walker et al. (2004) and Peterson et al. (2003). 6

Figure 1.2. Location of the two trenches. Modified from Boulianne-Verschelden et al. (2019, 2022) 8

Figure I. 1 Bedrock geology map modified by de Bronac de Vazelhes et al. (2021), after Hrabi et al. (2003). 20

Figure I. 2 Map of some glaciogenic features and glacial landsystems of the eastern Keewatin region. Modified from McMartin et al. (2021; 2022). KID=Keewatin Ice Divide (8 Ka BP). 21

Figure I.3 Regional Quaternary geology map of the Amaruq Area. Modified from Boulianne-Verschelden et al. (2022). 23

Figure I.4 Local Quaternary geology map of the Amaruq deposit area near the Whale Tail mineralization. Modified from Boulianne-Verschelden et al. (2019). Location of the Whale tail transect samples, number of gold grains (normalized to 10-kg) and the mudboil profile from de Bronac de Vazelhes et al. (2021) are shown. 24

Figure I.5 Localization of the two trenches and mudboils samples (MB=Mudboil). Ice-flow direction identified from fieldwork on small outcrop within a boulder field. Local Quaternary map modified from Boulianne-Verschelden et al. (2019). 27

Figure I.6 Sketches of the Trench 1. Top, the north wall. Bottom, the south wall. Red-bordered squares represent the vertical till sampling profiles. 28

Figure I.7 Sampling profiles in both mudboils from Trench 2. Red boxes represent till samples, dotted lines variations in the till character (see Figs. I.12 and I.13). 29

Figure I.8 Proportion of the 5-9.5 mm pebble lithologies in the glacial diamictons. 36

Figure I.9 Cryoturbation features identified on the surface in the study area. a) sorted circle, b) mudboil in Trench 2 area, c) and d) patterned ground in Trench 1 area. 37

Figure I.10 Buried organic matter in Trench 1. a) buried organic matter in the South wall, and b) deformed organic matter layer in the North wall. 38

Figure I. 11 North wall of the Trench 1. The bowl shapes represent at least four cryoturbation structures in this trench. 39

Figure I.12 Mudboil 1. a) Expression at the surface, b) cross-section, c) sketch of the cross-section. 40

Figure I.13 Mudboil 2. a) Expression at surface, b) cross-section, c) oxidized horizon at 90 cm depth, d) gleyed horizon above the permafrost, e) surface of permafrost table, and f) sketch of the mudboil profile. 41

Figure I.14 Vertical profiles pebble composition proportions in both mudboils from Trench 2. 42

Figure I.15 Ternary diagram showing the grain size composition of the samples, in distal till. 43

Figure I.16 Vertical and lateral profiles of the grain-size distribution in the distal till of both trenches. 44

Figure I.17 PCA score plots of geochemical results from this study. a) PC1/PC2 loading plot of ICP-ES/MS and multi-acid (MA) digestion, b) PC2/PC3 loading plot of ICP-ES/MS MA, c) sample projection in PC1/PC2 loading plot, and d) sample projection in PC2/PC3 loading plot. 46

Figure I.18 Principal component analysis using ICP-MS/Aqua-regia method. a) PC1/PC2 loading plot for log centered normalized values of distal till samples (this study) combined with Whale Tail transect and profile samples of de Bronac de Vazelhes (2019), and b) Samples of both trenches in distal till (this study) and WT samples from de Bronac de Vazelhes (2019) projected on the PC1/PC2 score plot.	47
Figure I.19 Vertical geochemical profiles in detailed mudboils (1 and 2) from Trench 2. a) Left, Major elements (ICP-ES/LBF method). Right, Trace metals (ICP-ES/MS and Aqua-regia). b) Trace metals analyzed by ICP-ES/MS and aqua-regia showing significant variation with depth.....	48
Figure I.20 Samples of both detailed mudboils from Trench 2 (this study) combined with profile samples in Whale Tail mudboil from de Bronac de Vazelhes (2019) projected on the Principal components PC1/PC2 ICP-MS/Aqua-regia method score plots.....	51
Figure I.21 Vertical profiles of the gold grain counts, length, and morphology. a) North side of Trench1, b) South side of Trench 1, c) Mudboil 1, and d) Mudboil 2. Grain counts normalized to 10-kg table feed.	52
Figure I.22 IM's characteristics in the lateral till sampling profile in Mudboil 1. a) IM grain counts, b) proportions of gold grain size and morphology.	54
Figure I.23 Histograms of gold grain sizes frequency a) Trench 1, classified by till, b) Trench 2, c) Mudboil 3, and d) Mudboil 4.....	55
Figure I.24 Fineness of gold grains. a) Values for the Amaruq Area, left bedrock mineralization (Liu and Beaudoin, 2021; Mendizabal, 2022) and right, grains recovered from tills from this study, and b) comparison with values of different gold mineral deposits (Morrison et al., 1991; Liu and Beaudoin, 2021).....	57
Figure I.25 Profiles showing the gold fineness measured in till samples through box plots.....	58
Figure I.26 Partial least square-discriminant analysis (PLS-DA) of the log-centered and normalized LA-ICP-MS of gold grains recovered from till (this study) compared to different gold mineral deposits based on Liu and Beaudoin (2021). a) The q_w^*1 - q_w^*2 loading plot, b) The $t1$ - $t2$ scores plot shows the distribution of gold grains according to till c) Samples of the gold grains within the two mudboils sampled in Trench 2 plotted in the PLS-DA score plots. Top, Mudboil 1. Bottom, Mudboil 2. Data for Amaruq deposit from Liu (2020) and Mendizabal (2022).	60
Figure I.27. Vertical profiles of the scheelite and pyrite grain counts. a) North side of Trench1, b) South side of Trench 1, c) Mudboil 1, and d) Mudboil 2. Grain counts normalized to 10-kg table feed.	62
Figure I.28 Binary plots to discriminate scheelite. Top, Eu^* anomaly vs Sr/Mo. Bottom, As (ppm) vs Sr/Mo.....	66
Figure I.29 Chalcopyrite discrimination diagrams. a) Ternary diagram of Cd, Se, and Ni (Duran et al., 2019), b) Cd vs Zn diagram for hydrothermal deposits (George et al., 2018), c) Binary plot Cd/Se vs Ni/Se (Mansur et al., 2021, after George et al., 2018), d) Vertical profiles of chalcopyrite grain counts of the two mudboils from Trench 2 and Mudboil 3. The thin black outline represents Amaruq data from Caraballo (2023).....	67
Figure I.30 Partial least square-discriminant analysis of the log-centered and normalized LA-ICP-MS of scheelite grains recovered from till compared to different gold mineral deposits based on Sciuba et al. (2020). Amaruq deposit data from de Bronac de Vazelhes (2019).	68
Figure I.31 Vertical profiles showing the proportion of scheelite grains discriminated by deposit type. Each section of the pie graphs is a scheelite grain.	68

Figure I.32 Vertical grain-size profiles in mudboils from the Northern Hemisphere compared to the study area mudboils. Left, sand content. Right, silt content.....	74
Figure I.33 Gold grains characteristics in the two mudboil profiles from Trench 2. a) Comparison of the gold grain abundance with the red line representing the percentage difference between the gold grain counts at specific depths; b) integration of the grain-size frequency with gold grain morphology	78
Figure I.34 Summary of a proposed classification of materials by depth based on the IM nature in the two mudboils analyzed in Trench 2.....	81

List of tables

Table 1. Major pebble lithology counts in the diamicton units of the two trenches.	35
Table 2. Gold grain counts (normalized to 10-kg table feed).....	50
Table 3. Gold grains morphology proportions classified by till and trench.....	53
Table 4. Summary statistics of EPMA and LA-ICP-MS element analyses on gold grains recovered from till (n=150 by EPMA and n=131 by LA-ICP-MS)	56
Table 5. Scheelite grain counts (normalized to 10-kg table feed)	61
Table 6. Summary statistics of EPMA and LA-ICP-MS element analyses on scheelite grains recovered from till (n=48 by EPMA and n=48 by LA-ICP-MS)	63
Table 7. Summary statistics of EPMA and LA-ICP-MS element analyses on chalcopyrite grains recovered from till (n=12 by EPMA and n=12 by LA-ICP-MS)	64

Acknowledgments

I would like to extend my heartfelt gratitude to all the individuals who have contributed to the successful completion of this research work. Without their unwavering support, guidance, and encouragement, this study would not have been possible.

First and foremost, I would like to express my special thanks to my academic advisors, Professor Georges Beaudoin and Dr. Isabelle McMartin. Throughout this "cold and glittering" research journey, their mentorship has been an invaluable guiding light. Their profound insights, constructive critiques, and constant encouragement have been instrumental in shaping the direction of this study. I am also deeply thankful to Professor Bertrand Rottier and the PhD Enzo Caraballo for their invaluable support during the "seminaire" and over the past two years. Additionally, I would like to extend my gratitude to my colleagues from around the world and my Latino-friends, whose continuous support and motivation have been a source of strength during this endeavor.

My sincere thanks also go to the staff at Université Laval, particularly Edmond Rousseau who assisted me in the preparation of the samples, Suzie Côté for her guidance in using the SEM, Marc Choquette for his support in EPMA analyses, and Professor Crystal Laflamme and Guillaume Barré for their assistance in the LA-ICP-MS analysis. I am also grateful to Brandon Boucher from the University of New Brunswick for making the analyses on tiny grains of gold possible. Furthermore, I want to acknowledge the support of the Agnico Eagle staff of the Amaruq project during the fieldwork, with special thanks to Olivier Côté-Mantha for making this project a reality.

I would also like to express my gratitude to the province of Québec and the city for allowing me to immerse myself into Québécoise culture. Merci for the enriching experience.

Above all, I want to extend my deepest appreciation to my family back in Colombia, especially my mom, my dad (whose memory will always be with me), and my godmother, for their love and unwavering support. Most importantly, I want to thank my wife, Silvia Castilla, who has been my biggest motivation and the pillar of unconditional support throughout this entire journey. She tirelessly helped me practice presentations and showered me with love.

¡Gracias!

Foreword

This thesis is an original work of the author Juan David Bello Rodríguez. It is composed of an introductory section, one research section and a conclusion. All tasks related to realization of this thesis, which include field sampling, sample preparation, data processing and interpretations, were conducted by the author and supervised by Prof. Georges Beaudoin (Université Laval) and co-supervised by Dr. Isabelle McMartin (GSC-Ottawa), who co-authored the article. Data from previous memoirs by Victor de Bronac de Vazelhes (2019) and Alexandre Mendizabal (2022) have been used by the author and are mentioned in each use.

Introduction

This master's project is part of a series of studies in the Industrial Research Chair CRSNG – Agnico Eagle in mineral exploration. The primary focus is to improve the understanding of indicator minerals (IM) scattered by glacial and post-glacial processes, with the aim to enhance drift prospecting techniques in glaciated terrains. This case study takes place on the Amaruq gold mine in Nunavut, where previous MSc studies have been conducted (Boulianne-Verschelden et al., 2019; de Bronac de Vazelhes, 2019; Mendizabal, 2022). The major goal of this project is to recognize the effects of cryoturbation processes on IM in till down-ice from an orogenic gold deposit, by analyzing their characteristics (abundance, size, morphology, and mineral chemistry) in the active layer above permafrost. This is in order to increase the knowledge of IM nature in periglacial areas with the goal of improving surface exploration strategies in permafrost terrain.

Research background

Drift prospecting

Mineral exploration programs conduct multiple geological studies to discover ore deposits. These studies are based on the prior understanding of favorable geological conditions to develop an ore deposit, such as lithospheric architecture (pathways), energy drivers, sources (metals and fluids), and depositional mechanisms (Wyborn et al., 1994; McCuaig et al., 2010; McCuaig and Hronsky, 2014). In addition, studies are also directed toward the understanding of geochemical and geophysical signatures generated by the ore bodies, alteration mineralogy, associated rocks, and subsequent weathering and erosional processes (Hawkes, 1957; Andrews-Jones, 1968; Beus and Grigorian, 1977). The weathering and erosional processes disperse the original signatures of the ore deposit by mechanical and chemical mechanisms. These processes are strongly dominated by the geographical location and the resulting climatic conditions.

In almost all of Canada, past continental glaciers have been the main process of erosion and media of sediment transport during the last glaciation, generating multiple landforms and clastic sediment deposits predominated by till (Fulton, 1989). This process is defined as glacial dispersal (Shilts and Menzies, 1996). Glacial dispersal trains of ore deposits are characterized by a particular geochemical signature and specific heavy minerals associated with mineralization (Shilts, 1977; Miller, 1984). These mineralization-related heavy minerals are defined as indicator minerals (IM). Till which is an unsorted and unstratified sediment deposited directly by glacier ice (Dreimanis, 1989) has been widely used for mineral exploration in glaciated terrains (drift prospecting) due to its relatively simple transport history, which allows easy determination of the bedrock source (McClenaghan et al., 2000; McMartin and McClenaghan, 2001). Dispersal trains may be affected by post-glacial processes in areas underlain by permafrost such as cryoturbation, which causes soil movement in the active layer above the permafrost table (Washburn, 1980).

Indicator minerals have been used worldwide to prospect several types of deposits such as lode-gold, diamond-bearing kimberlites, REE-mineralization, iron-oxide-copper-gold (IOCG), porphyry Cu, Ni-Cu, PGE, and W-Mo (McClenaghan and Paulen 2018, and references therein). The occurrence and concentration of IM in any sample media strongly relates to the mineral deposits or host rocks from which they were derived (McClenaghan, 2005; McClenaghan and Paulen, 2018). In the exploration of gold-bearing deposits, gold grains are the principal indicator mineral (Chapman et al., 2000; McClenaghan, 2005; McClenaghan and Cabri, 2011; Chapman et al., 2017; Moles and Chapman, 2019). Furthermore, other minerals such as scheelite, tourmaline, sulfides, PGM, tellurides, cassiterite, barite and rutile have been described as indicator minerals for lode-gold deposits in Canada (McClenaghan and Cabri, 2011; Duran et al., 2019; de Bronac de Vazelhes et al., 2021; Sciuba et al., 2021). Analysis of the IM properties (e.g., abundance, morphology, grain size, and mineral chemistry) provides vital information such as transport distance and nature of the mineral deposit (DiLabio, 1990; McClenaghan et al., 2000; Belousova et al., 2002; Townley et al., 2003; Nixon, 2003; Chapman et al., 2022). The process of glacial erosion, transport and dispersal generates a peak of IM abundance at or down-ice to the mineral deposit, and a subsequent abundance decrease in the direction of transport (Shilts, 1976). The

morphology of gold grains changes as the transport distance increases because its malleable character causes it to deform rather than be comminuted (DiLabio, 1990; Townley et al., 2003). Three main morphology types were proposed by DiLabio (1990): Pristine, Modified, and Reshaped; these typically reflect the shortest to the longest distance of transport, respectively. The size of the gold grains reflects the nature of the gold in the bedrock mineralization; most of the gold grains found in regional till studies in Canada are silt-sized (Averill et al., 1988; Averill and Huneault, 1991; McClenaghan, 2001; Girard et al., 2021). Finally, the mineral chemistry of some IM enables mineral deposit type source discrimination to aid exploration targeting, e.g., kimberlites, magnetite, gold, sulphides, scheelite, and tourmaline (Beaudoin et al., 2007; Chapman et al., 2009; Paulen et al., 2011; Layton-Matthews et al., 2014; Wilkinson et al., 2017; Duran et al., 2019; Sciuba, 2020; Liu and Beaudoin, 2021; Miranda et al., 2022; Layton-Matthews and McClenaghan, 2022).

Cryoturbation in glaciated terrains

The periglacial environment refers to regions close to glaciers or ice sheet edges, where the land is impacted by cold climatic conditions (Murton, 2021). Certain areas, such as northern Russia, northern Canada, Alaska, and Greenland have a foundation of permafrost, while others undergo seasonal ground-freezing. Permafrost regions in Canada, such as northern Quebec, Nunavut, Northwest Territories and Yukon (Heginbottom, 1995), the year-round presence of the frozen layer amplifies the intensity of perturbations within the till column by the freeze-thaw cycles, known as cryoturbation (Vandenberghe, 1988). Cryoturbation primarily occurs in the active layer above the permafrost table. In contrast, in areas without permafrost, cryoturbation can still occur although at a significantly lower rate.

In permafrost regions, freezing progresses from the top and the bottom of the active layer in cold seasons, while thawing is generated only from the top down in warm seasons. This seasonal freeze-thaw action produces cryoturbation structures (Vandenberghe, 1988; Vandenberghe, 2013). Several mechanisms have been proposed for the origin of these structures. Vandenberghe (2013) present three main processes for their formation: 1) periglacial loading; 2) cryohydrostatic flow; and 3) cryostatic heave. Periglacial loading

occurs when water-saturated soils have a reverse density gradient causing the less dense bottom soil to move upward. This is generated mostly by the formation of ice lenses in the upper part of the permafrost and subsequent thawing. Cryohydrostatic flow releases material to areas of lower pressure when the pore water pressure increases due to high amounts of trapped water between impermeable layers such as frozen soil. Cryostatic heave is generated by the expansion of freezing water and the formation of segregated ice, leading to soil movement.

In areas underlain by permafrost, geometrical features termed patterned ground dominate the ground surface (Shilts, 1973). Washburn (1956) described these symmetrical patterns and suggested 19 formation mechanisms involving various thermal, pressure, density, moisture and water content interactions by the freezing, thawing or a combination of both. One of the most common land surface features is the mudboil, also denominated frost boil and non-sorted circles, which are circular “mud” (silt, clay, sand, and minor pebbles) patches surrounded by stones or vegetation at the surface (Washburn, 1956; Shilts, 1978). Mudboils are created chiefly in poorly sorted silt-clay-rich materials (diamicton) with low liquid limits and restricted plasticity indices, and are ubiquitous in northern Canada (Shilts 1978; Egginton, 1979). In mudboils, the active layer is concave-shape and thicker than the peripheral area (Shilts, 1978; Egginton, 1979). Inner soil motion dynamics are thought of as circulation cell-like, resembling convection, as in Figure 1.1 (Mackay, 1980; Peterson et al., 2003; Hagedorn et al., 2008; Nicolsky et al., 2008). This is supported by the burial of organic materials at the edges (Zoltai and Tarnocai, 1981; Becher et al., 2013), and the upward movement of material at the central part which causes ejection of material at the surface (Egginton, 1979; Peterson et al., 2003; Nicolsky et al., 2008). The lifting of material in the central part facilitates its movement to the edges by creep, solifluction, and erosion (Walker et al., 2004; Klaminder et al., 2014; van Dijke, 2016). Rates of the internal circular soil movement have been determined by field evidence. Maximum rates of upward movement up to 35.5 cm y⁻¹ but mostly of 8.7 cm y⁻¹ have been identified, as well as horizontal movement rates at the surface are between 1 to 3 cm y⁻¹ (Egginton, 1979). These rates, however, contrast sharply with the downward rates of the “subducted” organic material at the edges which are less than 1 mm y⁻¹, as shown by radiocarbon dating (Dyke and Zoltai, 1980; Becher et al.,

2013). Furthermore, movement rates estimated by radionuclides such as ^{210}Pb show lesser net uplift velocities of 0.2-0.7 cm y^{-1} and higher net burial speeds of 0.3-1.2 cm y^{-1} (Klaminder et al., 2014). This cell-like movement is triggered by the opposite curvatures of the top (convex) and the bottom (concave) of the active layer, and thus, the contrary orientation of both freezing fronts (Mackay, 1980), and the thermal differences caused by the surrounding vegetation (Walker et al., 2004; Boike et al., 2008).

Differential frost heave and periglacial loading are the main cryogenic processes that occur inside mudboils. The first is generated as a result of the easier propagation of freezing temperatures in the bare central part than in surrounding soil insulated by vegetation cover and organic matter at the edges (Van Vliet-Lanoë, 1991; Peterson et al., 2003; Walker et al., 2004; Overduin and Kane, 2006; Nicolsky et al., 2008; Peterson, 2011). The second is produced because of the thawing of ice-rich material above the permafrost table increases the water content, which causes both a decrease in density and liquefaction (Swanson et al., 1999; Hallet and Waddington 2020). The participation of cryohydrostatic flow in mudboils as a main process was discarded since in the freezing back action, the unfrozen soil became desiccated rather than water saturated by the cryosuction generated by freezing fronts (Mackay and Mackay, 1976; Boike et al., 2008). Soils with higher clay content, however, can be injected as a liquid form into coarser layers through areas of weakness as evidence of pressure release (Ping et al., 2003).

Soil-related factors such as texture, moisture, bulk density, and pore water content influence the seasonal freezing and thawing aspects in mudboils (e.g., liquefaction, differential frost heave, freezing rate, ice content, and total heave). Fine-grained soil and high pore water content allow liquefaction to occur and are more frost-susceptible (Chamberlain, 1981; Walker et al., 2004; Peterson, 2011). Nevertheless, additional elements such as air temperature, snow depth, water availability, vegetation cover, altitude, slope, precipitation and active layer thickness may strongly influence the freeze-thaw action. Ice distribution at depth and freezing rate are highly controlled by air temperature and snow depth, whereas the total heave is mostly governed by soil availability (Overduin and Kane, 2006). A greater difference in frost heave is generated when the contrast in vegetation cover between the

central part of the mudboil and the peripheral area is larger (Peterson et al., 2003; Walker et al., 2004; Klaus et al., 2013). The size of the ground features, therefore the cryoturbated volume, is governed by the active layer depth (Peterson, 2011).

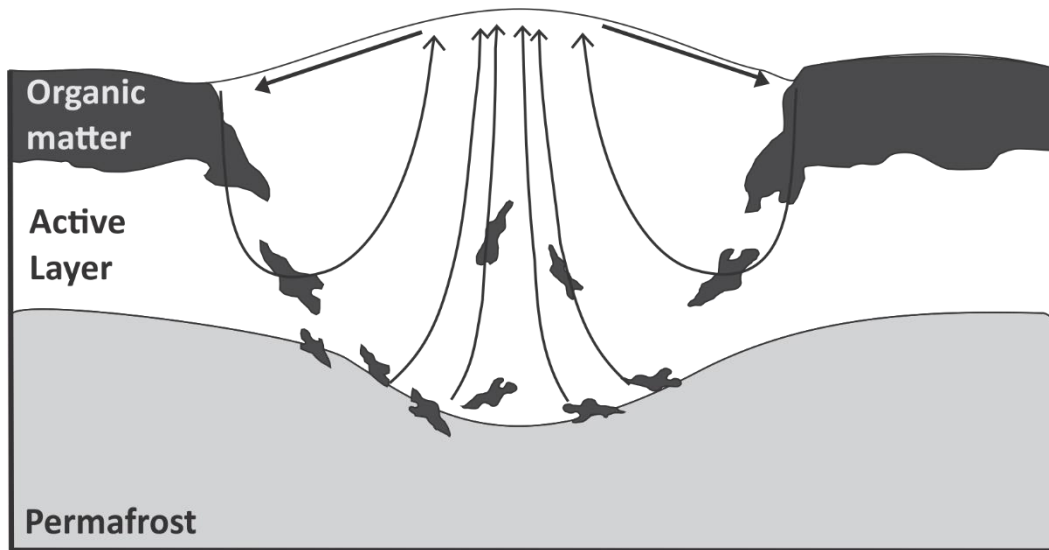


Figure 1.1. Internal long-term circular soil motion within mudboil. Modified from Walker et al. (2004) and Peterson et al. (2003).

Soil particles in permafrost regions may be sorted as a result of the seasonal freeze and thaw, creating mainly vertical sorting by decreasing the grain size with depth and sometimes accompanied by lateral sorting (Corte 1962a, b, 1963). Vertical sorting is governed by water content, freezing rate, size distribution of particles, particle density (mineralogy), grain shape, and the angle of the freezing front (Corte, 1962a, b). Slow freezing rates are the main processes that favor sorting (Corte 1962a, Derbyshire et al., 1979). Vertical sorting may be developed inside mudboils by migration on the freezing front, frost pull and frost push. Larger fragments have higher thermal conductivity, which favors the development of ice lenses beneath them. Moreover, fragments may adhere to the upper-freezing front (Derbyshire et al., 1979). Some authors present a vertical sorting of the matrix proportion (>2 mm) in mudboils, having a concentration of coarse material in the bottom as evidence of the long-term circular soil motion (Mackay, 1980; Zoltai and Tarnocai 1981; Ping et al., 2003). Nevertheless, this grain-size distribution is not uniform in all mudboils because concentration of coarse material at the top, as well as non sorted material at depth, have been

identified within mudboils (Dyke and Zoltai, 1980; Zoltai and Tarnocai, 1981; Klassen, 1995; Swanson et al., 1999; Overduin and Kane, 2006; Boike et al., 2008).

Problem Statement

Mudboils are the target for till sampling surveys in permafrost terrain (McMartin and McClenaghan, 2001). They have been extensively used for geochemical and indicator minerals surveys since they bring relatively unweathered till to the surface, are easy to recognize, and allow for easy sampling (Shilts, 1977, 1978; Batterson, 1989; Klassen, 1995; McClenaghan et al., 2000; McMartin and McClenaghan, 2001; Spirito et al., 2011). The major and trace element concentrations in mudboils do not vary considerably with depth (McMartin and McClenaghan, 2001; De Bronac de Vazelhes et al., 2021). For this reason, till samples are taken at shallow depths (Shilts, 1978; McMartin and McClenaghan, 2001; McClenaghan and Paulen, 2018). Notwithstanding, the distribution of indicator minerals inside mudboils has not been studied. The depth-invariant nature of till geochemistry cannot be assumed for IM. This is because geochemical analysis only comprises the <0.063 mm fraction, whereas IM processing involves fractions up to 2 mm. The long-term circular soil motion dynamics in mudboils may generate a sorting of IM in the till profile. Therefore, understanding the influence of cryoturbation on the IM properties (abundance, morphology, size, chemistry) will enable us to improve the indicator minerals strategies in permafrost regions.

Objective

The aim of this project is to develop new insights regarding the influence of cryogenic processes on indicator minerals derived from an orogenic-gold deposit in till underlain by permafrost by:

- Examining cryoturbation features in the glacial dispersal train from the Amaruq gold deposit;
- Systematically sampling vertical profiles into the selected cryoturbation structures;

- Determining the characteristics of indicator minerals (abundance, morphology, size, and mineral chemistry);
- Integrating and comparing the indicator minerals properties with features identified in the field; and
- Assessing the effects of cryogenic processes on indicator minerals and their implications for drift prospecting.

Methodology

Sampling and QA/QC

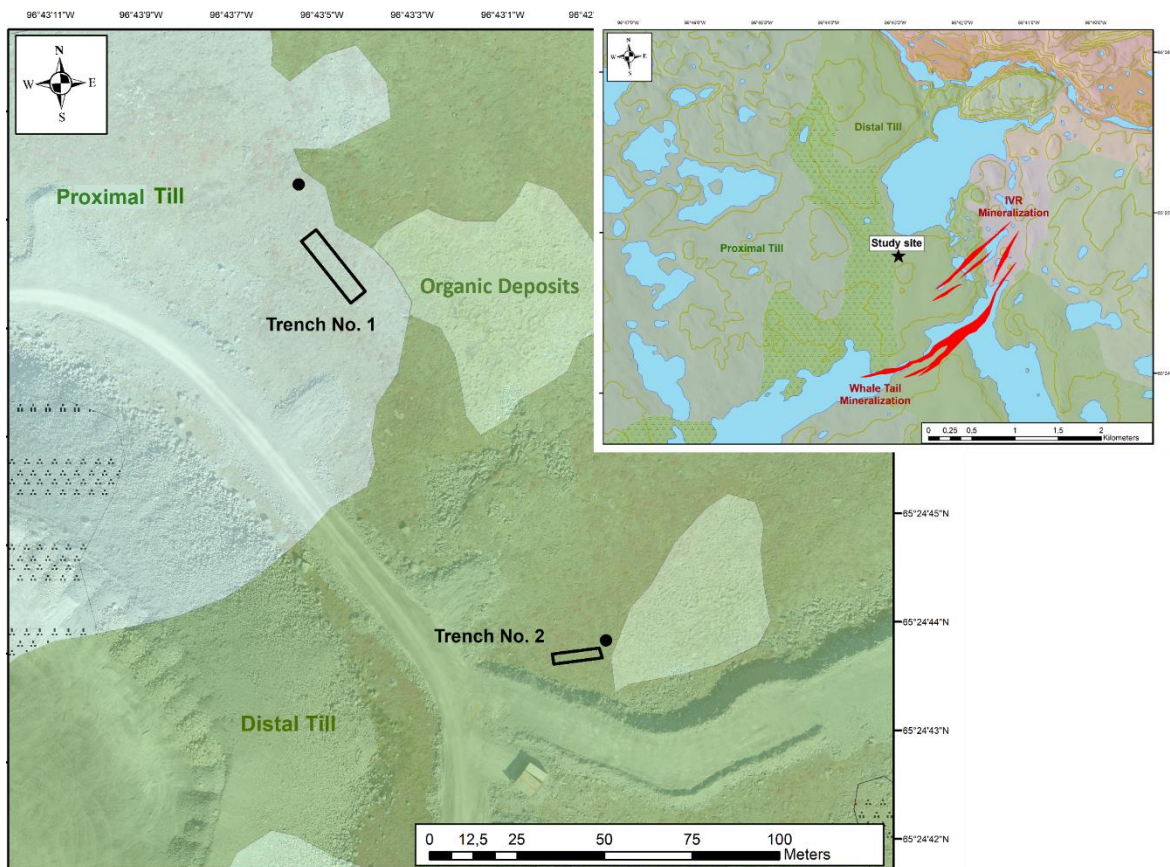


Figure 1.2. Location of the two trenches. Modified from Boulianne-Verschelden et al. (2019, 2022)

Two trenches (~3 m by 20 m) were made in 2021 at 1 km down-ice from the Amaruq gold deposit in 2021 (Figure 1.2). The first (Trench 1) is in the “proximal till” and underlain by diorite, and the second (Trench 2) is in the “distal till” and underlain by sedimentary bedrock, as mapped by Agnico Eagle Mines Limited and Boulianne-Verschelden et al. (2019). Each trench was examined, mapped and systematically sampled. In Trench 1, two main diamicton units were identified and seven vertical profiles down to ~1 m depth were made. In Trench 2, only one diamicton unit was recognized and two vertical profiles in two well-identified mudboils (one reaching the permafrost table) were sampled. Ten-kilogram samples for indicator minerals were collected according to the procedures of Spirito et al. (2011), McClenaghan et al. (2013), and Plouffe et al. (2013). The number of samples collected for IM was forty-two; forty in the vertical profiles inside the trenches, and two at ~35 cm depth in two mudboils from pits dug with a shovel (each one close to a trench; detailed sampling description is in the following section). Three quality control samples were inserted (two blanks and one field duplicate) for IM. In addition, twenty-four samples for matrix geochemical and textural analysis were taken. Six-teen of them are from the two well-identified mudboils in Trench 2. The average weight of these samples is ~3 kg.

Indicator Minerals

Indicator minerals preparation

Separation of heavy mineral concentrates, as well as morphology classification and counting of some IM (gold, scheelite, pyrite), were made by Overburden Drilling Management Limited (ODM). This process followed the Geological Survey of Canada’s methodology for till samples with the following steps (Spirito, et al., 2011): 1) concentration on the shaking table of the fraction <2 mm; 2) separation of the gold grains (minimum size 15 µm), particle size estimation and morphology description (DiLabio, 1990); preservation of separate gold grains in conical bottom vials; 3) preparation of heavy mineral concentrates (HMCs), using a heavy liquid separation at a 3.0 specific gravity, on the 0.25-2 mm fraction of the table concentrate; and 4) removal of the ferromagnetic fraction from the HMCs by magnetic separation.

The non-ferromagnetic HMC fraction (0.25-2 mm) was analyzed at Université Laval under a binocular microscope for IM classification, especially sulfides, tourmaline and scheelite. Ultraviolet (UV) light was used for scheelite identification. In addition, gold grains were characterized under a binocular microscope. Gold, scheelite, chalcopyrite and pyrite were mounted in epoxy resin.

Mineral chemistry

In order to identify any zonation or chemical variability, back-scattered analysis was performed on the gold and scheelite grains under the SEM (secondary electron microscope). In general, all grains exhibit a homogeneous texture and no significant variations at the edges.

-Electron Probe Micro-Analyzer (EPMA)

Mineral chemistry of major and minor elements was analyzed in gold, scheelite, and chalcopyrite grains by EPMA CAMECA SX-100, at Université Laval. The EPMA is equipped with five wavelength-dispersive spectrometers (WDS).

In the case of gold, the major elements Au and Ag, and minor elements such as Cu, Fe, Hg, S, and As were analyzed. The Au and Ag analyses were performed with a beam current of 20 nA, and an accelerating voltage of 15 kV. Minor elements were measured using a 20 kV accelerating voltage with a current of 100 nA. Major and minor were measured with a 5 µm beam size. In scheelite, W and Ca as major, and Mn, Na, Fe, Mo, Sr, and Y as minor elements were acquired. Major and minor element analyses were performed using a 15 kV accelerating voltage, and a 5 µm beam size. The current for the major element was 20 nA, and for the minor element was 100 nA. Finally, in chalcopyrite, the major elements S, Fe, and Cu, and minor elements such as Cd, Sb, Zn, Mn, Co, Ni, and As, were measured with a beam current of 20 nA, with an accelerating voltage at 15 kV, and a 5 µm beam size.

-Laser Ablation Inductively Coupled Plasma Mass Spectrometry (LA-ICP-MS)

The trace element concentration of gold, scheelite, and chalcopyrite was determined by the LA-ICP-MS method. Gold analyses were performed at the University of New Brunswick (UNB), while scheelite and chalcopyrite minerals were examined at Université Laval (UL). At University of New Brunswick, the trace element content was examined by the laser ablation system laser RESolution LR 193nm Excimer S-155-LR 193nm and a large cell coupled to an Agilent 8900 triple quadrupole. The frequency of operation was 2.5 Hz and the fluence was $2.25 \text{ J}\cdot\text{cm}^{-2}$. The size of the beam used was $45 \mu\text{m}$ and $33 \mu\text{m}$, depending on the size of the gold grains. The standards NIST-610, MASS-1, Au-30 and Au-31 were used for calibration. Silver¹⁰⁹ was used as an internal standard, being normalized to values acquired by EPMA. The isotopes measured were ²⁴Mg, ²⁷Al, ²⁹Si, ³⁴S, ⁴⁷Ti, ⁵³Cr, ⁵⁵Mn, ⁵⁷Fe, ⁵⁹Co, ⁶⁰Ni, ⁶⁵Cu, ⁶⁶Zn, ⁷⁵As, ⁷⁷Se, ⁹⁵Mo, ¹⁰⁸Pd, ¹¹¹Cd, ¹¹⁵In, ¹¹⁸Sn, ¹²¹Sb, ¹²⁵Te, ¹⁸⁵Re, ¹⁹⁵Pt, ²⁰²Hg, ²⁰⁵Tl, ²⁰⁶Pb, ²⁰⁷Pb, ²⁰⁸Pb, and ²⁰⁹Bi.

At Université Laval the trace element analysis was performed by LA-ICP-QQQ-MS at Université Laval using a RESolution S-155 Excimer laser with 193 nm wavelength and a large cell coupled to an Agilent 8900 (Inductively plasma triple quadruple mass spectrometer). For analyses on scheelite, the equipment operates with a frequency of 15 Hz and fluence of $4 \text{ J}\cdot\text{cm}^{-2}$. The beam size in line and spot analyses were $38 \mu\text{m}$ and $24 \mu\text{m}$ respectively. Lines were preferred over spots to evaluate possible chemical variations. The external standards were GSE-1g, NIST-610, and NIST-612. As an internal standard was used ⁴⁴Ca, fixed at 13.90 wt%. The isotopes analyzed were ⁷Li, ¹¹B, ²³Na, ²⁴Mg, ²⁸Si, ³¹P, ³⁴S, ³⁹K, ⁴³Ca, ⁴⁷Ti, ⁵¹V, ⁵²Cr, ⁵⁵Mn, ⁵⁶Fe, ⁵⁹Co, ⁶³Cu, ⁶⁶Zn, ⁷⁵As, ⁸⁸Sr, ⁸⁹Y, ⁹³Nb, ⁹⁵Mo, ¹⁰⁷Ag, ¹¹⁸Sn, ¹³⁷Ba, ¹³⁹La, ¹⁴⁰Ce, ¹⁴¹Pr, ¹⁴⁶Nd, ¹⁴⁷Sm, ¹⁵³Eu, ¹⁵⁷Gd, ¹⁵⁹Tb, ¹⁶³Dy, ¹⁶⁵Ho, ¹⁶⁶Er, ¹⁶⁹Tm, ¹⁷²Yb, ¹⁷⁵Lu, ¹⁸¹Ta, ¹⁸²W, ²⁰⁸Pb, ²³²Th, and ²³⁸U. For the determination of trace elements in chalcopyrite, the laser ablation system was conducted with a frequency of 15 Hz and a power of 2 J cm^{-2} , and a $38 \mu\text{m}$ beam size. The external standards NIST-610, MASS-1, GSE-1g, and synthetics FeS-4, and FeS-6 were analyzed. Iron⁵⁷ was used as an internal standard with stoichiometric iron values in chalcopyrite (30.43 wt%). The isotopes analyzed were ²⁴Mg, ²⁸Si, ³¹P, ³²S, ³⁴S, ⁴⁴Ca, ⁴⁹Ti, ⁵¹V, ⁵²Cr, ⁵⁵Mn, ⁵⁹Co, ⁶⁰Ni, ⁶³Cu, ⁶⁶Zn, ⁷¹Ga, ⁷²Ge, ⁷⁵As, ⁷⁸Se, ⁹⁵Mo, ¹⁰³Rh, ¹⁰⁵Pd, ¹⁰⁷Ag, ¹¹¹Cd, ¹¹⁵In, ¹¹⁸Sn, ¹²¹Sb, ¹²⁵Te, ¹³⁷Ba, ¹⁸²W, ¹⁸⁵Re, ¹⁹⁵Pt, ¹⁹⁷Au, ²⁰¹Hg, ²⁰⁵Tl, ²⁰⁸Pb, and ²⁰⁹Bi. The data was reduced using the Iolite software.

Till geochemistry

Sample preparation

Samples for geochemistry were prepared according to the Geological Survey of Canada protocols (Spirito et al., 2011). Samples were air-dried at the GSC Sedimentology Laboratory, then sieved to obtain the <0.063 mm fraction. Two silica blanks (#135), two lab duplicates, and two standards (Till-4) were inserted as QA/QC samples.

Analytical Methods

Till geochemistry was acquired by three analytical methods (AQ252-EXT +REE, LF200, and MA250) in Bureau Veritas. AQ252-EXT + REE is an aqua-regia digestion method (1:1:1 HNO₃:HCl:H₂O), with ICP-MS acquisition for ultra-low concentrations including rare earth elements. The elements measured were Li, Be, B, Na, Mg, Al, P, S, K, Ca, V, Cr, Ti, Mn, Fe, Co, Ni, Cu, Zn, Ga, Ge, As, Se, Rb, Sr, Y, Zr, Sc, Pr, Gd, Dy, Ho, Er, Tm, Nb, Mo, Pd, Ag, Cd, In, Sn, Sb, Te, Cs, Ba, La, Ce, Nd, Sm, Eu, Tb, Yb, Lu, Hf, Ta, W, Re, Pt, Au, Tl, Pb, Bi, Th, U, Hg. LF200 is a lithium borate fusion digestion method by ICP-ES, which is highly used for total element content. The elements analyzed were SiO₂, Al₂O₃, Fe₂O₃, MgO, CaO, Na₂O, K₂O, TiO₂, P₂O₅, MnO, Cr₂O₃, Ba, Ni, Sc, Cu, Zn, Mo, Pb, Be, Co, Cs, Ga, Hf, Nb, Rb, Sn, Sr, Ta, Th, U, V, W, Zr, Y, La, Ce, Pr, Nd, Sm, Eu, Gd, Tb, Dy, Ho, Er, Tm, Yb, Lu, as well as the total carbon and total sulphur. Finally, MA250 is a multi-acid (HNO₃:HClO₄:HF, and HCl) ultra-trace analytical method (ICP-ES/MS). The elements examined were Mo, Cu, Pb, Zn, Ag, Ni, Co, Mn, Fe, As, U, Th, Sr, Cd, Sb, Bi, V, Ca, P, La, Cr, Mg, Ba, Ti, Al, Na, K, W, Zr, Sn, Be, Sc, S, Y, Ce, Pr, Nd, Sm, Eu, Gd, Tb, Dy, Ho, Er, Tm, Yb, Lu, Hf, Li, Rb, Ta, Nb, Cs, Ga, In, Re, Se, Te, Tl.

Grain size analysis, total C, organic carbon and LOI

Particle Size Analysis

The analysis was performed in the GSC Sedimentology Laboratory, following the method described by Girard et al. (2004). The analyses include gravel, and sand-silt-clay grain sizes. The sizes >0.063mm are identified by wet sieving and the sizes <0.063mm are determined using the Camsizer & Beckham LS13-320 particle size analyzer. The sizes fractions are reported as % weight (>0.063 mm) and % volume (<0.063 mm). The fractions (mm) are 2-1.4; 1.4-1; 1-0.71; 0.71-0.50; 0.50-0.35; 0.35-0.25; 0.25-0.18; 0.18-0.12; 0.12-0.088; 0.088-0.063; 0.063-0.044; 0.044-0.031; 0.031-0.016; 0.016-0.008; 0.008-0.004; 0.004-0.002; 0.002-0.001; <0.001.

Total and Organic Carbon

The analysis of the organic and inorganic carbon was conducted in the GSC Sedimentology Laboratory according to the procedures in Girard et al. (2004). The fraction used for the analysis is <0.063 mm. The carbon content in soil samples was determined using a Leco CR412 1350C Carbon Analyser. The analysis also registered the loss on ignition (LOI) at 500°C.

Geostatistical treatment

To analyze the data, a range of statistical techniques were used, including both univariate and multivariate analyses. Univariate statistics, such as mean, median, mode, range, variance, and standard deviation, were used to describe and analyze individual variables in the dataset. Meanwhile, multivariate statistics tools, including correlation analysis, regression analysis, and multivariable statistics, were employed to examine the relationships between multiple variables, especially for the geochemical data (till and mineral chemistry).

Some of the variables were discarded when their percentage of data below detection limit, or censored values, was >40%. To address missing data, the censored values below the detection limit were imputed using the log-ratio Expectation-Maximization algorithm (lrEM), in the zComposition R-Package (Palarea-Albaladejo and Martín-Fernández, 2015; R Core Team, 2022). Two main multivariate statistics were used, the Principal Component Analysis (PCA)

and the Partial Least Squares Discriminant Analysis (PLS-DA) to understand the relationships between the various elements. Whereas PCA visually exhibits the correlation between elements, PLS-DA shows similar characteristics between the elements and the classes labelled. In the case of till geochemistry, PCA was the method used to compare with previous PCA results in the Amaruq area (de Bronac de Vazelhes et al., 2021). PLS-DA score plots were used to identify the possible mineral deposit source of the scheelite and gold according to the PLS-DA models of Sciuba et al., (2020) and Liu and Beaudoin (2021), respectively.

Presentation of the article

Chapter 1 is a manuscript entitled “ASSESSING THE EFFECTS OF CRYOTURBATION ON INDICATOR MINERALS FROM THE AMARUQ GOLD DEPOSIT (NUNAVUT, CANADA)”. It was written by Juan David Bello Rodríguez (first author) under the supervision of Prof. Georges Beaudoin (Université Laval) and Dr. Isabelle McMartin (Geological Survey of Canada). Following the introduction, this chapter provides an overview about the Quaternary and bedrock geological context of the Amaruq gold deposit including at the regional and local scales. Subsequently, it explains the methodology into the details of sampling processes, sample preparation, analysis parameters, and statistical methods employed for data processing. The chapter then focuses on till description, cryoturbation features, matrix analysis (grain-size and till geochemistry), and indicator mineral properties (abundance, gold morphology, gold grain size and mineral chemistry). Uni- and multivariate statistical methods are used to describe and discriminate the nature of gold, scheelite and chalcopyrite. The characteristics of the indicator minerals are compared with their position in the various cryoturbation structures. Finally, the chapter concludes with a comprehensive discussion of the results and a concluding statement.

Chapter 1

ASSESSING THE EFFECTS OF CRYOTURBATION ON INDICATOR MINERALS FROM THE AMARUQ GOLD DEPOSIT (NUNAVUT, CANADA)

1.1 Résumé

Les minéraux indicateurs (MI) fournissent des informations précieuses pour l'exploration minière dans les terrains glaciaires. Dans les régions pergélisolées, les ostioles sont une des manifestations de la cryoturbation les plus courantes dans les sédiments glaciaires et sont donc essentiels pour les études des MI. Nous avons étudié si la dynamique du mouvement interne dans les ostioles peut entraîner un tri vertical et/ou latéral des MI dans la couche active. Dans cette étude menée près du dépôt aurifère orogénique d'Amaruq, dans le nord du Canada (Nunavut), nous avons prélevé des échantillons de till sur plusieurs profils verticaux jusqu'à une profondeur d'environ 1,3 mètre dans deux tranchées situées à environ 1,5 km en aval glaciaire du dépôt, comprenant deux profils dans la partie centrale de deux ostioles bien identifiés (dont l'un atteint le pergélisol à 1,30 m de profondeur).

La fraction du concentré de minéraux lourds (<2 mm) de tous les échantillons de profils contient de l'or et de la scheelite. L'abondance de ces MI présente des variations verticales qui ne sont pas uniformes entre tous les profils. De même, la taille et la morphologie des grains d'or ne suivent aucun modèle cohérent. Le till dans le pergélisol présente la plus grande abondance des MI par rapport à celui de la couche active sus-jacent. La variation latérale des MI examinée dans un ostiole à une profondeur d'environ 30 cm indique que le nombre de grains d'or et de scheelite le plus élevé se trouve dans la partie centrale de l'ostiole. La composition chimique de l'or (<400 µm), de la scheelite et de la chalcopyrite (0.25-2.00 mm) a été déterminée par EPMA et LA-ICP-MS. La plupart de ces minéraux sont interprétés comme étant issus du dépôt aurifère d'Amaruq. Aucun d'entre eux ne présente de tendances verticales systématiques dans leur composition chimique.

En résumé, les ostioles ne montrent pas de variations systématiques dans les propriétés des MI (abondance des minéraux, morphologie, taille et composition minérale) à différentes profondeurs. L'étude suggère que les processus de cryoturbation ne génèrent pas de fractionnement vertical uniforme des minéraux indicateurs dans les ostioles en raison des multiples variables impliquées dans le processus de gel-dégel.

1.2 Abstract

Indicator minerals (IM) play a crucial role in mineral exploration in glaciated regions. In permafrost areas, mudboils (frost boils) are common features caused by cryoturbation in glacial sediments, making them significant for IM studies. Our investigation focused on understanding whether the internal motion dynamic within mudboils could lead to vertical sorting of IM in the active layer. The study took place at the Amaruq orogenic gold deposit in northern Canada (Nunavut), where we sampled till in vertical profiles down to approximately 1.3 m depth in two trenches located about 1.5 km down-ice from the deposit. Two of these profiles are in the central part of two well-defined mudboils, with one reaching the permafrost table (at 1.30 m depth).

The heavy mineral concentrate fraction (<2mm) of all profile samples contained gold and scheelite. However, the abundance of these IM exhibited vertical variations that are not consistent across all profiles, and the size and morphology of gold grains did not show any clear trends. The highest IM abundance was found in the till within the permafrost compared to the overlying active layer. The lateral variation of IM examined in one mudboil at approximately 30 cm depth revealed the highest grain count of gold and scheelite in the central part of the mudboil. The chemical composition of gold (<400), scheelite and chalcopyrite (0.25-2 mm) was analyzed using EPMA and LA-ICP-MS, with most of these minerals interpreted to originate from the Amaruq gold deposit. However, none of them displayed systematic vertical trends in chemical composition.

In conclusion, mudboils exhibit no systematic variations in IM properties (mineral abundance, morphology, size, and mineral chemistry) at different depths. The study suggests that cryoturbation processes do not lead to a uniform vertical fractionation of indicator minerals in mudboils due to the involvement of multiple variables in the freeze-thawing process.

1.3 INTRODUCTION

Mineral exploration programs conduct multi-disciplinary geological studies to discover ore deposits and consider factors like tectonic setting, hydrothermal composition, structural environment, host-rock, and ore formation processes. Additionally, these programs use geochemical and geophysical surveys to detect ore bodies. However, weathering and erosional processes can mask or disperse mineralization. These processes are influenced by the deposit's geographical location and weathering conditions. In Canada, past continental ice sheets have been the main factor of erosion and sediment transport, commonly generating streamlined landforms and clastic sediment deposits, mainly composed of till, a glacial diamicton deposited directly by ice (Shilts and Menzies, 1996). Consequently, till sampling is an important method for drift prospecting in Canada, as till is the preferred sample medium in glaciated areas (McMartin and McClenaghan, 2001). Glacial dispersal from mineral deposits forms distinct geochemical and heavy mineral (density higher than $\sim 3 \text{ g/cm}^3$) patterns. Certain minerals within this heavy mineral fraction can serve as indicators of various mineralization types and are referred to as 'indicator minerals' (IM; Shilts, 1977).

Periglacial environments, found near glaciers or ice sheet edges, and in areas underlain by permafrost, are characterized by cold climatic conditions. Permafrost regions have year-round frozen layers that intensify soil perturbations by cryoturbation, the process of freeze-thaw cycles (Vandenberghe, 1988). Cryoturbation primarily occurs in the active layer above the permafrost table, while non-permafrost areas with seasonally frozen ground also experience cryoturbation but at a lower rate. The most common cryogenic processes are periglacial loading, cryohydrostatic flow, and frost heave (Vandenberghe, 2013). These processes govern the soil particles' migration, mixing, and sorting, and contribute to weathering in permafrost areas. Particle sorting is influenced by a multitude of factors, encompassing both the nature of the particles and the environmental conditions in which they exist, such as water content, humidity, till texture, and freezing rate (Corte, 1962a).

Till samples for geochemistry and IM surveys in permafrost areas are commonly collected in mudboils (Shilts 1973; 1977; DiLabio and Shilts, 1979; Laurus and Fletcher, 1999; Klassen, 1995; Spirito et al., 2011; McClenaghan et al., 2013; McClenaghan and Paulen,

2018). Mudboils (frost boils or non-sorted circles) are the result of the seasonal freeze-thaw and are a common frost feature in periglacial environments (Washburn, 1956). Several studies have shown a uniform distribution of major and trace element concentrations with depth in mudboils, enabling representative sampling near surface, at about 30 cm depth (McMartin and McClenaghan, 2001; McMartin and Campbell, 2009; de Bronac de Vazelhes, 2019). However, the characteristics and distribution of IM within mudboils have not been thoroughly investigated.

The objective of this study is to investigate the nature of IMs in mudboils, and to assess how long-term soil motion produced by cryoturbation in the active layer may affect the distribution, morphology, grain size and provenance of IM in the till column. We analyzed the characteristics of orogenic gold IM in glacial sediments from two trenches located 1 km down-ice of the Whale Tail mineralization in the Amaruq banded iron formation-hosted orogenic gold deposit, Nunavut, Canada (Fig I.1). The study area is located within the continuous permafrost zone (Heginbottom et al., 1995) and along the proximal part of a well-documented dispersal train from the Whale Tail mineralization (de Bronac de Vazelhes et al., 2021; Mendizabal, 2022). Orogenic gold deposits and their dispersal trains in this northern region are known to contain several indicator mineral species, including gold, scheelite, tourmaline, and some sulfides such as pyrite, arsenopyrite, and pyrrhotite (Manégliia et al., 2018; de Bronac de Vazelhes, 2019; Sciuba, 2020; Liu et al., 2021; de Bronac de Vazelhes et al., 2021). Our research aims to provide valuable insights into the behavior of IM in cryoturbated glacial sediments and their use for mineral exploration in permafrost regions in order to contribute to the development of more efficient drift prospecting techniques in glaciated terrains.

1.4 GEOLOGICAL SETTING

1.4.1 Bedrock geology

The Amaruq gold deposit is in the Archean Rae domain of the western Churchill geological province. The Archean Rae domain consists of a Mesoarchean granodioritic to gneissic basement (2.9 -2.8 Ga) and several Neoproterozoic greenstone belts (2.73- 2.63 Ga) (Berman et al., 2010; Pehrsson et al., 2013). The Amaruq deposit is hosted in the Woodburn Lake Group which forms one of these greenstone belts. This group has been subdivided into six main volcanic-sedimentary rock assemblages (Sherlock et al., 2004; Janvier et al., 2015; Jefferson et al., 2015; Valette et al., 2020) and it has been affected by several deformation events in the Archean and Paleoproterozoic (Pehrsson et al., 2013; Valette et al., 2020). The Amaruq gold deposit is hosted in the Rumble assemblage (2735-2630 Ma; Valette et al., 2019, Valette et al., 2020).

In the Amaruq area, the Rumble assemblage has been divided into three stratigraphic domains: (1) North domain; (2) South domain; and (3) Central domain (Valette et al., 2020). The North domain with a minimum age of 2735 Ma presents the first volcanic cycle, with tholeiitic mafic-ultramafic igneous rocks interlayered with black shales. The South domain is the result of a second volcanic event, comprising transitional to calc-alkaline mafic-ultramafic rocks, with a crystallization age of 2710 Ma (Valette et al., 2022), and greywacke. The Central domain is characterized by clastic (greywacke and shale) and chemical (banded iron formation [BIF] and chert) sedimentary rocks. This assemblage is intruded by diorite bodies at 2.6 Ga (Snow Island Suite; Pehrsson et al., 2013; Jefferson et al., 2015; Valette et al., 2020), and lamprophyre and felsic dykes (Valette et al., 2020).

Three principal gold mineralized zones have been identified in the Amaruq gold deposit, the IVR, Mammoth, and Whale Tail, which exhibit different mineralization styles, structural domains, geometry, ore types, and textures (Coté-Mantha et al., 2017; Valette et al., 2019; Valette et al., 2020). In general, gold is found as inclusions, at sulfide crystal boundaries, free grains and fracture-fillings. The Whale Tail zone is the main gold-bearing mineralization,

and it is mostly hosted in chemical sedimentary rocks. Stratabound, disseminated and replacement are the three styles of ore which are characterized by actinolite-quartz-calcite-bearing veins, disseminated pyrrhotite-arsenopyrite-gersdorffite, and Ca-amphibole-siderophyllite-clinozoisite-garnet-apatite-titanite, respectively (Valette et al., 2020). Native Au and electrum in the Whale Tail zone typically form as inclusions in pyrrhotite and arsenopyrite. The shape of native Au and electrum is rounded to angular, and their size varies from <1 to 50 μm (Coté-Mantha et al., 2017; Lauzon et al., 2020).

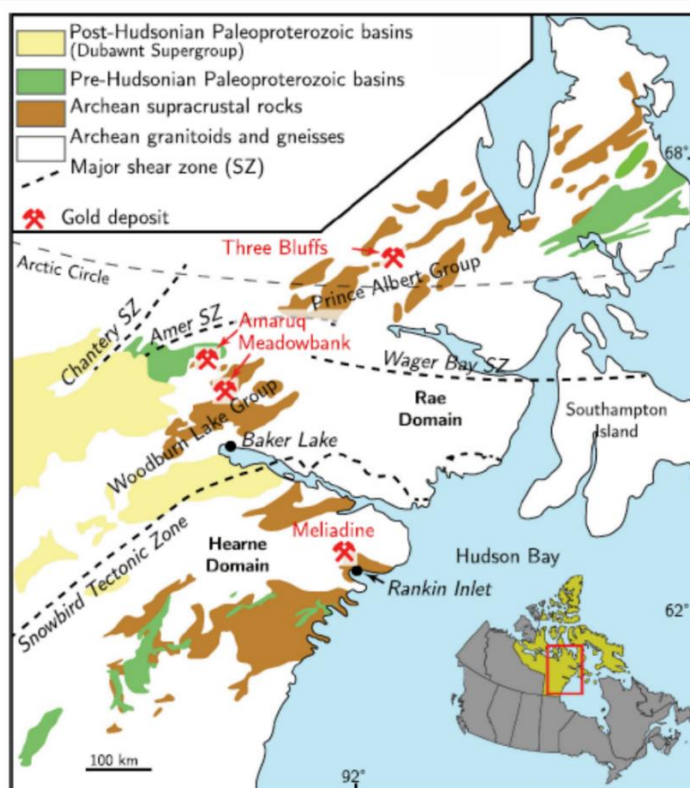


Figure I. 1 Bedrock geology map modified by de Bronac de Vazelhes et al. (2021), after Hradi et al. (2003).

1.4.2 Quaternary geology

The northwestern Canadian Shield was covered by the Laurentide Ice Sheet (LIS) of the Late Wisconsin North American ice sheet complex until its retreat at approximately 7 ka BP (Dyke and Dredge, 1989; Dyke, 2004). The current landscape is characterized by abundant glacial

landforms such as drumlins, glacial lineations, ribbed moraine, hummocky moraine, end moraines and eskers west of Hudson Bay in Nunavut (Keewatin region; Shilts et al., 1987). The orientation of some of these glacial landforms (eskers, drumlins, and ribbed moraine) radiate outwards from the Keewatin Ice Divide (Fig. I.2; Shilts et al., 1987; Aylsworth and Shilts, 1989; McMartin et al., 2021). The Keewatin Ice Divide migrated up to 500 km in different directions between ice-flow phases that generated several ice-flow directions in the region, especially in the areas close to the divide, producing a complex pattern of ice-flow indicators and glacial landforms (McMartin and Henderson, 2004).

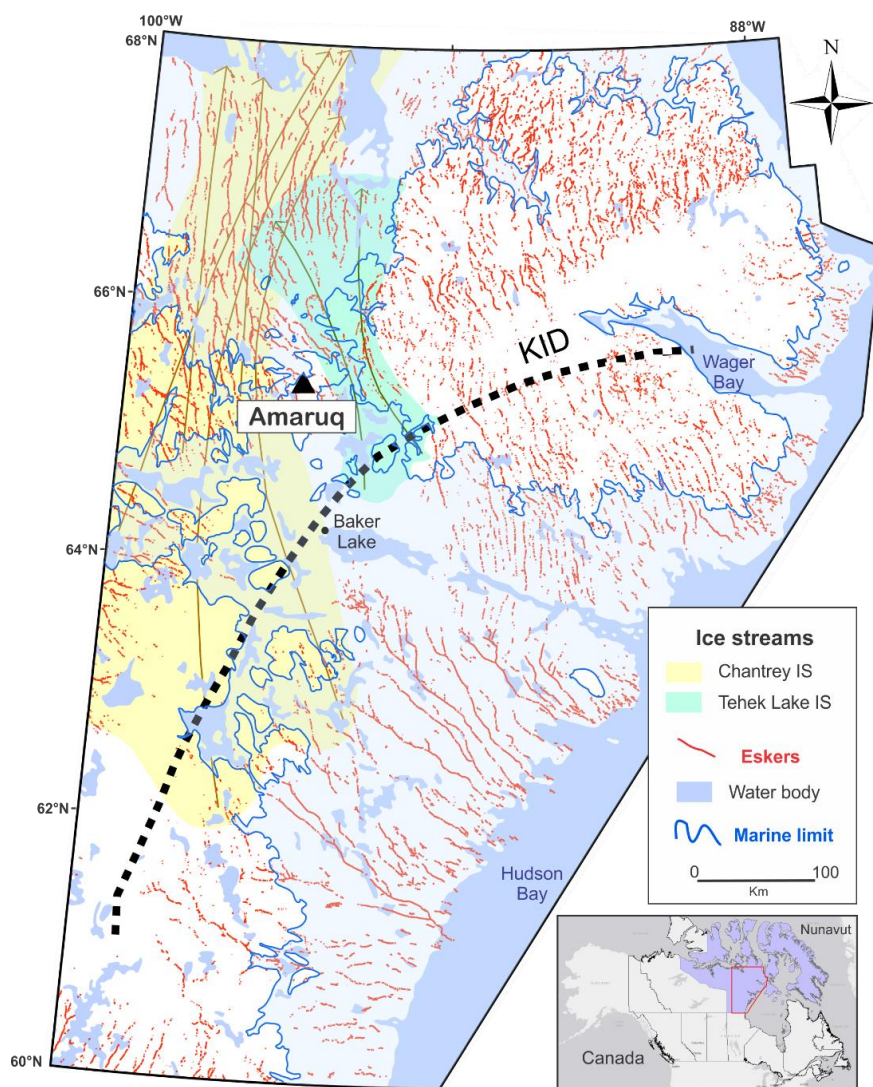


Figure I. 2 Map of some glaciogenic features and glacial landsystems of the eastern Keewatin region. Modified from McMartin et al. (2021; 2022). KID=Keewatin Ice Divide (8 Ka BP).

Mapping of glaciogenic features based on field and remote sensing data in the eastern Keewatin region has allowed the interpretation of different regional glacial landsystems such as ice streams, palimpsest streamlined landscapes, relict cold-based terrains (McMartin et al., 2021). At least six different ice streams with different ice flow directions have been documented in the region, and the Amaruq deposit area is located between the Chantrey ice stream and the Tehek Lake ice stream (Fig. I.2; McMartin et al., 2021). Furthermore, the geomorphology of the region is also influenced by marine postglacial inundation recorded at its maximum level (145 m above sea level) by high-raised boulder beaches, wave-washing limits, wave-cut notches in till and deltas (Fig I.2; McMartin et al., 2022). The Amaruq deposit is located above the post-glacial marine limit.

After the complete deglaciation and retreat of seawater in the region (~7000-8000 years BP; Dyke, 2004), cryoturbation processes commenced to occur in the active layer of glacial sediments. According to Zoltai (1995), continuous permafrost has existed in west-central Canada since at least 6000 years BP, regardless of the warm middle Holocene period. This continuous permafrost environment, as well as the cold climatic conditions, have generated the development of cryosols (Tarnocai and Bockheim, 2011). Radiocarbon dating of buried organic matter in mudboils and cryoturbated soils in the Keewatin region shows that cryoturbation processes began at least 7400 years BP (Dyke and Zoltai, 1980; Hugelius et al., 2010). Various cryoturbation features were observed in the Amaruq deposit area such as patterned ground (mudboils, sorted circles) and earth hummocks (Boulianne-Verschelden et al., 2019, 2022; De Bronac de Vazelhes et al., 2021).

The surficial geology of the Amaruq project area is dominated by glacial deposits including till blanket, ridged moraine, and till veneer, with minor glaciofluvial deposits along narrow corridors, and marine and/or glacial lake deposits in the north (Fig I.3; Boulianne-Verschelden et al., 2022; McMartin et al., 2022). Glacial deposits can be distinguished based on their texture, associated landforms, thickness, distribution and mudboil abundance. The ice-movement indicators show a general NNW to NW direction in the Amaruq deposit area, from the Keewatin Ice Divide (Utting and McMartin, 2004; Boulianne-Verschelden et al., 2019, 2022; McMartin et al., 2021).

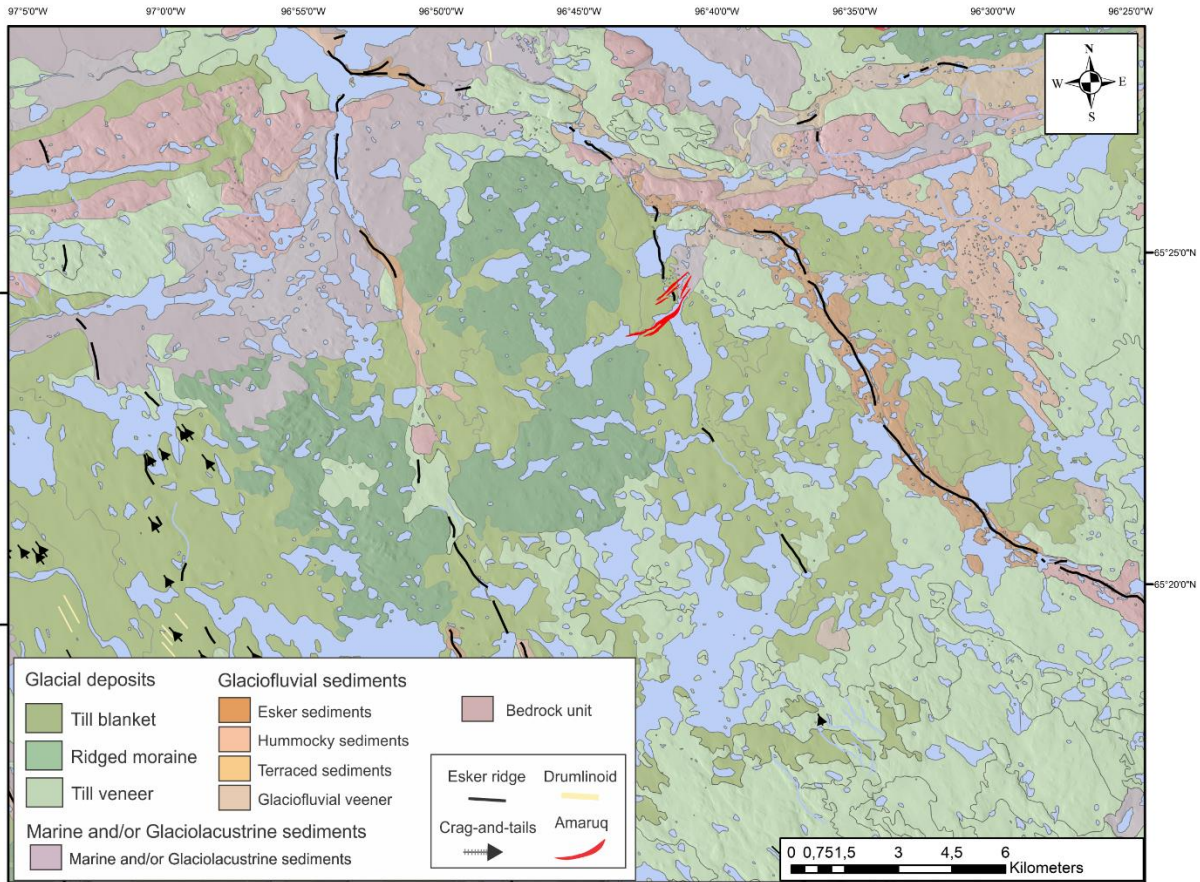


Figure I.3 Regional Quaternary geology map of the Amaruq Area. Modified from Boulianne-Verschelden et al. (2022).

Near the Amaruq deposit area at a local scale, four types of till deposits were mapped: proximal, distal, hybrid, and undifferentiated tills (Fig. I.4; Boulianne-Verschelden et al., 2019). The proximal till is commonly related to the ridged moraine mapped at the regional scale. It exhibits a matrix with less than 5% clay content, a high proportion of surface boulders (over 70%), a ribbed moraine shape, a thickness of less than 10 m, and rare mudboils. Pebble counts and matrix geochemistry suggests that the proximal till reflects limited glacial transport, containing a significant proportion of local bedrock material. The distal and hybrid tills, on the other hand, are associated with the till blanket (regional scale) and form a continuous cover that typically obscures the underlying topographic features. The distal till presents a clay content higher than 6% and less than a 20% of the surface is cover of boulders. It occurs in the form of drumlinoids, has a thickness of less than 20 m, and abundant proportion of the surface covered by mudboils. The finer grain-size of the distal till

facilitates the development of mudboils (Shilts, 1978). The hybrid till, although associated with the till blanket on a regional scale, exhibits a high surface boulder cover and geochemical characteristics of a proximal source, but with distal clasts. Undifferentiated till shows few or not enough distinct attributes to be classified.

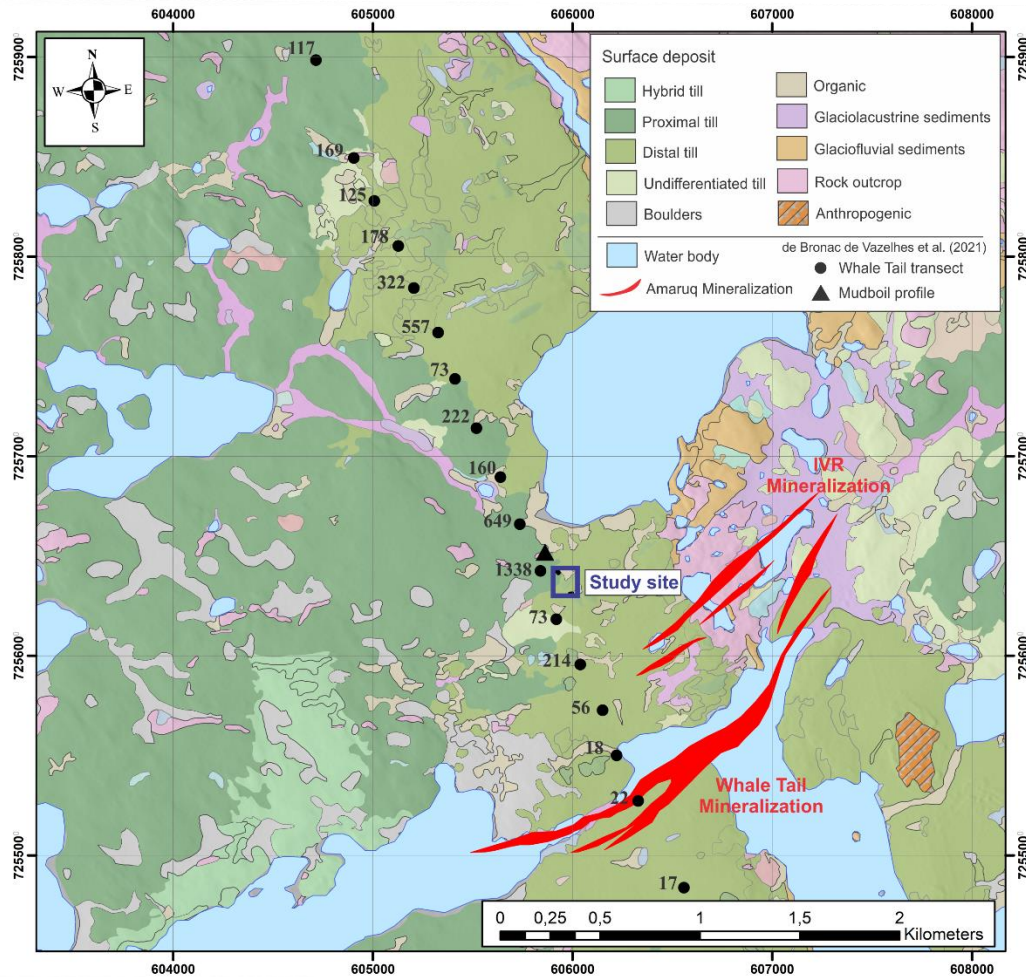


Figure I.4 Local Quaternary geology map of the Amaruq deposit area near the Whale Tail mineralization. Modified from Boulianne-Verschelden et al. (2019). Location of the Whale tail transect samples, number of gold grains (normalized to 10-kg) and the mudboil profile from de Bronac de Vazelhes et al. (2021) are shown.

De Bronac de Vazelhes et al. (2021) identified different glacial dispersal patterns along three transects (Whale Tail, Mammoth East and Mammoth West) perpendicular to the Amaruq deposit. The patterns were linked to variations in ice velocities, as shown by till thickness and sediment composition. The Whale Tail transect (Fig I.4) was mainly sampled in distal

till indicating a higher relative ice velocity, which lead to a longer glacial transport and greater lag distances (i.e., skip zone: the distance between the mineralization and the evidence of the plume at the surface) compared to the other transects in proximal till (de Bronac de Vazelhes et al., 2021). The Whale Tail transect shows a predominance of felsic elemental association derived from diorite and granite up-ice lithologies reflecting the significant cover of distal till. However, ~1700 m down-ice from mineralization, there is an increase in the mafic/ultramafic and gold mineralization signature probably associated with proximal till (Fig. I.4; 649 gold grains; de Bronac de Vazelhes et al., 2021). Another sample ~850 m down-ice exhibits a similar increase but to a lesser extent (214 gold grains), and this sample is from distal till. Up-ice from the mineralization, till exhibits less than 25 gold grains with a pristine proportion of around 15%. The highest gold peak occurs at 1400 m (near our study area) down-ice from the mineralization with 1338 gold grains, in proximal till. The gold abundance decreases rapidly in the direction of ice flow further along the transect (<400m), but even at 8 km down-ice from mineralization there are still 200 gold grains, significantly higher than background levels (Mendizabal, 2022). Down-ice gold grains have a pristine proportion that varies from 50 to >90%, with an average of 69%, and remain similar in proportion to the end of the transect. Most of the samples analyzed in this transect were taken in mudboils at ~35 cm depth.

1.5 METHODOLOGY

1.5.1 Sampling and QA/QC

Two trenches (up to 3 m wide, 20 m long) were made with an excavator in September 2021 at ~1.4 km down-ice from the Amaruq gold deposit (Fig I.5). The first (Trench 1) is in “proximal till” near the contact with “distal till” underlain by diorite, whereas the second (Trench 2) is in “distal till” overlying sedimentary rocks (Boulianne-Verschelden et al., 2019). Each trench was examined, mapped and systematically sampled. In Trench 1, both north and south walls were sampled and analyzed. Two main diamicton units were identified and seven vertical profiles down to ~1 m depth were sampled. The vertical sampling profiles were named according to their North or South wall and their position in meters: N6, N7, N10, N12, N16, S13, and S17 (Fig. I.6). In Trench 2, one diamicton unit was recognized and two vertical profiles in two well-identified mudboils (Mudboil 1 and Mudboil 2) were sampled (Fig. I.7). Mudboil 2 profile (MB2) reached the permafrost table at 1.30 m depth. In Mudboil 1 profile, three lateral samples were also taken, one on the left side and two on the right side of the mudboil. The number of till samples collected within the trenches for IM was 40, and 2 additional till samples were collected at ~35 cm depth in two mudboils from pits hand-dug with a shovel (MB3 close to Trench 2 and MB4 close to Trench 1; Fig. I.5). Ten-kilogram samples for indicator minerals were collected according to the procedures of Spirito et al. (2011), McClenaghan et al. (2013), and Plouffe et al. (2013). Three quality control samples were inserted (two blanks from Bathurst New Brunswick: 09-PTA-001 and one field duplicate) for IM processing and analysis. In addition, twenty-four samples for matrix geochemical and textural analysis were taken. Sixteen samples are from the two mudboils in Trench 2, 6 samples in Trench 1, and 2 samples in the adjacent mudboils. The weight of these samples is ~3 kg.

1.5.2 Till geochemistry

Sample preparation

Samples for geochemistry were prepared according to Girard et al. (2004). Samples were air-dried at the GSC Sedimentology Laboratory, then were sieved at 63 μm . Two silica blanks (J.T. Baker®), two lab duplicates, and two standards (Till-4) were inserted as QA/QC samples.

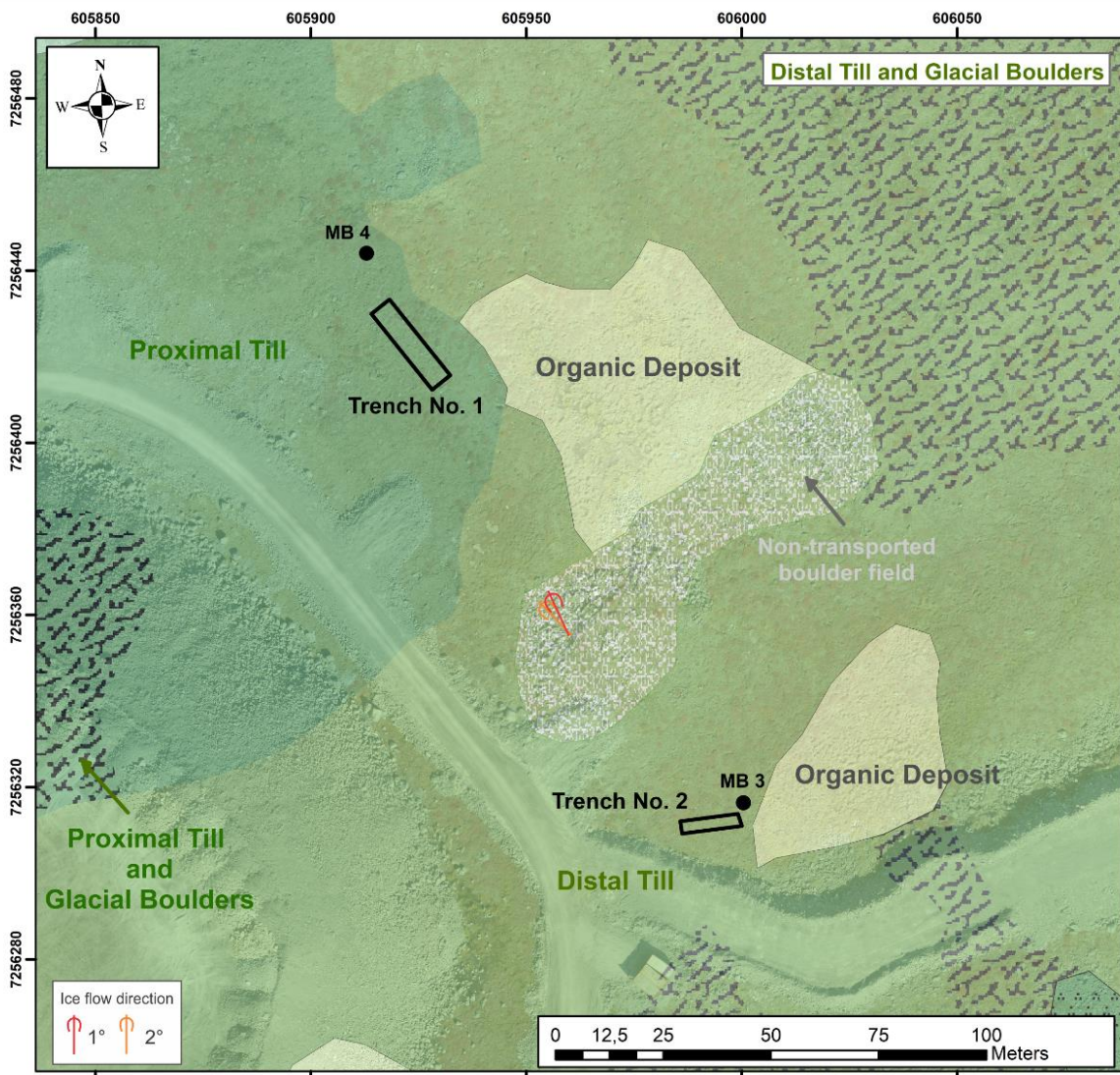


Figure I.5 Localization of the two trenches and mudboils samples (MB=Mudboil). Ice-flow direction identified from fieldwork on small outcrop within a boulder field. Local Quaternary map modified from Boulianne-Verschelden et al. (2019).

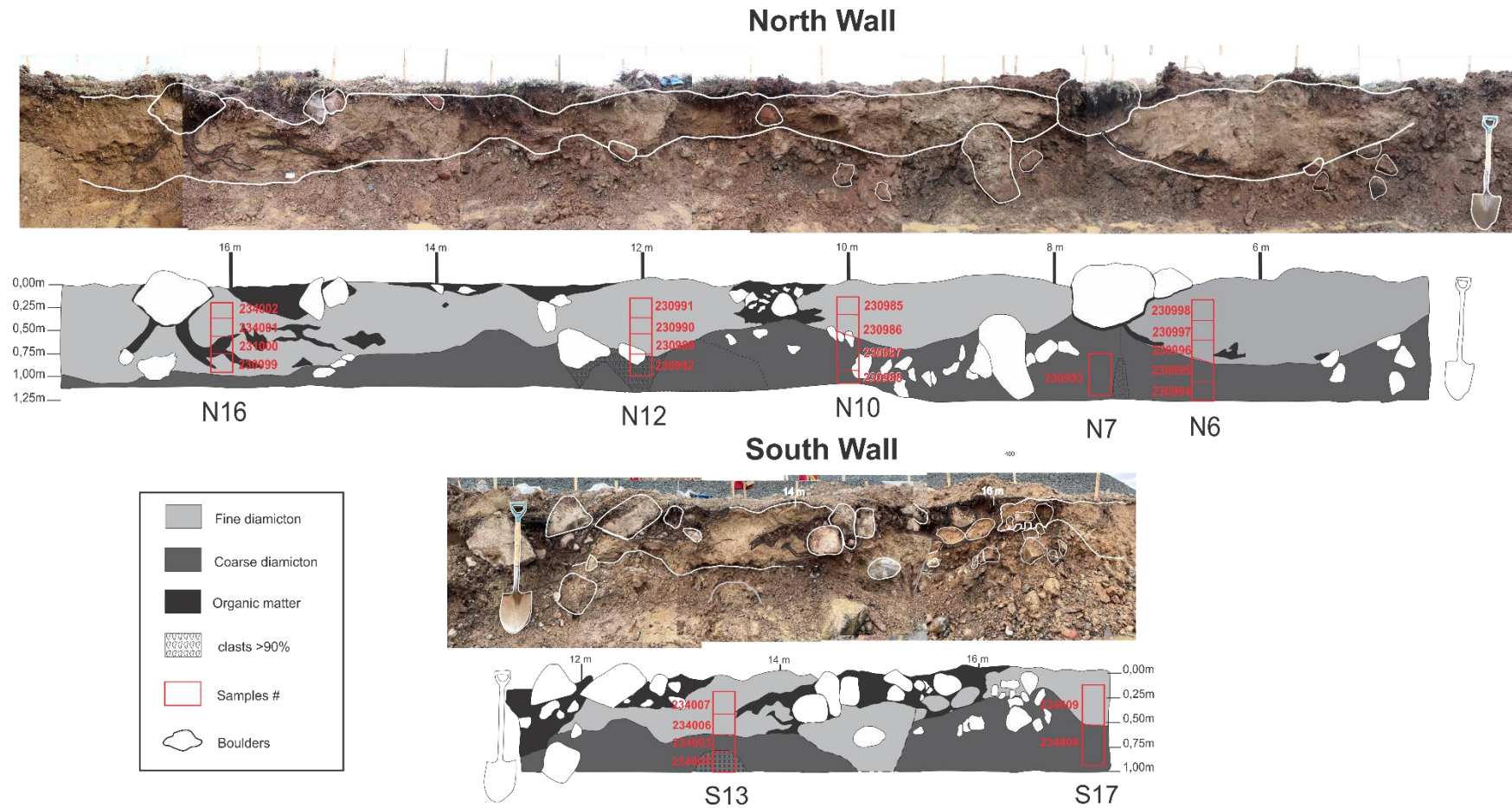


Figure I.6 Sketches of the Trench 1. Top, the north wall. Bottom, the south wall. Red-bordered squares represent the vertical till sampling profiles.

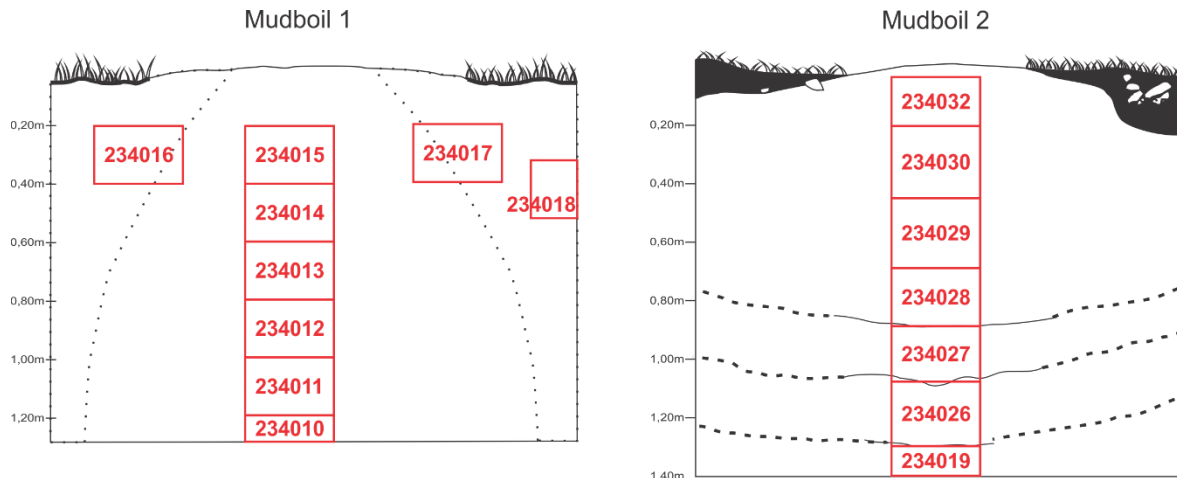


Figure I.7 Sampling profiles in both mudboils from Trench 2. Red boxes represent till samples, dotted lines variations in the till character (see Figs. I.12 and I.13).

Analytical procedure

Till geochemistry was acquired by three analytical methods (AQ252-EXT +REE, LF200, and MA250) at Bureau Veritas. AQ252-EXT + REE is an aqua-regia digestion method (1:1:1 HNO₃:HCl:H₂O), with ICP-MS acquisition for ultra-low concentrations including rare earth elements. The elements measured were Li, Be, B, Na, Mg, Al, P, S, K, Ca, V, Cr, Ti, Mn, Fe, Co, Ni, Cu, Zn, Ga, Ge, As, Se, Rb, Sr, Y, Zr, Sc, Pr, Gd, Dy, Ho, Er, Tm, Nb, Mo, Pd, Ag, Cd, In, Sn, Sb, Te, Cs, Ba, La, Ce, Nd, Sm, Eu, Tb, Yb, Lu, Hf, Ta, W, Re, Pt, Au, Tl, Pb, Bi, Th, U, Hg. LF200 is a lithium borate fusion digestion method by ICP-ES, which is highly used for total element content. The elements analyzed were SiO₂, Al₂O₃, Fe₂O₃, MgO, CaO, Na₂O, K₂O, TiO₂, P₂O₅, MnO, Cr₂O₃, Ba, Ni, Sc, Cu, Zn, Mo, Pb, Be, Co, Cs, Ga, Hf, Nb, Rb, Sn, Sr, Ta, Th, U, V, W, Zr, Y, La, Ce, Pr, Nd, Sm, Eu, Gd, Tb, Dy, Ho, Er, Tm, Yb, Lu, as well as the total carbon and total sulphur. Finally, MA250 is a multi-acid (HNO₃:HClO₄:HF, and HCl) ultra-trace analytical method (ICP-ES/MS). The elements examined were Mo, Cu, Pb, Zn, Ag, Ni, Co, Mn, Fe, As, U, Th, Sr, Cd, Sb, Bi, V, Ca, P, La, Cr, Mg, Ba, Ti, Al, Na, K, W, Zr, Sn, Be, Sc, S, Y, Ce, Pr, Nd, Sm, Eu, Gd, Tb, Dy, Ho, Er, Tm, Yb, Lu, Hf, Li, Rb, Ta, Nb, Cs, Ga, In, Re, Se, Te, Tl.

1.5.3 Grain size analysis, total C, organic carbon and LOI

Particle Size Analysis

The analysis was performed in the GSC Sedimentology Laboratory, following Girard et al. (2004). The analyses include gravel and sand-silt-clay grain sizes. The sizes >0.063mm are identified by wet sieving and the sizes <0.063mm are determined using the Camsizer & Beckham LS13-320 particle size analyzer. The sizes fractions are reported as % weight (>0.063mm) and % volume (<0.063mm). The fractions (mm) are 2-1.4; 1.4-1; 1-0.71; 0.71-0.50; 0.50-0.35; 0.35-0.25; 0.25-0.18; 0.18-0.12; 0.12-0.088; 0.088-0.063; 0.063-0.044; 0.044-0.031; 0.031-0.016; 0.016-0.008; 0.008-0.004; 0.004-0.002; 0.002-0.001; <0.001.

Total and Organic Carbon

The carbon content in soil samples was determined using a Leco CR412 1350C Carbon Analyser in the GSC Sedimentology laboratory. The organic and inorganic carbon analysis was conducted according to Girard et al. (2004), based on the measurement of the released CO₂ by infrared detection after sample combustion. The fraction used for the analysis is <0.063mm. The analysis also registered the loss on ignition (LOI) at 500°C.

1.5.4 Clast analysis

Samples were wet sieved at Université Laval to separate the 5-9.5mm fraction. The lithological classification of pebbles was carried out using a binocular microscope, into 1) felsic intrusive, 2) diorite, 3) mafic/ultramafic, 4) volcano-sedimentary, 5) quartzite, 6) milky quartz, 7) BIF, and 8) other (especially highly altered). The number of clasts analyzed on the 5-9.5mm fraction varies from 200 to 388 per sample.

1.5.5 Indicator Minerals

Separation of heavy mineral concentrates, as well as morphology classification and counting of some IMs (gold, scheelite), were made by Overburden Drilling Management Limited (ODM) in Ottawa, Ontario. This process followed Spirito et al. (2011): 1) concentration on

the shaking table of the fraction <2 mm; 2) separation of the gold grains (minimum size 15 µm), particle size estimation and morphology description (DiLabio, 1991); preservation of separate gold grains in conical bottom vials; 3) preparation of heavy mineral concentrates (HMCs), using a heavy liquid separation at a 3.0 specific gravity, on the 0.25-2 mm fraction of the table concentrate; and 4) removal of the ferromagnetic fraction from the HMCs by magnetic separation.

The non-ferromagnetic HMC fraction (0.25-2 mm) was analyzed at Université Laval under a binocular microscope for IM identification of sulfides, tourmaline and scheelite. Ultraviolet (UV) light was used for scheelite. In addition, gold grains were characterized under a binocular microscope. Gold, scheelite, chalcopyrite and pyrite were mounted in epoxy resin. Moreover, all counts were normalized to 10 kg table feed.

Mineral chemistry

In order to identify any zonation or chemical variability, back-scattered analysis was performed on the gold and scheelite grains using the secondary electron microscope (SEM) FEI Inspect F50 at Université Laval. In general, all grains exhibited a homogeneous texture and no significant variations at the edges.

-Electron Probe Micro-Analyzer (EPMA)

Mineral chemistry of major and minor elements was analyzed in gold, scheelite, and chalcopyrite grains using an EPMA CAMECA SX-100, at Université Laval. The EPMA is equipped with five wavelength-dispersive spectrometers (WDS). The elements measured in each mineral species were different.

In the case of gold, the major elements Au and Ag, and minor elements such as Cu, Fe, Hg, S, and As were analyzed. The Au and Ag analyses were performed with a beam current of 20 nA, and an accelerating voltage of 15 kV, using the methods of Liu et al. (2021). Minor elements were measured using a 20kV accelerating voltage with a current of 100 nA. Major and minor were measured with a 5 µm beam size. For scheelite, W and Ca as major, and Mn,

Na, Fe, Mo, Sr, and Y as minor elements were acquired. Major and minor element analyses were performed using a 15kV accelerating voltage, and a 5 μm beam size, using the methods of Sciuba et al. (2020). The current for the major element was 20nA, and for the minor element was 100nA. Finally, in chalcopyrite, the major elements S, Fe, and Cu, and minor elements such as Cd, Sb, Zn, Mn, Co, Ni, and As, were measured with a beam current of 20nA, with an accelerating voltage at 15kV, and a 5 μm beam size, using the methods of Caraballo et al. (2022).

-Laser Ablation Inductively Coupled Plasma Mass Spectrometry (LA-ICP-MS)

The trace element concentration of gold, scheelite, and chalcopyrite grains was determined by the LA-ICP-MS method. Gold analyses were performed at the University of New Brunswick, while scheelite and chalcopyrite minerals were analyzed at Université Laval.

At the University of New Brunswick, the trace element content was analyzed by the laser ablation system laser RESOLUTION LR 193nm Excimer S-155-LR 193nm and a large cell coupled to an Agilent 8900 triple quadrupole. The frequency of operation was 2.5Hz and the fluence was $2.25 \text{ J}\cdot\text{cm}^{-2}$. The size of the beam used was $45\mu\text{m}$ and $33\mu\text{m}$, depending on the size of the gold grains. The standards NIST-610, MASS-1, Au-30 and Au-31 were used for calibration. Silver¹⁰⁹ was used as an internal standard, being normalized to values acquired by EPMA. The isotopes measured were ²⁴Mg, ²⁷Al, ²⁹Si, ³⁴S, ⁴⁷Ti, ⁵³Cr, ⁵⁵Mn, ⁵⁷Fe, ⁵⁹Co, ⁶⁰Ni, ⁶⁵Cu, ⁶⁶Zn, ⁷⁵As, ⁷⁷Se, ⁹⁵Mo, ¹⁰⁸Pd, ¹¹¹Cd, ¹¹⁵In, ¹¹⁸Sn, ¹²¹Sb, ¹²⁵Te, ¹⁸⁵Re, ¹⁹⁵Pt, ²⁰²Hg, ²⁰⁵Tl, ²⁰⁶Pb, ²⁰⁷Pb, ²⁰⁸Pb, and ²⁰⁹Bi, following the methods of Liu et al. (2021)

At Université Laval, the trace element analysis was performed by LA-ICP-QQQ-MS using a RESOLUTION S-155 Excimer laser with 193 nm wavelength and a large cell coupled to an Agilent 8900 (Inductively plasma triple quadruple mass spectrometer). For analyses on scheelite, the equipment operates with a frequency of 15 Hz and fluence of $4 \text{ J}\cdot\text{cm}^{-2}$. The beam size in line and spot analyses were $38 \mu\text{m}$ and $24 \mu\text{m}$ respectively. Lines were preferred over spots to evaluate possible chemical variations. The external standards were GSE-1g, NIST-610, and NIST-612. As an internal standard was used ⁴⁴Ca, fixed at 13.90 wt%. The isotopes analyzed were ⁷Li, ¹¹B, ²³Na, ²⁴Mg, ²⁸Si, ³¹P, ³⁴S, ³⁹K, ⁴³Ca, ⁴⁷Ti, ⁵¹V, ⁵²Cr, ⁵⁵Mn,

⁵⁶Fe, ⁵⁹Co, ⁶³Cu, ⁶⁶Zn, ⁷⁵As, ⁸⁸Sr, ⁸⁹Y, ⁹³Nb, ⁹⁵Mo, ¹⁰⁷Ag, ¹¹⁸Sn, ¹³⁷Ba, ¹³⁹La, ¹⁴⁰Ce, ¹⁴¹Pr, ¹⁴⁶Nd, ¹⁴⁷Sm, ¹⁵³Eu, ¹⁵⁷Gd, ¹⁵⁹Tb, ¹⁶³Dy, ¹⁶⁵Ho, ¹⁶⁶Er, ¹⁶⁹Tm, ¹⁷²Yb, ¹⁷⁵Lu, ¹⁸¹Ta, ¹⁸²W, ²⁰⁸Pb, ²³²Th, and ²³⁸U, following the methods of Sciuba et al. (2020). For the determination of trace elements in chalcopyrite, the laser ablation system was conducted with a frequency of 15 Hz and a power of 2 J cm⁻², and a 38µm beam size. The external standards NIST-610, MASS-1, GSE-1g, and synthetics FeS-4, and FeS-6 were analyzed. Iron⁵⁷ was used as an internal standard with stoichiometric iron values in chalcopyrite (30.43 wt%). The isotopes analyzed were ²⁴Mg, ²⁸Si, ³¹P, ³²S, ³⁴S, ⁴⁴Ca, ⁴⁹Ti, ⁵¹V, ⁵²Cr, ⁵⁵Mn, ⁵⁹Co, ⁶⁰Ni, ⁶³Cu, ⁶⁶Zn, ⁷¹Ga, ⁷²Ge, ⁷⁵As, ⁷⁸Se, ⁹⁵Mo, ¹⁰³Rh, ¹⁰⁵Pd, ¹⁰⁷Ag, ¹¹¹Cd, ¹¹⁵In, ¹¹⁸Sn, ¹²¹Sb, ¹²⁵Te, ¹³⁷Ba, ¹⁸²W, ¹⁸⁵Re, ¹⁹⁵Pt, ¹⁹⁷Au, ²⁰¹Hg, ²⁰⁵Tl, ²⁰⁸Pb, and ²⁰⁹Bi, following the methods of Caraballo et al. (2022). The data was reduced using the Iolite software.

1.5.6 Statistical analysis

A range of statistical techniques were used to analyze the data, including univariate and multivariate analyses. Univariate statistics, such as mean, median, mode, range, variance, and standard deviation, were used to describe and analyze individual variables in the dataset. Multivariate statistics tools, including correlation analysis and regression analysis were employed to examine the relationships between the geochemical data, till and mineral chemistry variables.

Some of the variables were discarded when their proportion of values below detection limit, or censored value, was >40%. Values below the detection limit were imputed using the log-ratio Expectation-Maximization algorithm (lrEM), in the zComposition R-Package (Palarea-Albaladejo and Martín-Fernández, 2015; R Core Team, 2022). Two main multivariate statistics were used, the Principal Component Analysis (PCA) and the Partial Least Squares Discriminant Analysis (PLS-DA) to understand the relationships between the various elements. Whereas PCA visually exhibits the correlation between elements, PLS-DA shows similar characteristics between the elements and the labelled classes. In the case of till geochemistry, PCA was the method used to compare with previous PCA results in the Amaruq area (de Bronac de Vazelles et al., 2021). PLS-DA score plots were used to identify

the possible mineral deposit source of the scheelite and gold according to the PLS-DA models of Sciuba et al., (2020) and Liu and Beaudoin (2021), respectively.

1.6 RESULTS

1.6.1 Description of the till

In Trench 1 two till units were identified, a coarse-grained diamicton at depth overlain by a fine-grained diamicton at the surface (Fig. I.6). The contact between the two till units is commonly sharp (Fig. I.6). The upper diamicton is a massive, non-calcareous muddy sand, with a clay content ranging between 3.2 and 4.3 % (see below) and containing approximately 10-35% clasts. It is located from the surface to a maximum depth of 1 m. This till is composed mostly of clasts eroded from granitic rocks (mean=64.0%), and to a lesser extent, mafic/ultramafic (mean=7.6%) and volcano-sedimentary rocks (mean=9.9%; Table 1). The lower diamicton is a massive, non-calcareous silty sand, containing generally 60 to 75 % clasts, with lateral variations where the clast content increased to more than 90%. This till contains clasts derived from the same sources as for the upper unit but presents a lesser content of felsic rocks (mean=43.3%) and a higher content of mafic/ultramafic (mean=20.2%) and volcano-sedimentary (mean=23.3%) sources (Fig. I.8). The till in MB4 next to Trench 1 is a non-calcareous diamicton with a muddy sand texture, comprising approximately 4% clay content and less than 10% of clasts. This till consists primarily of fragments derived from felsic intrusive rocks (56.9%), with a smaller proportion of mafic/ultramafic rocks (8.7%) and volcano-sedimentary rocks (11.5%). The composition of the till in MB4 is similar to the fine-grained diamicton in Trench 1.

Trench 2 only contains a fine-grained diamicton with similar characteristics to the upper diamicton in Trench 1. It has a slightly higher clay content ranging from 3-7% (see below). Additionally, it exhibits a slightly different proportion of felsic clasts (mean=59.8%) and volcano-sedimentary fragments (mean=11.3%), and a higher proportion of mafic/ultramafic fragments (mean=14.4%). The till in MB3 next to Trench 2 is a non-calcareous, sandy mud

diamicton with a clay content of 6% (see below) and less than 10% clasts. This till contains a lower proportion of felsic intrusive clasts (40%) and a higher content in mafic/ultramafic pebbles (28.2%) than the till in Trench 2 (Table 1), but a similar volcano-sedimentary clast content (14.7%). The proportion of the pebble lithologies in this diamicton presents characteristics more like the coarse-grained diamicton in Trench 1, but the texture is the same as the fine-grained diamicton in Trench 2.

Table 1. Major pebble lithology counts in the diamicton units of the two trenches.

	Statistics	Trench 1		Trench 2
		Fine-grained	Coarse-grained	Fine-graine
Felsic-Intrusive (%)	Min	57.8	28.2	44.3
	Max	75.1	62.5	75.9
	Mean	64.0	43.3	59.8
	Median	63.8	44.7	60.3
	Std	4.5	10.3	7.9
Diorite (%)	Min	2.3	1.4	2.4
	Max	11.9	10.7	8.0
	Mean	7.6	5.5	5.7
	Median	7.9	5.5	6.1
	Std	2.8	3.1	1.8
Mafic/Ultramafic (%)	Min	3.9	10.0	5.1
	Max	16.5	37.1	25.6
	Mean	7.6	20.2	14.4
	Median	7.4	21.1	15.0
	Std	3.4	7.1	5.7
Volcano-sedimentary (%)	Min	4.4	11.0	3.0
	Max	18.6	36.4	21.7
	Mean	9.9	23.3	11.3
	Median	8.9	25.3	9.7
	Std	4.1	7.6	5.4
	Max	10.0	6.7	9.1
	Mean	6.9	4.9	5.7
	Median	6.7	5.0	5.3
	Std	1.6	1.0	2.1

Figure I.8 shows the variation of the pebble lithology proportions in each diamicton unit. In general, the fine-grained diamicton in both trenches exhibits a higher content of felsic intrusive lithologies (distal sources) and a lower content of mafic/ultramafic and volcano-

sedimentary pebbles (local sources) in comparison to the coarse-grained diamicton. In contrast, the coarse diamicton found only in Trench 1 presents a lower content of felsic intrusive clasts and a significant content of mafic/ultramafic and volcano-sedimentary lithologies. According to the classification of till units in the Amaruq area by Boulianne-Verschelden et al. (2019), the fine-grained diamicton corresponds to the distal till whereas the coarse-grained diamicton in Trench 1 is likely the proximal till.

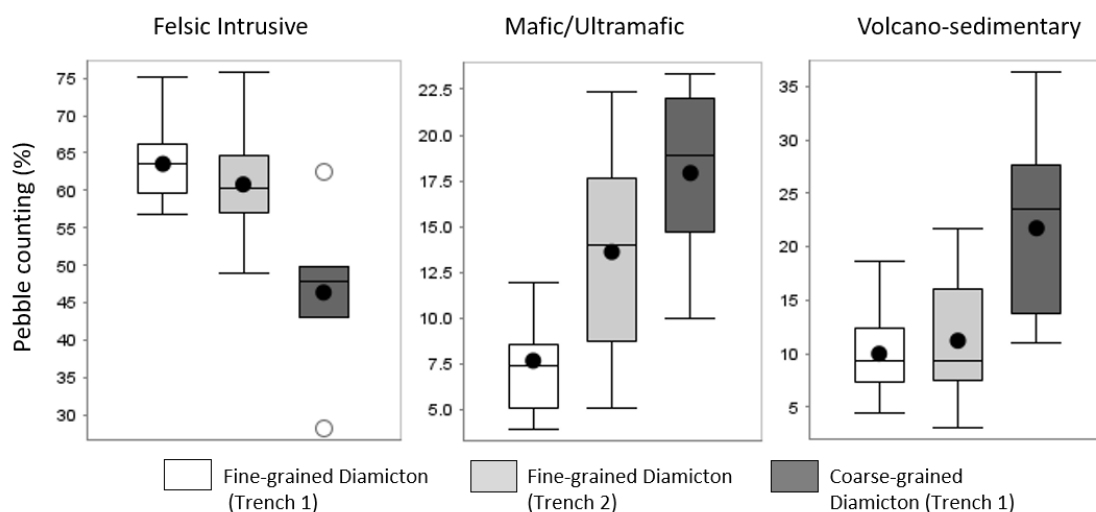


Figure I.8 Proportion of the 5-9.5 mm pebble lithologies in the glacial diamictons.

In comparison to the units mapped at a local scale in the study area, Trench 2 shows one unit (distal till) without any variation at depth. In Trench 1, a discrepancy is observed between the surface unit (distal till) and the mapped unit (proximal till). However, the mapped unit (proximal till) appears at a deeper level. Consequently, the stratigraphic relationship between these units can be described as the distal till overlaying the proximal till, as suspected by de Bronac de Vazelhes et al. (2021). It is worth emphasizing that the mapped contact between these two units is less than 10 meters from Trench 1 (Fig I.5).

1.6.2 Cryoturbation

Patterned ground was recognized in the study area such as mudboils, sorted circles, and hummocks (Fig. I.9). In Trench 1 area, there were mainly inactive mudboils and sorted circles

forming a poorly developed net, with a thin vegetation cover at the surface. In contrast, in Trench 2 area, there were primarily active mudboils, without much vegetation on top.

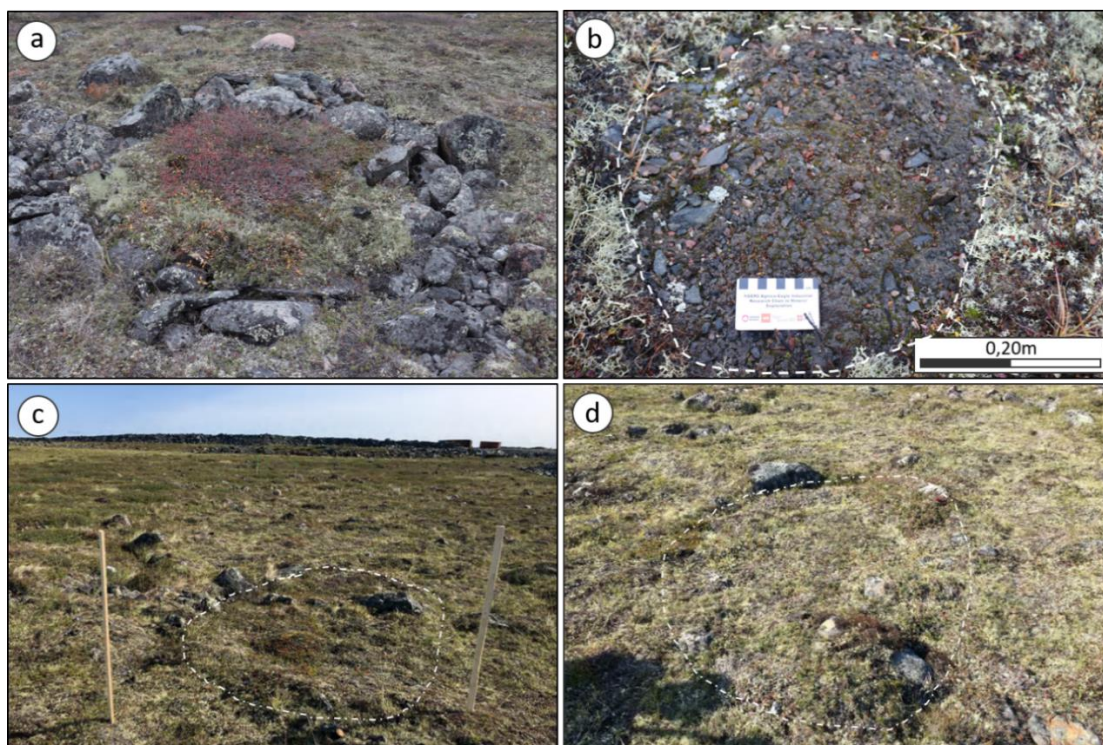


Figure I.9 Cryoturbation features identified on the surface in the study area. a) sorted circle, b) mudboil in Trench 2 area, c) and d) patterned ground in Trench 1 area.

In Trench 1, the fine-grained diamicton unit contains buried organic matter layers (Fig. I.10) at a depth of up to 90 cm, whereas some were at the contact between the two diamictons. This interface is characterized by at least four concave contour resembling a bowl shape (Fig. I.11) in the North wall. The combination of buried organic matter disposition, the bowl-shaped features, the distribution of larger boulders and organic matter (at the border of bowl shapes) and the circular appearance at surface suggests the presence of at least four cryoturbation structures characterized by long-term circular soil motion (Fig. I.11). These are likely to be poorly developed sorted circles. The vertical till sampling profiles are between and along these structures, while the N12 profile is likely in the central part of one of these structures.

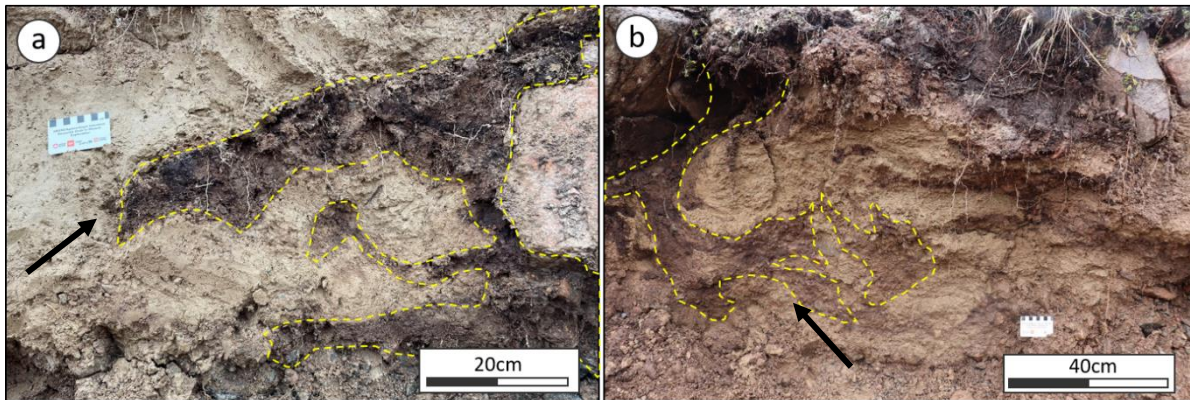
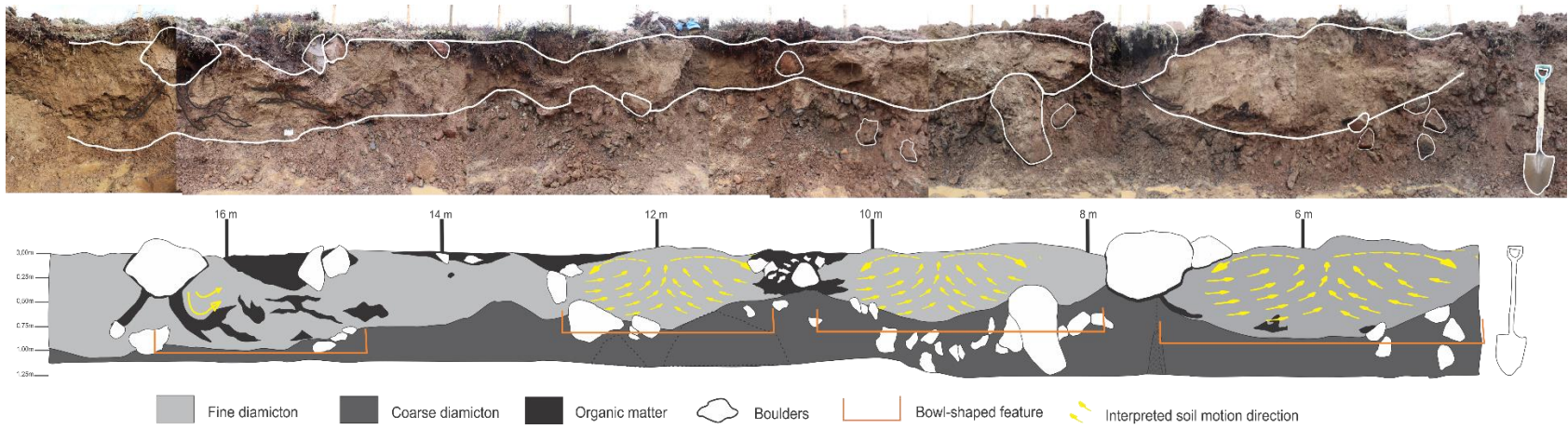


Figure I.10 Buried organic matter in Trench 1. a) buried organic matter in the South wall, and b) deformed organic matter layer in the North wall.

The cryoturbation structures identified in Trench 2 consisted of two mudboils, MB1 and MB2. These mudboils exhibit distinct circular expressions at the surface (Fig. I.12a and I.13a). The main contrast between them is their size, with MB1 being larger. Additionally, MB2 has lichen cover, while MB1 shows evidence of recent material (“mud”) ejected to the surface. Mudboil 1 (1 m diameter at the surface) exhibits a lateral variation in the character of the soil on the surface and at depth, having a weakly meteorized material at the centre and a moderately oxidized material on either side of the central section (Fig. I.12b, c). In addition, there are deformed layers of gleyed-colored material at the edges of the central section in MB1. Buried organic matter is also found mainly at 50 cm depth towards the edges (Fig. I.12c). Mudboil 2 (0.60 m diameter at the surface) does not present a lateral variation, but instead shows a vertical variation consisting, from top to bottom: (1) a slightly altered material (0-90 cm depth), (2) an oxidized reddish colored material (90-110 cm), and (3) a gleyed colored horizon (110-130 cm). These layers were mostly identified by their prominent color contrast. Below the gleyed-colored horizon, the permafrost table was reached at 1.30 m depth as shown by ice lenses and frozen till. Although portrayed in Fig. I.13f, the convex shape between the permafrost and the active layer was not examined. Moreover, a transitional thickening of the organic layer from the center to the edges of the mudboil was denoted at the surface (Fig I.13f).



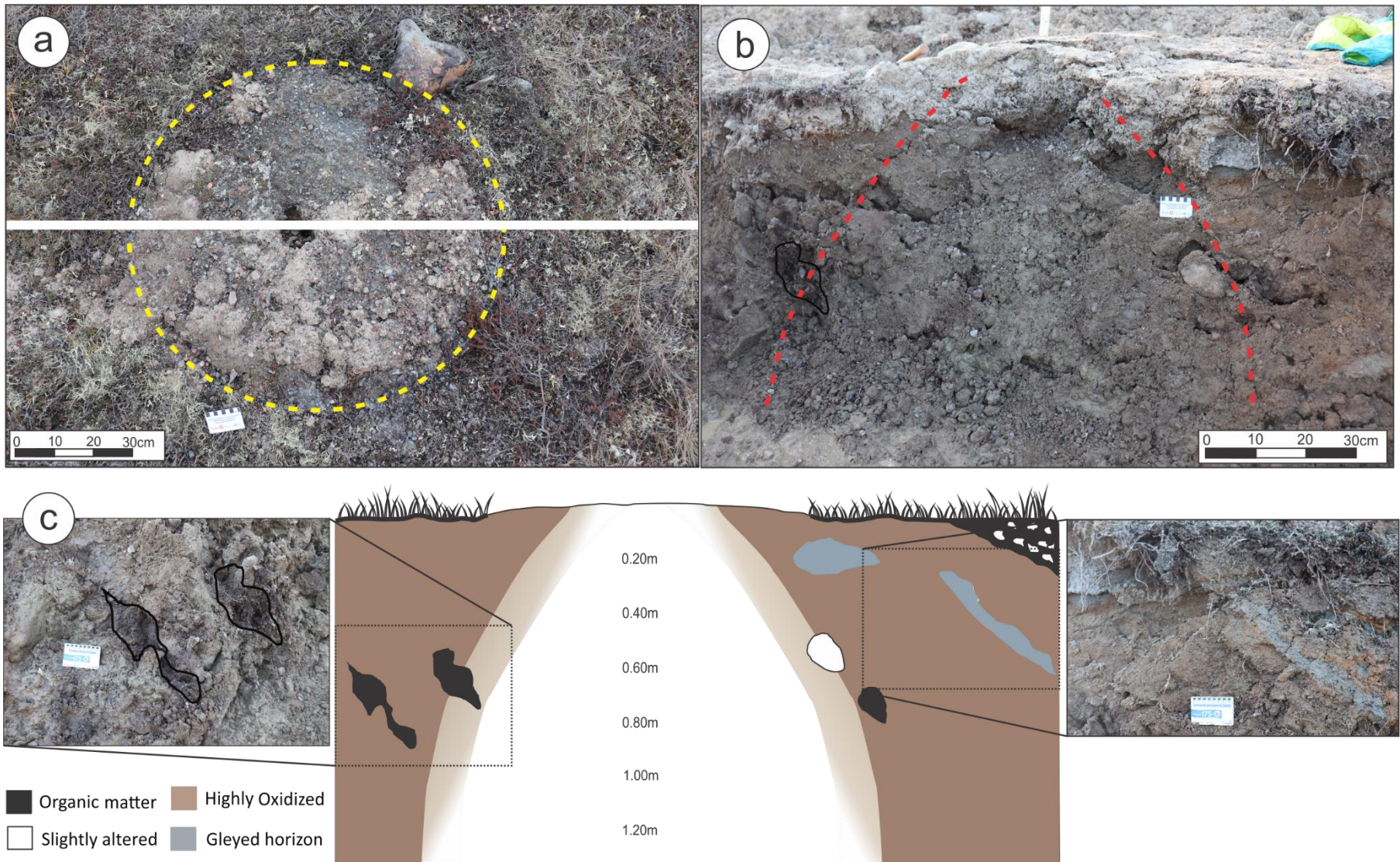


Figure I.12 Mudboil 1. a) Expression at the surface, b) cross-section, c) sketch of the cross-section.

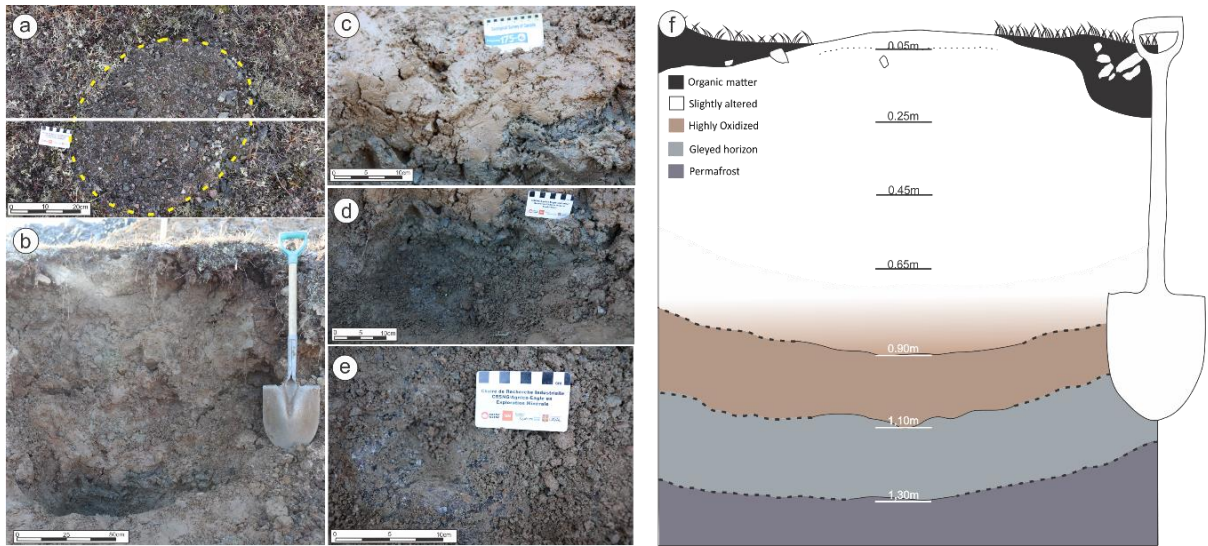


Figure I.13 Mudboil 2. a) Expression at surface, b) cross-section, c) oxidized horizon at 90 cm depth, d) gleyed horizon above the permafrost, e) surface of permafrost table, and f) sketch of the mudboil profile.

1.6.3 Pebble counts

The pebble count (5-9.5 mm) in Trench 1 distal till is uniform with depth. In Trench 2, the proportions of distal lithologies (felsic intrusive and diorite) slightly increase downwards compared to local lithologies (mafic/ultramafic and volcano-sedimentary) in both mudboils MB1 and MB2 (Fig I.14). This contrasts with the common pattern observed in till profiles, where the proportion of local bedrock component usually increases at depth near the bedrock surface. In MB2, the local components from the samples collected in and above the permafrost are elevated, deviating from the decreasing trend observed above in other samples within the mudboil (Fig I.14).

The mudboil surface sample next to Trench 2 (MB3) shows a proportion of distal and local lithologies that are closer together, resembling the shallowest sample in MB2. In contrast, the mudboil next to Trench 1 (MB4) exhibits a proportion of distal lithologies over 70%, similar to the average proportion found in the distal till in Trench 1.

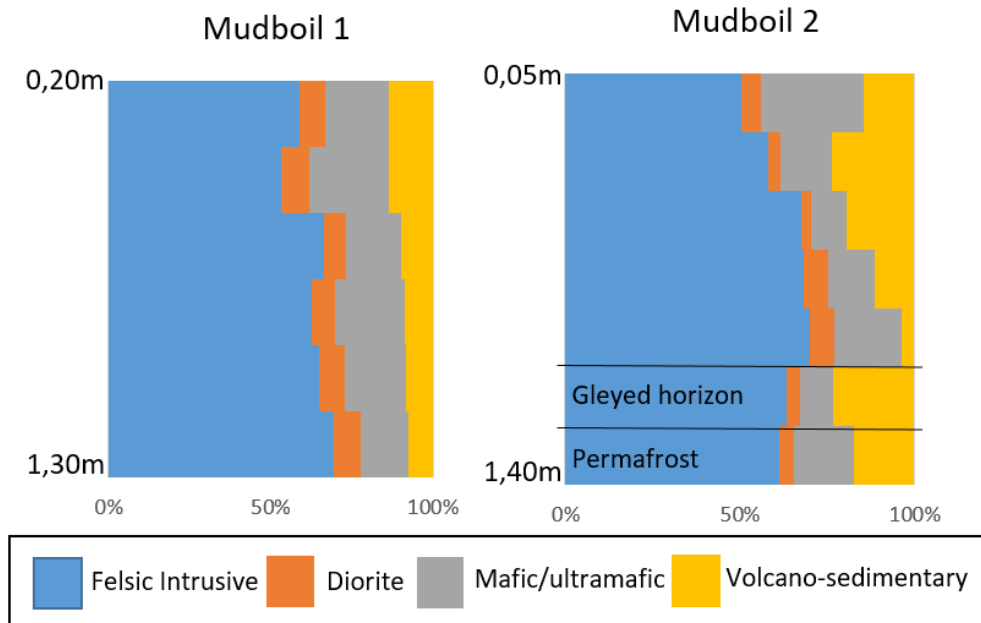


Figure I.14 Vertical profiles pebble composition proportions in both mudboils from Trench 2.

1.6.4 Grain-size distribution

The quantitative study of the particle sizes was performed in the distal till identified in the two trenches and the two mudboil surface samples. The distal till has a sand content that varies between 34-74% (mean=54%), a silt content between 23-60% (mean=40%), and a clay content between 2.9-7.8% (mean=5%). The distal till in Trench 1 has a silty sand matrix texture, whereas the distal till in Trench 2 varies from a silty sand to sandy silt matrix texture (Fig. I.15). The mean graphic diameter of the till samples from both trenches is (Φ) 3.848 and sorting is 3.050 (Folk and Ward, 1957). The matrix texture of Mudboil 4 till is silty sand and is within the range of the distal till matrix texture found in Trench 1. On the other hand, the distal till in Mudboil 3 has a finer-grained matrix (sandy silt) than the overall matrix texture of distal till observed in Trench 2 (Fig I.15). Mudboil 1 exhibits the lowest sand content and the highest silt content in the central part compared to samples collected on either side, while the matrix grain size remains constant down the vertical profile (Fig I.16). Mudboil 2 shows a general trend of increasing silt content down to the permafrost (Fig I.16). The short profile in the distal till of Trench 1 (N16) displays a consistent increase in sand proportion and decrease in silt amount with depth (Fig I.16).

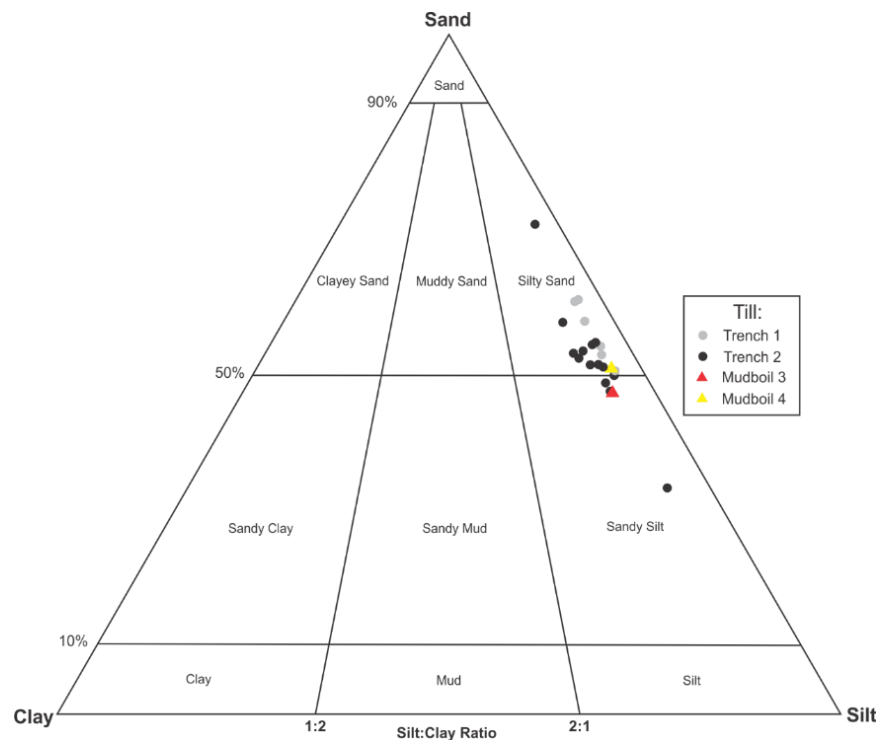


Figure I.15 Ternary diagram showing the grain size composition of the samples, in distal till.

1.6.5 Total carbon and LOI

Total carbon and LOI were analyzed in 24 samples, 22 in distal till and 2 in the mudboils (also distal till) adjacent to each trench. The total C content varies from <0.1 to 2.7%, with a mean of 0.4%. Most of the total C is organic carbon (>99%). LOI values range from 0.5 to 5.8%, with a mean of 1.6%. The N16 profile sample with the highest values of total C (2.7%) and LOI (5.8%) contains organic matter. The vertical distribution of these parameters in the two mudboils is similar. Values increase from the top toward the middle part and then decrease a little and increase again in the deepest part of each profile. The permafrost presents relatively low values in both total C (0.2%) and LOI (1.4%). As for horizontal variation, the sample exhibiting lower total C and LOI values is in the middle part of Mudboil 1. Values in mudboils adjacent to the trenches are the following: MB3 has a total C <0.1% and an LOI of 0.9%, while MB4 exhibits a total C of 0.6% and an LOI of 1.6%.

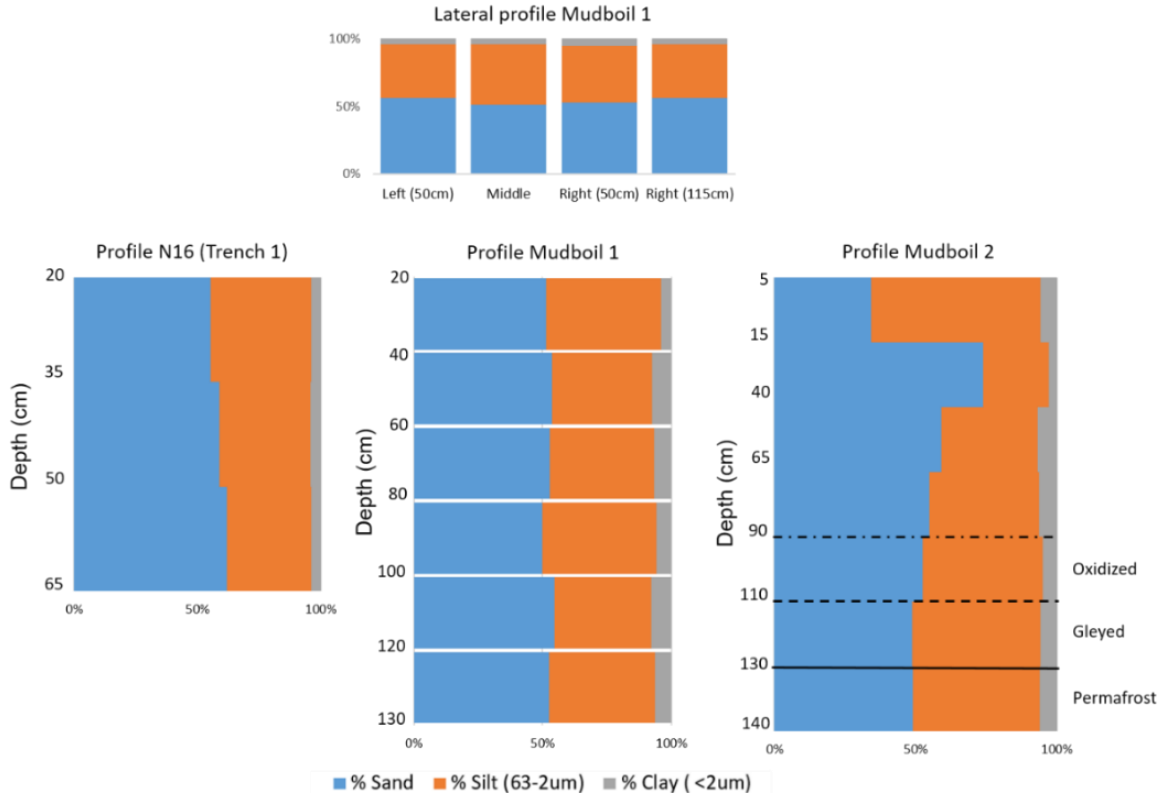


Figure I.16 Vertical and lateral profiles of the grain-size distribution in the distal till of both trenches.

1.6.6 Till geochemistry

The geochemical analysis of the 22 distal till samples and the two mudboil surface samples are in appendix B2.2, B2.4 and B2.6. These analysis yield elements with a mean concentration of less than 1 ppm analyzed by ICP-MS and aqua-regia digestion, and ICP-ES/MS and multiacid leach, are Mo, Sb, Bi, Tl, Se, Cd, Tb, Ho, Tm, and Lu. Using the same analytical methods, the elements Cs, Cu, Pb, Zn, Ni, Co, As, U, Th, Sr, V, La, Cr, Ba, B, Na, Sc, Ga, Nb, Rb, Zr, Y, Ce, Li, Pr, Nd, Sm, Eu, Gd, Dy, Er, and Yb have mean concentrations between 1 and 100 ppm. The oxides analyzed by ICP-ES and lithium borate fusion digestion technique with a mean concentration higher than 1% are SiO₂, Al₂O₃, Fe₂O₃, MgO, CaO, Na₂O, and K₂O, and lower than 1% are TiO₂, P₂O₅, MnO and Cr₂O₃. Metals such as Ag and Au analyzed by ICP-MS and aqua-regia leach have a mean concentration of 55 and 22 ppb respectively. Elements such as Te, In, Ge, Pt, Pd, Ta, Re, and Hg measured by ICP-MS and

aqua-regia digestion technique present more than 40% of values below the detection limit. Re, Se, and Te exhibit more than 40 % of values below the detection limit with the ICP-ES/MS method and multi-acid digestion technique.

Principal Component Analysis

Principal component analysis (PCA) was conducted on 24 samples of distal till (Fig. I.17). The first three principal components (multi-acid ultra-trace analytical method) explain approximately 87.3 % of the total variance in the data. The first component, which accounts for 65.9% of the variance (Fig. I.17a), primarily signifies the differentiation between elements (Na, Ca, P, Ta, Zr, Sr, Hf, and Nb) hosted in glacial-process-resistant minerals such as feldspar, zircon, and apatite, as opposed to elements found in less resistant minerals. The second component PC2 exhibits an elemental association with lanthanides and elements common in felsic rocks and an inverse relation with mafic/ultramafic and gold signature (Fig. I.17b). In the PC1/PC2 loading plot (Fig. I.17a), PC2 (14.5%) provides insights into the lithological sources of the till between a distal signature (felsic rocks) and a local signature (mafic/ultramafic and gold mineralization; de Bronac de Vazelhes, 2019). The sample projection in the loading plot of PC1/PC2 (Fig. I.17c) differentiates the till in Trench 1 and MB4 distal till that consistently show positive scores along PC1, whereas in Trench 2 (MB1 and MB2) and MB3 primarily occupy the negative PC1 space.

A principal component analysis (PCA) was conducted on 51 till samples combining the 24 samples from the current study and 27 samples from de Bronac de Vazelhes (2019) using ICP-MS/Aqua-regia data (Fig I.18). The first component, explaining 45.2% of the variance, is characterized to the mafic + gold mineralization with PC1 negative values for Fe, Ni, Co, Cr, Mg, and Mn related to mafic/ultramafic rocks and Au, Ag, As, Cd and Sb associated with gold mineralization. PC1 positive elements Na, Ti, Sr, Eu, La, Th, Tm, Ho, Nb, Pr, Dy, Gd, Sm, and Ce represent the felsic sources (Fig I.18a). PC2 (17.4% of variance) differentiates the mafic/ultramafic signature (negative) from the elements mostly related to mineralization (positive, Fig I.18a).

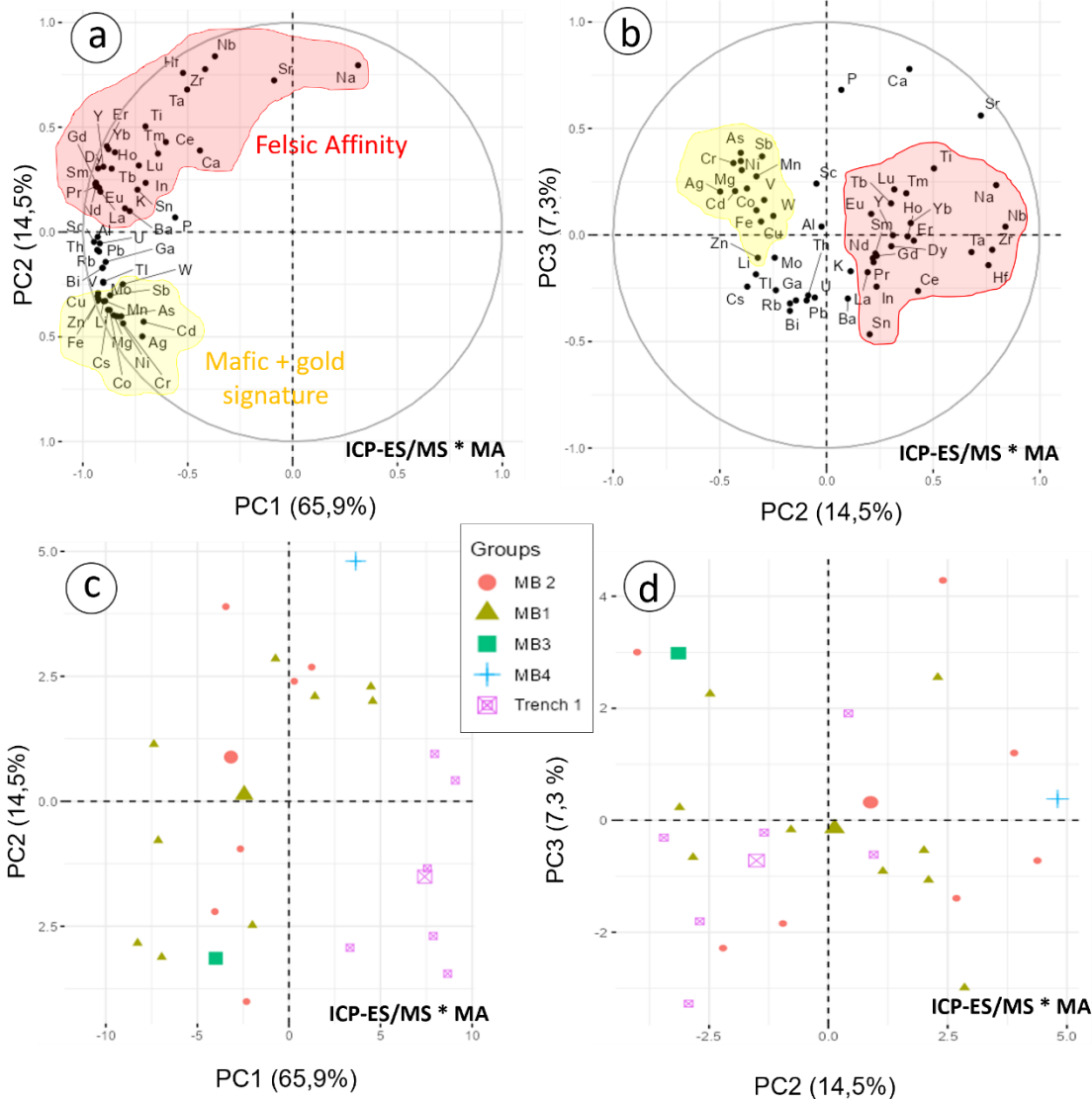


Figure I.17 PCA score plots of geochemical results from this study. a) PC1/PC2 loading plot of ICP-ES/MS and multi-acid (MA) digestion, b) PC2/PC3 loading plot of ICP-ES/MS MA, c) sample projection in PC1/PC2 loading plot, and d) sample projection in PC2/PC3 loading plot.

Most of our samples have negative values in PC1 and PC2 (Fig. I.18b). In general, the samples from Trench 2 exhibit a greater contribution from mafic sources (negative PC1), compared to the samples from Trench 1, which present a higher supply of felsic sources. The mudboil surface sample nearby Trench 2 (MB3) presents a similar behavior to the samples collected from that trench. The mudboil surface sample close to Trench 1 (MB4) has a significant felsic affinity input, slightly more so than the samples from Trench 1.

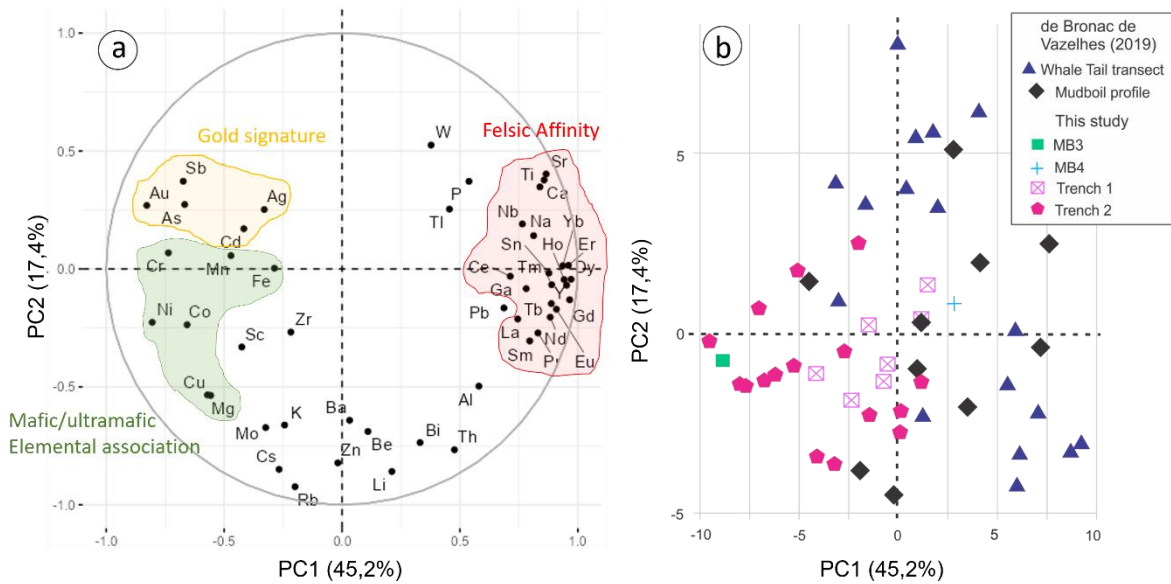


Figure I.18 Principal component analysis using ICP-MS/Aqua-regia method. a) PC1/PC2 loading plot for log centered normalized values of distal till samples (this study) combined with Whale Tail transect and profile samples of de Bronac de Vazelhes (2019), and b) Samples of both trenches in distal till (this study) and WT samples from de Bronac de Vazelhes (2019) projected on the PC1/PC2 score plot.

Geochemical profiles in mudboils

The major elements Al_2O_3 , MgO , CaO , Fe_2O_3 and K_2O in both mudboils from Trench 2 do not exhibit important changes with depth, as shown on Figure I.19a. Additionally, some trace elements such as Cu, Pb, Zn, and W show a slight variation of decreasing or increasing concentrations with depth, as illustrated on Figure 1.19a.

The concentrations of trace elements such as Ag, Ni, As and Au show greater variability along the profiles (Fig. I.19b). In Mudboil 1, the shallowest sample shows the lowest concentration in As, Ag and Ni, and then are relatively constant with depth. In terms of gold, its concentration is constant with depth, except for the sample collected at ~40 cm depth. The distribution of Ag, Ni, and As concentrations in Mudboil 2 show similar profiles (Fig I.19b).

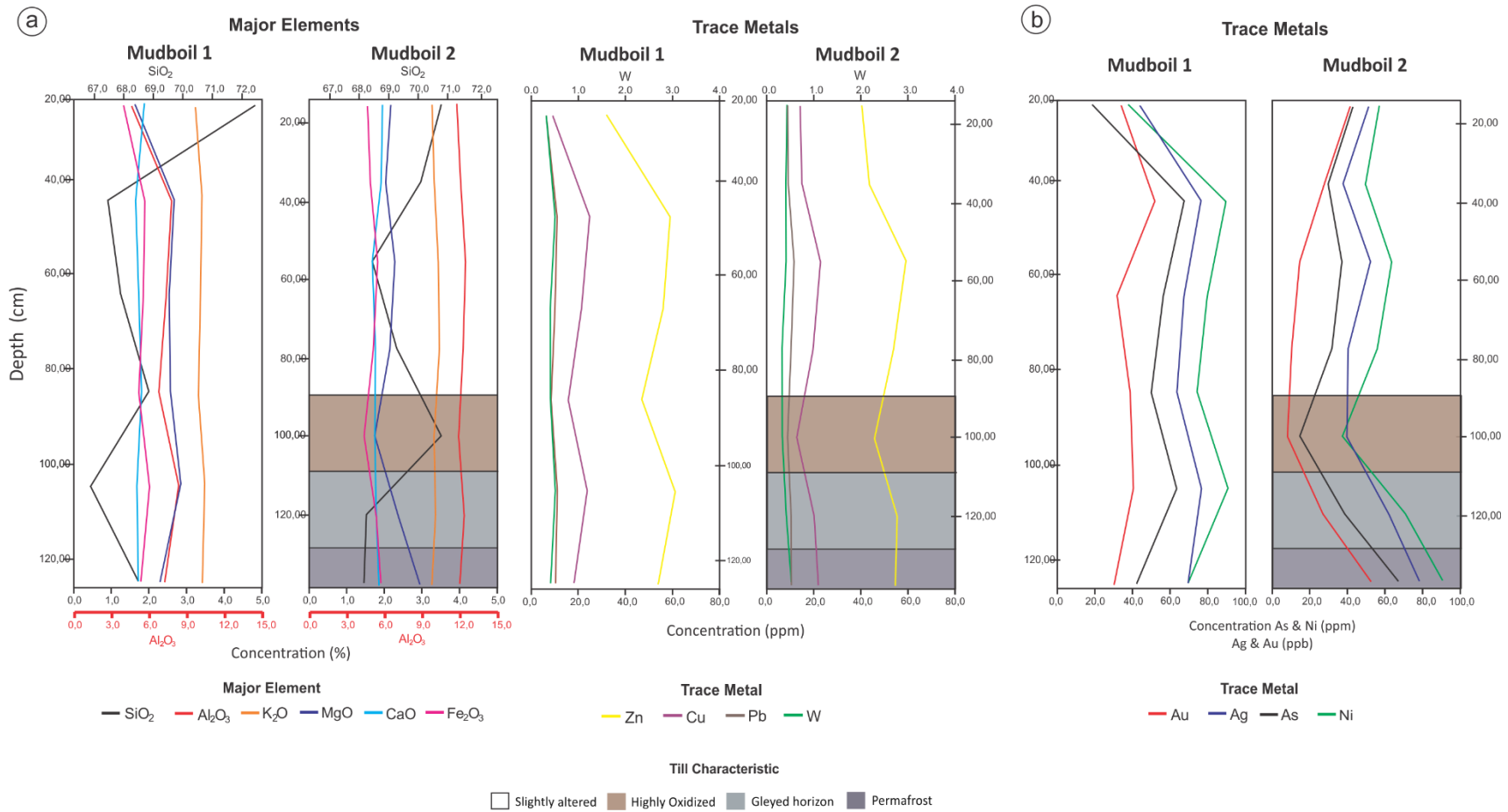


Figure I.19 Vertical geochemical profiles in detailed mudboils (1 and 2) from Trench 2. a) Left, Major elements (ICP-ES/LBF method). Right, Trace metals (ICP-ES/MS and Aqua-regia). b) Trace metals analyzed by ICP-ES/MS and aqua-regia showing significant variation with depth.

A constant value is observed down to 80 cm depth, then a significant decrease at 100 cm depth, and finally an increase to the deepest sample. Gold values show a constant decrease up to a depth of 100 cm. However, similar to Ag, Ni, and As, the gold content increases until reaching the permafrost. Permafrost has the greatest content of these elements (Ag, Ni, As, and Au). In general, there is a strong relation between the silica content and the concentration of the following trace elements: Pb, Zn, Ag, Ni, and As, with an R-squared value higher than 0.70. This relation is inverse as silica increases, the concentrations of the trace elements decrease. There is no covariation between silica and Au concentrations (R-squared =0.30).

A profile in a mudboil close to our study area (<100 m; Fig I.4) by de Bronac de Vazelhes (2019) does not show any pattern with depth (Fig. I.20). The shallowest samples in each profile, involving the above, exhibit a significant contribution of gold-related elements, plotted in the upper left of the PC1/PC2 loading plot (Fig. I.20). The till in the permafrost exhibits the highest negative value in PC1, which implies that there is greater contribution of mafic- or mineralization-related elements in this sample compared with the rest of the mudboil samples. Regarding the lateral profile, there is a significant variance between the samples taken at the edges compared to the one in the center of the mudboil, especially in PC2 values.

1.6.7 Indicator Minerals

Various indicator minerals of orogenic gold deposits were recovered from till in the study area. The minerals identified were scheelite, gold, chalcopyrite, and pyrite. Properties such as mineral abundance, morphology, size, and mineral chemistry were determined in some of them. 4486 gold grains were described with the abundance of grains per sample, the grain morphology and the grain size.

Gold

Mineral abundance

Gold grain counting was completed on the <2 mm size fraction and the counts were normalized to a 10-kg sample mass (Table 2). Results show significant differences in

statistical measures between the two till units in Trench 1 (Fig I.21). Proximal till exhibits a higher average gold grain counts (mean=108 grains) with a wide range, spanning from 11 to 1011 grains (coefficient of variation 2.77). These values are the minimum and maximum gold grain counts within the study area. The gold grain count average in distal till in Trench 2 is higher (mean=214) than distal till in Trench 1 (Table 2; with a narrower range), with the minimum count at 30 and the maximum count at 689. Notably, there is a contrast in the coefficient of variation (CV) between the distal till samples from Trench 2 and Trench 1 (Table 2). The CV in distal till in Trench 2 is nearly three times higher than that observed in distal till in Trench 1, showing a major variation within the distal unit. In the mudboils adjacent to the trenches, gold grain counts are 485 and 66 in MB3 (Trench 2) and MB4 (Trench 1), respectively.

Table 2. Gold grain counts (normalized to 10-kg table feed)

	Trench 1		Trench 2		
	Distal till	Proximal till	Distal till (total)	Mudboil1	Mudboil2
Mean	72	108	214	193	225
Median	61	100	130	167	156
Min	43	11	30	100	30
Max	122	1011	689	330	689
Std	28	299	198	94	265
CV	0.39	2.77	0.92	0.48	1.18

There is no uniform pattern of gold grain abundance observed with depth (Fig. I.21), but the Trench 1 profiles have contrasting counts between the two till units. This variation can involve higher and lower values, consistent with the large variance in the number of gold grain counts in the two units, especially in proximal till (Fig. I.21 a, b). Establishing trends with depth in the proximal till is difficult due to the limited number of samples per profile (1 or 2). In Trench 1 in the central part of a cryoturbation feature (N12), the profile exhibits relatively constant gold grain count with depth in the distal till, with a mean count of 108 ($\sigma=13$). However, in the underlying proximal till layer, the normalized gold grain count is 11. In contrast, the vertical profiles in Trench 2, also in the central part of a cryoturbation feature, vary with depth (Fig. I.21c, d). The mean gold grain count in Mudboil 1 is 193 ($\sigma=94$) and in Mudboil 2 is 225 ($\sigma=265$). In the latter, there is a trend of decreasing gold grain counts (n=689) from the shallowest sample (5-20cm) to 110 cm depth (n=32), whereas in the

following two deeper samples 110-130 cm and 130-140 cm (permafrost) the gold grain count increases considerably (n=390, n=506, respectively). The lateral profile in Mudboil 1 shows the largest number of gold grains in the central part of the mudboil (n=100), this is twice as much as the samples collected at the same depth on the sides of the mudboil (~30 cm; Fig. I.22a).

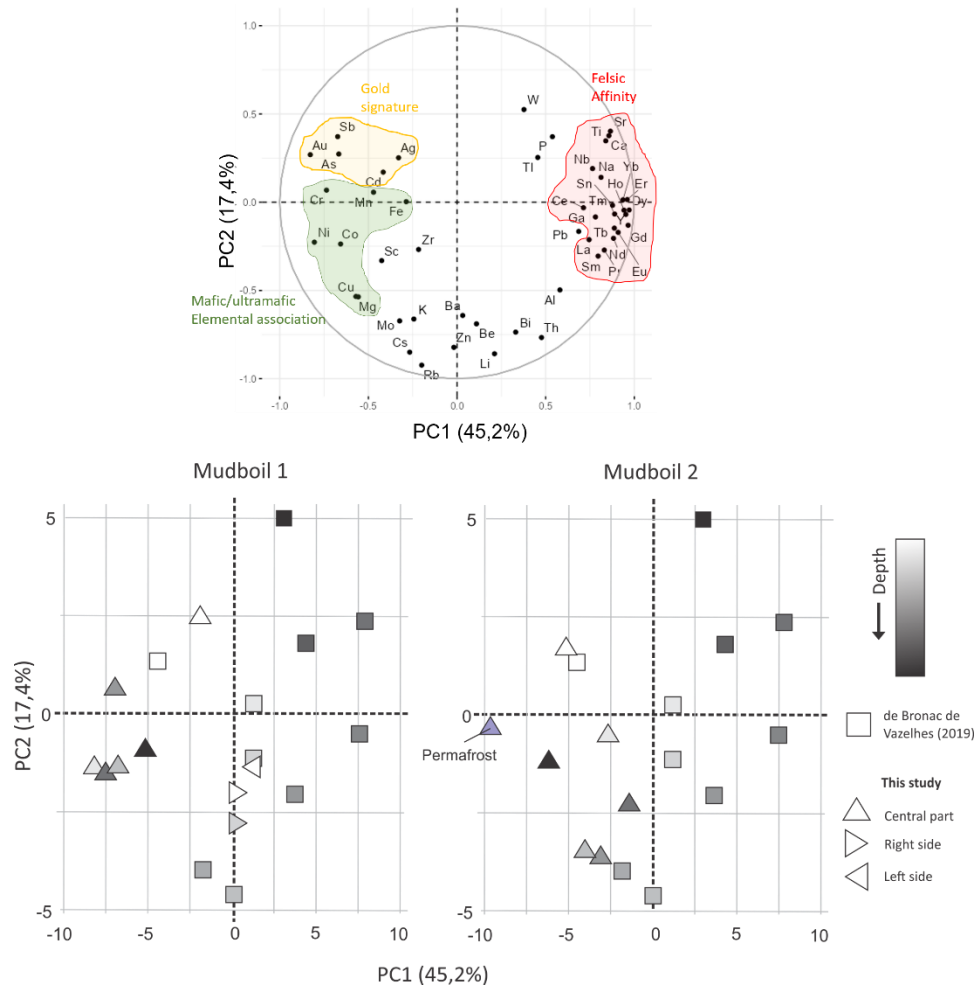


Figure I.20 Samples of both detailed mudboils from Trench 2 (this study) combined with profile samples in Whale Tail mudboil from de Bronac de Vazelhes (2019) projected on the Principal components PC1/PC2 ICP-MS/Aqua-regia method score plots.

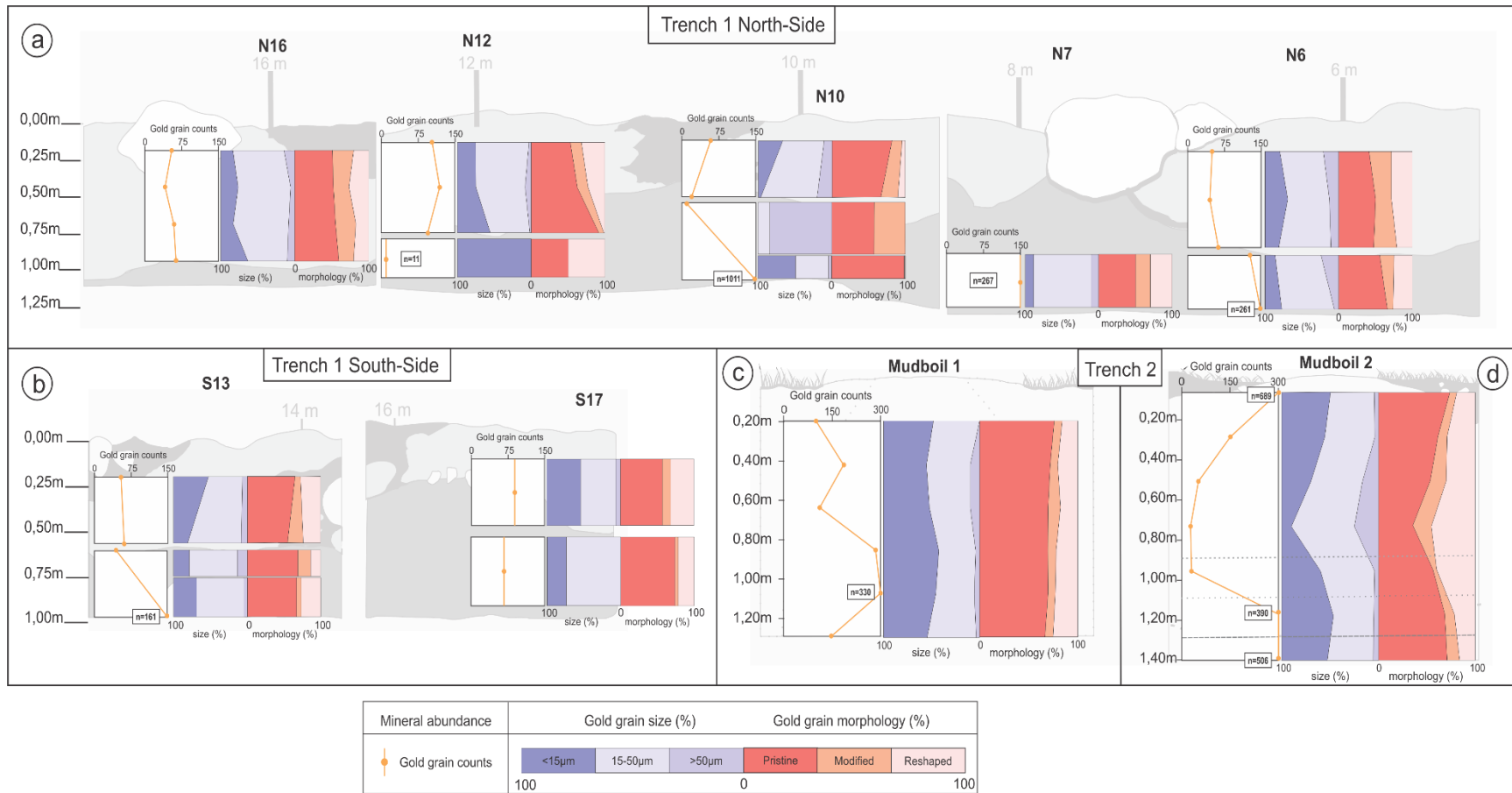


Figure I.21 Vertical profiles of the gold grain counts, length, and morphology. a) North side of Trench1, b) South side of Trench 1, c) Mudboil 1, and d) Mudboil 2. Grain counts normalized to 10-kg table feed.

Grain morphology

Each grain of gold was classified according to DiLabio's (1991) morphology scheme (pristine, modified and reshaped). The relative proportion of pristine gold grains varies depending on the till type and trench location (Table 3). Overall, distal till exhibits a lower relative proportion of pristine gold grains in comparison to the proximal till. The two mudboil surface samples show similar proportions for all morphologies. These samples, both collected in distal till, exhibit similar pristine gold grains proportions to the samples collected in distal till from the trenches.

The vertical distribution of grain morphology does not exhibit a consistent pattern (Fig. I.21). The three profiles interpreted as located in the central part of a cryoturbation feature (N12 in Trench 1, and MB1 and MB2 in Trench 2) display contrasting distributions of pristine, modified and reshaped gold grains. The N12 profile in Trench 1 shows an increase in the pristine shape proportion with depth in distal till (Fig I.21a). Mudboil 1 displays a slight but steady decrease in the pristine proportion from top to bottom (Fig I.21c). In contrast, Mudboil 2 displays an initial decrease of the pristine proportion up to the middle section and then increases towards and into the permafrost table (Fig I.21d). Moreover, the lateral profile of Mudboil 1 features the highest pristine proportion in the sample located in the middle part of the mudboil compared to the lateral samples taken at the same depth (~30 cm; Fig. I.22b).

Table 3. Gold grains morphology proportions classified by till and trench.

Morphology	Trench 1								Trench 2			
	Distal till				Proximal Till				Distal till			
	Min	Max	Mean	Med.	Min	Max	Mean	Med.	Min	Max	Mean	Med.
Pristine (%)	41.0	92.1	59.5	55.6	50.0	98.3	65.4	66	35.0	75.9	61.9	67.8
Modified (%)	6.3	31.3	19.6	21.1	0.0	42.9	13.3	7.8	4.0	23.5	11.1	9.5
Reshaped(%)	1.6	31.7	20.9	22.7	0.0	50.0	22.4	25.0	16.6	45.0	27.0	23.9

Grain size

The maximum length of all gold grains was classified according to the intervals <15, 15-25, 25-50, 50-75, 75-100, 100-125, 125-150, 150-175, 175-200 and >200 μm . The distribution

of the sizes differs in the different till types, as well as in the same till type but in different trenches (Fig. I.23a, b). The gold grain size distribution in both tills in Trench 1 is relatively similar, and the most common size falls within the range of 15-25 μm . In contrast, the number of gold grains in distal till in Trench 2 decreases with increasing gold grain size. Therefore, the gold grains $<15 \mu\text{m}$ are the most numerous in Trench 2. Samples collected in MB3 and MB4 display a similar size distribution between them but MB4 presents a higher abundance in the gold grain size 15-25 μm interval, similar to samples collected in the nearby trench (Fig. I.23c, d).

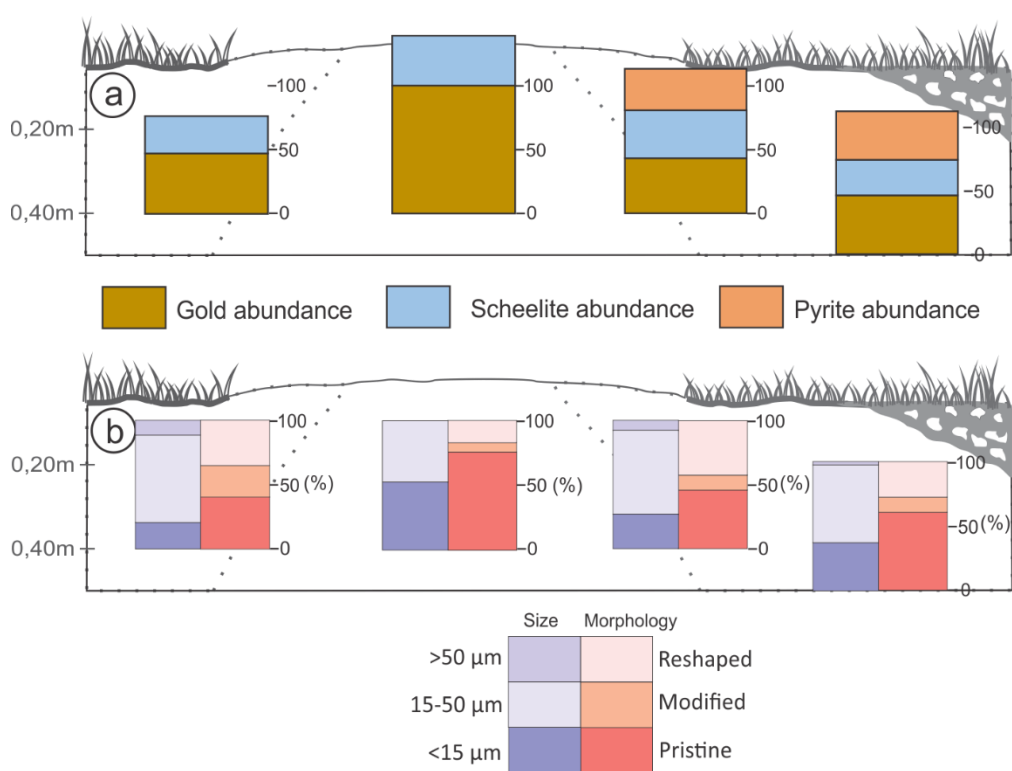


Figure I.22 IM's characteristics in the lateral till sampling profile in Mudboil 1. a) IM grain counts, b) proportions of gold grain size and morphology.

The distribution of the gold grain sizes along the profiles shows no systematic pattern (Fig. I.21). Vertical profiles display increasing, decreasing and relatively constant grain sizes with depth. More than 94% of the gold grains smaller than 15 μm are pristine in morphology, therefore, there is a strong relation between their distributions and depth (Fig I.21). In MB1 the gold grain sizes decrease in the central part compared to the lateral samples (Fig I.22b).

The three vertical profiles interpreted in the central part of a cryoturbation feature (N12, MB1 and MB2) demonstrate distinct characteristics in terms of grain sizes (Fig. I.21). In the case of the N12 profile, there is a significant increase in the number of gold grains smaller than 15 μm with depth, similar to the increase of pristine gold grains with depth, although not as significant. MB1 shows an overall uniform distribution of grain sizes as depth increases, in contrast to a slight but constant increase in the number of pristine gold grains with depth. MB2 has a particular trend where the general gold grain size decreases from the top to the middle section of the profile, followed by a subsequent increase in small gold grains (<15 and 15-50 μm) towards the gleyed horizon, and deeper, relatively stable sizes down to the permafrost table, overall mimicking the distribution of grain morphologies (Fig. I.21).

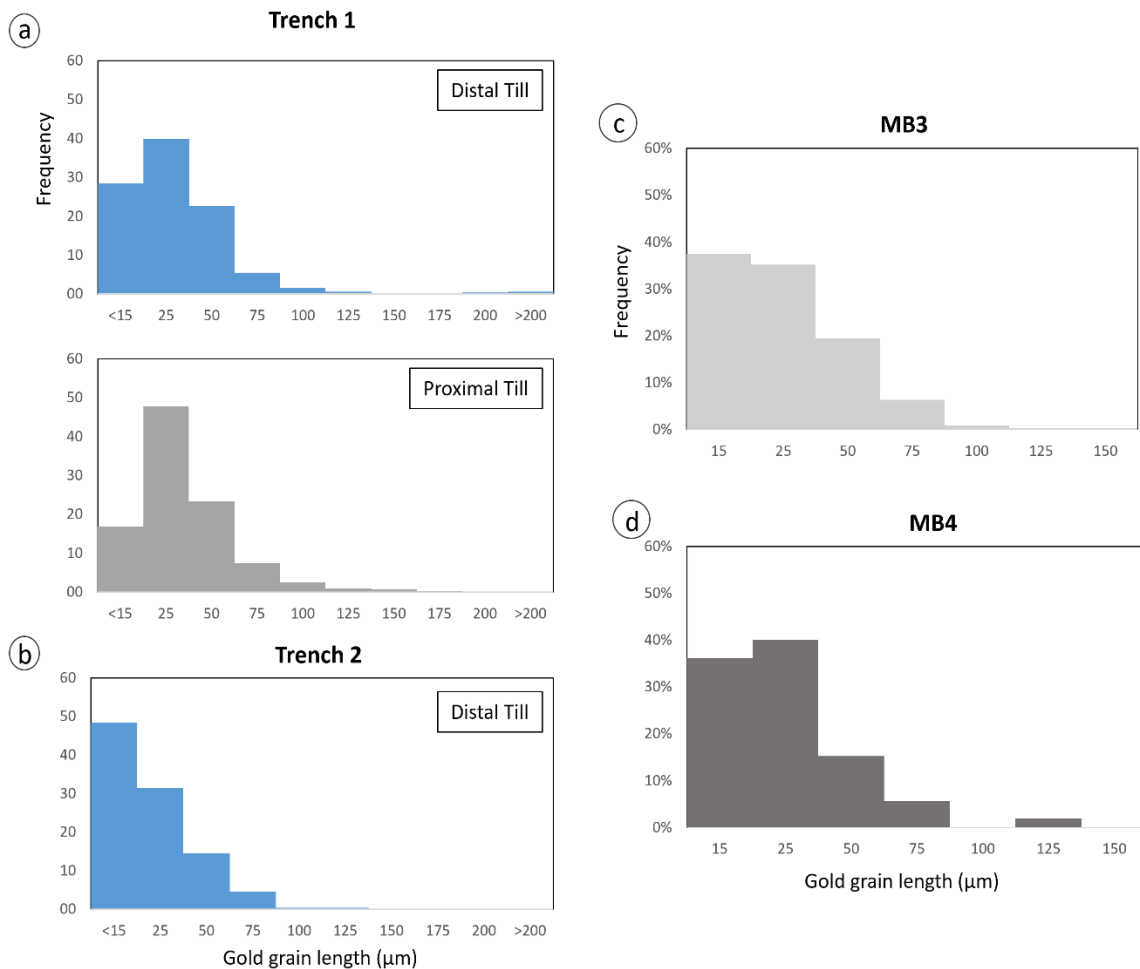


Figure I.23 Histograms of gold grain sizes frequency a) Trench 1, classified by till, b) Trench 2, c) Mudboil 3, and d) Mudboil 4.

Mineral chemistry

The mineral chemistry of gold was analyzed (Table 4) to determine whether the possible sorting by cryoturbation is based on the chemical variations in the gold grains and whether this process influences the discrimination of their source (Liu et al., 2021). Major (Au and Ag) and minor (S, Fe, Cu, Hg, and As) elements were analyzed in 150 gold grains located in vertical profiles, as well as in the two nearby mudboils (112 grains from distal till in both trenches, 29 grains from proximal till, 6 grains from MB3, and 3 grains from MB4). However, the trace element concentrations by LA-ICP-MS were only acquired in 131 gold grains larger than 30 μm (94 grains from distal till in both trenches, 29 from proximal till, 6 grains from MB3, and 2 grains from MB4).

Table 4. Summary statistics of EPMA and LA-ICP-MS element analyses on gold grains recovered from till (n=150 by EPMA and n=131 by LA-ICP-MS)

Element	Min	Max	Median	Sd	%<DL
Au (%)	53.14	98.91	75.99	8.83	0.00
Ag (%)	0.20	47.03	23.07	8.92	0.00
S (%)	0.00	0.08	0.02	0.01	0.00
Cu (%)	0.00	0.46	0.02	0.04	9.33
As (ppm)	0.32	6082	25.41	1050.80	29.01
Cr (ppm)	3.26	13552	16.07	1875.82	60.31
Mn (ppm)	11.02	4368	72.08	1053.02	57.25
Fe (ppm)	21.39	198477	2446.42	31956.86	11.45
Co (ppm)	0.07	714.94	1.84	75.04	21.37
Ni (ppm)	0.96	2977	12.40	320.74	27.48
Zn (ppm)	0.73	2149	45.08	310.58	12.98
Se (ppm)	0.62	32.71	1.91	9.26	91.60
Pd (ppm)	0.11	18286.78	0.83	1658.33	1.53
Cd (ppm)	0.03	41.66	0.37	8.28	52.67
Sn (ppm)	0.15	76.24	1.12	9.96	55.73
Sb (ppm)	0.23	877.83	11.49	121.21	29.01
Te (ppm)	0.12	291.95	1.39	42.55	64.12
Pt (ppm)	0.01	21.41	0.12	6.77	90.08
Hg (ppm)	144.67	49515	2197.28	5334.71	0.00
Pb (ppm)	0.07	14047	6.65	1288.14	8.40
Bi (ppm)	0.03	440.58	0.81	51.61	19.08
Mg (ppm)	0.88	17821	163.71	3057.61	14.29
Al (ppm)	3.59	39147	775.06	6187.81	13.33

Ti (ppm)	0.31	110030	37.33	13799.31	22.86
Mo (ppm)	0.03	36.77	0.43	6.01	62.86
Si (ppm)	898.54	125818	4240.07	20470.66	43.81
In (ppm)	0.00	0.37	0.02	0.09	81.90
Re (ppm)					100.00
Tl (ppm)	0.01	1.83	0.06	0.32	66.67

The gold content varies from 53.14 to 98.90%, with a mean value of 76.74% ($\sigma=8.83$). The range of fineness for the gold grains recovered from till samples varies from 530.5 to 998, with a median value of 766.85 ($\sigma=88.35$). More than 85% of the gold grains present a fineness value within the range of Amaruq gold bedrock which varies from 660 to 910 (Liu and Beaudoin, 2021; Mendizabal, 2022; Fig. I.24a left). Proximal till fineness plots mostly inside the Amaruq range, whereas distal till contains a greater proportion of gold grains with fineness values outside that range.

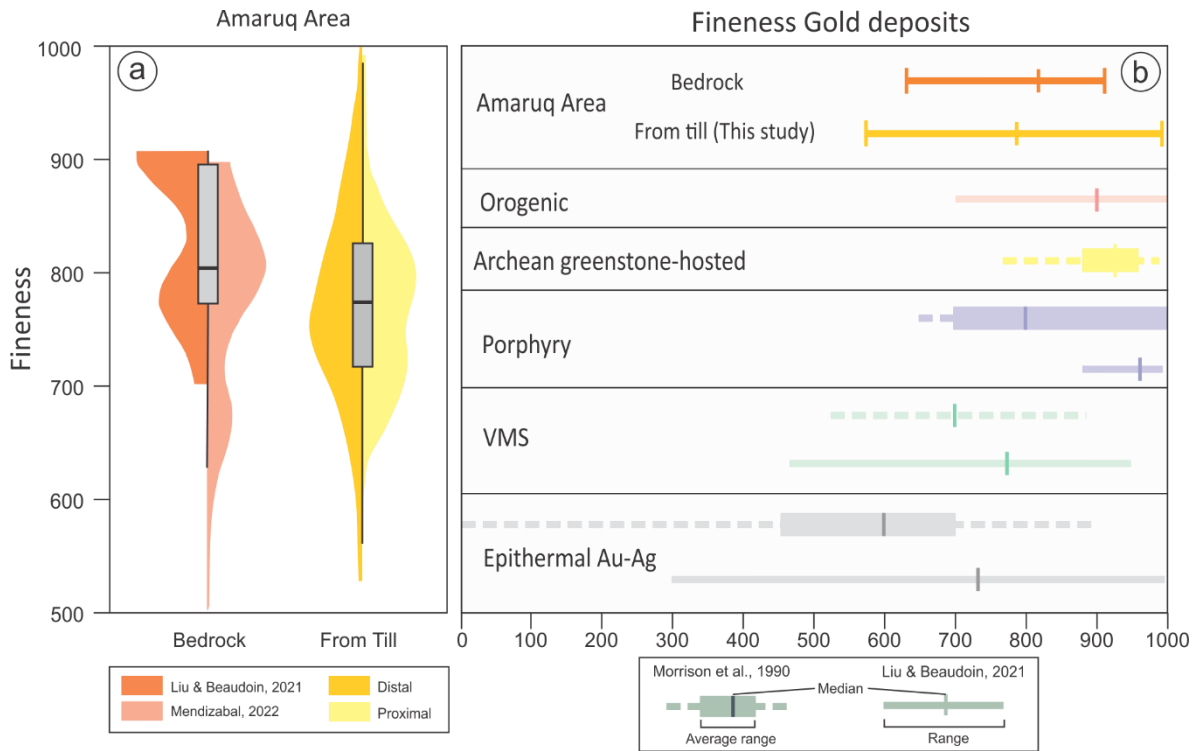


Figure I.24 Fineness of gold grains. a) Values for the Amaruq Area, left bedrock mineralization (Liu and Beaudoin, 2021; Mendizabal, 2022) and right, grains recovered from tills from this study, and b) comparison with values of different gold mineral deposits (Morrison et al., 1991; Liu and Beaudoin, 2021).

Silver concentration ranges from 0.19 to 47.02%, with a mean value of 22.43% ($\sigma=8.92$). The mean concentration of Fe and Hg is higher than 1000 ppm, with values of 14912 and 3532 ppm respectively. Trace elements with mean concentrations between 100 and 1000 ppm are Cr, Mn, Cu, Zn, As, Pd, and Pb. Elements with a mean lower than 100 ppm are Co, Ni, Cd, Sn, and Bi. Certain elements such as In, Se, Re, and Pt have a high percentage (>80%) of values below the detection limit.

No uniform patterns in the fineness grain values of gold grains with depth were recognized (Fig. I.25). In addition, gold grains in till with fineness values falling outside the Amaruq deposit range were observed across all profiles regardless of depth or till unit in which they were sampled (Fig. I.25). In Mudboil 1, they are found at different depths and in lateral samples in Mudboil 1, whereas in Mudboil 2, these gold grains were discovered only in the shallowest sample and in the gleyed horizon. However, the proportion of these grains was minor compared to the Amaruq-like gold grains in all the samples.

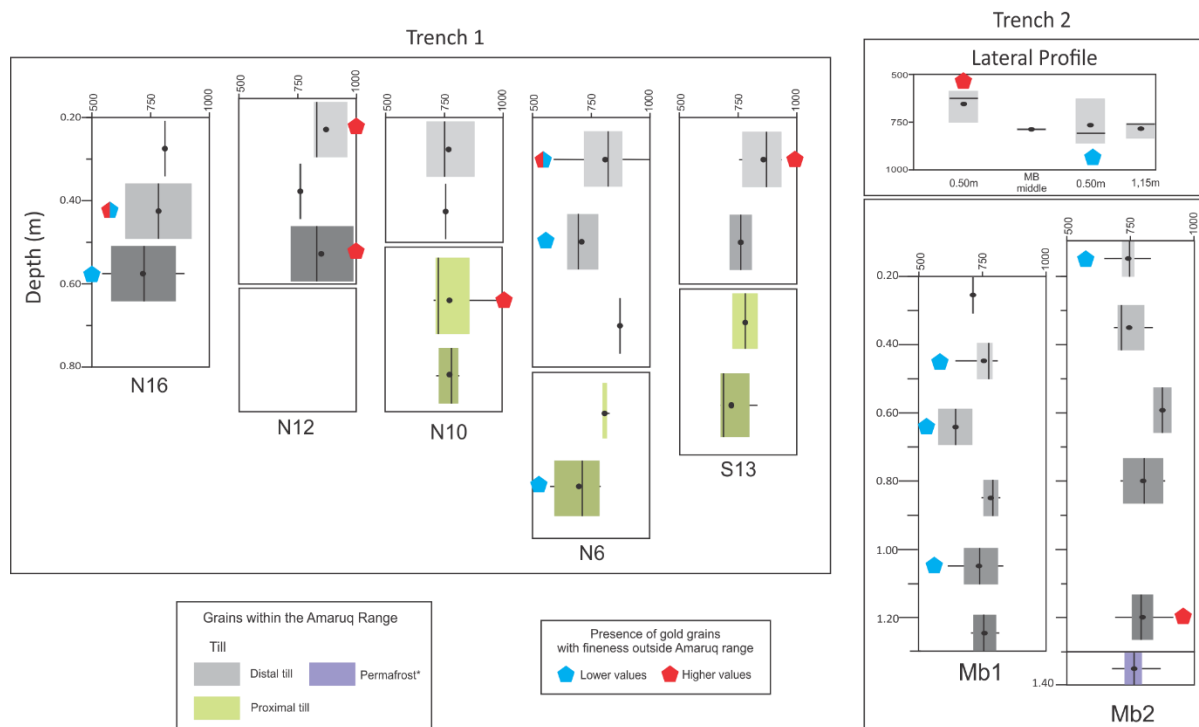


Figure I.25 Profiles showing the gold fineness measured in till samples through box plots.

The gold grains recovered from MB3 and MB4 display broad fineness values: MB3 ranges from 530 to 892, having a larger proportion plotting within the Amaruq range. In contrast, MB4 only presents values within the Amaruq range (from 696 to 897).

Partial least squares discriminant analysis (PLS-DA)

Liu and Beaudoin's (2021) PLS-DA model score plot enables the differentiation of gold deposits based on the Pd, As, Sb, Pb, Cu, Hg, and Te content of gold grains (Fig. I.26a). In our study, most gold grains (94%) plot within the fields of Amaruq gold and orogenic gold deposits (Fig. I.26b). However, as documented by Mendizabal (2022), gold from Amaruq bedrock shows contributions of the qw1 and qw2 loadings that are comparable to both porphyry and VMS deposits. This differs from the typical loadings in orogenic gold deposits, making it challenging to fully discriminate Amaruq-derived gold grains.

The majority of the gold grains outside of the Amaruq field (n=8) are from distal till samples (Fig. I.26b). The distribution of the gold grains from Trench 1 does not exhibit a correlation with depth. Likewise, the gold grains from MB1 and MB2 (Trench 2) within the PLS-DA score plot are independent of their position inside the profiles (Fig. I.26c). This implies that the location of the gold grains within the mudboils is regardless of their Pd, Sb, Cu, Hg, Ag, Pb, and Te content.

Scheelite and Fe-sulfides

Abundance

Scheelite grains have a bright blue color under short-wave ultraviolet light. Similarly to gold grains, the distal till in Trench 1 has a lower scheelite abundance than the proximal till (Table 5). Furthermore, distal till in Trench 2 has lower scheelite counts than in Trench 1. In the two mudboil surface samples, scheelite counts were 7 and 25 in MB3 (near Trench 2) and M4 (near Trench 1), respectively. Pyrite is the most common Fe-sulfide in the samples. Fe-

sulfides are scarce in both tills in Trench 1. In contrast, distal till in Trench 2 contains pyrite, chalcopyrite and arsenopyrite, especially in Mudboil 2.

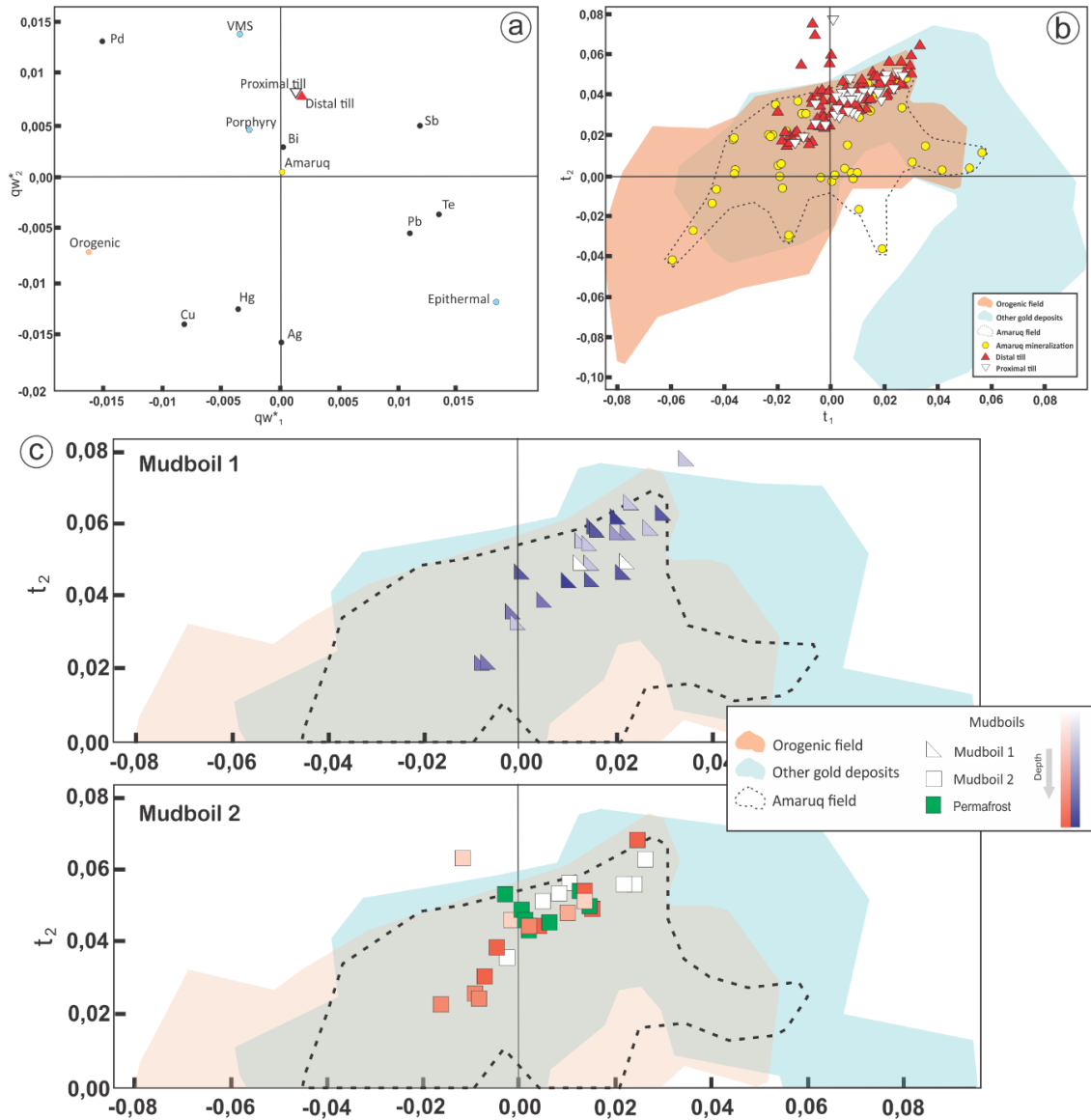


Figure I.26 Partial least square-discriminant analysis (PLS-DA) of the log-centered and normalized LA-ICP-MS of gold grains recovered from till (this study) compared to different gold mineral deposits based on Liu and Beaudoin (2021). a) The qw^*_1 - qw^*_2 loading plot, b) The t_1 - t_2 scores plot shows the distribution of gold grains according to till c) Samples of the gold grains within the two mudboils sampled in Trench 2 plotted in the PLS-DA score plots. Top, Mudboil 1. Bottom, Mudboil 2. Data for Amaruq deposit from Liu (2020) and Mendizabal (2022).

Table 5. Scheelite grain counts (normalized to 10-kg table feed)

	Trench 1		Trench 2		
	Distal till	Proximal till	Distal till(total)	Mudboil1	Mudboil2
Mean	179	201	54	49	38
Median	48	179	40	51	23
Min	24	16	13	39	13
Max	725	576	208	56	208
Std	243	217	51	38	78
CV	1.36	1.08	0.94	0.77	2.05

The abundance of scheelite grains does not show a systematic pattern in the vertical profiles (Fig. I.27). Within distal till, different profiles show varying trends, or absence of trends, with depth. Profiles such as N12 and N10 remain relatively constant with depth, whereas profiles such as N16 or N6 demonstrate major differences in scheelite counts with depth, without clear trends. In Trench 2, Mudboil 1 and Mudboil 2 show contrasting scheelite abundances with depth. Mudboil 1 exhibits a constant distribution with depth (mean of 46; Fig I.27). The greatest scheelite abundance is in the middle of the mudboil compared to the lateral samples at the same depth (Fig. I.22a). Mudboil 2 has the highest scheelite counts in permafrost (n=200) and in the gleyed sample above it (n=143; Fig I.27). Scheelite grains larger than 0.25 mm in distal till are primarily located at the top of the N12 and N16 profiles in Trench 1, as well as in the 1 m depth sample from Mudboil 1 and in the permafrost in Trench 2.

Pyrite (n=35) was observed in Mudboil 1 (Fig I.27), while chalcopyrite (n=6) was found in the middle section of the same profile (ranging from 0.40 m to 0.90 m depth), with no trend in mineral abundance with depth. In contrast, Mudboil 2 contains pyrite grains with a tendency (Fig I.27) to decrease from the shallowest sample (n=88) to the middle part of the profile (50-90 cm; n=0) and then increase to the permafrost table (n=200). Chalcopyrite grains (n=8) were only observed in the permafrost sample whereas arsenopyrite grains (n=4) were only found in the sample above the permafrost. Unlike scheelite, pyrite shows the highest abundance on the right-lateral samples in Mudboil 1 compared to the samples in the central and left side (Fig. I.22a). This is related to the deformed gleyed patches identified in that part (Fig. I.12c). In the two mudboils sampled next to the trenches, MB3 exhibits pyrite (n=28) and chalcopyrite (n=2), whereas MB4 contains only pyrite (n=13).

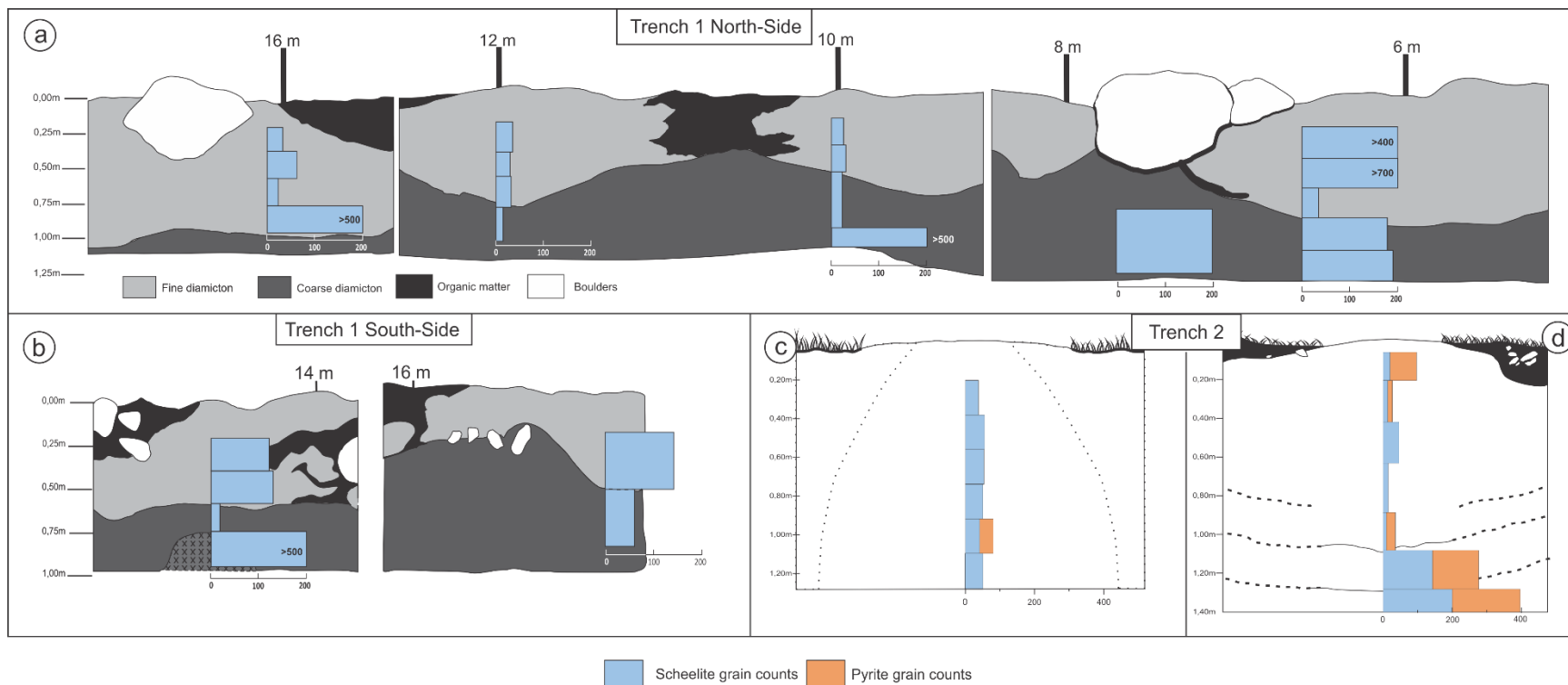


Figure I.27. Vertical profiles of the scheelite and pyrite grain counts. a) North side of Trench1, b) South side of Trench 1, c) Mudboil 1, and d) Mudboil 2. Grain counts normalized to 10-kg table feed.

Mineral chemistry

Major, minor and trace element concentrations of 48 scheelite grains (0.25-2 mm NM-HMC fraction) and 12 chalcopyrite grains (0.25-2 mm NM-HMC fraction) were determined (Table 6 and Table 7). Among the scheelite grains, 29 are from distal till from both trenches, while 19 grains were recovered from the proximal till. No scheelite grains (0.25-2 mm) were identified in the mudboils samples near the trenches (MB3 and MB4). Chalcopyrite grains are from distal till in both mudboils and MB3.

In scheelite, the mean values of WO_3 and CaO are 79.45 and 19.13% respectively. Among the minor and trace elements determined, only Sr presents a mean concentration higher than 1000 ppm, with a value of 1107.1 ppm. Elements with a mean content ranging from 100 to 1000 ppm are S, Fe, and Mo. Most of the elements determined exhibit a mean value varying from 1 to 100 ppm such as Na, Mg, K, Ti, Mn, Cu, As, Y, Nb, Ba, La, Ce, Pr, Nd, Sm, Eu, Gd, Tb, Dy, Ho, Er, Yb, and Pb. Elements with a mean concentration that are less than 1 ppm are B, V, Zn, As, Tm, Lu and Ta. Several elements such as Ti, V, As, Li, Cr, Co, Ag, Sn, Th and U have more than 40% of the values below detection limit.

Table 6. Summary statistics of EPMA and LA-ICP-MS element analyses on scheelite grains recovered from till (n=48 by EPMA and n=48 by LA-ICP-MS)

Element	Min	Max	Median	Sd	%<DL	Element	Min	Max	Median	Sd	%<DL
WO ₃ (%)	74.11	80.84	79.47	0.73	0.00	Mo (ppm)	0.12	3688.54	31.55	706.23	8.33
CaO (%)	17.80	19.98	19.13	0.20	0.00	Ag (ppm)	0.05	0.05	0.05	0.00	97.92
Li (ppm)	0.07	1.60	0.16	0.39	64.58	Sn (ppm)	0.14	0.14	0.14	0.00	97.92
B (ppm)	0.41	2.30	0.76	0.44	2.08	Ba (ppm)	0.28	7.69	1.66	1.74	12.50
Na (ppm)	2.13	154.80	18.89	28.83	0.00	La (ppm)	0.06	63.05	2.90	13.27	0.00
Mg(ppm)	1.69	1511.73	3.50	219.48	0.00	Ce (ppm)	0.40	178.97	6.02	40.33	0.00
S (ppm)	166.64	315.14	252.08	30.97	0.00	Pr (ppm)	0.11	47.03	1.23	8.22	0.00
K (ppm)	0.99	121.03	4.24	31.42	37.50	Nd (ppm)	0.53	373.97	8.42	58.61	0.00
Ti (ppm)	0.14	16.38	0.42	4.04	43.75	Sm (ppm)	0.29	187.77	3.35	28.15	4.17
V (ppm)	0.04	3.17	0.13	0.63	43.75	Eu (ppm)	0.11	33.18	3.28	7.79	2.08
Cr (ppm)	0.29	13.90	1.15	4.55	81.25	Gd (ppm)	0.39	263.70	5.26	40.18	0.00
Mn(ppm)	4.01	156.07	13.97	22.60	0.00	Tb (ppm)	0.06	36.78	0.80	5.66	0.00
Fe (ppm)	0.96	3758.09	10.87	632.68	2.08	Dy (ppm)	0.52	191.32	5.55	31.06	0.00
Co (ppm)	0.02	3.83	0.05	1.09	77.08	Ho (ppm)	0.14	27.04	1.12	5.38	0.00
Cu (ppm)	0.10	3.82	2.07	1.02	4.17	Er (ppm)	0.48	74.34	3.58	13.61	0.00

Zn (ppm)	0.19	4.06	0.42	0.67	37.50	Tm (ppm)	0.07	9.94	0.45	1.56	0.00
As (ppm)	0.62	5.14	1.10	1.25	41.67	Yb (ppm)	0.50	57.34	2.02	8.37	0.00
Sr (ppm)	60.45	5014.97	725.79	1147.45	0.00	Lu (ppm)	0.04	7.68	0.23	1.10	0.00
Y (ppm)	6.66	617.48	31.85	115.64	0.00	Ta (ppm)	0.07	0.67	0.15	0.10	0.00
Nb (ppm)	4.29	47.81	5.16	9.94	0.00	Pb (ppm)	3.97	28.49	9.84	5.63	0.00

In chalcopyrite, the mean concentration of S, Cu, and Fe is 35.5, 34.0 and 30.8% respectively. In terms of minor and trace elements, both Se and Zn have mean values greater than 100 ppm. Elements with a mean content ranging from 1 to 100 ppm are Mg, Ti, Cr, As, Rh, Pd, Ag, Cd, In, Sn, and Pb. Lastly, the elements with a mean quantity lower than 1 ppm are Co, Ga, Ge, Sb, Te, Ba, Hg, Au, and Bi. Moreover, some elements present high percentages (from 40 to 100%) of values below detection limit such as Sb, Ca, Ni, As, Ba, V, Mn, Mo, Ru, W, Re, Os, Pt, and Tl.

Table 7. Summary statistics of EPMA and LA-ICP-MS element analyses on chalcopyrite grains recovered from till (n=12 by EPMA and n=12 by LA-ICP-MS)

Element	Min	Max	Median	Sd	%<DL	Element	Min	Max	Median	Sd	%<DL
S (%)	35.28	35.87	35.56	0.18	0.00	Ru(ppm)	0.05	0.08	0.06	0.01	71.43
Fe (%)	30.54	31.10	30.82	0.20	0.00	Rh(ppm)	27.39	29.33	28.50	0.53	0.00
Cu (%)	33.58	34.51	33.90	0.32	0.00	Pd(ppm)	20.75	24.95	22.14	1.01	0.00
As (%)	0.00	0.07	0.03	0.02	18.18	Ag(ppm)	0.07	110.98	7.08	31.53	0.00
Mg(ppm)	0.08	13.88	0.55	4.38	14.29	Cd(ppm)	0.9	79.73	15.06	27.51	14.29
Si(ppm)	456.81	828.13	753.77	103.29	0.00	In(ppm)	0.10	9.69	3.75	2.69	0.00
P(ppm)	11.03	23.14	14.41	3.77	35.71	Sn(ppm)	0.06	7.33	2.14	2.69	0.00
Ca(ppm)	7.10	95.51	28.71	33.59	50.00	Sb(ppm)	0.05	1.39	0.33	0.56	42.86
Ti(ppm)	3.46	17.17	5.05	4.62	7.14	Te(ppm)	0.05	2.11	0.39	0.66	7.14
V(ppm)	0.02	0.30	0.11	0.11	64.29	Ba(ppm)	0.02	2.11	0.42	0.70	50.00
Cr(ppm)	2.63	5.99	3.66	0.84	7.14	W(ppm)	0.16	0.20	0.18	0.03	85.71
Mn(ppm)	1.19	10.55	4.10	3.75	64.29	Re(ppm)					100.00
Co(ppm)	0.03	1.67	0.10	0.46	21.43	Os(ppm)					100.00
Ni(ppm)	0.16	20.96	0.94	7.35	50.00	Pt(ppm)					100.00
Zn(ppm)	1.19	696.88	309.16	258.63	0.00	Au(ppm)	0.01	15.26	0.02	4.27	0.00
Ga(ppm)	0.01	0.10	0.05	0.03	7.14	Hg(ppm)	0.35	1.06	0.46	0.28	64.29
Ge(ppm)	0.28	0.38	0.31	0.02	0.00	Tl(ppm)					100.00
As(ppm)	0.70	18.51	3.71	6.69	50.00	Pb(ppm)	0.50	13.66	1.66	3.47	0.00
Se(ppm)	8.55	414.58	36.08	169.24	0.00	Bi(ppm)	0.03	2.34	0.42	0.68	0.00
Mo(ppm)	0.01	0.07	0.04	0.03	78.57						

Provenance

Binary and ternary plots

The concentration of Sr, Mo, As and Eu* in scheelite is useful for discriminating scheelite derived from orogenic gold deposits from other types of gold deposits (Sciuba et al., 2020). Two binary plots (Eu* vs Sr/Mo and As vs Sr/Mo) were used to detect the till-recovered scheelite originating from the Amaruq gold deposit (Fig. I.28). Most of the scheelite grains in the till plot within the field for scheelite Amaruq gold deposit (n=43). Four grains plot in the field for other types of deposits. These grains are from distal till, and are present in the profiles N10, MB1 and MB2 at different depths (Fig I.28), suggesting that these 4 scheelite grains are randomly distributed throughout the till column and do not exhibit preferential depths.

Concentrations of Cd, Zn, Ni and Se in chalcopyrite were used to discriminate their origin using various discrimination diagrams. The element concentration in chalcopyrite from the Amaruq gold deposit (Caraballo, 2023) is plotted in all diagrams (Fig I.29). Most chalcopyrite from till plot outside the field for the Amaruq gold deposit. The Se-Ni-Cd diagram serves to determine whether chalcopyrite is from magmatic or hydrothermal sources (Duran et al., 2015; 2019). The till chalcopyrite grains plot in both magmatic and hydrothermal sources (Fig. I.29a). Most of them, however, are located near the Se corner of the diagram. This complicates the identification of the chalcopyrite's origin. The ratio Cd/Zn is a useful indicator for distinguishing chalcopyrite originating from various hydrothermal mineral deposits (Fig. I.29b; George et al., 2018). In general, the Cd/Zn ratio of the till chalcopyrite grains is greater than that of chalcopyrite from most other hydrothermal deposits. According to the diagram of Mansur et al., (2022; Fig. I30c), most chalcopyrite grains plot in the hydrothermal field, with only one chalcopyrite grain in the magmatic field. This chalcopyrite also plots in the magmatic field of the Se-Ni-Cd ternary diagram (Fig I.29a). It contains low values of Cd (<5ppm) while displaying a relatively high Zn content (>250ppm), resulting in a different Cd/Zn ratio compared to the other chalcopyrite grains

(Fig. I.29b). Due to the absence of grains in the 0.25-2mm fraction, complete vertical profiles cannot be presented (Fig I.29d).

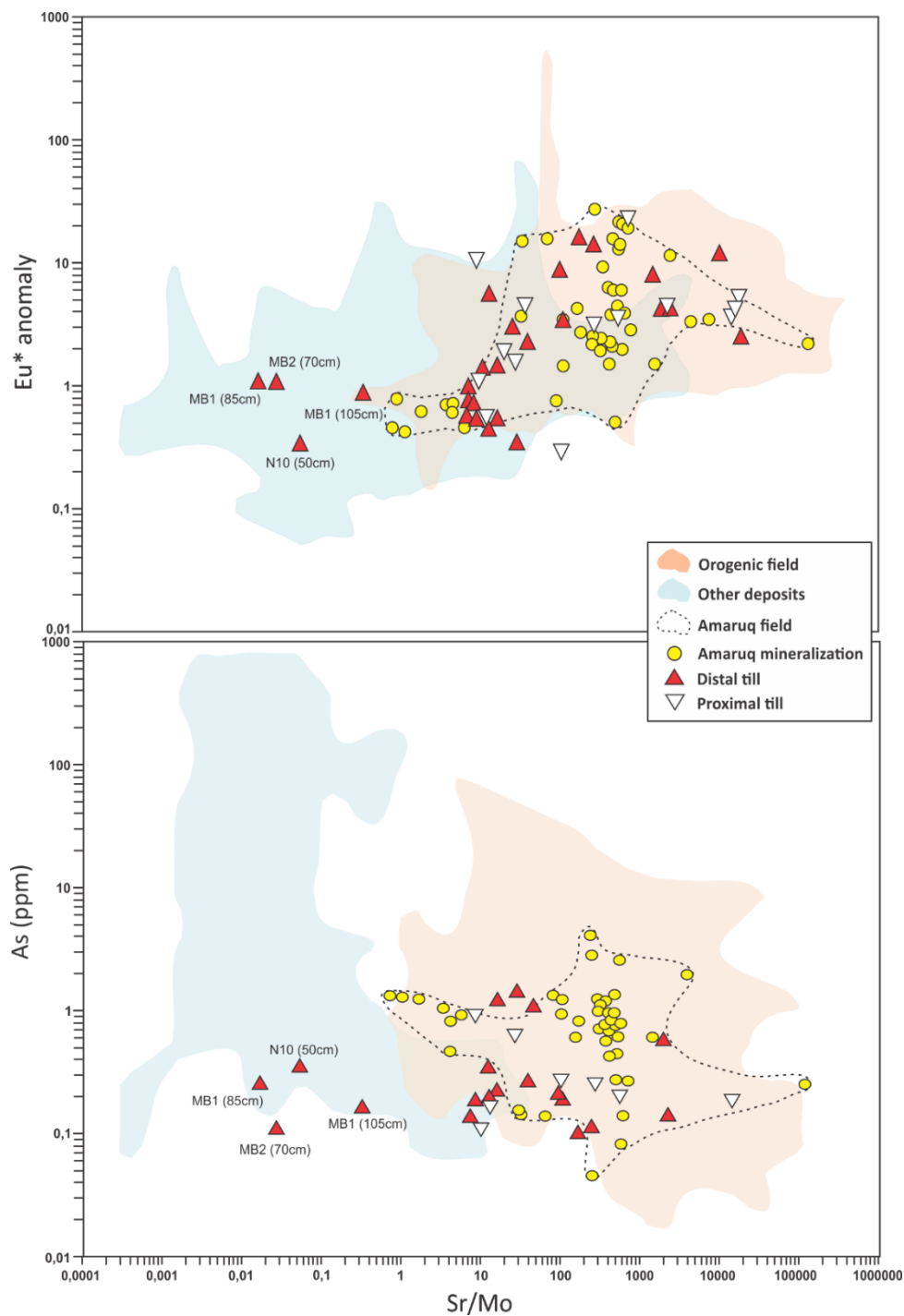


Figure I.28 Binary plots to discriminate scheelite. Top, Eu* anomaly vs Sr/Mo. Bottom, As (ppm) vs Sr/Mo

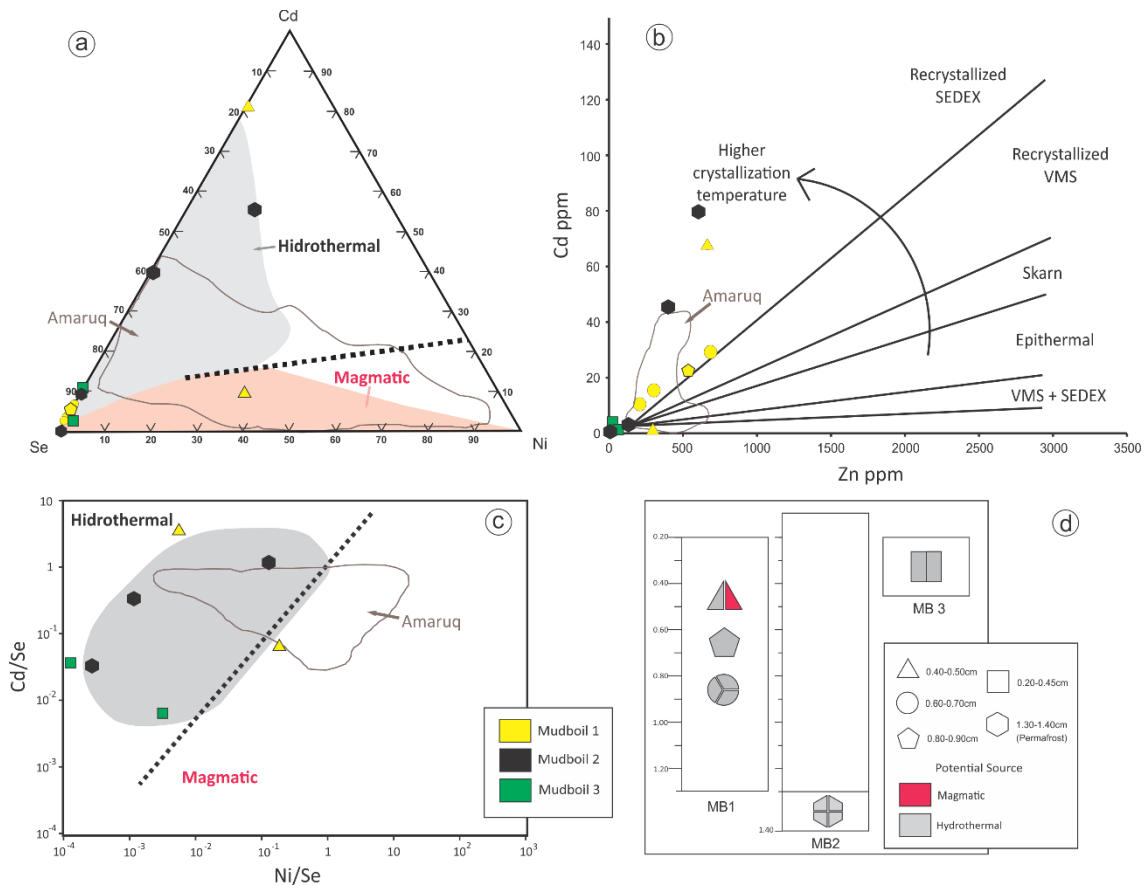


Figure I.29 Chalcopyrite discrimination diagrams. a) Ternary diagram of Cd, Se, and Ni (Duran et al., 2019), b) Cd vs Zn diagram for hydrothermal deposits (George et al., 2018), c) Binary plot Cd/Se vs Ni/Se (Mansur et al., 2021, after George et al., 2018), d) Vertical profiles of chalcopyrite grain counts of the two mudboils from Trench 2 and Mudboil 3. The thin black outline represents Amaruq data from Caraballo (2023)

PLS-DA

The chemical composition of scheelite grains from till was plotted in the PLS-DA model by Sciuba et al. (2020). The Amaruq deposit scheelite data from de Bronac de Vazelhes (2019) was used as a reference (n=47). About half of the till scheelite grains (n=24) plot in or close to the Amaruq gold deposit field (Fig. I.30). Till scheelite with orogenic gold deposit signature forms two groups: 1) group 1 consists of 4 samples from proximal till. These samples display positive t1 and t2 values, primarily associated with high positive Sr and Eu contributions, while negative Mo contributions, and 2) group 2 samples are from proximal and distal till, having positive t1 and negative t2 values, attributed from positive contributions of Er, Tm, Yb, and Ho and negative Pr, La, and Nd contributions (Fig. I.30).

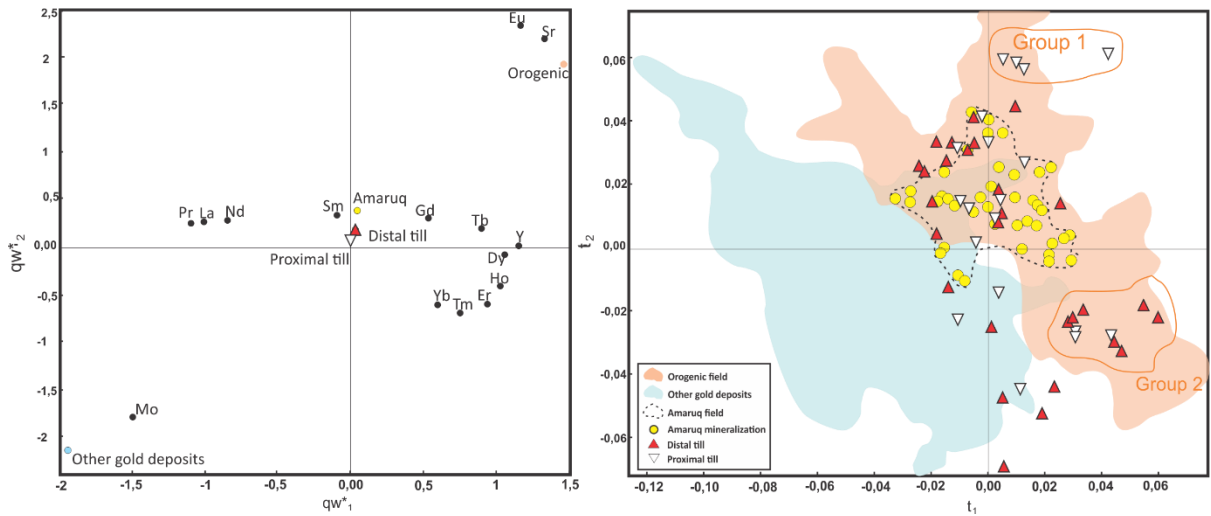


Figure I.30 Partial least square-discriminant analysis of the log-centered and normalized LA-ICP-MS of scheelite grains recovered from till compared to different gold mineral deposits based on Sciuba et al. (2020). Amaruq deposit data from de Bronac de Vazelhes (2019).

Several samples do not contain scheelite grains in the 0.25-2 mm fraction, making it difficult to establish depth-related trends (Fig. I.31). The vertical distribution profiles of scheelite from different sources do not exhibit a discernible pattern in relation to depth.

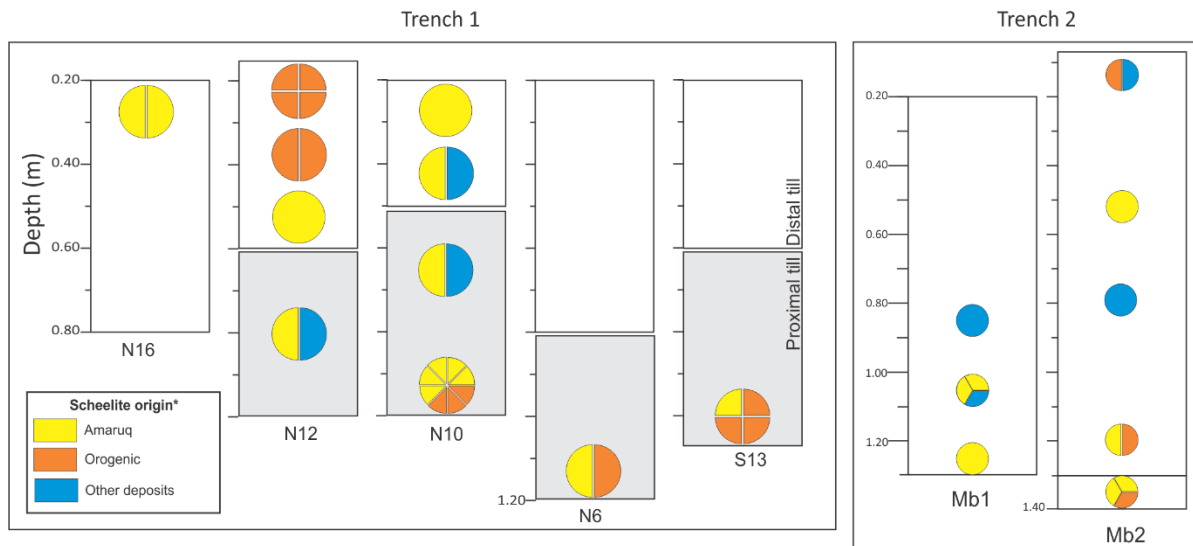


Figure I.31 Vertical profiles showing the proportion of scheelite grains discriminated by deposit type. Each section of the pie graphs is a scheelite grain.

1.7 DISCUSSION

1.7.1 Heterogeneity of composition, texture and IM in till units

The spatial relationship between the two till units in Trench 1, with distal till on top of proximal till (Fig I.6), suggests that distal till is younger than proximal till. Proximal till in Trench 1 shows significant changes in pebble composition, texture and IM abundance along the trench (Table 1; Fig I.8; Fig I.21). The Whale Tail transect sample with the greatest gold grain (1338) and scheelite grain counts (0.25-2mm; n=12) is located less than 100 m west of Trench 1 (~1400 m down-ice from mineralization), within proximal till (Fig. I.4). The till sample contains a proportion of >90% of pristine gold grains. This sample also shows the gold mineralization signature in till geochemistry (de Bronac de Vazelhes et al., 2021). One sample within the proximal till in Trench 1 shows high gold and scheelite grain counts (1011 and 9 [0.25-2mm], respectively) close to those values and a pristine proportion >95%. However, the overall values in the proximal till from this study are much lower than those in the transect sample. The proximal till identified in Trench 1 has more clasts and coarser-grained texture compared to the sandy diamicton texture characteristic of proximal till (Boulianne-Verschelden, 2019). These variations in texture and composition can be attributed to facies changes resulting from differences in glacial dynamics or subglacial processes, and changes in the nature of the subglacial bed. Further analysis would be necessary to determine the precise factors responsible for this variation.

The gold grain abundance in distal till at Trench 2 is higher than at Trench 1. As the thickness of the distal till layer increases from Trench 1 to Trench 2, there is an apparent relationship between till thickness and gold grain contents in the distal till. These observations suggest that perhaps near Trench 2 a more intensified glacial activity led to greater erosion of the proximal till and mineralized bedrock, leading to higher gold grain concentrations at Trench 2 than at Trench 1. This is further supported by the different geochemical signatures (Fig. I.16) and the clast lithology percentages (Fig I.8) between the distal till of both trenches, indicating a closer resemblance in composition between the distal till in Trench 2 and the

proximal till (de Bronac de Vazelhes et al., 2021; Mendizabal, 2022). The compositional variation in distal till is accompanied by differences in IM characteristics and geochemical signatures between till in Trench 2 and the nearest sample taken from distal till along the Whale Tail transect at 1150 m down-ice (Fig. I.4). The latter sample contains 73 gold grains with over 85% having a pristine shape. Trench 2 has nearly three times more gold grains on average, with a lower pristine proportion (65%) compared to the 1150 m down-ice Whale Tail sample. Notably, the geochemical signature of the down-ice Whale Tail sample at 1150m (de Bronac de Vazelhes et al., 2021) contrasts to the till in Trench 2 and MB3 (predominantly mafic/ultramafic signature; Fig. I.17). Variability in till composition between the distal tills in trenches 1 and 2, and the 1150 m down-ice Whale tail sample reflect the complex nature of till deposited by glacial processes, involving erosion of multiple bedrock and previous till layers (including proximal till), intricate mechanisms of sediment transportation and deposition, and possibly cryoturbation in permafrost regions. Till in the two mudboils surface samples (MB3 and MB4) exhibit contrasting characteristics. Till in MB3 displays a similar nature to the distal till in Trench 2, while that in MB4 is comparable to the distal till in Trench 1, emphasizing again the variations found within the same till unit.

Overall IM characteristics are different in the two till units in both trenches. In Trench 2, the presence of numerous gold grains smaller than 15 μm significantly raises the content of pristine gold grains, due to limited modification of smaller gold grains by glacial processes (Girard et al., 2021). This can lead to misinterpretations regarding the relative proportions of gold grains and their proximity to the source. The contrasting abundance of gold and scheelite grains in distal till profiles can be attributed to: 1) the intrinsic characteristics of these minerals and/or 2) heterogeneity in glacial deposits and sources. Mineral features like density and malleability influence erosion, transportation, and depositional processes. Additionally, these mineral features also play a role in how cryoturbation modifies them, as evidenced by the variations in gold and scheelite grain counts with depth in MB1 and MB2. Furthermore, around half of scheelites grains are likely not derived from the Amaruq deposit, suggesting significant input of distal-sourced scheelite from a different orogenic gold deposit.

Glacial and cryogenic processes govern the Fe-sulfides abundance in Trench 1 and 2. The Fe-sulfide absence in Trench 1 may be due to: 1) a short distance of dispersal, or a wide skip zone, or 2) exposure to the surface by cryogenic processes destroyed them by weathering (Shilts, 1977). Conversely, the presence of Fe-sulfides in distal till at Trench 2 may be attributed to a higher contribution by erosion of prior proximal till dispersal train closer to mineralization (de Bronac de Vazelhes, 2019), combined with better preservation conditions related to less weathering at depth. The sulfide grains in permafrost distal till, and in the overlying gleyed layer, are sporadically released to the surface by cryoturbation due to the thickening of the active layer caused by warmer conditions (French 2018).

1.7.2 Evidence for cryoturbation, and weathering

Interaction between till units

The findings from Trench 1 indicate that major differences in the textural characteristics of the proximal and distal tills prevent cryoturbation from generating a mixture of both units. In contrast, when materials have similar textures, such as fine-grained till and glacio-marine sediments, it is more common to observe a complete mixture of materials in the active layer (McMartin and Campbell, 2009; McClenaghan et al., 2013). The absence of mixing between the two till layers in Trench 1 is evidenced by the sharp contacts between both units, as well as contrasting data obtained from pebble and indicator minerals counts (Fig I.6 and Table 2). Cryoturbation altered the presumed horizontal shape of the contacts of the original surface at the time of deposition into bowl-shape contacts. These distinctive bottom concave-shapes are commonly observed in cryoturbation features characterized by circular soil-motion (Shilts 1978; Egginton, 1979). The contact between the two units serves as the lower limit of internal motion, which can be observed through the accumulation of organic matter along the contact (Fig I.6). This typically occurs along the permafrost table (Soil Classification Working Group, 1998). In Trench1, distal till is considerably disturbed by cryoturbation processes favored by its fine-grained texture (Walker et al., 2004; Tarnocai and Bockheim, 2011). The presence of bowl-shape contacts, buried organic matter layers, and a regular pattern of stones and organic matter suggests a cell-like soil motion, likely caused by the expansion and

contraction during freezing and thawing (Mackay, 1980; Petterson et al., 2003; Tarnocai and Bockheim, 2011; Hagedorn et al, 2008; Hallet, 2013). The effects of cryoturbation on the distribution of till units can be complex and influenced by a variety of factors, one of the most fundamental being the soil texture. The fine-grained texture character of distal till makes it much more frost susceptible than coarser grained proximal till (Chamberlain, 1981).

Moreover, cryoturbation processes create zones where proximal till, beneath distal till, can reach the surface, due to the increasing frost susceptibility towards the surface (Van Vliet-Lanoë and Coutard, 1984). This phenomenon has the potential to generate patterned ground, specifically sorted circles (Jahn, 1968; Van Vliet-Lanoë, 1985; Hallet, 2013) and to combine some of the features of both till units at the surface.

Mudboil characteristics

The nature of mudboils is variable, as seen in the distinct characteristics of the two mudboils in Trench 2, including surface diameter, active layer thickness, till characteristics, matrix grain-size distribution, pebble composition, IM features, and geochemical signatures. While both mudboils generally show a consistent content of major and trace elements with depth, indicating homogeneity, their specific characteristics differ. Mudboil 1 exhibits a greater diameter on surface and a thicker active layer compared to Mudboil 2. This suggests that larger mudboils at surface are correlated with increased active layer thickness, as reported by Shilts (1978) and Kokelj et al. (2007), possibly due to changes in the vegetation cover resulting in soil temperature modifications (Walker et al., 2004; Tarnocai and Bockheim, 2011).

Mudboil 1 shows no vertical variability, but a lateral variation in the character of the till is observed. The lateral variability is caused by cryoturbation, bringing homogenized, weakly altered, and moderately altered sediments in contact with each other (Fig I.12). The oxidized material at the edges of the MB1 could be associated with the B horizon identified in cryosols (Soil Classification Working Group, 1998). Clast lithology proportions and geochemical signatures (Fig. I.19) are similar among the lateral samples of MB1, but they differ from the

sample collected in the central part at analogous depth in the same mudboil, indicating cryoturbation's influence on geochemical signature within the till at the same level.

Mudboil 2 exhibits vertical variation in the till characteristics, with no apparent lateral heterogeneity. The possibility of vertical variation in MB1 at depth is not discarded as permafrost was not reached in this mudboil. The trenches were examined in September, so the thickness of the active layer probably corresponds to the maximum thawing depth for MB2, at 1.30 m, allowing us to recognize the complete layering of that mudboil. The gleyed layer above the permafrost shares similar attributes with the permafrost till (grain size, indicator minerals, geochemistry), suggesting minimal cryoturbation processes and recent incorporation of the gleyed material into the active layer. This phenomenon may be linked to recent global warmer conditions, which could have led to a thickening of the active layer in permafrost areas (French, 2018; Biskaborn et al., 2019). In addition, this gleyed horizon generated by high moisture above the permafrost is common in cryosolic soils (Soil Classification Working Group, 1998; Tarnocai and Bockheim, 2011). The interface between the highly oxidized till and the gleyed horizon (1.10 m depth) could represent the deepest permafrost table for a significant period, facilitating soil oxidation processes above the permafrost due to potential groundwater flow.

Limited information exists regarding the variation of multiple characteristics with depth in mudboils. Some studies have focused on grain-size distribution, revealing diverse trends (Fig. I.32). For instance, sorted-particle profiles with increasing sand content with depth have been documented in mudboils from North America (Mackay, 1980; Zoltai and Tarnocai, 1981; Ping et al., 2003), and in fieldwork observations in the Amaruq area (de Bronac de Vazelhes, 2019). This increase of the coarse fraction with depth has been used as evidence of circular dynamics within mudboils (Mackay, 1980). On the other hand, uniform grain-size distributions, as identified in MB1, and random grain-size vertical distributions have also been described by several authors in mudboils from Canada, USA and Norway (Fig. I. 32; Mackay, 1980; Dyke and Zoltai, 1980; Zoltai and Tarnocai, 1981; Swanson et al., 1998; Ping et al., 2003; Overduin and Kane, 2006; Boike et al., 2008; Tarnocai and Bocheim, 2011). Notably, the general trend of increasing silt and decreasing sand content with depth in MB2 has not been previously described. These findings suggest that mudboils do not consistently

exhibit specific grain-size distributions with depth, and particle sorting is not typical. As a result, no variation in the grain-size distribution with depth within mudboils should also be expected. Moreover, this lack of systematic behavior with depth may also extend to other mudboil features, including the characteristics of IM identified in this study.

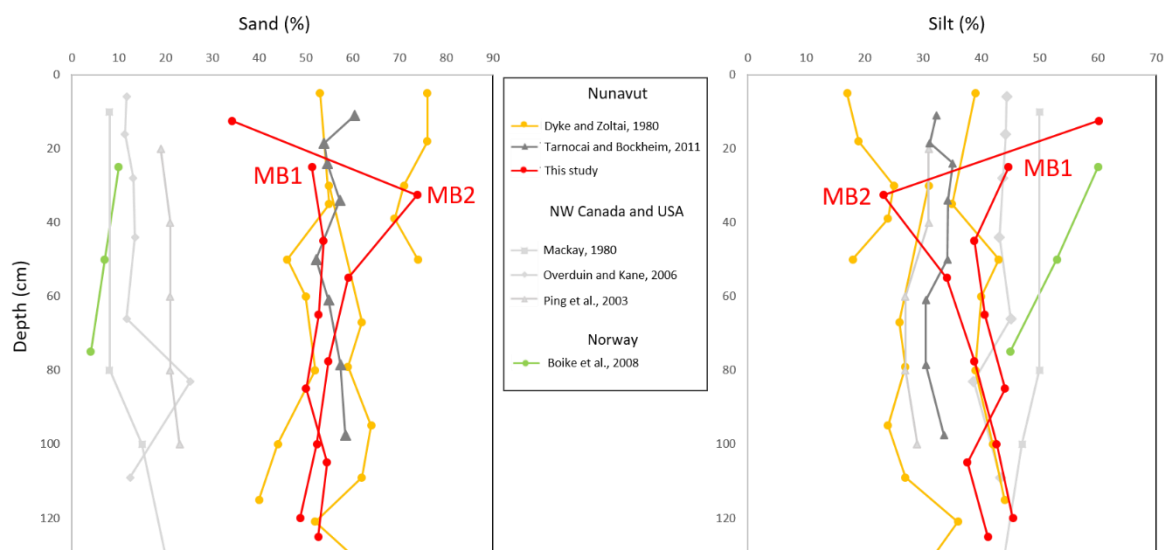


Figure I.32 Vertical grain-size profiles in mudboils from the Northern Hemisphere compared to the study area mudboils. Left, sand content. Right, silt content.

Till in permafrost has the greatest amount of scheelite and Fe-sulfides, and a high count of gold grains, distinct from the till sampled in the active layer. In the central part of a cryoturbation structure, the indicator minerals are mobilized towards the surface by a net upward movement which also causes their dilution by mixing weathered and weakly-altered till by freeze-thaw cycles. The relative depletion of sulfides in the active layer is caused by the partial destruction of sulfides by exposure in an oxidizing environment (Shilts, 1977; Klassen, 1995). Another factor potentially causing the difference in IM abundance between the active layer and permafrost is the expected increase of mineralization debris with depth closer to the ore-bedrock source (Miller, 1984; Sarala et al., 2007). However, the substantial variation observed over a depth of less than 1.5 m, when compared to the dispersal train system of the complete Amaruq mineral deposit, suggests that the variations in IM abundance between the active layer and the permafrost is primarily attributed to weathering enhanced by cryogenic processes within the active layer.

The observations from this study suggest that the distribution of indicator minerals in cryoturbated soils with a long-term circular soil motion is influenced by multiple factors. The dissimilar nature of both mudboils may be attributed to different cryogenic processes and/or distinct interactions with their respective natural environments, including original heterogeneity. Two main cryogenic mechanisms can be involved in mudboil activity: frost heave and periglacial loading (Washburn, 1956; Mackay, 1980; Van Vliet-Lanoë, 1985; 1991; Swanson et al., 1999, Peterson and Krantz, 2003; Vandenberghe, 2013; Peterson, 2011). MB1 does not show sorting and a diapir-like shape. These features are likely generated by the homogenization resulting from the continuous migration of fine-grained material from the bottom to the surface due to the thawing of ice-rich material above the permafrost. This suggests a major contribution of the periglacial loading process in MB1. In contrast, MB2 characteristics such as matrix grain size and gold grain sorting, a lack of lateral variation, and the presence of a finer texture layer on the top (5-20 cm), may indicate contributions of both frost heave and periglacial loading. Frost heave is recognized as the primary mechanism for generating grain size sorting in permafrost areas (Hallet, 2013), while the presence of the fine texture layer could be more associated with the migration of fine-grained material. However, the significance of frost heave may outweigh that of periglacial loading in MB2. Evidence of cryogenic fabric that would indicate frost heave was not found, which may be due to the low clay/silt ratio of the distal diamicton (Van Vliet-Lanoë, 1985). Regardless of the possible causes, this analysis suggests that shared characteristics (till unit) and environmental conditions (proximity) do not necessarily lead to the same characteristics and composition of material in mudboils.

1.7.3 Vertical fractionation of composition and IM

A difference in distal till features is evident between Trench 1 and Trench 2. Trench 1, experienced a lower level of cryoturbation, likely due to a thinner frost-susceptible layer, shows a distribution of till characteristics primarily associated with the inherent heterogeneity of till deposits. In contrast, Trench 2 exhibits significant evidence of cryoturbation, indicating that the characteristics of the till are primarily related to cryogenic activity.

Both mudboils in Trench 2 show relatively constant concentrations of major and some trace elements with depth, consistent with previous studies (Klassen, 1995; McMartin and McClenaghan, 2001; Spirito et al., 2011; McMartin and Campbell, 2009; de Bronac de Vazelhes, 2019). Nevertheless, slight variations in trace metals, including Ag, Ni, As, and Au, are observed with depth in the mudboil profiles (Fig. I.19b), similar to previously described vertical variations in trace metal concentration and U content in mudboils (Shilts, 1975; DiLabio 1979; Laurus and Fletcher, 1999, de Bronac de Vazelhes, 2019). These findings highlight the stable geochemical composition of the material in the active layer of mudboils, while the small fluctuations in certain trace metals suggest local influences such as redox conditions, weathering or organic matter presence. For instance, a decrease of Zn, Cu, Ni, and As content is observed in the highly oxidized 90-110 cm depth sample of MB2. The higher trace metal concentrations in the permafrost and the above gleyed horizon of this mudboil likely result from limited exposure to weathering at depth. In the active layer a correlation between the clay content and metal concentrations is observed (except Au), suggesting that metal cations released by weathering are adsorbed by clay minerals (Shilts, 1975; Klassen, 2001). Varying behavior of metals such as Cu, Zn and Mn with depth in mudboils may also reflect the presence of organic-rich material at depth (McMartin et al., 2000; McMartin and Campbell, 2009).

In contrast to the generally constant chemical concentrations with depth, particle sizes, pebble lithologies, IM characteristics (gold, scheelite, and Fe-sulfides) and gold content within the two cryoturbated till profiles (MB1 and MB2) exhibit variability but show no systematic patterns with depth suggesting that cryoturbation processes do not generate a uniform vertical fractionation. It is noteworthy that some mudboils may present sorting of particle sizes with depth, as shown in MB2, a phenomenon not observed in MB1 or in other mudboils studied in the Northern Hemisphere (Fig I.32).

The general trend observed of a slight increase in distal clast lithologies with depth within the active layer of both mudboils (Fig I.14) suggests some influence from cryoturbation processes on pebble distribution. In contrast to IM grain counts (< 2 mm) which do not show

uniform trends with depth, vertical sorting of the relatively large pebbles (5-9.5 mm) can be favored by the repetitive passage of a freezing front for larger clasts (Derbyshire et al., 1979). In addition, vertical variations in distal and local lithologies within mudboils may result from different physical characteristics of the lithologies, such as texture, rather than reflecting changes in their proximity to source (proximal or distal). Local rocks (i.e. volcanic and sedimentary rocks) in the trenches predominantly display fine grain-sizes textures, resulting in higher erosion and disintegration during glacial transport, whereas distal rocks (i.e. felsic intrusive rocks) exhibit coarse-grained textures and are more resistant to glacial transport.

Figure I.33 depicts variations in gold grain characteristics at various depths in both studied mudboils of Trench 2. Assuming that the composition of till in the permafrost reflects the closest gold grain sizes, morphology and abundance generated by glacial processes in distal till for this area, without postglacial modifications, any sample composition above the permafrost potentially reflects cryoturbation effects on the original gold grains characteristics and abundance, providing that the permafrost table has not been deeper in the past. Results show that cryoturbation potentially contributes to the most significant differences in gold grain counts and characteristics (shapes and sizes) between the two mudboils in the middle and deep part of the profiles (0.60-1.20 m), while the shallow part of the profiles (< 40 cm) shows less variations (Fig. I.33).

On the other hand, the observed trend of decreasing gold grain abundance in MB2 aligns with similar findings of decreasing gold concentrations in the till matrix of other mudboils in northern Canada (Laurus and Fletcher, 1999), suggesting a possible but small effect from cryoturbation in mudboils (Fig I.32). The concentration of gold measured in the till matrix in the active layers is mainly determined by the amount of fine-sized gold grains and gold inclusions in sulfides, rather than weather-scavenging process or enrichment in organic-rich layers (Laurus and Fletcher, 1999; McMartin, 2009). Consequently, a decrease in gold content in the till matrix is mostly related to a reduction on gold grain abundance.

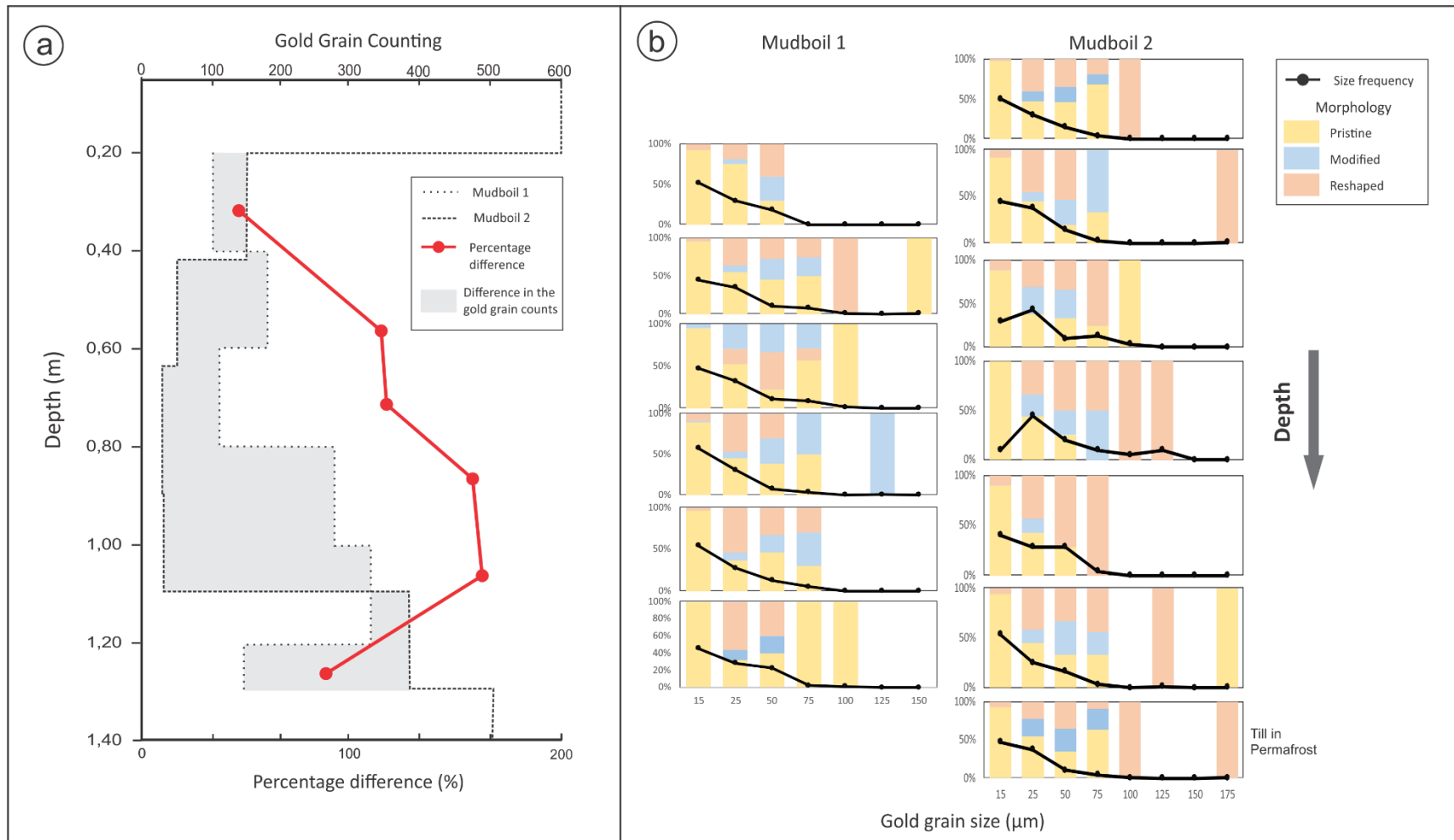


Figure I.33 Gold grains characteristics in the two mudboil profiles from Trench 2. a) Comparison of the gold grain abundance with the red line representing the percentage difference between the gold grain counts at specific depths; b) integration of the grain-size frequency with gold grain morphology

In summary, the results show that the vertical organization of till composition and IM in mudboils is influenced by many factors, including cryogenic mechanisms (Corte, 1962a; 1962b; Chamberlain, 1981; Derbyshire et al., 1979; Overduin and Kane, 2006; French, 2008) and additional factors such as till provenance, till matrix texture, particle shape, size and density, redox conditions, weathering, organic matter presence, and nature of transported clasts. These complex interactions lead to non-uniform arrangement compositional patterns within mudboils with depth, albeit with some discernible trends, as seen in this study.

1.7.4 Provenance of IM

No depth variations based on the potential provenance of the indicator minerals were identified in the till profiles (Figs I.25, I.29 and I.31). The provenance of gold based on fineness allows differentiation of two groups of grains likely not derived from the Amaruq deposit. The higher fineness gold grains values (>910) could be derived mostly from Archean greenstone-hosted deposits, orogenic deposits (with higher fineness gold values than Amaruq), and/or porphyry deposits (Fig. I.24b). However, there is no indication of porphyry mineralization in the region. In contrast, the source of the gold grains with the lowest fineness values (< 660) could be VMS and/or epithermal deposits (Fig. I.24b). Nevertheless, these ore deposit types are not known to be present in the area, although VMS deposits do have potential in greenstone belts. According to PLS-DA models (Liu and Beaudoin, 2021), the gold grains falling outside of the Amaruq deposit field are mostly associated with VMS and porphyry.

The scheelite PLS-DA model (Sciuba et al., 2020) allows for better differentiation of the provenance of scheelite grains compared to binary plots. It enables the identification of additional groups of scheelite grains originating from orogenic-type deposits distinct from Amaruq. Due to the lack of scheelite crystals between 0.25-2.00 mm, it is not possible to observe depth trends in all profiles. However, in the profiles where it is feasible, the lack of systematic distribution of grains from Amaruq, other orogenic deposits, or other mineral deposits becomes evident. For chalcopyrite, very few crystals were identified, and the current binary or ternary diagrams do not allow for a complete discrimination of the grains. However,

one grain has a composition that suggests a magmatic source. Depth trends could not be identified due to the lack of crystals.

The study suggests that cryoturbation mechanisms in till deposits do not generate sorting in the till column based on the mineral chemistry of each mineral species, even in some cases where significant variations in major elements occurs such as the fineness in gold grains.

1.7.5 Mineral exploration implications

Field sample collection in indicator mineral survey can be costly, especially in remote areas of Northern Canada. Consequently, research has focused on improving sampling techniques in permafrost terrains, with mudboils being common targets sites for till sampling (Shilts, 1978; McMartin and McClenaghan, 2001; McClenaghan et al., 2023)

To develop a practical guide for mineral exploration in permafrost areas, understanding the characteristics of indicator minerals, particularly in mudboils, is crucial. We propose a classification of materials based on the examination of IM in two mudboils from Trench 2 (Fig. 1.35). The central part of the mudboils, which exhibits the highest concentration of indicator minerals, is considered here (based on one lateral profile). Material at 5-20 cm depth in MB2 shows an enrichment of gold grains (greater than in permafrost), especially in the <15 μm size, along with an increase in pristine morphology proportions. However, additional samples within this depth range would be needed to fully comprehend the processes involved in this enrichment. Material in the 20-40 cm depth range demonstrates low variance in the abundance of IM in both mudboils. Despite having a lower content of IM compared to material in permafrost, this depth range still exhibits high abundance of IM. The gold grain size frequency and morphology proportions resemble those found in the till of permafrost. Material at a depth interval >40 cm exhibits a probable high variance in IM counts between both mudboils, with a potential decrease in abundance with depth, particularly in gold grains. There is also a significant variation in both gold grain sizes and morphology proportions among mudboils and compared to till in permafrost. This decrease in gold content at this depth aligns with the documented decrease in gold content in mudboils with a maximum depth of 0.80 m by Laurus and Fletcher (1999). Permafrost material (at variable depth)

displays the highest abundance of IM, likely representing the most original values unaffected by post-glacial processes. Notwithstanding, due to the limited number of mudboils analyzed, further studies are necessary to assess the broad generalization of this classification of material by depth.

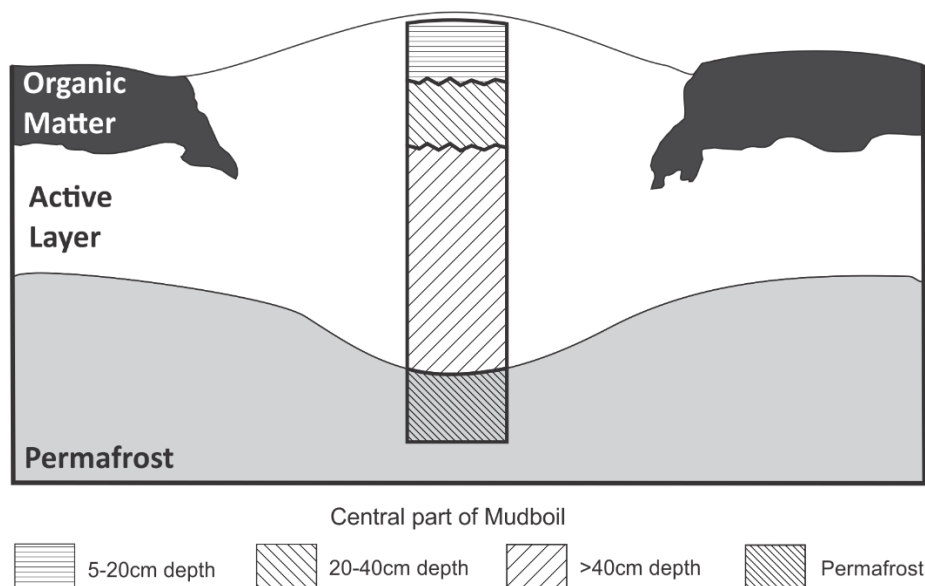


Figure I.34 Summary of a proposed classification of materials by depth based on the IM nature in the two mudboils analyzed in Trench 2.

Based on our study, we propose preferential sampling depths within mudboils using the subdivision by depth developed in Fig. I.34, considering factors such as: 1) ease of sampling, 2) resemblance to undisturbed IM characteristics after glacial deposition, 3) significant and representative abundance, 4) potential variation in IM abundance among mudboils, and 5) weathering grade. The recommended depth is between 20-40 cm, followed by the permafrost layer, while the deeper part of the mudboil (>40 cm depth) is the least recommended. We discourage sampling from the lateral parts of the mudboils. It should be noted that the shallowest sample of MB2 has not been considered, as no other sample with a similar depth is available. Further investigations are required to determine whether the 5-20 cm depth would present more appropriate conditions for IM sampling.

References

- Aylsworth, J. M. and Shilts, W. W. (1989): Glacial features around the Keewatin Ice divide: districts of MacKenzie and Keewatin. Geological Survey of Canada, Paper 88-24, 21 pp.
- Berman, R. G., Sanborn-Barrie, M., Rayner, N., Carson, C., Sandeman, H. A., and Skulski, T. (2010). Petrological and in situ SHRIMP geochronological constraints on the tectonometamorphic evolution of the Committee Bay belt, Rae Province, Nunavut. *Precambrian Research*, 181(1-4), 1-20.
- Biskaborn, B. K., Smith, S. L., Noetzli, J., Matthes, H., Vieira, G., Streletskiy, D. A., ... and Lantuit, H. (2019). Permafrost is warming at a global scale. *Nature communications*, 10(1), 264.
- Boike, J., Ippisch, O., Overduin, P. P., Hagedorn, B., and Roth, K. (2008). Water, heat and solute dynamics of a mud boil, Spitsbergen. *Geomorphology*, 95(1-2), 61-73.
- Boulianne-Verschelden, N., De Bronac de Vazelhes, V., McMartin, I., and Beaudoin, G., (2022). Surficial geology, Amaruq deposit area, Kivalliq Region, Nunavut, NTS 66-H southeast; Geological Survey of Canada, Canadian Geoscience Map 441, scale 1:50 000. <https://doi.org/10.4095/329418>
- Boulianne-Verschelden, N., De Bronac de Vazelhes, V., McMartin, I. et Beaudoin, G., (2019). Cartographie du Quaternaire dans la région du gisement Amaruq, Nunavut; Commission géologique du Canada, Dossier public 8651, 1 fichier .zip. central mainland Nunavut and northern Manitoba; Geological Survey of Canada, Open File 8921, 1 .zip file.
- Caraballo, E. (2023). Composition en éléments traces de la chalcopyrite: Son potentiel comme minéral indicateur et les implications dans l'exploration minière. Ph.D. thesis, Université Laval, 457p.
- Chamberlain, E. J. (1981). Frost susceptibility of soil, review of index tests. Cold Regions Research and Engineering Lab Hanover NH.
- Corte, A. E. (1962a). The frost behavior of soils. I. Vertical sorting. Highway Research Board Bulletin, (317).
- Corte, A. E. (1962b). Vertical migration of particles in front of a moving freezing plane. *Journal of Geophysical Research*, 67(3), 1085-1090.
- Côté-Mantha, O., Gosselin, G., Vaillancourt, D., Blackburn, A., (2017). The Amaruq deposits – building a customized toolset and using a flexible geomodel: optimization from discovery to mine development. In: In: Tschihart, V. and Thomas, M. D. (Eds) Proceedings of Exploration 17: Sixth Decennial International Conference on Mineral Exploration, pp. 553–567.
- de Bronac de Vazelhes, V., Beaudoin, G., McMartin, I., Côté-Mantha, O., and Boulianne-Verschelden, N. (2021). Assessment of the Amaruq gold deposit signature in glacial sediments using multivariate geochemical data analysis and indicator minerals. *Journal of Geochemical Exploration*, 228, 106800. <https://doi.org/10.1016/j.gexplo.2021.106800>
- de Bronac de Vazlhés, V., (2019). Étude de la dispersion d'un gisement d'or dans les sédiments glaciaires: le cas d'Amaruq (Nunavut, Canada). Master thesis. Université Laval.
- Derbyshire, E. Gregory, K.J. Hails, J.R. (1979). *Geomorphological processes*. London, Wm Dawson & Sons, Ltd.

DiLabio, R. N. W. (1991). Classification and interpretation of the shapes and surface textures of gold grains from till. (N.o 90-1C; pp. 90-1C).

DiLabio, R. N. W., and Shilts, W. W. (1979). Composition and dispersal of debris by modern glaciers, Bylot Island, Canada. *Moraines and Varves. Balkema. Rotterdam*, 146-155.

Dreimanis, A. (1989). Tills: their genetic terminology and classification. *Genetic classification of glacial deposits*, 17-83.

Duran, C. J., Barnes, S. J., and Corkery, J. T. (2015). Chalcophile and platinum-group element distribution in pyrites from the sulfide-rich pods of the Lac des Iles Pd deposits, Western Ontario, Canada: Implications for post-cumulus re-equilibration of the ore and the use of pyrite compositions in exploration. *Journal of Geochemical Exploration*, 158, 223-242.

Duran, C. J., Dubé-Loubert, H., Pagé, P., Barnes, S.-J., Roy, M., Savard, D., Cave, B. J., Arguin, J.-P., and Mansur, E. T. (2019). Applications of trace element chemistry of pyrite and chalcopyrite in glacial sediments to mineral exploration targeting: Example from the Churchill Province, northern Quebec, Canada. *Journal of Geochemical Exploration*, 196, 105-130.

Dyke, A. S., and Dredge, L. A. (1989). Quaternary geology of the northwestern Canadian Shield.

Dyke, A. S., and Zoltai, S. C. (1980). Radiocarbon-dated mudboils, central Canadian Arctic. Geological Survey of Canada Paper, 80, 271-275.

Dyke, A.S., (2004). An outline of North American deglaciation with emphasis on central and northern Canada. *Developments in Quaternary Sciences* 2, 373–424.

French, H. M. (2018). The periglacial environment. John Wiley & Sons.

George, L. L., Cook, N. J., Crowe, B. B., and Ciobanu, C. L. (2018). Trace elements in hydrothermal chalcopyrite. *Mineralogical Magazine*, 82(1), 59-88.

Girard, I., Klassen, R. A., and Laframboise, R. R. (2004). Sedimentology laboratory manual. *Terrain Sciences Division*, 1.

Girard, R., Tremblay, J., Néron, A., Longuépée, H., and Makvandi, S. (2021). Automated Gold Grain Counting. Part 2: What a Gold Grain Size and Shape Can Tell! *Minerals*, 11(4), Art. 4.

Hagedorn, B., Aalto, R., Sletten, R. S., and Hallet, B. (2008). Frost boil dynamics using ²¹⁰Pb as a tracer for soil movement. In *Proceedings of the Ninth International Conference on Permafrost—Fairbanks, Alaska* (pp. 613-618).

Hallet, B. (2013). Stone circles: form and soil kinematics. *Philosophical Transactions of the Royal Society A: Mathematical, Physical and Engineering Sciences*, 371(2004), 20120357.

Hallet, B., and Waddington, E. D. (2020). Buoyancy forces induced by freeze-thaw in the active layer: implications for diapirism and soil circulation. In *Periglacial geomorphology* (pp. 251-279). Routledge.

Hrabi, R. B., Barclay, W. A., Fleming, D. and Alexander, R. B. (2003). Structural evolution of the Woodburn Lake group in the area of the Meadowbank gold deposit, Nunavut; Geological Survey of Canada, Current Research 2003-C27, 10 p.

Hugelius, G., Kuhry, P., Tarnocai, C., and Virtanen, T. (2010). Soil organic carbon pools in a periglacial landscape: a case study from the central Canadian Arctic. *Permafrost and Periglacial Processes*, 21(1), 16-29.

Jahn A. (1968). Patterned ground. In R.W. Fairbridge (ed.): Encyclopedia of geomorphology. Pp. 814-817. New York, Reinhold

Janvier, V., Castonguay, S., Mercier-Langevin, P., Dubé, B., McNicoll, V., Pehrsson, S., Malo, M., De Chavigny, B., Côté-Mantha, O., (2015). Preliminary results of the geology of the portage deposit, Meadowbank Gold Mine, Churchill Province, Nunavut. Geological Survey of Canada, Current Research 2015-2, 21

Jefferson, C.W., White, J.C., Young, G.M., Patterson, J., Tschirhart, V.L., Pehrsson, S.J., Calhoun, L., Rainbird, R.H., Peterson, T.D., Davis, W.J., Tella, S., Chorlton, L.B., Scott, J.M.J., Percival, J.A., Morris, W.A., Keating, P., Anand, A., Shelat, Y., MacIsaac, D., (2015). Outcrop and Remote Predictive Geology of the Amer Belt and Basement Beside and Beneath the Northeast Thelon Basin, in Parts of NTS 66-A, B, C, F, G and H, Kivalliq Region, Nunavut. Geological Survey of Canada, Open File 7242.

Klassen, R. A. (1995). Drift Composition and Glacial Dispersal Trains, Baker Lake Area, District of Keewatin, Northwest Territories. Geological Survey of Canada, Bulletin 485

Klassen, R. A. (2001). The interpretation of background variation in regional geochemical surveys—an example from Nunavut, Canada. *Geochemistry: Exploration, Environment, Analysis*, 1(2), 163-173.

Kokelj, S. V., Burn, C. R., and Tarnocai, C. (2007). The structure and dynamics of earth hummocks in the subarctic forest near Inuvik, Northwest Territories, Canada. *Arctic, Antarctic, and Alpine Research*, 39(1), 99-109.

Laurus, K. A., and Fletcher, W. K. (1999). Gold distribution in glacial sediments and soils at Boston Property, Nunavut, Canada. *Journal of Geochemical Exploration*, 67(1-3), 271-285.

Lauzon, M.-C., Mercier-Langevin, P., Valette, M., Beaudoin, G., De Souza, S., Côté-Mantha, O., Simard, M., (2020). Ore mineralogy and mineral chemistry of the Whale Tail zone, Amaruq gold deposit, Nunavut; in Targeted Geoscience Initiative 5: Contributions to the Understanding of Canadian Gold Systems, (ed.) P. Mercier-Langevin, C.J.M. Lawley, and S. Castonguay; Geological Survey of Canada. Open File 8712, 267–279.

Liu, H., and Beaudoin, G. (2021). Geochemical signatures in native gold derived from Au-bearing ore deposits. *Ore Geology Reviews*, 132, 104066. <https://doi.org/10.1016/j.oregeorev.2021.104066>

Liu, H., Beaudoin, G., Makvandi, S., Jackson, S. E., and Huang, X. (2021). Multivariate statistical analysis of trace element compositions of native gold from orogenic gold deposits: implication for mineral exploration. *Ore Geology Reviews*, 131, 104061.

Mackay, J. R. (1980). The origin of hummocks, western Arctic coast, Canada. *Canadian Journal of Earth Sciences*, 17(8), 996-1006.

Manégli, N., Beaudoin, G., and Simard, M. (2018). Indicator minerals of the Meliadine orogenic gold deposits, Nunavut (Canada), and application to till surveys. *Geochemistry: Exploration, Environment, Analysis*, 18(3), 241-251.

Mansur, E.T., Barnes, S.J. and Duran, C.J. (2021). An overview of chalcophile element contents of pyrrhotite, pentlandite, chalcopyrite, and pyrite from magmatic Ni-Cu-PGE sulfide deposits. *Miner Deposita* 56, 179–204.

McClenaghan, M. B., Paulen, R. C., Smith, I. R., Rice, J. M., Plouffe, A., McMartin, I., Campbell, J.E., Lehtonen, M., Parsasadr, M., and Beckett-Brown, C. E. (2023). Review of till geochemistry and indicator mineral methods for mineral exploration in glaciated terrain. *Geochemistry: Exploration, Environment, Analysis*, geochem2023-013.

McClenaghan, M.B. and Paulen, R.C. (2018). Mineral Exploration in Glaciated Terrain, Chapter 20. In: Menzies, J. and van der Meer J.J-M. (eds) Past Glacial Environments (Sediments, Forms and Techniques) A new & revised edition. Elsevier, 689–751.

McClenaghan, M.B., Plouffe, A., McMartin, I., Campbell, J.E., Spirito, W.A., Paulen, R.C., Garrett, R.G. and Hall, G.E.M. (2013). Till sampling and geochemical analytical protocols used by the Geological Survey of Canada. *Geochemistry: Exploration, Environment, Analysis*, 13, 285–301.

McMartin, I., and McClenaghan, M. B. (2001). Till geochemistry and sampling techniques in glaciated shield terrain: A review. Geological Society, London, Special Publications, 185(1), 19-43.

McMartin, I. and Campbell J.E. (2009). Near-surface till sampling protocols in shield terrain, with examples from western and northern Canada. In: R.C. Paulen and I. McMartin (eds.), Application of Till and Stream Sediment Heavy Mineral and Geochemical Methods to Mineral Exploration in Western and Northern Canada; Geological Association of Canada, GAC Short Course Notes 18, p. 75-95.

McMartin, I., Gauthier, M.S., and Page, A.V., (2022). Updated postglacial marine limits along western Hudson Bay, central mainland Nunavut and northern Manitoba. Geological Survey of Canada, Open File 8921.

McMartin, I., Godbout, P. M., Campbell, J. E., Tremblay, T., and Behnia, P. (2021). A new map of glacial features and glacial landsystems in central mainland Nunavut, Canada. *Boreas*, 50(1), 51-75.

McMartin, I., Hall, G. E. M., Kerswill, J. A., Sangster, A. L. and Valve, J. (2000). Mercury cycling in perennially frozen soils of Arctic Canada, Kaminak Lake area, Nunavut. In: Proceedings of the 25th Anniversary International Conference on Heavy Metals in the Environment. University of Michigan, USA.

McMartin, I. and Henderson, P., (2004). Evidence from Keewatin (central Nunavut) for paleo-ice divide migration. *Geog. Phys. Quatern.* 58 (2–3), 163–186

Mendizabal, A. (2022). Étude de la composition des minéraux indicateurs et de la géochimie du till en aval d'un gisement d'or : Le cas d'Amaruq (Nunavut, Canada). mémoire de maîtrise, Université Laval.

Miller, J.K. (1984). Model for clastic indicator trains in till: Prospecting in Areas of Glaciated Terrain. *The Institution of Mining and Metallurgy, London.* pp. 69–77.

Morrison, G. W., Rose, W. J., and Jaireth, S. (1991). Geological and geochemical controls on the silver content (fineness) of gold in gold-silver deposits. *Ore Geology Reviews*, 6(4), 333-364.

Overduin, P. P., and Kane, D. L. (2006). Frost boils and soil ice content: Field observations. *Permafrost and Periglacial Processes*, 17(4), 291-307.

Palarea-Albaladejo, J., and Martín-Fernández, J. A. (2015). zCompositions—R package for multivariate imputation of left-censored data under a compositional approach. *Chemometrics and Intelligent Laboratory Systems*, 143, 85-96.

Pehrsson, S. J., Berman, R. G., Eglington, B., and Rainbird, R. (2013). Two Neoproterozoic supercontinents revisited: The case for a Rae family of cratons. *Precambrian Research*, 232, 27-43.

Peterson, R. A. (2011). Assessing the role of differential frost heave in the origin of non-sorted circles. *Quaternary Research*, 75(2), 325-333.

Peterson, R. A., and Krantz, W. B. (2003). A mechanism for differential frost heave and its implications for patterned-ground formation. *Journal of Glaciology*, 49(164), 69-80.

Peterson, R. A., Walker, D. A., Romanovsky, V. E., Knudson, J. A., Raynolds, M. K., and Krantz, W. B. (2003). A differential frost heave model: cryoturbation-vegetation interactions. In *Proceedings of the eighth international conference on permafrost (Vol. 2, pp. 885-890)*. Lisse, Zurich, Switzerland: AA Balkema.

Ping, C. L., Michaelson, G. J., Overduin, P. P., and Stiles, C. A. (2003). Morphogenesis of frost boils in the Galbraith Lake area, Arctic Alaska. In *Proceedings of the Eighth International Conference on Permafrost, Zürich, Switzerland (pp. 897-900)*.

Plouffe, A., McClenaghan, M. B., Paulen, R. C., McMartin, I., Campbell, J. E., and Spirito, W. A. (2013). Processing of glacial sediments for the recovery of indicator minerals: protocols used at the Geological Survey of Canada. *Geochemistry: Exploration, Environment, Analysis*, 13(4), 303-316.

Pollard, W. (2018). Periglacial processes in glacial environments. In *Past Glacial Environments (pp. 537-564)*. Elsevier.

R Core Team (2022). R: A language and environment for statistical computing. R Foundation for Statistical Computing, Vienna, Austria. URL <https://www.R-project.org/>. Sarala, 2007

Sarala, P., Nykänen, V., Sarapää, O., Peltoniemi, A., and Ojala, J. (2007). Quaternary geological and till geochemical studies in verifying GIS-based prospectivity mapping in the Central Lapland Greenstone Belt, northern Finland. In 23rd International Applied Geochemistry Symposium (IAGS): Exploring our environment, Oviedo, Spain (pp. 14-19).

Sciuba, M. (2020). *Texture and composition of scheelite, tourmaline and rutile in orogenic gold deposits* (Doctoral dissertation, Université Laval).

Sciuba, M., Beaudoin, G., Grzela, D., and Makvandi, S. (2020). Trace element composition of scheelite in orogenic gold deposits. *Mineralium Deposita*, 55, 1149-1172.

Sherlock, R., Pehrsson, S., Logan, A.V., Hrabí, R.B., Davis, W.J., 2004. Geological setting of the Meadowbank Gold Deposits, Woodburn Lake Group, Nunavut. *Explor. Min. Geol.* 13 (1–4), 67–107.

Shilts, W. W. (1973). Drift prospecting; geochemistry of eskers and till in permanently frozen terrain: District of Keewatin; Northwest Territories.

Shilts, W. W. (1975). Principles of geochemical exploration for sulphide deposits using shallow samples of glacial drift. *Canadian Institute of Mining and Metallurgy, Bulletin* 68, 73-80.

Shilts, W. W. (1977). Geochemistry of till in perennially frozen terrain of the Canadian Shield—Application to prospecting. *Boreas*, 6(2), 203-212.

Shilts, W. W. (1978). Nature and genesis of mudboils, central Keewatin, Canada. *Canadian Journal of Earth Sciences*, 15(7), 1053-1068.

Shilts, W.W. (1996). Drift exploration. In: Menzies, J. (ed.) *Past Glacial Environment: Sediments, Forms and Techniques*, Butterworth-Heinemann Ltd., *Glacial Environment: Volume 2*, Oxford, 411–439.

Shilts, W. W., Aylsworth, J. M., Kaszycki, C. A., and Klassen, R. A. (1987). Canadian shield. *Geomorphic Systems of North America*, 2, 119-161.

Shilts, W.W., Aylsworth, J. M., Kaszycki, C. A., and Klassen, R. A. (1987): Canadian Shield. In Graf, W. L. (ed.): *Geomorphic systems of North America*, 119–161. Centennial Special Volume 2, Geological Society of America.

Soil Classification Working Group, National Research Council Canada, Canada. Agriculture, & Agri-Food Canada. Research Branch. (1998). *The Canadian system of soil classification* (No. 1646). NRC Research. Spirito, W.A., McClenaghan, M. B., Plouffe, A. et al. 2011. Till sampling and analytical protocols for GEM projects: From field to archive. Geological Survey of Canada, Open File 6850.

Spirito, W. A., McClenaghan, M. B., Plouffe, A., McMartin, I., Campbell, J. E., Paulen, R. C., and Hall, G. E. M. (2011). Till sampling and analytical protocols for GEM projects: From field to archive. Geological Survey of Canada, Open File 6850.

Swanson, D. K., Ping, C. L., and Michaelson, G. J. (1999). Diapirism in soils due to thaw of ice-rich material near the permafrost table. *Permafrost and Periglacial Processes*, 10(4), 349-367.

Tarnocai, C., and Bockheim, J. (2011). Cryosolic soils of Canada: genesis, distribution, and classification. *Canadian journal of soil science*, 91(5), 749-762.

Thiffault, E. (2019). Boreal forests and soils. In *Developments in Soil Science* (Vol. 36, pp. 59-82). Elsevier.

Utting, D. J. and McMartin, I. (2004). Ice-movement Indicator Mapping North of the Keewatin Ice Divide, Meadowbank Area, Nunavut. Geological Survey of Canada, Current Research 2004-C8, 6,

Valette, M., De Souza, S., Mercier-Langevin, P., Coté-Mantha, O., Simard, M., Wodicka, N., McNicoll, V.J., and Barbe, P., (2020). Lithological and tectonic controls on banded iron formation-associated gold at the Amaruq deposit, Churchill Province, Nunavut, and implications for exploration; in Targeted Geoscience Initiative 5: Contributions to the Understanding of Canadian Gold Systems, (ed.) P. Mercier-Langevin, C.J.M. Lawley, and S. Castonguay; Geological Survey of Canada, Open File 8712, p. 251–266.

Valette, M., De Souza, S., Mercier-Langevin, P., McNicoll, V.J., Wodicka, N., Creaser, R. A., Cote-Mantha, O., Simard, M., (2019). Geological setting of the 5.2 Moz au Amaruq banded iron formation-hosted gold deposit, Churchill Province, Nunavut. In: Rogers, N. (Ed.), Targeted Geoscience Initiative: 2018 Report of Activities, Geological Survey of Canada, Open File, vol. 8549, pp. 83–87.

Van Vliet-Lanoë, B. (1985). Frost effects in soils. *Soils and quaternary landscape evolution*, 117, 158.

Van Vliet-Lanoë, B. (1991). Differential frost heave, load casting and convection: converging mechanisms; a discussion of the origin of cryoturbations. *Permafrost and periglacial processes*, 2(2), 123-139.

Van Vliet-Lanoë, B., Coutard, J. P., and Pissart, A. (1984). Structures caused by repeated freezing and thawing in various loamy sediments: a comparison of active, fossil and experimental data. *Earth Surface Processes and Landforms*, 9(6), 553-565.

Vandenberghe, J. (1988). Cryoturbations. *Advances in Periglacial Geomorphology*. Wiley

Vandenberghe, J. (2013). Cryoturbation structures. *Encyclopedia of Quaternary Science*, 3, 430-435.

Walker, D. A., Epstein, H. E., Gould, W. A., Kelley, A. M., Kade, A. N., Knudson, J. A., and Shur, Y. (2004). Frost-boil ecosystems: complex interactions between landforms, soils, vegetation and climate. *Permafrost and Periglacial Processes*, 15(2), 171-188.

Washburn, A. L. (1956). Classification of patterned ground and review of suggested origins. *Geological Society of America Bulletin*, 67(7), 823-866.

Zoltai, S. C. (1995). Permafrost distribution in peatlands of west-central Canada during the Holocene warm period 6000 years BP. *Géographie physique et Quaternaire*, 49(1), 45-54.

Zoltai, S. C., and Tarnocai, C. (1981). Some nonsorted patterned ground types in northern Canada. *Arctic and Alpine Research*, 13(2), 139-151.

Conclusion

Results collected in two trenches in glacial sediments from the proximal part of the Amaruq gold dispersal train in Nunavut demonstrates that glacial and postglacial processes are complex and can lead to considerable changes in the dispersal patterns of a mineral deposit. In this study, we adopted a multidisciplinary approach that includes Quaternary geology knowledge, till geochemistry and indicator mineral methods, combined with field observations of cryogenic features, essential in drift prospecting campaigns in the northern part of Canada underlain by permafrost. This approach allows for an understanding of dispersal trains across different till deposits, which are associated with distinct glacial dynamics, and for assessing the potential effects of cryoturbation on the composition of the surface till.

The texture of the till is a major factor that governs cryoturbation. The distinct textural properties of the two till units identified (i.e., coarse-grained proximal till and fine-grained distal till) hinders the formation of a mixture through cryoturbation when both units are superimposed (distal over proximal). However, the seasonal freezing-thawing action does generate an interaction between the two till units, which can be observed on the surface through the development of sorted circles and minor mudboils (non-sorted circles). In addition, features of both till units, overlying and underlying, can be identified at the surface. The fine-grained distal till favors the development of cryoturbation features (i.e. mudboils) as it is more-frost susceptible.

Cryoturbation processes in the active layer affect considerably the abundance of some minerals that, although resistant to chemical weathering, shows a relative decrease in counts compared to permafrost. On the other hand, cryoturbation structures, characterized by long-term circular soil motion, do not generate a systematic arrangement of indicator minerals throughout the till column. Furthermore, the distribution of gold grain characteristics, including size, morphology, and mineral chemistry, lacks a consistent pattern with depth. It is worth mentioning that cryoturbation processes in some mudboils may lead to the sorting of gold grains based on their size, as reflected in MB2, which is associated with proportions of grain shape. This sorting process can result in a decrease of gold grains with depth,

consequently disturbing the gold content along vertical profiles as documented by other authors. Notwithstanding, it is important to note that not all mudboils demonstrate this gold-sorted profile and consistent arrangement of grain-size particles across different depths, as shown by MB1. Due to the limited number of mudboils analyzed, further studies are required to assess the broad applicability of the differentiated layers and indicator mineral distributions identified.

The nature of the indicator minerals identified in the mudboils of the Amaruq deposit area provides valuable insights for identifying optimal sites within mudboils for till sampling. Among these, the 20-40 cm depth range is recommended for several reasons. Firstly, accessibility, compared to permafrost, of reaching the 20-40 cm depth range within mudboils is relatively easier facilitating more efficient sampling procedures. Secondly, this range exhibits a significant amount of indicator minerals which enhances the probability of successful identification and analysis. Moreover, the mineral abundance within the 20-40 cm depth range displays less variability compared to other depths. This simplifies the comparison of results. Finally, the characteristics of the indicator minerals found at this depth show similarities to those observed after glacial deposition unaffected by postglacial processes (in permafrost). This resemblance suggests that the mineral features at this depth are more likely to reflect the influence of glacial processes. Notwithstanding, additional research is required to evaluate the wide-ranging applicability of this categorization of IM based on their depth.

Bibliography

Andrews-Jones, D. A. (1968). The application of geochemical techniques to mineral exploration. Colorado School of Mines. Mineral industries bulletin, Vol. 11 No. 6

Averill, S. A., and Huneault, R. (1991). Using silt-sized visible gold grains to explore for gold deposits concealed by Quaternary overburden: Nevada vs. Canada: *Explore*, 72(1), 10-12.

Averill, S. A., MacDonald, D. R., and Mills, K. A. (1988). Regional variations in the gold content of till in Canada. In *Prospecting in Areas of Glaciated Terrain* (Vol. 1, pp. 14-20). Montréal, QC, Canada: Canadian Institute of Mining and Metallurgy.

Aylsworth, J. M. and Shilts, W. W. (1989): Glacial features around the Keewatin Ice divide: districts of MacKenzie and Keewatin. Geological Survey of Canada, Paper 88-24, 21 pp.

Batterson, M.J. (1989). Till geochemistry of the Letitia Lake area (NTS 13L/1), Labrador. Newfoundland Department of Mines and Energy Open File (L) 13L/0069.

Beaudoin, G., Dupuis, C., Gosselin, P., and Jébrak, M. (2007). Mineral chemistry of iron oxides: application to mineral exploration. In Ninth Biennial SGA meeting, SGA, Dublin (pp. 497-500).

Becher, M., Olid, C., and Klaminder, J. (2013). Buried soil organic inclusions in non-sorted circles fields in northern Sweden: Age and paleoclimatic context. *Journal of Geophysical Research: Biogeosciences*, 118(1), 104-111.

Belousova, E. A., Griffin, W. L., O'Reilly, S. Y., and Fisher, N. I. (2002). Apatite as an indicator mineral for mineral exploration: trace-element compositions and their relationship to host rock type. *Journal of Geochemical Exploration*, 76(1), 45-69.

Berman, R. G., Sanborn-Barrie, M., Rayner, N., Carson, C., Sandeman, H. A., and Skulski, T. (2010). Petrological and in situ SHRIMP geochronological constraints on the tectonometamorphic evolution of the Committee Bay belt, Rae Province, Nunavut. *Precambrian Research*, 181(1-4), 1-20.

Beus, A. A., and Grigorian, S. V. (1977). *Geochemical exploration methods for mineral deposits*. Applied Publishing Ltd., USA, 31-270.

Biskaborn, B. K., Smith, S. L., Noetzli, J., Matthes, H., Vieira, G., Streletskiy, D. A., and Lantuit, H. (2019). Permafrost is warming at a global scale. *Nature communications*, 10(1), 264. Boike, J., Ippisch, O., Overduin, P. P., Hagedorn, B., and Roth, K. (2008). Water, heat and solute dynamics of a mud boil, Spitsbergen. *Geomorphology*, 95(1-2), 61-73.

Boike, J., Ippisch, O., Overduin, P. P., Hagedorn, B., and Roth, K. (2008). Water, heat and solute dynamics of a mud boil, Spitsbergen. *Geomorphology*, 95(1-2), 61-73.

Boulianne-Verschelden, N., De Bronac de Vazelhes, V., McMartin, I. et Beaudoin, G., (2019). Cartographie du Quaternaire dans la région du gisement Amaruq, Nunavut; Commission géologique du Canada, Dossier public 8651, 1 fichier .zip.

Boulianne-Verschelden, N., De Bronac de Vazelhes, V., McMartin, I., and Beaudoin, G., (2022). Surficial geology, Amaruq deposit area, Kivalliq Region, Nunavut, NTS 66-H southeast; Geological Survey of Canada, Canadian Geoscience Map 441, scale 1:50 000.

Caraballo, E. (2023). Composition en éléments traces de la chalcopirite: Son potentiel comme minéral indicateur et les implications dans l'exploration minérale. Ph.D. thesis, Université Laval, 457p.

Chamberlain, E. J. (1981). Frost susceptibility of soil, review of index tests. Cold Regions Research and Engineering Lab Hanover NH.

Chapman, R. J., Leake, R. C., Bond, D. P. G., Stedra, V., and Fairgrieve, B. (2009). Chemical and Mineralogical Signatures of Gold Formed in Oxidizing Chloride Hydrothermal Systems and their Significance within Populations of Placer Gold Grains Collected during Reconnaissance. *Economic Geology*, 104(4), 563-585. <https://doi.org/10.2113/gsecongeo.104.4.563>

Chapman, R. J., Leake, R. C., Moles, N. R., Earls, G., Cooper, C., Harrington, K., and Berzins, R. (2000). The application of microchemical analysis of alluvial gold grains to the understanding of complex local and regional gold mineralization: a case study in the Irish and Scottish Caledonides. *Economic Geology*, 95(8), 1753-1773.

Chapman, R. J., Moles, N. R., Bluemel, B., and Walshaw, R. D. (2022). Detrital gold as an indicator mineral. *Geological Society, London, Special Publications*, 516(1), 313-336. <https://doi.org/10.1144/SP516-2021-47>

Chapman, R.J., Banks, D.A. and Spence-Jones, C. (2017): Detrital gold as a deposit-specific indicator mineral, British Columbia: analysis by laser-ablation inductively coupled plasma–mass spectrometry; in *Geoscience BC Summary of Activities 2016*, Geoscience BC, Report 2017-1, p. 201–212.

Corte, A. E. (1962a). Vertical migration of particles in front of a moving freezing plane. *Journal of Geophysical Research*, 67(3), 1085-1090.

Corte, A. E. (1962b). The frost behavior of soils. I. Vertical sorting. *Highway Research Board Bulletin*, (317).

Corte, A. E. (1963). Particle sorting by repeated freezing and thawing. *Science*, 142(3591), 499-501.

Côté-Mantha, O., Gosselin, G., Vaillancourt, D., Blackburn, A., (2017). The Amaruq deposits – building a customized toolset and using a flexible geomodel: optimization from discovery to mine development. In: In: Tschihart, V. and Thomas, M. D. (Eds) *Proceedings of Exploration 17: Sixth Decennial International Conference on Mineral Exploration*, pp. 553–567.

de Bronac de Vazelhes, V. (2019). Étude de la dispersion d'un gisement d'or dans les sédiments glaciaires: le cas d'Amaruq (Nunavut, Canada). mémoire de maîtrise, Université Laval.

de Bronac de Vazelhes, V., Beaudoin, G., McMartin, I., Côté-Mantha, O., and Boulianne-Verschelden, N. (2021). Assessment of the Amaruq gold deposit signature in glacial sediments using multivariate geochemical data analysis and indicator minerals. *Journal of Geochemical Exploration*, 228, 106800.

Derbyshire E., Gregory K.J., Hails J.R., (1979). 5 - Cryonival and Glacial Processes, *Geomorphological Processes*, Butterworth-Heinemann, Pages 187-285, ISBN 9780408107358,

Derbyshire, E. Gregory, K.J. Hails, J.R. (1979). *Geomorphological processes*. London, Wm Dawson & Sons, Ltd.

- Dilabio, R. N. W. (1991). Classification and interpretation of the shapes and surface textures of gold grains from till. (N.o 90-1C; pp. 90-1C).
- Dilabio, R. N. W., and Shilts, W. W. (1979). Composition and dispersal of debris by modern glaciers, Bylot Island, Canada. *Moraines and Varves. Balkema. Rotterdam*, 146-155.
- Duran, C. J., Barnes, S. J., and Corkery, J. T. (2015). Chalcophile and platinum-group element distribution in pyrites from the sulfide-rich pods of the Lac des Iles Pd deposits, Western Ontario, Canada: Implications for post-cumulus re-equilibration of the ore and the use of pyrite compositions in exploration. *Journal of Geochemical Exploration*, 158, 223-242.
- Duran, C. J., Dubé-Loubert, H., Pagé, P., Barnes, S.-J., Roy, M., Savard, D., Cave, B. J., Arguin, J.-P., and Mansur, E. T. (2019). Applications of trace element chemistry of pyrite and chalcopyrite in glacial sediments to mineral exploration targeting: Example from the Churchill Province, northern Quebec, Canada. *Journal of Geochemical Exploration*, 196, 105-130.
- Dyke, A. S., and Dredge, L. A. (1989). Quaternary geology of the northwestern Canadian Shield.
- Dyke, A. S., and Zoltai, S. C. (1980). Radiocarbon-dated mudboils, central Canadian Arctic. Geological Survey of Canada Paper, 80, 271-275.
- Dyke, A.S., (2004). An outline of North American deglaciation with emphasis on central and northern Canada. *Developments in Quaternary Sciences* 2, 373–424.
- Eggington, P. A. (1979). Mudboil activity, central District of Keewatin. In: Current Research. Part B, Geological Survey of Canada, Paper 79-1B, 349-356.
- French, H. M. (2018). The periglacial environment. John Wiley & Sons.
- Fulton, R. J. (Ed.). (1989). *Quaternary geology of Canada and Greenland* (Vol. 2). pp. Ottawa: Geological Survey of Canada.
- George, L. L., Cook, N. J., Crowe, B. B., and Ciobanu, C. L. (2018). Trace elements in hydrothermal chalcopyrite. *Mineralogical Magazine*, 82(1), 59-88.
- Girard, I., Klassen, R. A., and Laframboise, R. R. (2004). Sedimentology laboratory manual. *Terrain Sciences Division*, 1.
- Girard, R., Tremblay, J., Néron, A., Longuépée, H., and Makvandi, S. (2021). Automated Gold Grain Counting. Part 2: What a Gold Grain Size and Shape Can Tell! *Minerals*, 11(4), Art. 4.
- Hagedorn, B., Aalto, R., Sletten, R. S., and Hallet, B. (2008). Frost boil dynamics using ²¹⁰Pb as a tracer for soil movement. In *Proceedings of the Ninth International Conference on Permafrost—Fairbanks, Alaska* (pp. 613-618).
- Hallet, B. (2013). Stone circles: form and soil kinematics. *Philosophical Transactions of the Royal Society A: Mathematical, Physical and Engineering Sciences*, 371(2004), 20120357.
- Hallet, B., and Waddington, E. D. (2020). Buoyancy forces induced by freeze-thaw in the active layer: implications for diapirism and soil circulation. In *Periglacial geomorphology* (pp. 251-279). Routledge.

Hawkes, H. E. (1957). *Principles of geochemical prospecting* (No. 1000). US Government Printing Office.

Heginbottom, J. A. (1995). Canada-permafrost. *National Atlas of Canada*.

Hrabi, R. B., Barclay, W. A., Fleming, D. and Alexander, R. B. (2003). Structural evolution of the Woodburn Lake group in the area of the Meadowbank gold deposit, Nunavut; Geological Survey of Canada, Current Research 2003-C27, 10 p.

Hugelius, G., Kuhry, P., Tarnocai, C., and Virtanen, T. (2010). Soil organic carbon pools in a periglacial landscape: a case study from the central Canadian Arctic. *Permafrost and Periglacial Processes*, 21(1), 16-29.

Jahn A. (1968). Patterned ground. In R.W. Fairbridge (ed.): *Encyclopedia of geomorphology*. Pp. 814-817. New York: Reinhold

Janvier, V., Castonguay, S., Mercier-Langevin, P., Dubé, B., McNicoll, V., Pehrsson, S., Malo, M., De Chavigny, B., Coté-Mantha, O., (2015). Preliminary results of the geology of the portage deposit, Meadowbank Gold Mine, Churchill Province, Nunavut. Geological Survey of Canada, Current Research 2015-2, 21

Jefferson, C.W., White, J.C., Young, G.M., Patterson, J., Tschirhart, V.L., Pehrsson, S.J., Calhoun, L., Rainbird, R.H., Peterson, T.D., Davis, W.J., Tella, S., Chorlton, L.B., Scott, J.M.J., Percival, J.A., Morris, W.A., Keating, P., Anand, A., Shelat, Y., MacIsaac, D., (2015). Outcrop and Remote Predictive Geology of the Amer Belt and Basement Beside and Beneath the Northeast Thelon Basin, in Parts of NTS 66-A, B, C, F, G and H, Kivalliq Region, Nunavut. Geological Survey of Canada, Open File 7242.

Klaminder, J., Yoo, K., Olid, C., Ramebäck, H., and Vesterlund, A. (2014). Using short-lived radionuclides to estimate rates of soil motion in frost boils. *Permafrost and periglacial processes*, 25(3), 184-193.

Klassen, R. A. (2001). The interpretation of background variation in regional geochemical surveys— an example from Nunavut, Canada. *Geochemistry: Exploration, Environment, Analysis*, 1(2), 163-173.

Klassen, R. A. (1995). Drift Composition and Glacial Dispersal Trains, Baker Lake Area, District of Keewatin, Northwest Territories. Geological Survey of Canada, Bulletin 485

Klaus, M., Becher, M., and Klaminder, J. (2013). Cryogenic soil activity along bioclimatic gradients in northern Sweden: insights from eight different proxies. *Permafrost and Periglacial Processes*, 24(3), 210-223.

Kokelj, S. V., Burn, C. R., and Tarnocai, C. (2007). The structure and dynamics of earth hummocks in the subarctic forest near Inuvik, Northwest Territories, Canada. *Arctic, Antarctic, and Alpine Research*, 39(1), 99-109.

Laurus, K. A., and Fletcher, W. K. (1999). Gold distribution in glacial sediments and soils at Boston Property, Nunavut, Canada. *Journal of Geochemical Exploration*, 67(1-3), 271-285.

Lauzon, M.-C., Mercier-Langevin, P., Valette, M., Beaudoin, G., De Souza, S., Coté- Mantha, O., Simard, M., (2020). Ore mineralogy and mineral chemistry of the Whale Tail zone, Amaruq gold

deposit, Nunavut; in Targeted Geoscience Initiative 5: Contributions to the Understanding of Canadian Gold Systems, (ed.) P. Mercier- Langevin, C.J.M. Lawley, and S. Castonguay; Geological Survey of Canada. Open File 8712, 267–279.

Layton-Matthews, D., and McClenaghan, M. B. (2022). Current Techniques and Applications of Mineral Chemistry to Mineral Exploration; Examples from Glaciated Terrain: A Review. *Minerals*, 12(1), 59.

Layton-Matthews, D., Hamilton, C., and McClenaghan, M. B. (2014). Mineral chemistry: modern techniques and applications to exploration. *Application of Indicator Mineral Methods to Mineral Exploration*, 7553, 9-18.

Liu, H., and Beaudoin, G. (2021). Geochemical signatures in native gold derived from Au-bearing ore deposits. *Ore Geology Reviews*, 132, 104066. <https://doi.org/10.1016/j.oregeorev.2021.104066>

Liu, H., Beaudoin, G., Makvandi, S., Jackson, S. E., and Huang, X. (2021). Multivariate statistical analysis of trace element compositions of native gold from orogenic gold deposits: implication for mineral exploration. *Ore Geology Reviews*, 131, 104061.

Mackay, J. R. (1980). The origin of hummocks, western Arctic coast, Canada. *Canadian Journal of Earth Sciences*, 17(8), 996-1006.

Mackay, J. R., and MacKay, D. K. (1976). Cryostatic pressures in nonsorted circles (mud hummocks), Inuvik, Northwest Territories. *Canadian Journal of Earth Sciences*, 13(7), 889-897.

Manégliá, N., Beaudoin, G., and Simard, M. (2018). Indicator minerals of the Meliadine orogenic gold deposits, Nunavut (Canada), and application to till surveys. *Geochemistry: Exploration, Environment, Analysis*, 18(3), 241-251.

Mansur, E.T., Barnes, S.J. and Duran, C.J. (2021). An overview of chalcophile element contents of pyrrhotite, pentlandite, chalcopyrite, and pyrite from magmatic Ni-Cu-PGE sulfide deposits. *Miner Deposita* 56, 179–204. <https://doi.org/10.1007/s00126-020-01014-3>

McClenaghan, M. B. (2001). Regional and local-scale gold grain and till geochemical signatures of lode Au deposits in the western Abitibi Greenstone Belt, central Canada. Geological Society, London, Special Publications, 185(1), 201-224. <https://doi.org/10.1144/GSL.SP.2001.185.01.09>

McClenaghan, M. B. (2005). Indicator mineral methods in mineral exploration. *Geochemistry: Exploration, Environment, Analysis*, 5(3), 233-245.

McClenaghan, M. B., and Cabri, L. J. (2011). Review of gold and platinum group element (PGE) indicator minerals methods for surficial sediment sampling. *Geochemistry: Exploration, Environment, Analysis*, 11(4), 251-263. <https://doi.org/10.1144/1467-7873/10-IM-026>

McClenaghan, M.B. and Paulen, R.C. (2018). Mineral Exploration in Glaciated Terrain, Chapter 20. In: Menzies, J. and van der Meer J.J-M. (eds) Past Glacial Environments (Sediments, Forms and Techniques) A new & revised edition. Elsevier, 689–751.

McClenaghan, M. B., Plouffe, A., McMartin, I., Campbell, J. E., Spirito, W. A., Paulen, R. C., and Hall, G. E. M. (2013). Till sampling and geochemical analytical protocols used by the Geological Survey of Canada.

- McClenaghan, M. B., Thorleifson, L. H., and DiLabio, R. N. W. (2000). Till geochemical and indicator mineral methods in mineral exploration. *Ore Geology Reviews*, 16(3-4), 145-166.
- McCuaig, T. C., and Hronsky, J. M. A. (2014). The Mineral System Concept The Key to Exploration Targeting. En K. D. Kelley & H. C. Golden, *Building Exploration Capability for the 21st Century*. Society of Economic Geologists.
- McCuaig, T. C., Beresford, S., and Hronsky, J. (2010). Translating the mineral systems approach into an effective exploration targeting system. *Ore Geology Reviews*, 38(3), 128-138.
- McMartin, I., and McClenaghan, M. B. (2001). Till geochemistry and sampling techniques in glaciated shield terrain: A review. Geological Society, London, Special Publications, 185(1), 19-43.
- McMartin, I., Campbell, J. E., and Paulen, R. C. (2009). Near-surface till sampling protocols in shield terrain, with examples from western and northern Canada. *Application of Till and Stream Sediment Heavy Mineral and Geochemical Methods to Mineral Exploration in Western and Northern Canada*. Geological Association of Canada, St. John's, Newfoundland, 61-78.
- McMartin, I., Gauthier, M.S., and Page, A.V. (2022). Updated postglacial marine limits along western Hudson Bay, central mainland Nunavut and northern Manitoba. Geological Survey of Canada, Open File 8921.
- McMartin, I., Godbout, P. M., Campbell, J. E., Tremblay, T., and Behnia, P. (2021). A new map of glacial features and glacial landsystems in central mainland Nunavut, Canada. *Boreas*, 50(1), 51-75.
- McMartin, I., Hall, G. E. M., Kerswill, J. A., Sangster, A. L. and Valve, J. (2000). Mercury cycling in perennially frozen soils of Arctic Canada, Kaminak Lake area, Nunavut. In: Proceedings of the 25th Anniversary International Conference on Heavy Metals in the Environment. University of Michigan, USA.
- McMartin, I., and Henderson, P., (2004). Evidence from Keewatin (central Nunavut) for paleo-ice divide migration. *Geog. Phys. Quatern.* 58 (2-3), 163-186
- Mendizabal, A. (2022). Étude de la composition des minéraux indicateurs et de la géochimie du till en aval d'un gisement d'or : Le cas d'Amaruq (Nunavut, Canada). mémoire de maîtrise, Université Laval.
- Miller, J.K. (1984). Model for clastic indicator trains in till: Prospecting in Areas of Glaciated Terrain. The Institution of Mining and Metallurgy, London. pp. 69-77.
- Miranda, A. C. R., Beaudoin, G., and Rottier, B. (2022). Scheelite chemistry from skarn systems: implications for ore-forming processes and mineral exploration. *Mineralium Deposita*, 57(8), 1469-1497.
- Moles, N. R., and Chapman, R. J. (2019). Integration of Detrital Gold Microchemistry, Heavy Mineral Distribution, and Sediment Geochemistry to Clarify Regional Metallogeny in Glaciated Terrains: Application in the Caledonides of Southeast Ireland. *Economic Geology*, 114(2), 207-232. <https://doi.org/10.5382/econgeo.2019.4628>
- Morrison, G. W., Rose, W. J., and Jaireth, S. (1991). Geological and geochemical controls on the silver content (fineness) of gold in gold-silver deposits. *Ore Geology Reviews*, 6(4), 333-364.

- Overduin, P. P., and Kane, D. L. (2006). Frost boils and soil ice content: Field observations. *Permafrost and Periglacial Processes*, 17(4), 291-307.
- Murton, J. B. (2021). What and where are periglacial landscapes?. *Permafrost and Periglacial Processes*, 32(2), 186-212.
- Nicolovsky, D. J., Romanovsky, V. E., Tipenko, G. S., and Walker, D. A. (2008). Modeling biogeophysical interactions in nonsorted circles in the Low Arctic. *Journal of Geophysical Research: Biogeosciences*, 113(G3).
- Nixon, G. T. (2003). Use of Spinel in Mineral Exploration: The Enigmatic Giant Mascot Ni-Cu-PGE Deposit: Possible Ties to Wrangellia and Metallogenic Significance. *British Columbia Geological Survey. Geological Fieldwork 2002*.
- Overduin, P. P., and Kane, D. L. (2006). Frost boils and soil ice content: Field observations. *Permafrost and Periglacial Processes*, 17(4), 291-307.
- Palarea-Albaladejo, J., and Martín-Fernández, J. A. (2015). zCompositions—R package for multivariate imputation of left-censored data under a compositional approach. *Chemometrics and Intelligent Laboratory Systems*, 143, 85-96.
- Pehrsson, S. J., Berman, R. G., Eglington, B., and Rainbird, R. (2013). Two Neoproterozoic supercontinents revisited: The case for a Rae family of cratons. *Precambrian Research*, 232, 27-43.
- Peterson, R. A. (2011). Assessing the role of differential frost heave in the origin of non-sorted circles. *Quaternary Research*, 75(2), 325-333.
- Peterson, R. A., and Krantz, W. B. (2003). A mechanism for differential frost heave and its implications for patterned-ground formation. *Journal of Glaciology*, 49(164), 69-80.
- Peterson, R. A., Walker, D. A., Romanovsky, V. E., Knudson, J. A., Reynolds, M. K., and Krantz, W. B. (2003). A differential frost heave model: cryoturbation-vegetation interactions. In *Proceedings of the eighth international conference on permafrost (Vol. 2, pp. 885-890)*. Lisse, Zurich, Switzerland: AA Balkema.
- Ping, C. L., Michaelson, G. J., Overduin, P. P., and Stiles, C. A. (2003). Morphogenesis of frost boils in the Galbraith Lake area, Arctic Alaska. In *Proceedings of the Eighth International Conference on Permafrost, Zürich, Switzerland (pp. 897-900)*.
- Plouffe, A., McClenaghan, M. B., Paulen, R. C., McMartin, I., Campbell, J. E., and Spirito, W. A. (2013). Processing of glacial sediments for the recovery of indicator minerals: protocols used at the Geological Survey of Canada. *Geochemistry: Exploration, Environment, Analysis*, 13(4), 303-316.
- Pollard, W. (2018). Periglacial processes in glacial environments. In *Past Glacial Environments (pp. 537-564)*. Elsevier.
- R Core Team (2022). *R: A language and environment for statistical computing*. R Foundation for Statistical Computing, Vienna, Austria.
- Sarala, P., Nykänen, V., Sarapää, O., Peltoniemi, A., and Ojala, J. (2007). Quaternary geological and till geochemical studies in verifying GIS-based prospectivity mapping in the Central Lapland Greenstone Belt, northern Finland. In *23rd International Applied Geochemistry Symposium (IAGS): Exploring our environment, Oviedo, Spain (pp. 14-19)*.

Sciuba, M. (2020). *Texture and composition of scheelite, tourmaline and rutile in orogenic gold deposits* (Doctoral dissertation, Université Laval).

Sciuba, M., Beaudoin, G., and Makvandi, S. (2021). Chemical composition of tourmaline in orogenic gold deposits. *Mineralium Deposita*, 56(3), 537-560. <https://doi.org/10.1007/s00126-020-00981-x>

Sciuba, M., Beaudoin, G., Grzela, D., and Makvandi, S. (2020). Trace element composition of scheelite in orogenic gold deposits. *Mineralium Deposita*, 55, 1149-1172.

Sherlock, R., Pehrsson, S., Logan, A.V., Hrabi, R.B., Davis, W.J., (2004). Geological setting of the Meadowbank Gold Deposits, Woodburn Lake Group, Nunavut. *Explor. Min. Geol.* 13 (1–4), 67–107.

Shilts, W. W. (1973). Drift prospecting: Geochemistry of eskers and till in permanently frozen terrain, District of Keewatin, Northwest Territories. Geological Survey of Canada, Paper 72–45.

Shilts, W. W. (1975). Principles of geochemical exploration for sulphide deposits using shallow samples of glacial drift. *Canadian Institute of Mining and Metallurgy, Bulletin* 68, 73-80.

Shilts, W. W. (1976). Glacial till and mineral exploration. *Glacial Till, An Interdisciplinary Study*. Edited by RF Legget. Royal Society of Canada, Special Publication, 12, 205-223.

Shilts, W. W. (1977). Geochemistry of till in perennially frozen terrain of the Canadian Shield—Application to prospecting. *Boreas*, 6(2), 203-212.

Shilts, W. W. (1978). Nature and genesis of mudboils, central Keewatin, Canada. *Canadian Journal of Earth Sciences*, 15(7), 1053-1068.

Shilts, W.W. (1996). Drift exploration. In: Menzies, J. (ed.) *Past Glacial Environment: Sediments, Forms and Techniques*, Butterworth-Heinemann Ltd., *Glacial Environment: Volume 2*, Oxford, 411–439.

Shilts, W. W., Aylsworth, J. M., Kaszycki, C. A., and Klassen, R. A. (1987). Canadian shield. *Geomorphic Systems of North America*, 2, 119-161.

Shilts, W.W., Aylsworth, J. M., Kaszycki, C. A., and Klassen, R. A. (1987): Canadian Shield. In Graf, W. L. (ed.): *Geomorphic systems of North America*, 119–161. Centennial Special Volume 2, Geological Society of America.

Soil Classification Working Group, National Research Council Canada, Canada. Agriculture, & Agri-Food Canada. Research Branch. (1998). *The Canadian system of soil classification* (No. 1646). NRC Research.

Spirito, W. A., McClenaghan, M. B., Plouffe, A., McMartin, I., Campbell, J. E., Paulen, R. C., and Hall, G. E. M. (2011). Till sampling and analytical protocols for GEM projects: From field to archive. Geological Survey of Canada, Open File 6850.

Swanson, D. K., Ping, C. L., and Michaelson, G. J. (1999). Diapirism in soils due to thaw of ice-rich material near the permafrost table. *Permafrost and Periglacial Processes*, 10(4), 349-367.

Tarnocai, C., and Bockheim, J. (2011). Cryosolic soils of Canada: genesis, distribution, and classification. *Canadian journal of soil science*, 91(5), 749-762.

- Thiffault, E. (2019). Boreal forests and soils. In *Developments in Soil Science* (Vol. 36, pp. 59-82). Elsevier.
- Townley, B. K., Hérail, G., Maksaev, V., Palacios, C., Parseval, P. de, Sepulveda, F., Orellana, R., Rivas, P., and Ulloa, C. (2003). Gold grain morphology and composition as an exploration tool: Application to gold exploration in covered areas. *Geochemistry: Exploration, Environment, Analysis*, 3(1), 29-38. <https://doi.org/10.1144/1467-787302-042>
- Utting, D. J. and McMartin, I. (2004). Ice-movement Indicator Mapping North of the Keewatin Ice Divide, Meadowbank Area, Nunavut. Geological Survey of Canada, Current Research 2004-C8, 6,
- Valette, M., De Souza, S., Mercier-Langevin, P., Côté-Mantha, O., Simard, M., Wodicka, N., McNicoll, V.J., and Barbe, P., (2020). Lithological and tectonic controls on banded iron formation-associated gold at the Amaruq deposit, Churchill Province, Nunavut, and implications for exploration; in *Targeted Geoscience Initiative 5: Contributions to the Understanding of Canadian Gold Systems*, (ed.) P. Mercier-Langevin, C.J.M. Lawley, and S. Castonguay; Geological Survey of Canada, Open File 8712, p. 251–266.
- Valette, M., De Souza, S., Mercier-Langevin, P., McNicoll, V.J., Wodicka, N., Creaser, R. A., Cote-Mantha, O., Simard, M., (2019). Geological setting of the 5.2 Moz au Amaruq banded iron formation-hosted gold deposit, Churchill Province, Nunavut. In: Rogers, N. (Ed.), *Targeted Geoscience Initiative: 2018 Report of Activities*, Geological Survey of Canada, Open File, vol. 8549, pp. 83–87.
- van Dijke, A. A. H. (2016). Non-sorted circle occurrence. Master's thesis. Wageningen University
- Van Vliet-Lanoë, B. (1985). Frost effects in soils. *Soils and quaternary landscape evolution*, 117, 158.
- Van Vliet-Lanoë, B. (1991). Differential frost heave, load casting and convection: converging mechanisms; a discussion of the origin of cryoturbations. *Permafrost and periglacial processes*, 2(2), 123-139.
- Van Vliet-Lanoë, B., Coutard, J. P., and Pissart, A. (1984). Structures caused by repeated freezing and thawing in various loamy sediments: a comparison of active, fossil and experimental data. *Earth Surface Processes and Landforms*, 9(6), 553-565.
- Vandenberghe, J. (1988). Cryoturbations. *Advances in Periglacial Geomorphology*. Wiley
- Vandenberghe, J. (2013). Cryoturbation structures. *Encyclopedia of Quaternary Science*, 3, 430-435.
- Walker, D. A., Epstein, H. E., Gould, W. A., Kelley, A. M., Kade, A. N., Knudson, J. A., and Shur, Y. (2004). Frost-boil ecosystems: complex interactions between landforms, soils, vegetation and climate. *Permafrost and Periglacial Processes*, 15(2), 171-188.
- Washburn, A. L. (1956). Classification of patterned ground and review of suggested origins. *Geological Society of America Bulletin*, 67(7), 823-866.
- Washburn, A.L. (1980). *Geocryology*. John Wiley & Sons, New York.

Wilkinson, J. J., Cooke, D. R., Baker, M. J., Chang, Z., Wilkinson, C. C., Chen, H., and Brugge, E. R. (2017). Porphyry indicator minerals and their mineral chemistry as vectoring and fertility tools. Geological Survey of Canada.

Wyborn, L.A.I., Heinrich, C.A. and Jaques, A.L. (1994) Australian Proterozoic Mineral Systems: Essential Ingredients and Mappable Criteria. Proceedings of the Australian Institute of Mining and Metallurgy Annual Conference, Melbourne, 109-115.

Zoltai, S. C. (1995). Permafrost distribution in peatlands of west-central Canada during the Holocene warm period 6000 years BP. *Géographie physique et Quaternaire*, 49(1), 45-54.

Zoltai, S. C., and Tarnocai, C. (1981). Some nonsorted patterned ground types in northern Canada. *Arctic and Alpine Research*, 13(2), 139-151.

Appendix A - Field data

A.1 Location of trenches and the two mudboils (MB3 and MB4), coordinates in NAD83 YTM 14N.

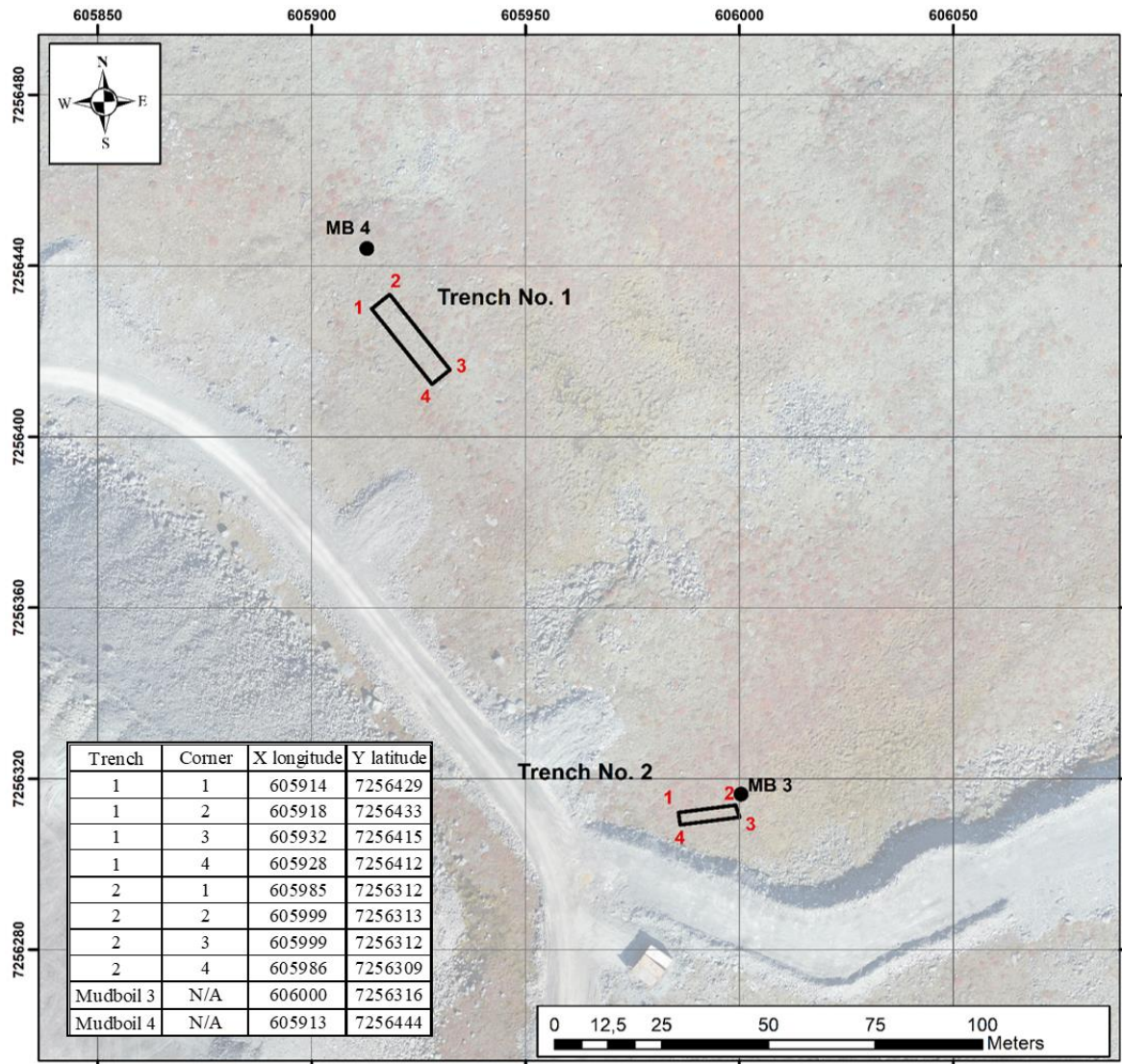


Figure A.3 Location of trenches (two rectangles) and the two adjacent mudboils (black dots). The map projection used: NAD83 UTM zone 14N.

A.2 Till sample list and description

Sample ID	Trench	Depth from surface (cm)		Location/ profile	Colour	Organic matter
		From	To			
230985	1	20	35	N10	2.5y 4/4	N
230986	1	35	50	N10	2.5y 4/4	N
230987	1	50	95	N10	2.5y 4/4	N
230988	1	95	105	N10	2.5y 5/3	N
230989	1	45	60	N12	2.5y 4/4	N
230990	1	30	45	N12	2.5y 4/4	N
230991	1	15	30	N12	2.5y 4/4	N
230992	1	60	95	N12	2.5y 4/3	N
230993	1	75	120	N7	2.5y 4/3	N
230994	1	100	125	N6	2.5y 5/4	N
230995	1	80	100	N6	2.5y 5/4	Y
230996	1	60	80	N6	2.5y 4/4	N
230997	1	40	60	N6	2.5y 4/4	N
230998	1	20	40	N6	2.5y 4/4	N
230999	1	65	80	N16	2.5y 4/4	Y
231000	1	50	65	N16	2.5y 4/3	Y
234001	1	35	50	N16	2.5y 4/3	N
234002	1	20	35	N16	2.5y 5/4	N
234003	1	60	80	S13	2.5y 5/4	N
234005	1	80	105	S13	2.5y 5/4	N
234006	1	40	60	S13	2.5y 5/4	N
234007	1	20	40	S13	2.5y 4/4	N
234008	1	50	100	S17	2.5y 4/4	N
234009	1	20	50	S17	2.5y 4/4	N
234010	2	120	130	MB 1	2.5y 5/4	N
234011	2	100	110	MB 1	2.5y 5/4	N
234012	2	80	90	MB 1	2.5y 5/4	N
234013	2	60	70	MB 1	2.5y 5/4	N
234014	2	40	50	MB 1	2.5y 5/4	N
234015	2	20	30	MB 1	2.5y 5/4	N
234016	2	15	30	50cm L (MB1)	10YR 5/8	N
234017	2	15	30	50cm R (MB1)	10YR 5/8	N
234018	2	25	40	115cm R (MB1)	10YR 5/8	N
234019	2	130	140	MB 2	5y 5/3	N
247526	2	110	130	MB 2	5y 5/1	N
247527	2	90	110	MB 2	10YR 5/8	N
247528	2	65	90	MB 2	2.5y 5/4	N
247529	2	40	65	MB 2	2.5y 4/4	N

Sample ID	Trench	Depth from surface (cm)		Location/ profile	Colour	Organic matter
		From	To			
247530	2	15	40	MB 2	2.5y 4/4	N
247532	2	5	15	MB 2	2.5y 4/4	N
247533	N/A	25	40	MB 3	2.5y 5/4	N
247534	N/A	20	30	MB 4	2.5y 5/4	N

Appendix B – Laboratory data

B.1 Pebble counting percentage of the 5-9.5mm fraction

Sample ID	FI	Dio	Mafic	VS	Qzite	Qz	BIF	Others
230985	58.1	2.3	11.9	13.2	10.0	0.0	0.3	4.2
230986	63.2	3.4	11.7	12.6	6.7	0.0	0.0	2.5
230987	44.7	3.7	15.4	27.6	5.7	0.0	0.0	2.8
230988	28.6	1.4	37.1	25.4	3.3	0.0	0.0	4.2
230989	57.8	7.9	5.9	17.0	7.3	1.5	0.0	2.6
230990	68.0	6.1	3.9	11.7	6.1	1.7	0.0	2.6
230991	62.3	5.0	5.0	18.6	6.0	2.0	0.5	0.5
230992	62.5	6.7	10.0	13.8	5.0	1.3	0.0	0.8
230993	28.2	5.8	23.4	36.4	4.8	0.7	0.0	0.7
230994	47.9	5.5	14.7	23.5	5.0	0.4	0.0	2.9
230994	47.9	5.5	14.7	23.5	5.0	0.4	0.0	2.9
230995	43.2	2.1	22.0	25.3	4.1	0.8	0.0	2.5
230995	43.2	2.1	22.0	25.3	4.1	0.8	0.0	2.5
230996	64.0	8.4	7.4	7.1	8.8	1.7	0.0	2.7
230997	59.6	9.6	7.9	7.9	10.0	1.7	0.0	3.3
230998	62.4	11.9	5.0	8.4	5.9	2.0	0.0	4.5
230999	63.8	10.8	7.7	9.9	5.6	0.6	0.3	1.2
231000	65.8	7.0	7.6	8.9	5.1	0.0	0.0	5.7
234001	68.4	7.8	5.1	6.3	7.4	1.6	0.0	3.5
234002	66.4	8.0	5.2	10.0	6.8	0.8	0.0	2.8
234003	49.7	6.6	18.9	14.6	6.1	1.1	0.0	2.9
234005	31.3	10.7	23.3	30.3	3.7	0.7	0.0	0.0
234006	75.1	6.2	5.9	4.5	5.2	1.0	0.0	2.1
234007	65.2	11.9	7.4	4.4	7.4	1.9	0.4	1.5
234008	48.6	10.1	21.1	11.0	6.7	0.6	0.0	1.8
234009	60.1	8.2	16.5	8.0	5.4	0.3	0.0	1.5
234010	64.6	7.8	14.0	6.8	3.7	1.6	0.0	1.6
234011	60.9	7.7	17.6	7.7	5.1	0.0	0.3	0.6
234012	57.9	6.9	19.7	8.1	4.8	1.2	0.3	1.2
234013	62.9	6.3	16.1	9.4	2.2	1.3	0.0	1.8
234014	48.9	8.0	22.3	12.5	4.5	1.5	0.4	1.9
234015	54.9	7.5	18.2	12.6	3.6	1.2	0.0	2.0
234016	66.1	5.8	7.7	8.8	9.1	0.7	0.4	1.5
234017	75.9	6.1	5.1	7.5	3.7	0.3	0.0	1.4
234018	71.9	4.1	8.1	5.9	6.7	0.7	0.4	2.2

Sample ID	FI	Dio	Mafic	VS	Qzite	Qz	BIF	Others
234019	57.0	4.0	16.1	16.1	4.4	0.0	0.4	2.0
247526	58.7	3.5	8.7	21.7	6.1	0.0	0.0	1.3
247527	60.3	6.0	16.8	3.0	7.3	0.0	0.0	6.5
247528	60.4	6.5	11.8	10.0	9.0	0.0	0.2	2.1
247529	60.3	2.4	9.1	17.2	7.2	0.0	0.0	3.8
247530	51.6	3.2	13.0	21.1	8.8	0.0	0.0	2.5
247532	44.3	4.9	25.6	12.8	5.4	1.5	0.5	4.9
247533	40.0	5.7	28.2	14.7	6.9	0.4	0.0	4.1
247534	62.5	6.7	10.0	13.8	5.0	1.3	0.0	0.8

FI: Felsic intrusive

Dio: Diorite

Mafic: Mafic/ultramafic

VS: Volcano-sedimentary

Qzite: Quartzite

Qz: Milky quartz

BIF: Banded Iron Formation

Others: Unidentified clasts

B.2 Till geochemistry (<0.063mm fraction)

B.2.1 Detection Limit of the ICP-ES Analyses and lithium borate fusion digestion method

Element	Detection Limit	Unit
SiO ₂	0.01	%
Al ₂ O ₃	0.01	%
Fe ₂ O ₃	0.04	%
MgO	0.01	%
CaO	0.01	%
Na ₂ O	0.01	%
K ₂ O	0.01	%
TiO ₂	0.01	%
P ₂ O ₅	0.01	%
MnO	0.01	%
Cr ₂ O ₃	0.002	%
Ba	1	ppm
Ni	20	ppm
Sc	1	ppm
Cu	5	ppm
Zn	5	ppm
Mo	1	ppm
Pb	5	ppm
Be	1	ppm
Co	0.2	ppm
Cs	0.1	ppm
Ga	0.5	ppm
Hf	0.1	ppm
Nb	0.1	ppm
Rb	0.1	ppm
Sn	1	ppm
Sr	0.5	ppm
Ta	0.1	ppm
Th	0.2	ppm
U	0.1	ppm
V	8	ppm
W	0.5	ppm
Zr	0.1	ppm
Y	0.1	ppm
La	0.1	ppm
Ce	0.1	ppm

Element	Detection Limit	Unit
Pr	0.02	ppm
Nd	0.3	ppm
Sm	0.05	ppm
Eu	0.02	ppm
Gd	0.05	ppm
Tb	0.01	ppm
Dy	0.05	ppm
Ho	0.02	ppm
Er	0.03	ppm
Tm	0.01	ppm
Yb	0.05	ppm
Lu	0.01	ppm

B.2.2 ICP-ES and lithium borate fusion digestion method results

Sample ID	SiO2 (%)	Al2O3 (%)	Fe2O3 (%)	MgO (%)	CaO (%)	Na2O (%)	K2O (%)	TiO (%)	P2O5 (%)	MnO (%)	Cr2O3 (%)	Ba (ppm)	Ni (ppm)	Sc (ppm)	Cu (ppm)	Zn (ppm)	Mo (ppm)
230998	71.62	11.88	3.91	1.49	1.63	2.39	3.43	0.55	0.15	0.05	0.02	718.00	37.00	9.00	8.00	43.00	bdl
231000	66.62	12.12	4.46	1.73	1.49	2.11	3.32	0.54	0.16	0.05	0.02	698.00	48.00	9.00	16.00	49.00	bdl
231001	70.51	11.87	4.06	1.59	1.58	2.25	3.32	0.54	0.16	0.05	0.02	721.00	43.00	9.00	16.00	46.00	bdl
231002	73.42	11.32	3.55	1.37	1.65	2.33	3.24	0.54	0.16	0.05	0.01	707.00	37.00	9.00	8.00	40.00	bdl
231006	70.66	11.56	3.95	1.54	1.56	2.25	3.31	0.52	0.17	0.05	0.02	708.00	46.00	9.00	29.00	45.00	bdl
231007	73.43	11.12	3.63	1.33	1.75	2.32	3.21	0.56	0.18	0.05	0.01	665.00	35.00	9.00	8.00	40.00	bdl
234010	68.47	12.45	5.37	2.34	1.75	2.18	3.44	0.57	0.17	0.07	0.03	726.00	90.00	11.00	20.00	60.00	2.00
234011	66.88	12.83	6.07	2.87	1.71	2.15	3.50	0.56	0.17	0.08	0.03	743.00	115.00	12.00	32.00	71.00	2.00
234012	68.86	12.29	5.30	2.60	1.84	2.23	3.35	0.57	0.18	0.07	0.03	722.00	105.00	11.00	22.00	56.00	1.00
234013	67.90	12.49	5.62	2.58	1.76	2.13	3.39	0.56	0.18	0.07	0.03	715.00	102.00	11.00	26.00	62.00	1.00
234014	67.47	12.63	5.76	2.70	1.70	2.15	3.45	0.56	0.20	0.08	0.03	711.00	105.00	11.00	24.00	58.00	bdl
234015	72.48	11.56	4.11	1.67	1.91	2.40	3.29	0.59	0.19	0.06	0.02	685.00	51.00	10.00	11.00	41.00	bdl
234016	72.20	11.83	3.97	1.52	1.74	2.34	3.31	0.57	0.16	0.05	0.01	714.00	40.00	10.00	10.00	44.00	1.00
234017	70.62	12.20	4.45	1.64	1.67	2.30	3.42	0.56	0.15	0.05	0.02	731.00	45.00	10.00	18.00	51.00	1.00
234018	70.89	11.82	4.58	1.58	1.72	2.26	3.24	0.57	0.17	0.06	0.02	723.00	47.00	10.00	15.00	50.00	bdl
234019	68.02	12.09	5.70	2.93	1.83	2.14	3.27	0.56	0.19	0.07	0.03	675.00	127.00	11.00	28.00	61.00	bdl
247526	68.10	12.45	5.24	2.35	1.78	2.16	3.36	0.57	0.18	0.07	0.02	685.00	90.00	11.00	44.00	63.00	1.00
247527	70.92	12.04	4.33	1.72	1.74	2.31	3.31	0.57	0.15	0.05	0.02	686.00	53.00	10.00	15.00	51.00	1.00
247528	69.25	12.42	5.09	2.14	1.72	2.23	3.46	0.55	0.17	0.06	0.02	697.00	72.00	11.00	21.00	62.00	bdl
247529	68.32	12.53	5.38	2.25	1.66	2.14	3.43	0.54	0.17	0.07	0.02	721.00	78.00	11.00	90.00	65.00	bdl
247530	70.15	12.15	4.79	2.02	1.90	2.31	3.34	0.62	0.18	0.06	0.02	695.00	67.00	11.00	16.00	52.00	2.00
247532	70.94	11.76	4.65	2.15	1.95	2.35	3.27	0.59	0.20	0.06	0.03	654.00	75.00	10.00	15.00	46.00	bdl
247533	68.28	12.39	5.68	2.83	1.86	2.18	3.35	0.57	0.18	0.08	0.03	697.00	120.00	11.00	22.00	61.00	1.00
247534	71.29	11.94	3.88	1.42	1.84	2.41	3.36	0.62	0.20	0.05	0.01	710.00	36.00	10.00	8.00	40.00	bdl

Sample ID	Pb (ppm)	Be (ppm)	Co (ppm)	Cs (ppm)	Ga (ppm)	Hf (ppm)	Nb (ppm)	Rb (ppm)	Sn (ppm)	Sr (ppm)	Ta (ppm)	Th (ppm)	U (ppm)	V (ppm)	W (ppm)	Zr (ppm)
230998	16.00	2.00	9.00	1.90	13.60	7.30	13.00	104.50	2.00	201.90	1.10	11.30	3.40	42.00	1.60	275.00
231000	19.00	4.00	9.50	2.40	14.00	6.50	12.30	106.50	2.00	179.20	1.00	13.60	3.90	46.00	2.50	237.10
231001	17.00	2.00	9.40	2.00	14.00	8.00	12.70	105.10	2.00	188.10	1.10	11.60	3.40	42.00	1.50	291.50
231002	17.00	2.00	7.90	1.60	12.50	8.10	12.80	95.90	2.00	194.50	1.10	11.80	3.10	37.00	1.80	303.90
231006	16.00	3.00	9.50	1.90	13.60	7.40	12.70	102.10	2.00	188.00	1.10	11.70	3.60	40.00	2.60	274.60
231007	16.00	1.00	7.50	1.60	12.50	9.00	13.40	92.70	2.00	201.70	1.20	10.50	3.00	40.00	2.40	321.70
234010	19.00	1.00	14.10	2.30	15.70	7.30	13.10	108.60	2.00	193.60	1.10	15.30	5.30	52.00	2.00	274.40
234011	21.00	bdl	16.50	2.90	16.50	7.10	12.40	113.90	3.00	184.70	1.10	16.20	5.60	60.00	3.00	269.80
234012	21.00	2.00	15.00	2.30	14.30	6.90	12.60	105.00	2.00	194.70	1.10	13.90	4.30	56.00	1.80	248.30
234013	20.00	1.00	14.90	2.60	15.20	7.10	12.60	108.60	2.00	185.60	1.00	15.90	5.20	65.00	2.30	260.20
234014	19.00	bdl	14.00	2.90	16.30	7.00	13.00	113.60	2.00	180.70	1.30	16.40	5.20	55.00	1.90	247.70
234015	18.00	bdl	9.30	1.40	12.20	8.10	13.30	92.30	2.00	205.20	1.20	11.50	3.50	44.00	1.90	282.10
234016	17.00	1.00	9.60	1.80	13.40	7.90	13.40	99.50	2.00	198.30	1.10	12.10	3.40	41.00	1.80	297.40
234017	18.00	2.00	9.40	2.10	14.40	7.80	13.50	106.40	2.00	191.80	1.20	14.80	4.50	44.00	2.00	290.40
234018	19.00	4.00	10.00	2.10	13.40	7.80	13.70	100.90	2.00	196.80	1.20	15.10	4.60	43.00	1.90	291.80
234019	20.00	1.00	16.70	2.60	14.30	7.10	12.40	105.40	2.00	186.20	1.00	14.70	4.70	59.00	1.90	261.70
247526	19.00	2.00	13.40	2.50	14.60	7.60	13.00	107.80	2.00	192.60	1.10	15.80	5.00	56.00	2.40	276.10
247527	19.00	2.00	9.00	2.10	14.00	8.00	13.20	104.00	2.00	193.30	1.20	13.80	4.10	48.00	2.00	290.90
247528	20.00	bdl	11.50	2.30	14.80	7.40	12.80	109.00	2.00	187.20	1.00	16.40	5.50	53.00	1.80	267.60
247529	20.00	3.00	13.10	2.90	16.10	7.80	13.30	119.50	3.00	195.60	1.00	18.90	6.00	53.00	2.20	280.10
247530	18.00	3.00	10.80	2.00	13.60	7.60	14.30	101.20	2.00	201.70	1.20	15.10	4.60	51.00	2.00	290.00
247532	17.00	1.00	10.70	1.80	12.20	7.10	13.00	92.70	2.00	200.00	1.20	12.00	3.60	50.00	1.50	262.00
247533	17.00	3.00	14.20	2.50	13.30	6.80	12.00	102.70	2.00	189.20	1.10	15.00	3.80	57.00	1.90	241.60
247534	17.00	bdl	8.50	1.70	14.10	7.80	14.50	98.30	2.00	211.50	1.20	11.60	3.60	42.00	2.00	294.10

Sample ID	Y (ppm)	La (ppm)	Ce (ppm)	Pr (ppm)	Nd (ppm)	Sm (ppm)	Eu (ppm)	Gd (ppm)	Tb (ppm)	Dy (ppm)	Ho (ppm)	Er (ppm)	Tm (ppm)	Yb (ppm)	Lu (ppm)
230998	26.50	46.40	89.30	10.11	35.10	6.05	1.04	5.44	0.78	4.63	0.92	2.65	0.40	2.51	0.39
231000	25.20	50.10	99.20	10.59	38.30	6.31	1.03	5.15	0.75	4.65	0.87	2.62	0.37	2.40	0.37
231001	27.20	48.80	92.20	10.41	37.40	6.15	1.08	5.19	0.79	4.66	0.94	2.69	0.40	2.58	0.42
231002	27.80	47.10	91.20	10.30	37.40	6.58	1.07	5.36	0.79	4.82	0.97	2.80	0.42	2.64	0.42
231006	25.90	46.50	92.20	10.14	35.60	6.11	1.06	5.25	0.74	4.39	0.87	2.77	0.37	2.74	0.39
231007	29.00	47.50	91.90	10.42	37.10	6.23	1.12	5.45	0.81	4.90	0.99	3.00	0.44	2.86	0.44
234010	30.90	57.10	100.10	12.82	47.00	7.93	1.36	6.66	0.96	5.68	1.06	3.29	0.46	2.94	0.48
234011	31.00	62.00	102.00	13.36	47.70	7.88	1.35	6.50	0.97	5.42	1.07	3.10	0.46	2.96	0.48
234012	29.60	54.80	93.70	11.97	43.20	7.38	1.32	6.12	0.90	5.20	1.08	3.12	0.46	2.87	0.47
234013	29.80	60.50	100.30	12.99	47.20	7.76	1.38	6.54	0.92	5.44	1.08	3.18	0.45	2.95	0.46
234014	30.60	56.40	95.10	12.87	45.50	7.53	1.36	6.64	0.98	5.45	1.16	3.37	0.46	3.13	0.47
234015	28.70	51.20	90.70	11.13	41.50	7.11	1.23	5.95	0.85	4.95	1.04	2.93	0.42	2.87	0.45
234016	28.30	53.00	104.60	11.55	41.80	7.13	1.19	5.59	0.85	4.85	1.02	3.13	0.43	2.80	0.45
234017	29.70	54.40	100.70	12.19	43.90	7.68	1.28	6.27	0.92	5.17	1.05	3.05	0.46	3.02	0.46
234018	30.70	59.70	117.10	13.02	47.30	7.88	1.34	6.59	0.94	5.44	1.12	3.42	0.47	3.05	0.46
234019	28.50	50.60	92.20	11.41	42.00	6.96	1.25	5.76	0.81	4.86	0.98	2.91	0.40	2.66	0.41
247526	32.00	58.50	113.10	12.58	45.10	7.67	1.29	6.38	0.95	5.36	1.09	3.21	0.46	3.02	0.44
247527	30.00	51.70	91.90	11.52	42.20	7.15	1.20	6.04	0.85	5.18	1.06	3.16	0.45	3.02	0.46
247528	32.20	59.40	92.50	12.98	46.80	7.94	1.28	6.63	0.95	5.28	1.07	3.32	0.46	3.03	0.46
247529	33.30	63.40	96.90	13.86	48.80	8.32	1.43	6.86	0.96	5.61	1.06	3.24	0.45	3.05	0.45
247530	31.40	57.20	92.30	12.77	46.20	7.74	1.39	6.60	0.94	5.48	1.12	3.23	0.47	2.99	0.47
247532	29.00	48.60	82.10	10.77	39.20	6.60	1.19	5.64	0.80	4.91	0.98	2.87	0.42	2.76	0.42
247533	28.20	54.00	89.00	11.67	42.00	6.98	1.27	5.89	0.82	4.85	0.98	2.87	0.38	2.71	0.42
247534	30.40	53.80	107.40	11.94	42.30	7.38	1.25	5.93	0.86	5.08	1.04	2.93	0.43	2.83	0.44

bdl: Below detection limit

B.2.3 Detection Limit of the ICP-MS Analyses and aqua-regia digestion method

Element	Detection limit	Unit
Mo	0.01	ppm
Cu	0.01	ppm
Pb	0.01	ppm
Zn	0.1	ppm
Ag	2	ppb
Ni	0.1	ppm
Co	0.1	ppm
Mn	1	ppm
Fe	0.01	%
As	0.1	ppm
U	0.1	ppm
Au	0.2	ppb
Th	0.1	ppm
Sr	0.5	ppm
Cd	0.01	ppm
Sb	0.02	ppm
Bi	0.02	ppm
V	1	ppm
Ca	0.01	%
P	0.001	%
La	0.5	ppm
Cr	0.5	ppm
Mg	0.01	%
Ba	0.5	ppm
Ti	0.001	%
B	1	ppm
Al	0.01	%
Na	0.001	%
K	0.01	%
W	0.1	ppm
Sc	0.1	ppm
Tl	0.02	ppm
S	0.02	%
Hg	5	ppb
Se	0.1	ppm
Te	0.02	ppm
Ga	0.1	ppm
Cs	0.02	ppm
Ge	0.1	ppm

Element	Detection limit	Unit
Hf	0.02	ppm
Nb	0.02	ppm
Rb	0.1	ppm
Sn	0.1	ppm
Ta	0.05	ppm
Zr	0.1	ppm
Y	0.01	ppm
Ce	0.1	ppm
In	0.02	ppm
Re	1	ppb
Be	0.1	ppm
Li	0.1	ppm
Pr	0.02	ppm
Nd	0.02	ppm
Sm	0.02	ppm
Eu	0.02	ppm
Gd	0.02	ppm
Tb	0.02	ppm
Dy	0.02	ppm
Ho	0.02	ppm
Er	0.02	ppm
Tm	0.02	ppm
Yb	0.02	ppm
Lu	0.02	ppm
Pd	10	ppb
Pt	2	ppb

B.2.4 ICP-MS and aqua-regia digestion method results

Sample ID	Mo (ppm)	Cu (ppm)	Pb (ppm)	Zn (ppm)	Ag (ppb)	Ni (ppm)	Co (ppm)	Mn (ppm)	Fe (%)	As (ppm)	U (ppm)	Au (ppb)	Th (ppm)	Sr (ppm)
230998	0.50	6.39	7.69	37.70	25.00	27.60	7.80	267.00	2.06	7.40	1.80	8.80	8.00	31.80
231000	0.76	9.48	9.73	42.60	59.00	35.30	8.30	281.00	2.42	12.90	2.50	6.30	7.60	29.70
231001	0.55	7.65	8.35	40.10	34.00	30.30	8.00	272.00	2.13	8.00	2.00	7.60	8.20	31.40
231002	0.41	5.83	6.82	32.40	25.00	23.70	6.30	220.00	1.78	5.00	1.60	8.80	7.70	32.00
231006	0.54	7.42	8.06	40.90	46.00	31.50	7.90	268.00	2.10	7.70	2.00	12.30	7.40	29.90
231007	0.41	5.58	6.75	33.00	24.00	25.10	6.30	223.00	1.83	5.50	1.60	5.70	7.20	32.20
234010	0.85	18.38	10.22	53.80	69.00	68.40	11.60	386.00	2.92	42.00	3.60	30.00	13.10	39.10
234011	0.83	23.78	11.50	61.00	76.00	90.20	14.00	439.00	3.25	62.70	3.80	40.40	13.80	37.00
234012	0.75	15.87	8.90	46.90	63.00	73.50	12.20	376.00	2.77	49.60	2.60	38.50	10.50	38.60
234013	0.98	21.97	10.41	56.10	67.00	78.70	12.50	405.00	3.08	56.10	3.70	31.40	12.90	39.10
234014	0.85	24.83	11.05	59.00	76.00	89.00	13.10	409.00	3.20	67.00	3.80	51.90	13.50	37.50
234015	0.53	8.61	6.79	32.60	44.00	37.10	7.40	254.00	2.00	18.10	1.90	34.20	8.20	34.80
234016	0.50	8.09	7.59	38.60	24.00	28.70	7.50	254.00	2.04	7.00	2.00	4.80	9.20	32.70
234017	0.73	12.31	9.44	45.70	41.00	38.20	8.50	288.00	2.40	14.40	3.10	3.40	11.50	34.20
234018	0.80	12.78	9.83	46.60	29.00	39.50	9.40	329.00	2.66	14.00	3.30	10.60	12.30	36.60
234019	0.91	21.49	9.92	54.10	79.00	91.20	15.30	389.00	3.09	67.40	3.30	52.00	11.60	37.60
247526	0.95	19.73	10.02	54.90	62.00	70.70	12.50	379.00	2.84	37.90	3.70	26.30	12.70	38.80
247527	0.62	12.29	8.31	45.20	39.00	37.00	7.70	264.00	2.30	13.90	2.60	7.70	10.90	33.90
247528	0.96	19.16	10.11	53.20	40.00	55.90	10.20	339.00	2.72	31.20	3.90	9.10	13.60	36.70
247529	0.91	22.43	10.86	58.30	52.00	63.40	11.30	375.00	2.98	37.10	4.40	13.90	14.60	36.90
247530	0.84	14.60	8.91	43.10	37.00	49.30	9.00	304.00	2.49	28.80	3.10	26.90	11.90	39.10
247532	0.55	13.76	7.88	39.80	51.00	56.50	9.50	312.00	2.49	42.50	2.30	40.70	10.00	39.20
247533	0.96	21.51	9.69	54.20	65.00	92.70	12.60	394.00	3.05	64.30	2.40	66.60	11.90	38.40
247534	0.40	5.69	7.31	32.50	27.00	25.10	6.50	242.00	1.99	6.10	2.00	6.60	8.00	35.80

Sample ID	Cd (ppm)	Sb (ppm)	Bi (ppm)	V (ppm)	Ca (%)	P (%)	La (ppm)	Cr (ppm)	Mg (%)	Ba (ppm)	Ti (%)	B (ppm)	Al (%)	Na (%)	K (%)
230998	0.04	0.08	0.31	19.00	0.33	0.07	35.30	55.50	0.54	34.70	0.08	2.00	0.99	0.01	0.10
231000	0.05	0.09	0.38	23.00	0.30	0.07	40.80	74.00	0.64	48.70	0.08	3.00	1.25	0.01	0.12
231001	0.04	0.08	0.33	20.00	0.33	0.07	39.40	59.40	0.58	41.20	0.08	2.00	1.07	0.01	0.11
231002	0.04	0.07	0.25	16.00	0.32	0.07	35.20	47.70	0.47	30.40	0.07	2.00	0.86	0.01	0.09
231006	0.05	0.09	0.29	20.00	0.31	0.07	35.90	64.10	0.55	31.70	0.08	2.00	1.01	0.01	0.10
231007	0.05	0.07	0.24	17.00	0.34	0.08	35.00	49.50	0.45	23.90	0.07	2.00	0.84	0.01	0.08
234010	0.05	0.18	0.43	28.00	0.41	0.08	49.40	127.40	0.89	73.30	0.10	3.00	1.39	0.01	0.25
234011	0.06	0.23	0.47	32.00	0.39	0.08	51.10	164.60	1.07	89.10	0.10	3.00	1.57	0.01	0.29
234012	0.05	0.22	0.39	27.00	0.40	0.08	43.30	149.40	0.88	61.50	0.09	2.00	1.23	0.01	0.22
234013	0.05	0.20	0.44	29.00	0.40	0.08	48.20	144.30	0.97	84.00	0.10	3.00	1.45	0.01	0.27
234014	0.05	0.25	0.45	31.00	0.39	0.08	48.20	151.70	1.00	97.60	0.09	3.00	1.55	0.01	0.30
234015	0.04	0.12	0.25	19.00	0.37	0.08	38.70	69.60	0.53	37.00	0.07	2.00	0.84	0.01	0.12
234016	0.04	0.08	0.30	19.00	0.35	0.07	41.20	53.50	0.54	40.90	0.08	2.00	0.97	0.01	0.12
234017	0.04	0.10	0.40	22.00	0.36	0.07	45.20	61.60	0.62	56.80	0.09	3.00	1.18	0.01	0.17
234018	0.04	0.11	0.41	23.00	0.39	0.08	52.70	65.40	0.63	61.90	0.09	3.00	1.21	0.01	0.18
234019	0.05	0.26	0.37	32.00	0.44	0.08	43.20	172.80	1.08	64.30	0.10	3.00	1.57	0.01	0.29
247526	0.06	0.18	0.42	27.00	0.42	0.08	46.70	116.20	0.87	63.20	0.09	4.00	1.45	0.01	0.26
247527	0.04	0.11	0.35	22.00	0.38	0.07	42.30	66.40	0.64	52.70	0.09	3.00	1.17	0.01	0.17
247528	0.04	0.16	0.44	25.00	0.38	0.07	48.90	89.00	0.78	81.30	0.09	3.00	1.36	0.01	0.25
247529	0.04	0.17	0.49	29.00	0.40	0.07	51.90	103.90	0.88	85.20	0.09	4.00	1.51	0.01	0.28
247530	0.04	0.16	0.38	25.00	0.41	0.08	48.00	94.20	0.71	62.10	0.09	3.00	1.16	0.01	0.20
247532	0.03	0.18	0.29	25.00	0.42	0.09	42.00	118.70	0.75	56.10	0.08	2.00	1.07	0.01	0.19
247533	0.05	0.25	0.38	30.00	0.41	0.09	44.30	167.70	0.99	79.90	0.09	3.00	1.48	0.01	0.28
247534	0.04	0.08	0.27	18.00	0.37	0.08	40.60	52.00	0.48	28.70	0.08	2.00	0.93	0.01	0.09

Sample ID	W (ppm)	Sc (ppm)	Tl (ppm)	S (%)	Hg (ppb)	Se (ppm)	Te (ppm)	Ga (ppm)	Cs (ppm)	Ge (ppm)	Hf (ppm)	Nb (ppm)	Rb (ppm)	Sn (ppm)	Ta (ppm)
230998	0.30	2.90	0.10	bdl	bdl	0.20	bdl	4.30	1.01	bdl	0.16	1.13	15.30	0.70	bdl
231000	0.30	3.20	0.13	bdl	17.00	0.30	bdl	5.40	1.35	bdl	0.11	1.66	20.10	0.80	bdl
231001	0.30	3.00	0.10	bdl	8.00	0.20	bdl	4.50	1.09	bdl	0.14	1.41	15.60	0.70	bdl
231002	0.30	2.60	0.08	bdl	bdl	0.10	bdl	3.50	0.81	bdl	0.13	0.90	11.70	0.60	bdl
231006	0.40	2.80	0.09	bdl	7.00	0.30	bdl	4.20	0.96	bdl	0.07	1.19	14.10	0.60	bdl
231007	0.30	2.60	0.07	bdl	bdl	0.20	bdl	3.40	0.71	bdl	0.12	1.04	10.90	0.60	bdl
234010	0.40	4.10	0.16	bdl	bdl	0.30	bdl	5.60	1.54	bdl	0.39	0.56	24.40	0.80	bdl
234011	0.50	4.40	0.20	bdl	bdl	0.30	0.03	6.20	1.86	bdl	0.47	0.40	28.60	0.80	bdl
234012	0.40	3.70	0.14	bdl	bdl	0.30	0.03	4.80	1.35	bdl	0.38	0.29	21.10	0.70	bdl
234013	0.40	4.30	0.18	bdl	bdl	0.30	bdl	5.90	1.66	bdl	0.32	0.47	26.70	0.80	bdl
234014	0.50	4.40	0.20	bdl	bdl	0.30	0.02	6.00	1.84	bdl	0.50	0.32	29.20	0.80	bdl
234015	0.30	2.70	0.08	bdl	bdl	0.20	bdl	3.30	0.79	bdl	0.23	0.35	12.90	0.50	bdl
234016	0.30	3.00	0.10	bdl	bdl	0.30	bdl	4.00	0.96	bdl	0.20	0.71	15.50	0.60	bdl
234017	0.30	3.60	0.12	bdl	6.00	0.30	bdl	4.90	1.25	bdl	0.24	0.84	19.40	0.80	bdl
234018	0.30	3.80	0.13	bdl	bdl	0.30	0.02	4.80	1.32	bdl	0.26	1.03	21.70	0.80	bdl
234019	0.50	4.40	0.18	bdl	bdl	0.30	0.03	5.70	1.71	bdl	0.38	0.47	27.10	0.70	bdl
247526	0.40	4.20	0.17	bdl	bdl	0.30	0.02	5.70	1.59	bdl	0.33	0.81	25.50	0.80	bdl
247527	0.30	3.60	0.13	bdl	bdl	0.30	bdl	5.00	1.22	bdl	0.25	0.85	19.80	0.70	bdl
247528	0.30	4.00	0.16	bdl	bdl	0.40	bdl	5.60	1.55	bdl	0.37	0.47	24.50	0.80	bdl
247529	0.40	4.40	0.19	bdl	bdl	0.30	bdl	6.20	1.78	bdl	0.35	0.69	27.80	0.80	bdl
247530	0.40	3.70	0.12	bdl	bdl	0.20	bdl	4.70	1.25	bdl	0.33	0.38	19.90	0.70	bdl
247532	0.40	3.30	0.12	bdl	bdl	0.10	bdl	4.20	1.11	bdl	0.33	0.32	18.10	0.60	bdl
247533	0.50	4.20	0.18	bdl	bdl	0.20	0.02	5.60	1.69	bdl	0.36	0.22	25.50	0.70	bdl
247534	0.30	2.90	0.08	bdl	bdl	0.20	bdl	3.70	0.85	bdl	0.11	1.18	12.40	0.70	bdl

Sample ID	Zr (ppm)	Y (ppm)	Ce (ppm)	In (ppm)	Re (ppb)	Be (ppm)	Li (ppm)	Pr (ppm)	Nd (ppm)	Sm (ppm)	Eu (ppm)	Gd (ppm)	Tb (ppm)	Dy (ppm)	Ho (ppm)
230998	8.20	11.93	68.90	bdl	bdl	0.50	10.70	8.14	27.87	4.56	0.70	3.32	0.41	2.30	0.40
231000	5.80	12.70	78.00	bdl	bdl	0.60	11.80	9.02	30.95	5.00	0.75	3.65	0.45	2.51	0.43
231001	6.80	11.99	74.00	bdl	bdl	0.50	11.60	8.77	30.24	4.86	0.73	3.50	0.43	2.39	0.42
231002	7.40	11.57	68.30	bdl	bdl	0.40	9.10	8.02	27.74	4.46	0.68	3.25	0.40	2.20	0.38
231006	3.90	11.61	71.40	bdl	bdl	0.50	10.20	8.36	28.11	4.57	0.69	3.28	0.41	2.27	0.40
231007	6.50	11.64	67.20	bdl	bdl	0.40	8.60	7.99	27.38	4.46	0.67	3.22	0.39	2.21	0.39
234010	20.90	17.44	82.60	0.03	bdl	0.70	14.60	11.33	41.22	6.60	1.02	4.94	0.61	3.39	0.60
234011	23.50	17.90	84.50	0.02	bdl	0.80	15.80	11.91	43.49	6.87	1.06	5.14	0.63	3.55	0.62
234012	19.20	15.14	75.00	bdl	bdl	0.50	12.20	10.01	35.96	5.77	0.92	4.30	0.53	2.92	0.52
234013	19.00	17.45	79.50	0.02	bdl	0.70	14.80	10.96	40.18	6.51	1.01	4.93	0.60	3.34	0.59
234014	24.60	17.55	77.50	0.02	bdl	0.80	15.50	10.99	40.47	6.52	1.02	4.96	0.60	3.39	0.60
234015	11.90	13.09	68.40	bdl	bdl	0.40	8.20	9.05	31.17	5.12	0.78	3.68	0.44	2.48	0.44
234016	10.60	13.31	81.50	bdl	bdl	0.50	10.20	9.41	33.52	5.28	0.80	3.86	0.47	2.59	0.46
234017	13.40	15.54	82.70	bdl	bdl	0.60	12.90	10.50	37.83	6.04	0.92	4.48	0.55	3.10	0.55
234018	14.50	17.55	99.80	0.02	bdl	0.70	12.30	11.93	41.58	6.74	1.02	4.99	0.62	3.40	0.60
234019	21.90	15.54	77.10	0.02	bdl	0.70	15.20	9.91	35.89	5.83	0.91	4.34	0.53	3.00	0.53
247526	19.40	16.88	89.10	0.02	bdl	0.80	14.90	10.68	37.91	6.15	0.95	4.64	0.57	3.21	0.56
247527	13.80	14.69	70.90	bdl	bdl	0.70	12.40	9.65	33.99	5.50	0.84	4.08	0.50	2.80	0.50
247528	19.90	17.68	73.40	0.02	bdl	0.80	14.90	11.20	40.34	6.53	0.99	4.96	0.61	3.44	0.61
247529	19.30	18.63	78.00	0.02	bdl	0.90	16.50	11.87	43.15	6.97	1.06	5.23	0.65	3.61	0.64
247530	17.70	16.93	73.10	bdl	bdl	0.60	12.30	11.27	40.95	6.33	0.97	4.67	0.57	3.20	0.56
247532	16.20	14.56	67.80	bdl	bdl	0.50	10.90	9.58	33.40	5.52	0.86	4.06	0.50	2.77	0.49
247533	18.70	15.79	72.80	0.02	bdl	0.70	15.00	10.19	36.20	5.83	0.93	4.39	0.55	3.01	0.53
247534	6.00	13.37	80.60	bdl	bdl	0.50	9.50	9.56	31.98	5.26	0.79	3.77	0.46	2.56	0.44

Sample ID	Er (ppm)	Tm (ppm)	Yb (ppm)	Lu (ppm)	Pd (ppb)	Pt (ppb)
230998	1.11	0.14	0.93	0.12	bdl	bdl
231000	1.16	0.15	0.96	0.13	bdl	bdl
231001	1.14	0.15	0.96	0.12	bdl	bdl
231002	1.06	0.14	0.87	0.12	bdl	bdl
231006	1.08	0.14	0.89	0.12	bdl	bdl
231007	1.05	0.14	0.87	0.12	bdl	bdl
234010	1.63	0.22	1.37	0.19	bdl	bdl
234011	1.70	0.22	1.45	0.20	bdl	bdl
234012	1.41	0.19	1.19	0.16	bdl	bdl
234013	1.62	0.21	1.37	0.19	bdl	bdl
234014	1.65	0.21	1.39	0.19	bdl	bdl
234015	1.18	0.15	1.00	0.13	bdl	bdl
234016	1.24	0.16	1.04	0.14	bdl	bdl
234017	1.50	0.20	1.27	0.17	bdl	bdl
234018	1.63	0.21	1.38	0.19	bdl	bdl
234019	1.47	0.19	1.24	0.17	bdl	bdl
247526	1.54	0.21	1.31	0.18	bdl	bdl
247527	1.35	0.18	1.15	0.16	bdl	bdl
247528	1.66	0.22	1.40	0.19	bdl	bdl
247529	1.75	0.23	1.48	0.20	bdl	bdl
247530	1.55	0.20	1.28	0.18	bdl	bdl
247532	1.34	0.17	1.11	0.15	bdl	bdl
247533	1.46	0.19	1.22	0.17	bdl	bdl
247534	1.21	0.16	1.00	0.13	bdl	bdl

B.2.5 Detection Limit of the ICP-ES/MS Analyses and multi-acid digestion method

Element	Detection limit	Unit
Mo	0.05	ppm
Cu	0.1	ppm
Pb	0.02	ppm
Zn	0.2	ppm
Ag	20	ppb
Ni	0.1	ppm
Co	0.2	ppm
Mn	1	ppm
Fe	0.01	%
As	0.2	ppm
U	0.1	ppm
Th	0.1	ppm
Sr	1	ppm
Cd	0.02	ppm
Sb	0.02	ppm
Bi	0.04	ppm
V	2	ppm
Ca	0.01	%
P	0.001	%
La	0.1	ppm
Cr	1	ppm
Mg	0.01	%
Ba	1	ppm
Ti	0.001	%
Al	0.01	%
Na	0.001	%
K	0.01	%
W	0.1	ppm
Zr	0.2	ppm
Sn	0.1	ppm
Be	1	ppm
Sc	0.1	ppm
S	0.04	%
Y	0.1	ppm
Ce	0.02	ppm
Pr	0.1	ppm
Nd	0.1	ppm

Element	Detection limit	Unit
Sm	0.1	ppm
Eu	0.1	ppm
Gd	0.1	ppm
Tb	0.1	ppm
Dy	0.1	ppm
Ho	0.1	ppm
Er	0.1	ppm
Tm	0.1	ppm
Yb	0.1	ppm
Lu	0.1	ppm
Hf	0.02	ppm
Li	0.1	ppm
Rb	0.1	ppm
Ta	0.1	ppm
Nb	0.04	ppm
Cs	0.1	ppm
Ga	0.02	ppm
In	0.01	ppm
Re	0.002	ppm
Se	0.3	ppm
Te	0.05	ppm
Tl	0.05	ppm

B.2.6 ICP-ES/MS and multi-acid digestion method results

Sample ID	Mo (ppm)	Cu (ppm)	Pb (ppm)	Zn (ppm)	Ag (ppb)	Ni (ppm)	Co (ppm)	Mn (ppm)	Fe (%)	As (ppm)	U (ppm)	Th (ppm)	Sr (ppm)	Cd (ppm)	Sb (ppm)	Bi (ppm)	V (ppm)
230998	0.55	6.00	15.26	42.70	bdl	40.00	8.80	396.00	2.62	8.20	2.60	9.10	187.00	0.05	0.25	0.34	38.00
231000	0.78	9.00	17.46	48.50	48.00	49.90	9.60	393.00	2.88	13.80	3.50	12.20	174.00	0.04	0.26	0.42	39.00
231001	0.61	7.20	15.34	44.70	27.00	42.20	9.00	379.00	2.56	9.20	2.70	9.90	174.00	0.05	0.24	0.35	36.00
231002	0.47	5.60	15.16	39.70	bdl	35.40	7.50	351.00	2.31	6.80	2.50	9.00	186.00	0.04	0.23	0.31	34.00
231006	0.59	6.80	14.55	43.90	28.00	43.10	8.70	381.00	2.53	8.60	2.70	10.10	177.00	0.05	0.22	0.31	36.00
231007	0.45	5.40	14.24	38.80	20.00	36.80	7.50	373.00	2.43	6.90	2.40	8.70	192.00	0.04	0.24	0.27	36.00
234010	0.93	17.90	18.57	62.00	57.00	92.10	13.80	543.00	3.57	43.40	4.50	14.30	190.00	0.06	0.42	0.54	48.00
234011	0.93	22.10	19.32	68.80	63.00	118.60	16.20	609.00	3.95	63.70	4.80	15.20	179.00	0.06	0.47	0.53	53.00
234012	0.86	15.10	16.84	54.00	62.00	103.60	14.00	544.00	3.36	50.40	3.60	12.20	183.00	0.06	0.43	0.41	47.00
234013	1.06	20.70	18.47	65.00	53.00	106.00	14.80	550.00	3.67	58.00	4.70	15.30	185.00	0.06	0.45	0.49	49.00
234014	0.94	22.80	18.68	65.90	61.00	112.30	14.90	577.00	3.85	68.50	4.70	14.60	177.00	0.07	0.48	0.50	49.00
234015	0.62	8.20	15.10	40.00	bdl	53.40	9.30	411.00	2.60	20.30	2.90	9.90	197.00	0.05	0.29	0.30	37.00
234016	0.54	7.40	15.68	43.80	21.00	40.20	8.90	378.00	2.55	8.10	2.90	11.00	183.00	0.04	0.25	0.34	37.00
234017	0.79	11.20	17.47	50.10	24.00	48.40	9.60	398.00	2.82	15.20	4.00	12.90	180.00	0.04	0.28	0.44	39.00
234018	0.79	11.10	16.05	48.30	bdl	47.50	10.00	427.00	2.96	14.10	3.70	12.40	182.00	0.04	0.27	0.39	40.00
234019	0.93	19.70	16.55	60.30	55.00	124.70	17.00	565.00	3.73	67.10	3.80	12.20	179.00	0.05	0.48	0.40	50.00
247526	1.11	20.50	19.73	68.70	49.00	100.70	15.60	571.00	3.75	42.10	5.10	15.90	201.00	0.06	0.42	0.51	51.00
247527	0.70	11.40	16.16	50.10	bdl	49.60	9.10	398.00	2.86	15.50	3.40	12.30	184.00	0.04	0.28	0.39	41.00
247528	1.01	17.90	17.15	58.60	23.00	70.60	11.60	470.00	3.28	32.60	4.60	15.00	179.00	0.05	0.35	0.47	45.00
247529	0.96	20.90	17.70	64.60	31.00	79.70	12.80	507.00	3.56	39.30	4.90	15.30	174.00	0.06	0.36	0.49	48.00
247530	0.89	14.10	16.83	50.90	33.00	67.60	10.80	463.00	3.15	30.90	4.00	13.20	205.00	0.05	0.36	0.41	44.00
247532	0.59	12.60	15.47	46.50	39.00	78.60	11.40	479.00	3.06	44.50	3.10	10.90	209.00	0.05	0.38	0.34	43.00
247533	1.02	20.00	16.75	60.70	57.00	118.80	14.20	572.00	3.73	65.80	3.20	12.80	184.00	0.06	0.48	0.41	50.00
247534	0.47	5.20	15.33	37.80	bdl	36.70	7.70	375.00	2.52	7.30	2.90	10.10	195.00	0.04	0.26	0.32	36.00

Sample ID	Ca (%)	P (%)	La (ppm)	Cr (ppm)	Mg (%)	Ba (ppm)	Ti (%)	Al (%)	Na (%)	K (%)	W (ppm)	Zr (ppm)	Sn (ppm)	Be (ppm)	Sc (ppm)	S (%)	Y (ppm)
230998	1.04	0.072	36.90	74.00	0.85	654.00	0.26	5.63	1.76	2.76	1.30	179.30	1.90	2.00	8.70	bdl	21.90
231000	0.93	0.073	46.60	104.00	0.96	687.00	0.27	5.72	1.59	2.63	1.30	170.80	2.00	2.00	9.20	bdl	22.30
231001	0.91	0.069	41.40	79.00	0.85	657.00	0.26	5.18	1.63	2.61	1.10	169.10	1.80	2.00	8.30	bdl	21.10
231002	1.01	0.069	39.80	67.00	0.76	669.00	0.26	5.12	1.75	2.63	1.40	184.60	1.80	2.00	8.20	bdl	21.70
231006	1.00	0.074	40.10	84.00	0.84	648.00	0.25	5.56	1.68	2.65	1.00	165.60	1.80	2.00	8.50	bdl	21.20
231007	1.15	0.080	39.10	71.00	0.76	612.00	0.26	5.41	1.79	2.65	1.20	192.50	1.80	2.00	8.70	bdl	22.60
234010	1.11	0.080	54.30	141.00	1.34	726.00	0.31	6.13	1.70	2.92	1.60	192.90	2.10	2.00	10.40	bdl	28.20
234011	1.09	0.078	53.60	182.00	1.61	728.00	0.29	6.16	1.59	2.89	1.70	188.00	2.00	2.00	10.50	bdl	26.80
234012	1.15	0.084	48.30	158.00	1.41	703.00	0.29	5.74	1.66	2.77	1.50	169.40	1.80	2.00	9.90	bdl	24.70
234013	1.12	0.080	55.50	160.00	1.43	718.00	0.29	6.09	1.64	2.79	1.70	194.90	2.00	2.00	10.60	bdl	28.10
234014	1.14	0.080	54.40	164.00	1.49	700.00	0.28	6.15	1.59	2.75	1.70	181.30	2.00	2.00	10.70	bdl	27.00
234015	1.20	0.079	46.20	84.00	0.90	652.00	0.29	5.48	1.75	2.58	1.10	180.10	1.80	2.00	9.10	bdl	25.10
234016	1.08	0.069	45.60	76.00	0.84	657.00	0.29	5.52	1.77	2.70	1.10	184.80	1.80	2.00	9.00	bdl	24.20
234017	1.05	0.069	51.70	78.00	0.89	723.00	0.27	5.77	1.73	2.71	1.30	190.80	2.00	2.00	9.40	bdl	26.30
234018	1.10	0.075	51.20	75.00	0.89	648.00	0.28	5.66	1.68	2.65	1.20	195.90	1.90	2.00	9.40	bdl	26.10
234019	1.20	0.082	45.00	183.00	1.65	637.00	0.29	5.90	1.60	2.68	1.40	176.40	1.90	2.00	10.70	bdl	24.20
247526	1.22	0.091	56.60	149.00	1.43	744.00	0.32	6.39	1.81	3.04	1.50	209.30	2.20	2.00	11.30	bdl	29.30
247527	1.11	0.070	47.50	85.00	0.97	670.00	0.28	5.83	1.73	2.77	1.20	198.40	2.00	2.00	9.50	bdl	24.90
247528	1.07	0.074	52.60	103.00	1.16	676.00	0.27	5.83	1.64	2.78	1.50	180.80	2.00	2.00	9.90	bdl	27.40
247529	1.02	0.076	52.00	120.00	1.24	669.00	0.27	5.87	1.62	2.84	1.40	183.10	2.10	2.00	10.00	bdl	26.90
247530	1.25	0.081	53.80	109.00	1.12	679.00	0.30	6.03	1.75	2.76	1.40	196.90	2.00	2.00	10.30	bdl	28.40
247532	1.28	0.089	46.40	127.00	1.21	668.00	0.30	5.80	1.79	2.70	1.30	188.50	1.80	2.00	10.00	bdl	25.30
247533	1.21	0.088	49.40	168.00	1.56	683.00	0.28	6.03	1.63	2.73	1.70	176.40	1.90	2.00	10.90	bdl	26.00
247534	1.13	0.080	47.00	76.00	0.78	667.00	0.29	5.51	1.74	2.67	1.30	193.70	2.00	2.00	9.20	bdl	24.10

Sample ID	Ce (ppm)	Pr (ppm)	Nd (ppm)	Sm (ppm)	Eu (ppm)	Gd (ppm)	Tb (ppm)	Dy (ppm)	Ho (ppm)	Er (ppm)	Tm (ppm)	Yb (ppm)	Lu (ppm)	Hf (ppm)	Li (ppm)	Rb (ppm)	Ta (ppm)
230998	75.28	9.00	32.00	5.70	1.00	4.60	0.70	3.90	0.80	2.30	0.30	2.20	0.30	4.77	13.90	101.20	0.90
231000	91.28	10.90	37.80	6.60	1.10	5.10	0.70	4.20	0.80	2.40	0.30	2.20	0.30	4.70	15.20	109.60	0.90
231001	80.17	9.80	34.20	6.00	1.00	4.70	0.60	3.90	0.80	2.20	0.30	2.20	0.30	4.64	14.20	100.30	0.90
231002	81.18	9.80	34.70	6.20	1.10	4.90	0.70	4.20	0.80	2.40	0.40	2.30	0.30	5.18	12.40	94.20	0.90
231006	81.45	9.60	33.80	5.90	1.00	4.60	0.70	3.90	0.80	2.20	0.30	2.10	0.30	4.38	12.80	100.30	0.80
231007	78.27	9.50	33.40	5.90	1.00	4.70	0.70	4.00	0.80	2.30	0.30	2.30	0.30	4.89	11.70	93.70	0.80
234010	92.68	13.10	46.10	8.00	1.40	6.40	0.90	5.10	1.00	2.90	0.40	2.70	0.40	5.19	18.20	118.80	1.00
234011	91.17	13.00	46.20	8.10	1.30	6.40	0.90	5.10	1.00	2.80	0.40	2.70	0.40	5.20	20.60	119.20	0.90
234012	85.82	11.60	41.50	7.30	1.30	5.80	0.80	4.70	0.90	2.60	0.40	2.50	0.40	4.71	15.80	107.90	0.90
234013	94.46	13.20	47.20	8.20	1.40	6.40	0.90	5.10	0.90	2.80	0.40	2.70	0.40	5.24	18.70	117.80	0.90
234014	89.83	12.80	45.90	8.00	1.40	6.30	0.80	5.10	1.00	2.80	0.40	2.70	0.40	4.95	19.20	115.50	0.90
234015	83.78	11.30	39.70	6.90	1.20	5.50	0.80	4.50	0.90	2.60	0.40	2.50	0.40	4.95	11.30	95.70	0.90
234016	90.59	10.90	39.00	6.70	1.10	5.30	0.70	4.40	0.90	2.50	0.40	2.50	0.40	5.09	13.10	101.70	0.90
234017	95.01	12.10	43.90	7.70	1.30	6.10	0.80	5.00	1.00	2.80	0.40	2.70	0.40	5.34	15.70	108.70	1.00
234018	98.69	12.10	42.40	7.40	1.20	5.90	0.80	4.80	0.90	2.70	0.40	2.50	0.40	5.08	14.30	103.50	0.90
234019	84.08	10.90	38.80	6.90	1.20	5.40	0.80	4.50	0.90	2.50	0.40	2.40	0.40	4.81	18.10	106.20	0.90
247526	113.31	13.80	48.60	8.50	1.40	6.70	0.90	5.50	1.10	3.10	0.40	2.90	0.40	5.80	19.90	121.80	1.10
247527	83.32	11.40	40.30	7.10	1.20	5.60	0.80	4.60	0.90	2.60	0.40	2.50	0.40	5.42	15.30	108.30	1.00
247528	82.97	12.40	44.30	7.80	1.30	6.20	0.80	5.00	0.90	2.80	0.40	2.60	0.40	5.00	18.10	112.20	0.90
247529	84.03	12.60	44.70	7.80	1.30	6.10	0.80	4.90	0.90	2.80	0.40	2.60	0.40	4.94	19.90	115.30	0.90
247530	86.22	12.90	45.50	8.00	1.40	6.20	0.90	5.10	1.00	2.90	0.40	2.70	0.40	5.35	16.00	107.60	1.00
247532	83.19	11.20	40.30	7.20	1.30	5.60	0.80	4.70	0.90	2.70	0.40	2.60	0.40	5.07	13.90	101.80	1.00
247533	85.10	11.80	41.90	7.30	1.30	5.70	0.80	4.70	0.90	2.70	0.40	2.60	0.40	4.85	18.10	107.70	0.90
247534	95.26	11.30	40.10	7.10	1.20	5.50	0.80	4.60	0.90	2.70	0.40	2.50	0.40	5.27	12.20	95.80	1.00

Sample ID	Nb (ppm)	Cs (ppm)	Ga (ppm)	In (ppm)	Re (ppm)	Se (ppm)	Te (ppm)	Tl (ppm)
230998	11.09	1.90	15.46	0.03	bdl	bdl	bdl	0.50
231000	11.10	2.60	16.37	0.04	bdl	bdl	bdl	0.56
231001	11.20	1.90	15.13	0.04	bdl	bdl	bdl	0.49
231002	11.19	1.60	14.03	0.04	bdl	bdl	bdl	0.48
231006	10.27	1.80	14.60	0.03	bdl	bdl	bdl	0.47
231007	11.19	1.40	14.21	0.03	bdl	bdl	bdl	0.44
234010	12.22	2.60	17.43	0.05	bdl	bdl	bdl	0.60
234011	11.14	3.00	17.66	0.04	bdl	0.30	bdl	0.63
234012	11.26	2.30	15.59	0.04	bdl	bdl	bdl	0.55
234013	11.89	2.70	16.98	0.04	bdl	0.30	bdl	0.58
234014	11.04	2.90	16.85	0.04	bdl	0.40	0.05	0.59
234015	11.60	1.60	14.07	0.03	bdl	bdl	bdl	0.47
234016	11.54	1.80	14.90	0.04	bdl	bdl	bdl	0.50
234017	11.75	2.30	15.91	0.04	bdl	0.30	bdl	0.55
234018	11.50	2.00	15.36	0.04	bdl	0.30	bdl	0.49
234019	11.07	2.50	16.18	0.04	bdl	bdl	bdl	0.55
247526	12.77	2.80	18.54	0.05	bdl	0.50	bdl	0.62
247527	12.00	2.10	15.95	0.04	bdl	0.40	bdl	0.53
247528	11.02	2.50	16.63	0.04	bdl	0.30	bdl	0.55
247529	10.95	2.70	17.48	0.04	bdl	0.30	bdl	0.57
247530	12.35	2.20	16.28	0.04	bdl	0.30	bdl	0.53
247532	11.83	1.90	15.19	0.04	bdl	bdl	bdl	0.49
247533	11.06	2.60	16.15	0.04	bdl	0.40	0.05	0.56
247534	12.58	1.70	14.60	0.04	bdl	0.40	bdl	0.47

B.3 Indicator minerals counting

B.3.1 Gold grains counting by ODM (non-normalized)

Sample ID	Total	Reshaped	Modified	Pristine	Table feed (Kg)
230985	92	4	13	75	7.7
230986	30	3	7	20	6.8
230987	7	0	3	4	5.1
230988	900	4	11	885	8.9
230989	63	1	4	58	6.5
230990	88	20	13	55	7.2
230991	73	23	11	39	6.9
230992	2	1	0	1	1.9
230993	136	40	27	69	5.1
230994	141	37	11	93	5.4
230995	72	18	14	40	5.6
230996	48	10	15	23	7.5
230997	32	9	7	16	6.9
230998	39	11	12	16	7.5
230999	30	6	6	18	5.6
231000	36	6	10	20	8.4
234001	38	10	8	20	6.5
234002	49	10	14	25	7.6
234003	23	3	4	16	5.2
234004	0	0	0	0	6.2
234005	92	24	6	62	5.7
234006	47	11	10	26	7.7
234007	44	12	3	29	8.2
234008	23	5	1	17	3.3
234009	63	20	7	36	7.1
234010	88	22	7	59	6.0
234011	188	43	14	131	5.7
234012	172	38	14	120	6.1
234013	84	15	10	59	7.4
234014	103	21	8	74	5.5
234015	54	9	4	41	5.4
234016	34	12	8	14	7.1
234017	26	11	3	12	6.0
234018	33	9	4	20	7.2
234019	253	42	32	179	5.0
247020	0	0	0	0	6.4
247526	273	60	26	187	7.0
247527	25	10	1	14	7.7
247528	20	9	4	7	6.7
247529	30	9	5	16	5.9

Sample ID	Total	Reshaped	Modified	Pristine	Table feed (Kg)
247530	106	31	10	65	6.8
247532	393	76	28	289	5.7
247533	344	111	32	201	7.1
247534	52	19	3	30	7.9
247539	40	9	5	26	6.0

B.3.1 Scheelite grains counting (non-normalized)

Sample ID	<0.25 mm	0.25-2.00mm	Table Feed (Kg)
230985	20	1	7.7
230986	20	2	6.8
230987	10	2	5.1
230988	500	13	8.9
230989	20	1	6.5
230990	20	2	7.2
230991	20	4	6.9
230992	3	0	1.9
230993	100	2	5.1
230994	100	3	5.4
230995	100	0	5.6
230996	25	1	7.5
230997	500	0	6.9
230998	300	0	7.5
230999	400	0	5.6
231000	20	0	8.4
234001	40	0	6.5
234002	20	4	7.6
234003	10	0	5.2
234005	300	8	5.7
234006	100	0	7.7
234007	100	0	8.2
234008	20	0	3.3
234009	100	2	7.1
234010	30	1	6.0
234011	20	4	5.7
234012	30	1	6.1
234013	40	0	7.4
234014	30	1	5.5
234016	20	1	7.1
234015	20	1	5.4
234017	20	2	6.0
234018	20	0	7.2
234019	100	4	5.0
247526	100	2	7.0
247527	10	0	7.7
247528	10	1	6.7
247529	30	1	5.9
247530	10	0	6.8
247532	10	3	5.7
247533	5	0	7.1
247534	20	0	7.9
247539	10	0	6.0

B.3.1 Sulfide grains counting (non-normalized)

Sample ID	Pyrite (<0.25mm)	Chalcopyrite (0.25-2.00mm)
230985	0	0
230986	0	0
230987	0	0
230988	0	0
230989	0	0
230990	0	0
230991	0	0
230992	0	0
230993	0	0
230994	0	0
230995	0	0
230996	0	0
230997	0	0
230998	0	0
230999	0	0
231000	0	0
234001	0	0
234002	0	0
234003	0	0
234005	0	0
234006	0	0
234007	0	0
234008	0	0
234009	0	0
234010	0	0
234011	20	0
234012	0	3
234013	0	1
234014	0	2
234016	0	0
234015	0	0
234017	20	0
234018	30	0
234019	100	4
247526	100	0
247527	20	0
247528	0	0
247529	0	0
247530	10	0
247532	50	0
247533	20	2
247534	10	0
247539	0	0

B.4 Mineral chemistry of indicator minerals

B.4.1 Gold analysis

B.4.1.1 Detection limits in gold analysis

Element	Range of Detection Limits	Unit	Method
Au	3277-3645	ppm	EPMA
Ag	330-415	ppm	EPMA
S	20-22	ppm	EPMA
Fe	37-41	ppm	EPMA
Cu	59-63	ppm	EPMA
As	79-86	ppm	EPMA
Hg	126-131	ppm	EPMA
⁵³ Cr	1.98-50.98	ppm	LA-ICP-MS
⁵⁵ Mn	3.60-79.80	ppm	LA-ICP-MS
⁵⁷ Fe	9.72-263.75	ppm	LA-ICP-MS
⁵⁹ Co	0.018-1.268	ppm	LA-ICP-MS
⁶⁰ Ni	0.44-13.09	ppm	LA-ICP-MS
⁶⁵ Cu	0.22-34.75	ppm	LA-ICP-MS
⁶⁶ Zn	0.31-9.82	ppm	LA-ICP-MS
⁷⁵ As	0.24-23.51	ppm	LA-ICP-MS
⁷⁷ Se	0.36-10.96	ppm	LA-ICP-MS
¹⁰⁸ Pd	0.013-0.712	ppm	LA-ICP-MS
¹¹¹ Cd	0.015-1.539	ppm	LA-ICP-MS
¹¹⁸ Sn	0.089-2.565	ppm	LA-ICP-MS
¹²¹ Sb	0.17-5.921	ppm	LA-ICP-MS
¹²⁵ Te	0.069-8.831	ppm	LA-ICP-MS
¹⁹⁵ Pt	0.004-0.406	ppm	LA-ICP-MS
²⁰² Hg	3.28-337.80	ppm	LA-ICP-MS
²⁰⁶ Pb	0.005-2.002	ppm	LA-ICP-MS
²⁰⁹ Bi	0.021-0.980	ppm	LA-ICP-MS

B.4.1.2 EPMA results in gold grains

Gold grain	Ag (%)	Au (%)	Total (%)	S (%)	Fe (%)	Cu (%)	As (%)	Hg (%)
230985_0	24.46	74.17	98.63	0.0101	0.0114	0.0247	bdl	bdl
230985_1	11.88	86.09	97.97	0.0100	bdl	0.0269	bdl	bdl
230985_2	31.94	66.08	98.02	0.0354	bdl	0.0153	bdl	bdl
230986_0	24.22	74.74	98.96	0.0034	0.0072	0.0171	bdl	bdl
230986_1	24.40	75.80	100.20	0.0136	0.0038	0.0172	bdl	bdl
230986_3	24.45	75.98	100.43	0.0147	bdl	0.0117	0.0149	bdl
230987_1	27.25	73.30	100.54	0.0142	0.0363	0.0074	bdl	bdl
230987_2	29.88	71.74	101.62	0.0185	bdl	bdl	0.0086	bdl
230987_3	0.84	97.25	98.10	0.0174	0.0157	0.0191	bdl	bdl
230987_4	28.03	73.07	101.10	0.0187	bdl	0.0062	0.0084	bdl
230987_5	27.80	73.96	101.76	0.0162	bdl	bdl	0.0122	bdl
230988_2	18.46	81.66	100.12	0.0118	0.0050	0.0166	bdl	bdl
230988_3	23.73	75.83	99.56	0.0034	0.0051	0.0172	0.0132	bdl
230988_4	27.62	69.90	97.52	0.0064	bdl	0.0120	bdl	bdl
230988_7	19.80	80.15	99.95	0.0052	0.0052	0.0256	bdl	bdl
230989_1	28.21	73.05	101.26	0.0263	bdl	0.0172	0.0183	bdl
230989_2	1.28	98.55	99.82	0.0156	bdl	0.4649	0.0085	bdl
230989_3	16.65	83.31	99.96	0.0234	bdl	0.0366	bdl	bdl
230990_1	23.80	77.06	100.85	0.0178	bdl	0.0167	bdl	bdl
230990_2	24.78	76.24	101.03	0.0180	bdl	0.0173	0.0090	bdl
230991_0	4.03	94.60	98.63	0.0229	0.2290	0.0299	0.0082	bdl
230991_1	9.72	88.00	97.72	0.0348	bdl	0.0395	bdl	0.0307
230991_2	17.34	83.78	101.13	0.0120	bdl	0.0176	bdl	bdl
230991_3	18.39	81.51	99.89	0.0158	bdl	0.0117	0.0131	bdl
230993_1	23.49	75.99	99.48	0.0246	bdl	0.0135	bdl	bdl
230993_3	28.54	70.90	99.44	0.0049	bdl	0.0086	0.0093	bdl
230993_4	21.09	77.08	98.18	0.0105	0.0070	0.0239	bdl	bdl
230993_6	19.58	78.99	98.57	0.0088	0.0046	0.0097	0.0095	bdl
230994_1	20.70	78.12	98.83	0.0327	bdl	0.0258	bdl	bdl
230994_2	34.73	63.85	98.59	0.0335	0.0042	bdl	bdl	bdl
230994_3	42.51	57.54	100.05	0.0063	0.0037	bdl	bdl	bdl
230994_4	21.88	76.20	98.07	0.0069	bdl	0.0169	0.0109	bdl
230995_0	19.64	81.52	101.15	0.0167	bdl	0.0099	bdl	bdl
230995_1	19.56	78.08	97.65	0.0278	bdl	0.0186	bdl	bdl
230995_2	20.35	80.70	101.05	0.0139	bdl	0.0119	bdl	0.0131
230995_4	20.31	80.81	101.12	0.0114	bdl	0.0120	0.0079	bdl
230995_7	17.12	83.33	100.46	0.0147	bdl	0.0135	0.0117	bdl
230996_0	12.96	86.37	99.32	0.0170	0.0037	0.0314	bdl	bdl
230996_1	12.74	89.18	101.92	0.0159	bdl	0.0282	bdl	bdl

Gold grain	Ag (%)	Au (%)	Total (%)	S (%)	Fe (%)	Cu (%)	As (%)	Hg (%)
230997_2	30.20	69.65	99.85	0.0228	bdl	0.0077	bdl	0.0167
230997_3	34.82	64.83	99.65	0.0273	bdl	0.0087	bdl	bdl
230997_4	21.78	78.36	100.13	0.0112	0.0053	0.0188	bdl	bdl
230998_1.1	18.31	80.47	98.78	0.0162	bdl	0.0285	bdl	bdl
230998_0	16.26	82.58	98.84	0.0168	bdl	0.0258	bdl	bdl
230998_1	41.96	59.41	101.36	0.0164	bdl	0.0090	bdl	bdl
230998_2	28.98	72.57	101.54	0.0125	bdl	0.0144	bdl	bdl
230998_2.1	17.81	80.13	97.95	0.0317	bdl	0.0256	bdl	bdl
230998_3	12.09	88.76	100.84	0.0107	0.0058	0.0410	bdl	bdl
230998_4	0.20	98.91	99.10	0.0206	bdl	0.0158	bdl	bdl
230999_1	8.80	60.75	69.55	0.0131	bdl	0.0212	bdl	bdl
231000_2	30.76	70.11	100.88	0.0181	bdl	bdl	bdl	bdl
231000_3	46.15	54.43	100.57	0.0276	0.0277	0.0096	bdl	bdl
231000_4	25.36	75.55	100.92	0.0164	bdl	0.0067	bdl	bdl
231000_5	10.49	89.40	99.89	0.0148	bdl	0.0189	bdl	bdl
234001_2	36.23	64.59	100.82	0.0199	bdl	0.0077	0.0170	bdl
234001_3	7.26	93.46	100.72	0.0396	bdl	0.0279	bdl	bdl
234002_1	19.06	82.15	101.22	0.0142	0.0052	0.0218	0.0099	bdl
234003_1	16.49	83.29	99.78	0.0121	bdl	0.0253	bdl	bdl
234003_2	27.88	73.55	101.43	0.0137	0.0095	bdl	bdl	bdl
234005_1	16.72	83.02	99.74	0.0091	bdl	0.0219	bdl	bdl
234005_2	31.59	66.57	98.16	0.0076	bdl	0.0108	0.0084	bdl
234005_3	28.99	66.81	95.81	0.0079	bdl	0.0152	0.0082	bdl
234005_4	31.48	64.96	96.44	0.0063	bdl	0.0140	0.0121	bdl
234006_1	29.13	72.32	101.45	0.0134	bdl	0.0068	0.0116	bdl
234006_2	19.50	81.59	101.10	0.0116	bdl	0.0159	bdl	bdl
234007_1	6.63	92.97	99.60	0.0089	bdl	0.0365	bdl	bdl
234007_2	25.22	75.98	101.20	0.0129	0.0062	0.0094	bdl	0.0245
234007_3	19.42	81.30	100.72	0.0086	bdl	0.0105	bdl	bdl
234007_4	7.10	93.03	100.13	0.0161	bdl	0.0273	bdl	bdl
234008_1	4.37	95.96	100.33	0.0127	bdl	0.0625	bdl	bdl
234009_1	21.70	79.60	101.29	0.0205	0.0676	0.0216	bdl	bdl
234009_2	23.71	77.28	100.99	0.0304	0.0060	0.0273	0.0089	bdl
234009_3	18.92	80.66	99.57	0.0141	bdl	0.0114	0.0102	bdl
234010_1	29.88	71.32	101.20	0.0288	bdl	0.0171	bdl	bdl
234010_2	18.65	83.03	101.68	0.0147	bdl	0.0185	bdl	bdl
234010_3	23.24	77.15	100.40	0.0199	0.0253	0.0184	bdl	bdl
234010_4	26.02	74.71	100.72	0.0133	0.0085	0.0118	bdl	bdl
234011_10	25.98	74.17	100.15	0.0197	0.0047	bdl	bdl	bdl
234011_12	38.93	62.56	101.49	0.0578	bdl	0.0071	0.0125	bdl
234011_5	19.41	81.57	100.99	0.0131	bdl	0.0100	bdl	bdl

Gold grain	Ag (%)	Au (%)	Total (%)	S (%)	Fe (%)	Cu (%)	As (%)	Hg (%)
234011_6	16.83	84.61	101.44	0.0170	bdl	0.0276	bdl	bdl
234011_7	30.11	70.50	100.61	0.0300	0.6289	0.0093	bdl	bdl
234011_8	26.10	75.27	101.37	0.0239	bdl	0.0094	bdl	bdl
234012_0	20.84	80.06	100.90	0.0159	bdl	0.0157	0.0138	bdl
234012_1	24.96	74.18	99.15	0.0170	0.0040	0.0171	0.0084	bdl
234012_2	19.47	81.62	101.08	0.0113	bdl	0.0128	0.0154	bdl
234012_2.1	15.58	69.19	84.76	0.0168	0.0041	0.0276	bdl	bdl
234012_3	17.79	81.93	99.72	0.0169	0.0094	0.0309	bdl	bdl
234012_4	23.17	74.61	97.78	0.0208	bdl	0.0179	bdl	bdl
234013_1	43.04	58.57	101.61	0.0774	0.0046	0.0087	bdl	bdl
234013_2	29.36	72.29	101.65	0.0312	0.0079	0.0124	0.0098	bdl
234014_0	21.08	80.08	101.16	0.0178	bdl	0.0147	bdl	bdl
234014_1	21.09	77.75	98.84	0.0315	0.0056	0.0099	bdl	bdl
234014_2	27.13	73.18	100.31	0.0258	bdl	0.0088	bdl	bdl
234014_3	18.28	78.93	97.21	0.0231	0.0037	0.0090	bdl	bdl
234014_3	22.68	78.66	101.34	0.0245	bdl	0.0204	bdl	bdl
234014_4	35.09	63.79	98.88	0.0257	bdl	0.0108	0.0094	bdl
234014_6	24.71	76.52	101.23	0.0150	bdl	0.0152	bdl	bdl
234015_1	28.47	72.34	100.81	0.0326	bdl	0.0128	0.0094	bdl
234015_2	29.28	70.64	99.91	0.0376	0.0085	bdl	0.0118	bdl
234016_1	8.66	91.01	99.67	0.0105	bdl	0.0277	bdl	bdl
234016_2	12.69	87.84	100.52	0.0079	bdl	0.0119	bdl	bdl
234016_3	25.66	76.22	101.88	0.0162	0.0041	0.0170	bdl	bdl
234017_1	12.27	84.87	97.14	0.0138	bdl	0.0647	bdl	bdl
234017_2	36.80	65.32	102.12	0.0256	bdl	0.0117	0.0165	bdl
234017_3	30.57	68.79	99.36	0.0361	0.0137	bdl	bdl	bdl
234018_0	25.74	73.27	99.01	0.0260	bdl	0.0124	bdl	bdl
234018_1	33.56	67.05	100.61	0.0143	0.0373	bdl	bdl	0.0203
234018_2	25.38	73.97	99.35	0.0167	bdl	0.0172	bdl	bdl
234019_0	31.59	65.84	97.43	0.0071	0.0044	0.0141	0.0142	bdl
234019_1	24.26	75.06	99.33	0.0068	0.0067	0.0087	bdl	bdl
234019_2	22.02	63.28	85.30	0.0099	0.0050	0.0078	bdl	bdl
234019_3	22.59	74.99	97.58	0.0045	bdl	0.0179	bdl	bdl
234019_4	13.15	86.66	99.81	0.0090	bdl	0.0155	bdl	bdl
234019_7	22.67	75.52	98.19	0.0062	0.0076	0.0140	bdl	bdl
234019_8	25.54	73.08	98.62	0.0068	0.0040	0.0155	bdl	bdl
247526_0	22.72	76.81	99.54	0.0091	0.0091	0.0099	0.0081	bdl
247526_1	8.50	89.53	98.02	0.0308	bdl	0.0632	bdl	bdl
247526_2	18.66	81.86	100.52	0.0067	0.0041	0.0215	bdl	bdl
247526_2.1	19.17	73.18	92.35	0.0204	bdl	0.0239	bdl	bdl
247526_3	30.85	68.86	99.71	0.0235	bdl	0.0107	bdl	bdl

Gold grain	Ag (%)	Au (%)	Total (%)	S (%)	Fe (%)	Cu (%)	As (%)	Hg (%)
247526_6	24.16	74.38	98.54	0.0062	bdl	0.0196	bdl	bdl
247526_7	15.86	82.79	98.64	0.0064	bdl	0.0175	bdl	0.1424
247528_0	29.50	71.45	100.96	0.0107	0.0043	0.0171	0.0111	bdl
247528_1	11.28	86.98	98.26	0.0315	bdl	0.0527	bdl	bdl
247528_2	24.05	72.21	96.26	0.0402	bdl	0.0156	bdl	bdl
247528_3	13.81	81.86	95.67	0.0417	0.0042	0.0386	bdl	bdl
247529_1	16.22	84.15	100.37	0.0171	bdl	0.0218	bdl	bdl
247529_2	8.96	90.90	99.86	0.0144	0.0093	0.0852	bdl	bdl
247530_1	28.68	71.22	99.89	0.0125	0.0048	0.0203	bdl	bdl
247530_2	22.97	77.36	100.33	0.0164	0.0050	0.0098	bdl	bdl
247530_3	29.01	71.44	100.45	0.0252	bdl	bdl	bdl	bdl
247530_4	31.71	68.33	100.03	0.0322	bdl	0.0131	bdl	bdl
247530_5	16.49	84.27	100.76	0.0104	bdl	0.0193	0.0194	bdl
247532_0	25.45	72.77	98.22	0.0085	bdl	0.0087	0.0094	bdl
247532_1	24.91	72.73	97.64	0.0217	bdl	0.0063	0.0097	bdl
247532_2	16.52	81.45	97.98	0.0072	0.0064	0.0111	bdl	bdl
247532_2.1	28.50	71.44	99.94	0.0181	bdl	0.0104	bdl	bdl
247532_3	35.57	64.66	100.23	0.0073	bdl	0.0096	bdl	bdl
247532_3.1	23.37	75.84	99.21	0.0214	bdl	0.0099	0.0105	bdl
247532_4	24.94	73.13	98.07	0.0067	0.0083	0.0091	0.0160	bdl
247533_0	16.84	81.21	98.04	0.0094	bdl	0.0303	bdl	bdl
247533_1	10.25	84.87	95.12	0.0308	bdl	0.0423	bdl	bdl
247533_2	22.36	75.00	97.36	0.0187	bdl	0.0230	bdl	bdl
247533_3	47.03	53.14	100.16	0.0417	bdl	0.0085	bdl	bdl
247533_4	43.96	56.22	100.18	0.0233	bdl	bdl	bdl	bdl
247533_5	23.17	75.26	98.42	0.0123	bdl	0.0198	bdl	bdl
247534_0	12.75	87.86	100.61	0.0138	bdl	0.0532	0.0109	bdl
247534_1	10.08	88.03	98.11	0.0422	bdl	0.0241	bdl	bdl
247534_2	29.97	68.88	98.86	0.0297	bdl	0.0062	bdl	bdl

247534_0: 247534: ID Sample 0: ID gold grain

bdl: below detection limit

B.4.1.3 LA-ICP-MS results in gold grains

Gold grain	Cr (ppm)	Mn (ppm)	Fe (ppm)	Co (ppm)	Ni (ppm)	Cu (ppm)	Zn (ppm)	Se (ppm)	As (ppm)	Pd (ppm)	Cd (ppm)
230985_0	bdl	162.47	7552.75	0.13	1.28	35.99	2.18	bdl	1.94	0.31	bdl
230985_1	34.08	93.10	9770.42	6.78	104.14	327.16	153.71	bdl	24.73	12.50	0.51
230985_2	6.45	107.56	12556.51	3.45	51.52	54.34	87.49	bdl	60.93	4.65	bdl
230986_0	bdl	bdl	569.79	0.08	bdl	17.08	6.87	bdl	4.66	0.55	0.13
230986_1	6.10	200.51	38394.99	1.84	8.31	26.84	105.98	bdl	297.54	0.79	0.16
230986_3	bdl	bdl	202.92	bdl	bdl	12.29	24.18	bdl	0.68	0.50	bdl
230987_1	17.08	525.38	171290.63	1.27	21.30	212.00	491.79	1.91	6082.46	1.14	0.81
230987_2	42.67	2372.38	19668.56	1.67	9.60	673.56	217.38	0.62	8.92	1.08	0.56
230987_3	230.47	411.30	127727.83	63.36	152.62	661.76	1148.28	32.71	75.19	18286.78	0.36
230987_4	bdl	bdl	1214.62	0.14	bdl	30.65	16.42	bdl	25.41	0.78	bdl
230987_5	N-A	N-A	413.00	0.17	1.79	19.63	12.68	N-A	2.54	0.35	0.00
230988_2	922.93	4170.58	101758.18	173.36	758.60	92.82	343.00	bdl	104.74	1.84	0.37
230988_3	8.20	15.55	1630.58	4.02	21.29	60.77	23.82	bdl	39.01	2.98	2.48
230988_4	54.93	154.00	18158.34	89.40	448.44	463.98	912.13	1.70	5599.85	2.49	8.40
230988_7	bdl	bdl	bdl	bdl	bdl	33.12	bdl	bdl	bdl	0.28	0.16
230989_2	15.06	37.40	2776.02	2.51	8.03	3828.03	58.53	bdl	34.10	453.10	18.20
230989_3	94.18	82.29	5989.55	4.00	9.92	126.47	66.12	bdl	198.50	5.82	bdl
230990_2	N-A	N-A	7936.66	6.02	25.54	61.05	71.94	N-A	12.32	1.05	0.00
230991_1	bdl	bdl	bdl	bdl	bdl	192.00	bdl	bdl	bdl	2.41	bdl
230993_1	bdl	bdl	bdl	bdl	bdl	22.20	bdl	bdl	bdl	0.44	bdl
230993_3	bdl	bdl	1720.39	0.37	bdl	16.29	2.61	bdl	918.63	1.08	bdl
230993_4	bdl	bdl	393.20	0.10	1.74	79.12	5.95	bdl	2.64	0.37	0.27
230993_6	14.55	22.41	949.02	bdl	bdl	36.79	0.80	bdl	bdl	11.37	0.05
230994_1	bdl	bdl	235.92	bdl	bdl	29.35	3.69	bdl	1.30	0.25	bdl
230994_2	15.00	26.63	12322.78	0.48	4.72	53.93	58.94	bdl	44.00	0.18	0.22
230994_3	bdl	bdl	265.41	0.16	1.15	4.13	4.71	bdl	1.63	0.43	bdl
230994_4	bdl	bdl	277.47	0.16	bdl	53.33	4.12	bdl	1.56	0.41	0.28

Gold grain	Cr (ppm)	Mn (ppm)	Fe (ppm)	Co (ppm)	Ni (ppm)	Cu (ppm)	Zn (ppm)	Se (ppm)	As (ppm)	Pd (ppm)	Cd (ppm)
230995_0	N-A	N-A	462.96	0.00	2.11	29.35	0.00	N-A	0.00	0.24	0.00
230995_1	285.28	4368.24	68720.70	46.68	189.00	620.23	1634.43	3.68	2658.94	0.29	1.28
230995_2	bdl	35.10	257.07	0.44	1.05	35.73	19.54	bdl	1.33	0.41	bdl
230995_4	4.21	27.70	772.60	0.35	2.82	38.78	27.18	bdl	11.06	7.16	0.10
230995_7	bdl	120.29	1515.86	1.13	6.65	54.17	59.89	bdl	336.98	0.27	bdl
230996_0	bdl	bdl	bdl	bdl	bdl	133.76	bdl	bdl	bdl	0.32	0.10
230997_2	bdl	bdl	bdl	bdl	bdl	15.27	bdl	bdl	bdl	0.43	bdl
230997_3	5.88	29.70	1545.36	0.70	4.10	101.25	23.69	bdl	1.43	1.06	bdl
230997_4	35.21	162.18	12897.94	2.77	11.93	1011.21	303.81	bdl	879.99	1.69	12.81
230998_0	bdl	bdl	bdl	bdl	bdl	30.84	bdl	bdl	bdl	55.40	bdl
230998_1	4.36	54.92	2406.88	51.65	6.48	47.40	37.55	bdl	846.48	1.03	0.05
230998_1.1	44.38	149.78	6831.31	3.58	18.90	111.37	212.77	bdl	21.22	528.94	0.13
230998_2	8.53	15.91	724.07	0.33	2.98	23.95	20.28	bdl	0.52	0.41	bdl
230998_2.1	10.26	22.15	2163.04	0.81	5.23	66.19	66.84	bdl	4.84	193.79	0.10
230998_3_	5.81	35.84	1410.65	1.69	5.65	325.29	85.61	1.68	1.50	3.31	bdl
230998_4	bdl	bdl	4103.81	6.52	19.37	257.56	372.54	bdl	bdl	2936.85	bdl
231000_2	5.28	11.02	1250.75	0.49	2.87	23.60	16.07	bdl	bdl	0.63	bdl
231000_3	N-A	N-A	198477.02	58.51	102.93	720.86	1286.39	N-A	320.39	0.54	2.63
231000_4	3.53	20.84	1542.87	0.82	4.77	26.05	17.06	bdl	bdl	0.83	bdl
231000_5	3.29	12.48	558.44	0.62	3.04	68.39	19.92	bdl	0.32	0.74	0.26
234001_2	N-A	N-A	4896.63	3.76	10.34	27.61	44.29	N-A	114.66	0.34	0.24
234001_3	bdl	bdl	56.53	0.07	bdl	530.21	2.20	bdl	bdl	0.63	bdl
234002_1	31.84	61.87	6368.92	3.59	20.15	63.00	148.24	bdl	3.86	0.41	0.08
234003_1	N-A	N-A	2721.83	0.83	4.28	197.45	18.23	N-A	38.67	2.92	41.66
234003_2	48.39	3501.30	87132.50	7.03	28.86	124.91	147.76	bdl	527.76	1.30	bdl
234005_1	N-A	N-A	9391.39	8.63	60.78	68.68	141.49	N-A	34.68	0.00	0.00
234005_2	N-A	N-A	7064.64	0.58	4.60	29.01	32.07	N-A	607.53	0.88	0.00
234005_3	6.65	97.52	326.43	bdl	bdl	14.73	bdl	bdl	bdl	4.82	0.05
234005_4	bdl	bdl	181.51	bdl	bdl	11.57	bdl	bdl	bdl	0.38	bdl

Gold grain	Cr (ppm)	Mn (ppm)	Fe (ppm)	Co (ppm)	Ni (ppm)	Cu (ppm)	Zn (ppm)	Se (ppm)	As (ppm)	Pd (ppm)	Cd (ppm)
234006_1	102.63	101.30	14692.15	4.03	30.21	96.14	82.90	bdl	65.98	2.70	0.46
234006_2	N-A	N-A	2728.06	1.37	3.70	104.34	29.65	N-A	6.09	1.73	11.43
234007_1	bdl	bdl	29.23	bdl	bdl	154.54	2.60	bdl	bdl	0.77	bdl
234007_4	41.21	168.52	4516.89	2.38	38.02	156.11	161.79	bdl	3.32	3.32	0.38
234008_1	135.41	304.74	19808.03	12.14	64.55	490.16	479.09	bdl	4.50	11.51	bdl
234009_1	94.71	1622.64	25009.34	7.71	22.93	301.40	208.61	4.17	3196.87	1.22	2.29
234009_2	145.99	3292.20	27786.25	8.44	21.45	155.38	181.82	bdl	188.50	0.90	1.60
234009_3	20.00	23.95	2064.31	2.36	5.78	32.71	48.96	bdl	2.24	0.53	bdl
234010_1	N-A	N-A	8649.68	27.47	142.38	43.29	128.67	N-A	88.72	0.55	0.00
234010_4	N-A	N-A	7337.67	36.42	37.63	72.75	45.86	N-A	336.82	2.58	0.48
234011_10	N-A	N-A	60910.06	31.09	367.71	397.68	318.54	N-A	101.81	6.71	0.00
234011_12	N-A	N-A	97041.80	5.00	43.08	885.63	251.62	N-A	1970.87	2.55	0.46
234011_5	10.14	33.92	2489.83	0.67	5.50	108.35	27.86	0.74	46.97	0.77	bdl
234011_6	N-A	N-A	1291.82	0.00	6.41	235.36	26.52	N-A	0.00	2.73	34.16
234011_7	N-A	N-A	17672.64	9.63	62.39	258.75	221.53	N-A	18.06	0.46	0.00
234011_8	bdl	bdl	bdl	bdl	bdl	15.45	1.08	bdl	bdl	15.54	0.05
234012_0	N-A	N-A	1095.77	0.26	1.74	33.32	12.77	N-A	36.20	0.34	0.37
234012_1	9.79	21.10	1426.00	0.96	4.55	71.77	47.18	bdl	25.27	1.02	12.08
234012_2	N-A	N-A	18875.64	12.15	236.33	75.90	180.65	N-A	19.57	0.53	0.00
234012_2.1	bdl	bdl	271.85	0.19	2.79	69.34	10.45	bdl	1.65	0.11	bdl
234012_3	bdl	bdl	318.21	0.14	0.96	61.13	8.88	bdl	bdl	0.22	bdl
234012_4	bdl	bdl	23.56	bdl	bdl	28.40	0.92	bdl	bdl	0.24	bdl
234013_1	N-A	N-A	263.18	0.00	0.00	3.85	4.20	N-A	0.00	0.66	0.03
234013_2	N-A	N-A	18719.11	2.41	21.68	84.29	82.59	N-A	715.72	1.05	0.15
234014_0	28.01	1909.64	36454.82	7.40	21.87	71.33	183.64	bdl	388.16	1.00	4.21
234014_1	bdl	bdl	72.35	0.26	bdl	38.57	4.92	bdl	0.53	0.37	bdl
234014_2	41.75	85.04	27759.81	6.75	22.75	84.25	218.40	0.97	551.64	0.42	0.48
234014_3	212.85	647.37	26172.36	12.56	88.89	74.82	217.24	bdl	57.42	2.37	bdl
234014_3.1	N-A	N-A	354.04	0.57	0.00	46.21	6.28	N-A	0.00	0.36	0.14

Gold grain	Cr (ppm)	Mn (ppm)	Fe (ppm)	Co (ppm)	Ni (ppm)	Cu (ppm)	Zn (ppm)	Se (ppm)	As (ppm)	Pd (ppm)	Cd (ppm)
234014_4	bdl	bdl	338.88	0.35	1.44	5.89	8.60	bdl	2.08	6.91	bdl
234014_6	N-A	N-A	12338.79	2.28	9.07	117.81	62.84	N-A	77.31	10.01	0.69
234015_1	bdl	bdl	1091.51	bdl	bdl	11.65	8.26	bdl	3.17	0.29	bdl
234015_2	N-A	N-A	48942.11	4.41	27.57	103.66	350.43	N-A	4233.24	0.30	0.30
234016_2	14.72	17.46	3741.02	1.15	9.74	44.98	77.57	bdl	2.24	12.68	0.09
234016_3	8.88	23.97	2081.74	0.94	6.97	28.40	74.14	bdl	0.83	0.90	bdl
234017_2	N-A	N-A	6794.66	1.54	16.42	33.86	215.44	N-A	2.77	2.21	0.00
234018_0	bdl	bdl	bdl	bdl	bdl	38.20	bdl	bdl	bdl	0.16	bdl
234018_1	146.33	147.14	25256.22	7.80	51.23	318.83	474.77	bdl	14.03	0.18	0.27
234019_0	35.58	144.09	5583.82	120.34	455.39	114.29	307.98	5.71	25.78	0.71	bdl
234019_1	bdl	bdl	34.86	0.28	1.01	7.39	0.90	bdl	bdl	12.17	bdl
234019_2	bdl	bdl	21.39	0.10	bdl	5.68	bdl	bdl	bdl	0.46	bdl
234019_3	bdl	bdl	bdl	bdl	bdl	18.55	bdl	bdl	bdl	0.52	bdl
234019_4	bdl	bdl	bdl	bdl	bdl	86.65	bdl	bdl	bdl	0.11	0.81
234019_7	9.47	36.57	1842.58	17.27	65.84	27.55	40.80	bdl	25.08	1.32	bdl
234019_8	4.47	bdl	495.59	7.58	30.09	16.26	24.75	bdl	2.15	1.19	bdl
247526_0	N-A	N-A	1139.88	19.36	126.78	29.24	130.24	N-A	0.00	3.45	0.04
247526_1	bdl	bdl	524.11	5.81	18.80	340.76	18.75	bdl	1.40	1.31	bdl
247526_2	N-A	N-A	6987.63	164.90	262.87	215.05	187.73	N-A	1284.59	8.69	9.24
247526_2.1	bdl	bdl	bdl	bdl	bdl	66.85	bdl	bdl	bdl	0.24	bdl
247526_3	bdl	bdl	bdl	0.22	bdl	3.54	0.73	bdl	bdl	0.30	bdl
247526_6	5.85	25.92	2805.84	17.63	90.60	32.24	104.98	bdl	14.12	2.60	bdl
247526_7	N-A	N-A	581.00	4.36	13.38	123.91	21.47	N-A	5.64	2.28	30.10
247528_0	6.59	23.40	1967.83	0.65	12.40	48.85	81.97	bdl	111.16	0.94	0.48
247528_1	bdl	bdl	bdl	bdl	bdl	351.22	bdl	bdl	bdl	0.47	0.20
247528_2	bdl	12.09	903.60	0.53	13.40	43.03	85.18	bdl	0.93	0.12	bdl
247528_3	bdl	bdl	343.40	0.17	2.90	122.62	12.63	bdl	0.78	bdl	bdl
247529_1	N-A	N-A	580.45	0.15	2.38	25.59	19.74	N-A	0.00	1.98	0.00
247530_1	41.91	90.57	6684.30	2.08	21.38	73.24	166.08	bdl	bdl	3723.35	bdl

Gold grain	Cr (ppm)	Mn (ppm)	Fe (ppm)	Co (ppm)	Ni (ppm)	Cu (ppm)	Zn (ppm)	Se (ppm)	As (ppm)	Pd (ppm)	Cd (ppm)
247530_2	N-A	N-A	3165.61	0.00	0.00	25.21	29.36	N-A	103.08	0.29	0.28
247530_3	bdl	bdl	790.40	bdl	2.98	11.35	18.20	bdl	3.75	11.33	bdl
247532_0	bdl	bdl	107.34	0.22	1.11	30.15	3.98	bdl	bdl	0.47	bdl
247532_1	12.70	21.96	3042.05	0.47	4.74	20.62	36.89	bdl	373.89	0.37	bdl
247532_2	N-A	N-A	63814.57	28.57	242.83	80.05	424.25	N-A	21.59	9.81	0.06
247532_2.1	N-A	N-A	2485.96	0.37	2.33	29.88	15.94	N-A	33.35	0.72	0.10
247532_3	N-A	N-A	24913.56	16.82	49.81	192.95	131.41	N-A	1068.05	1.37	2.96
247532_3.1	13552.40	1160.17	42344.18	714.94	2977.30	196.75	2149.96	bdl	266.66	0.84	0.44
247532_4	N-A	N-A	6366.11	0.54	8.42	10.53	9.50	N-A	52.09	0.31	0.00
247533_0	N-A	N-A	1328.27	0.67	0.00	120.89	20.21	N-A	0.00	0.81	13.20
247533_1	bdl	bdl	bdl	bdl	bdl	86.25	bdl	bdl	bdl	0.80	bdl
247533_2	bdl	13.90	bdl	0.53	bdl						
247533_3	3.26	13.17	617.13	0.68	5.61	18.42	15.56	6.98	8.42	0.56	0.13
247533_4	46.28	44.09	56834.00	24.80	82.14	101.54	218.89	bdl	934.03	0.32	0.33
247533_5	N-A	N-A	568.65	0.55	0.00	49.39	21.38	N-A	0.00	2.24	0.00
247534_1	bdl	bdl	215.65	bdl	bdl	218.12	7.28	bdl	bdl	0.20	bdl
247534_2	bdl	bdl	728.67	0.22	1.86	17.43	11.57	bdl	0.55	1.46	bdl

247534_1: 247534: ID Sample 1: ID gold grain N-A: Not measured bdl: below detection limit

Gold grain	Pt (ppm)	Sn (ppm)	Sb (ppm)	Te (ppm)	Hg (ppm)	Pb (ppm)	Bi (ppm)
230985_0	bdl	bdl	30.90	bdl	4780.77	0.13	1.55
230985_1	bdl	1.19	bdl	bdl	15351.96	7.30	1.01
230985_2	bdl	0.27	93.37	0.39	10507.95	3.24	0.52
230986_0	bdl	bdl	4.60	0.62	1377.48	4.56	11.53
230986_1	bdl	0.21	5.54	28.12	2851.53	172.17	440.58
230986_3	bdl	bdl	3.02	bdl	3484.01	0.12	0.25
230987_1	bdl	bdl	50.71	3.93	6740.86	54.14	9.07
230987_2	bdl	76.24	1.24	0.63	1839.66	49.19	7.17
230987_3	21.41	3.49	1.16	4.12	5648.97	226.91	9.49
230987_4	bdl	bdl	37.24	bdl	4065.06	1.18	0.22
230987_5	N-A	0.00	41.43	0.00	7826.82	0.21	0.00
230988_2	bdl	0.80	1.01	0.94	1245.32	5.26	0.53
230988_3	0.03	bdl	2.09	bdl	1457.10	4.13	0.56
230988_4	0.12	1.95	339.40	23.14	1410.42	73.89	0.99
230988_7	bdl	bdl	0.97	bdl	8256.18	bdl	0.11
230989_2	bdl	1.32	407.60	bdl	13562.37	2.06	52.20
230989_3	bdl	1.25	2.69	bdl	3845.36	13.87	3.92
230990_2	N-A	0.00	47.28	0.00	1722.90	10.67	2.68
230991_1	bdl	bdl	0.66	bdl	49515.29	bdl	bdl
230993_1	bdl	bdl	bdl	bdl	2542.62	bdl	bdl
230993_3	bdl	bdl	9.13	6.22	1434.13	0.45	bdl
230993_4	bdl	bdl	19.92	bdl	3177.02	0.33	0.14
230993_6	bdl	bdl	2.06	bdl	2292.55	0.11	bdl
230994_1	0.01	0.28	1.58	bdl	1841.01	2.02	0.03
230994_2	bdl	0.36	85.87	0.25	3793.19	142.28	1.37
230994_3	bdl	bdl	91.01	bdl	4249.92	0.92	0.16
230994_4	bdl	bdl	259.84	0.53	3157.60	1.82	0.18
230995_0	N-A	0.00	0.00	1.68	2646.97	0.21	0.54
230995_1	bdl	7.18	45.97	5.93	1116.44	282.75	131.77

Gold grain	Pt (ppm)	Sn (ppm)	Sb (ppm)	Te (ppm)	Hg (ppm)	Pb (ppm)	Bi (ppm)
230995_2	bdl	bdl	0.81	bdl	2398.57	0.35	bdl
230995_4	bdl	bdl	0.57	bdl	1780.32	15.48	0.08
230995_7	bdl	bdl	0.57	bdl	3379.21	1.35	0.29
230996_0	bdl	bdl	bdl	bdl	144.67	bdl	bdl
230997_2	bdl	bdl	bdl	bdl	288.22	bdl	0.05
230997_3	bdl	bdl	bdl	0.19	4985.45	3.63	0.08
230997_4	bdl	1.58	99.49	3.48	4382.31	54.41	1.20
230998_0	bdl	bdl	bdl	bdl	1088.57	bdl	bdl
230998_1	bdl	bdl	16.24	13.41	3832.63	62.10	2.10
230998_1.1	0.14	0.74	5.06	bdl	2935.30	56.29	2.41
230998_2	bdl	0.16	bdl	bdl	1459.12	11.37	0.57
230998_2.1	0.05	0.37	4.12	bdl	2334.13	27.59	0.88
230998_3_	bdl	0.36	bdl	bdl	2437.91	15.90	3.37
230998_4	14.31	2.54	bdl	bdl	14560.82	42.76	9.41
231000_2	bdl	bdl	bdl	0.72	402.11	189.68	10.77
231000_3	N-A	5.40	2.50	0.45	7761.77	360.47	1.98
231000_4	bdl	bdl	bdl	bdl	1205.71	2.78	bdl
231000_5	bdl	bdl	1.93	bdl	1103.49	0.99	2.86
234001_2	N-A	0.00	2.93	0.00	1951.57	4.95	0.14
234001_3	bdl	bdl	bdl	bdl	2052.32	0.11	0.03
234002_1	bdl	0.77	0.23	bdl	2664.63	3.23	0.09
234003_1	N-A	0.36	61.75	0.00	1392.20	1.86	0.12
234003_2	bdl	1.12	46.08	3.81	14700.36	11.66	0.59
234005_1	N-A	1.23	0.00	0.00	2157.47	9.79	0.56
234005_2	N-A	0.77	26.65	1.43	5179.42	19.65	10.45
234005_3	bdl	bdl	14.68	1.05	1467.62	0.80	bdl
234005_4	bdl	bdl	bdl	0.44	377.74	0.15	9.01
234006_1	bdl	0.98	132.27	bdl	1869.51	253.30	0.56
234006_2	N-A	0.00	17.57	0.00	2331.19	101.16	0.30

Gold grain	Pt (ppm)	Sn (ppm)	Sb (ppm)	Te (ppm)	Hg (ppm)	Pb (ppm)	Bi (ppm)
234007_1	bdl	bdl	bdl	bdl	6385.67	0.17	bdl
234007_4	bdl	0.93	bdl	bdl	2231.25	7.77	0.73
234008_1	bdl	2.60	bdl	1.52	3974.23	366.83	4.92
234009_1	0.55	2.92	25.75	291.95	2664.98	69.57	12.91
234009_2	0.27	0.83	24.16	21.19	3166.22	6.17	1.89
234009_3	bdl	bdl	bdl	bdl	614.89	2.00	0.26
234010_1	N-A	1.24	0.00	0.00	848.26	25.34	0.64
234010_4	N-A	0.39	76.16	1.39	2197.28	17.19	1.07
234011_10	N-A	8.32	8.67	0.00	1048.56	1112.44	7.64
234011_12	N-A	6.72	35.43	19.50	2060.05	14047.18	63.97
234011_5	bdl	1.08	bdl	1.55	817.56	112.98	1.02
234011_6	N-A	0.00	15.25	0.00	318.82	120.78	1.33
234011_7	N-A	0.00	3.12	3.24	1724.83	343.41	1.65
234011_8	bdl	bdl	2.94	bdl	4139.67	1.16	bdl
234012_0	N-A	0.31	158.02	0.00	1030.30	6.91	1.19
234012_1	bdl	bdl	219.73	0.44	986.78	3.96	0.27
234012_2	N-A	0.54	0.87	0.00	1603.89	6.38	0.09
234012_2.1	bdl	bdl	bdl	bdl	450.80	0.40	bdl
234012_3	bdl	bdl	bdl	bdl	5263.95	0.61	bdl
234012_4	bdl	bdl	3.76	bdl	6967.93	0.09	0.05
234013_1	N-A	0.00	35.75	0.00	2928.69	8.04	0.89
234013_2	N-A	1.33	6.35	1.13	1518.81	530.32	7.46
234014_0	bdl	1.35	5.53	2.11	3194.78	299.71	270.00
234014_1	bdl	bdl	2.28	bdl	3986.75	0.54	bdl
234014_2	bdl	2.57	106.13	0.64	5962.58	550.42	6.50
234014_3	bdl	1.36	1.58	bdl	710.18	164.35	2.71
234014_3.1	N-A	0.00	52.08	0.00	4161.42	4.24	0.25
234014_4	bdl	bdl	6.75	0.12	3850.79	5.10	0.11
234014_6	N-A	0.00	225.83	25.65	241.87	411.52	7.81

Gold grain	Pt (ppm)	Sn (ppm)	Sb (ppm)	Te (ppm)	Hg (ppm)	Pb (ppm)	Bi (ppm)
234015_1	bdl	bdl	27.76	bdl	2376.34	3.03	0.20
234015_2	N-A	2.53	11.49	3.73	5230.35	35.59	1.87
234016_2	bdl	0.38	bdl	bdl	927.74	7.07	0.36
234016_3	bdl	bdl	0.43	0.21	1906.40	4.06	1.02
234017_2	N-A	0.49	0.54	0.00	5673.02	53.37	1.62
234018_0	bdl	bdl	bdl	bdl	428.91	bdl	0.07
234018_1	bdl	2.97	bdl	0.74	480.93	407.39	7.79
234019_0	bdl	1.13	40.79	bdl	632.38	24.90	0.52
234019_1	bdl	bdl	1.41	bdl	407.01	0.12	0.03
234019_2	bdl	bdl	1.48	bdl	330.96	0.07	0.28
234019_3	bdl	bdl	0.84	bdl	1573.13	6.19	0.23
234019_4	bdl	bdl	3.37	0.34	1094.79	9.43	1.31
234019_7	0.06	bdl	1.04	bdl	7739.30	4.06	0.20
234019_8	bdl	bdl	bdl	bdl	1059.81	7.08	1.78
247526_0	N-A	0.00	0.85	0.00	3257.81	6.94	0.00
247526_1	bdl	0.23	bdl	bdl	1450.45	4.17	bdl
247526_2	N-A	3.07	21.57	16.97	779.31	563.56	3.59
247526_2.1	bdl	bdl	3.92	bdl	3513.12	bdl	0.12
247526_3	bdl	bdl	877.83	bdl	25157.97	0.21	bdl
247526_6	bdl	0.17	7.05	0.22	1628.52	14.09	0.16
247526_7	N-A	2.47	39.05	0.00	1642.59	3.02	0.00
247528_0	bdl	0.31	11.87	bdl	4301.42	0.80	0.10
247528_1	bdl	bdl	bdl	bdl	1495.35	bdl	bdl
247528_2	bdl	bdl	bdl	bdl	630.86	0.83	0.10
247528_3	bdl	bdl	bdl	bdl	435.38	0.19	0.69
247529_1	N-A	0.00	0.00	1.11	4518.11	7.79	0.36
247530_1	3.12	bdl	bdl	bdl	1117.66	5.89	0.58
247530_2	N-A	1.75	2.53	0.00	415.60	12.71	0.93
247530_3	bdl	0.35	1.62	bdl	2133.83	0.49	bdl

Gold grain	Pt (ppm)	Sn (ppm)	Sb (ppm)	Te (ppm)	Hg (ppm)	Pb (ppm)	Bi (ppm)
247532_0	bdl	bdl	bdl	bdl	2261.39	1.84	0.40
247532_1	bdl	0.17	12.00	bdl	1036.72	3.59	3.24
247532_2	N-A	0.40	1.39	0.00	3955.74	106.75	0.25
247532_2.1	N-A	0.00	43.04	7.29	4592.78	2.03	0.23
247532_3	N-A	3.35	102.18	4.21	4728.52	1039.34	7.63
247532_3.1	bdl	1.74	21.80	bdl	1292.11	39.05	1.61
247532_4	N-A	0.00	376.77	0.00	4539.12	34.24	0.00
247533_0	N-A	0.00	28.61	0.00	606.16	1.86	0.00
247533_1	bdl	bdl	bdl	bdl	1361.32	bdl	bdl
247533_2	bdl	bdl	bdl	bdl	2259.26	bdl	bdl
247533_3	0.08	0.15	187.45	0.15	1042.29	13.22	0.31
247533_4	0.98	1.30	329.22	0.68	8646.36	570.87	1.30
247533_5	N-A	0.00	0.00	0.00	1286.19	0.57	1.02
247534_1	bdl	bdl	bdl	bdl	342.48	1.05	0.07
247534_2	bdl	bdl	7.56	0.39	3088.70	0.60	0.12

247534_1: 247534: ID Sample 1: ID gold grain bdl: Below detection limit N-A: No measured

B.4.2 Scheelite analysis

B.4.2.1 Detection limits in scheelite analysis

Element	Detection Limit	Unit	Method
WO ₃	1422-1508	ppm	EPMA
CaO	112-118	ppm	EPMA
MnO	580-698	ppm	EPMA
Na ₂ O	15-16	ppm	EPMA
FeO	33-34	ppm	EPMA
MoO ₃	35-40	ppm	EPMA
SrO	98-111	ppm	EPMA
Y ₂ O ₃	33	ppm	EPMA
⁷ Li	0.032-0.102	ppm	LA-ICP-MS
¹¹ B	0.167-0.580	ppm	LA-ICP-MS
²³ Na	1.21-3.06	ppm	LA-ICP-MS
²⁴ Mg	0.049-1.390	ppm	LA-ICP-MS
²⁸ Si	117.4-320.6	ppm	LA-ICP-MS
³⁴ S	25.37-71.27	ppm	LA-ICP-MS
³⁹ K	0.780-2.143	ppm	LA-ICP-MS
⁴⁷ Ti	0.076-0.365	ppm	LA-ICP-MS
⁵¹ V	0.025-0.072	ppm	LA-ICP-MS
⁵² Cr	0.216-0.574	ppm	LA-ICP-MS
⁵⁵ Mn	0.332-0.835	ppm	LA-ICP-MS
⁵⁶ Fe	0.336-1.150	ppm	LA-ICP-MS
⁵⁹ Co	0.012-0.040	ppm	LA-ICP-MS
⁶³ Cu	0.065-0.161	ppm	LA-ICP-MS
⁶⁶ Zn	0.166-0.515	ppm	LA-ICP-MS
⁷⁵ As	0.427-1.295	ppm	LA-ICP-MS
⁸⁸ Sr	0.030-0.466	ppm	LA-ICP-MS
⁸⁹ Y	0.029-0.077	ppm	LA-ICP-MS
⁹³ Nb	0.012-0.040	ppm	LA-ICP-MS
⁹⁵ Mo	0.042-0.291	ppm	LA-ICP-MS
¹⁰⁷ Ag	0.025-0.112	ppm	LA-ICP-MS
¹¹⁸ Sn	0.033-0.139	ppm	LA-ICP-MS
¹³⁷ Ba	0.131-0.390	ppm	LA-ICP-MS
¹³⁹ La	0.009-0.036	ppm	LA-ICP-MS

Element	Detection Limit	Unit	Method
¹⁴⁰ Ce	0.022-0.081	ppm	LA-ICP-MS
¹⁴⁶ Nd	0.098-0.248	ppm	LA-ICP-MS
¹⁴⁷ Sm	0.125-0.310	ppm	LA-ICP-MS
¹⁵³ Eu	0.019-0.060	ppm	LA-ICP-MS
¹⁵⁷ Gd	0.118-0.294	ppm	LA-ICP-MS
¹⁵⁹ Tb	0.006-0.21	ppm	LA-ICP-MS
¹⁶³ Dy	0.024-0.062	ppm	LA-ICP-MS
¹⁶⁵ Ho	0.003-0.037	ppm	LA-ICP-MS
¹⁶⁶ Er	0.008-0.046	ppm	LA-ICP-MS
¹⁶⁹ Tm	0.003-0.018	ppm	LA-ICP-MS
¹⁷² Yb	0.018-0.085	ppm	LA-ICP-MS
¹⁷⁵ Lu	0.006-0.031	ppm	LA-ICP-MS
¹⁸¹ Ta	0.005-0.027	ppm	LA-ICP-MS
²⁰⁸ Pb	0.036-0.120	ppm	LA-ICP-MS
²³² Th	0.011-0.052	ppm	LA-ICP-MS

B.4.2.2 EPMA results in scheelite grains

Scheelite_ spot	WO3 (%)	CaO (%)	MnO (%)	Total (%)	Na (%)	Fe (%)	Mo (%)	Sr (%)	Y (%)
230985 1c	79.79	19.09	bdl	98.88	0.012	0.004	bdl	0.048	bdl
230985 1r	79.01	19.16	bdl	98.21	0.013	0.006	0.005	0.063	bdl
230986 1c	79.79	19.23	0.10	99.12	0.011	bdl	bdl	bdl	bdl
230986 1r	79.71	19.08	bdl	98.80	0.009	bdl	0.003	0.035	bdl
230986 2c	79.41	19.33	bdl	98.74	0.010	bdl	0.089	bdl	bdl
230986 2r	80.13	19.35	bdl	99.48	0.008	bdl	0.073	bdl	bdl
230987 1c	77.26	19.98	bdl	97.24	0.009	0.005	bdl	0.085	bdl
230987 1r	79.14	19.18	bdl	98.32	0.011	0.003	bdl	0.131	bdl
230987 3c	79.29	19.13	bdl	98.44	0.013	bdl	bdl	0.041	bdl
230987 3r	79.26	19.16	bdl	98.42	0.016	bdl	bdl	0.040	bdl
230988 1c	79.68	19.11	bdl	98.79	0.007	0.008	bdl	0.137	bdl
230988 1r	79.74	19.05	bdl	98.78	0.008	bdl	bdl	0.146	bdl
230988 2c	79.99	19.05	bdl	99.05	0.008	bdl	bdl	bdl	bdl
230988 2r	79.33	19.11	bdl	98.44	0.006	0.012	bdl	0.050	bdl
230988 3c	79.50	18.82	bdl	98.32	0.008	0.021	bdl	0.427	bdl
230988 3r	79.83	18.88	bdl	98.72	0.013	bdl	bdl	0.349	bdl
230988 4c	79.67	19.09	bdl	98.76	0.010	bdl	0.004	0.025	bdl
230988 4r	79.56	19.15	bdl	98.71	0.009	bdl	bdl	bdl	bdl
230988 5c	78.94	18.90	0.06	97.90	0.012	0.007	bdl	0.330	bdl
230988 5r	79.81	19.04	bdl	98.86	0.010	0.004	bdl	0.196	bdl
230988 6c	80.14	19.15	bdl	99.29	0.010	0.003	bdl	0.036	bdl
230988 6r	79.85	19.09	bdl	98.94	0.008	bdl	bdl	0.035	bdl
230988 7c	79.53	18.85	bdl	98.38	0.010	0.005	0.004	0.459	bdl
230988 7r	79.33	19.21	0.08	98.63	0.011	0.022	bdl	0.193	bdl
230988 8c	80.05	19.24	bdl	99.29	0.006	bdl	0.010	bdl	bdl
230988 8r	79.45	19.16	bdl	98.61	0.010	0.004	bdl	bdl	bdl
230988 9c	79.92	19.17	bdl	99.09	0.011	bdl	bdl	0.009	bdl
230988 9r	79.41	19.05	0.06	98.52	0.012	bdl	bdl	bdl	bdl
230989 1c	79.74	19.07	bdl	98.81	0.014	bdl	bdl	0.185	bdl
230989 1r	80.00	19.02	bdl	99.02	0.013	0.005	bdl	0.080	bdl
230990 1c	79.63	19.12	bdl	98.75	0.009	0.003	0.007	0.012	bdl
230990 1r	80.27	19.01	bdl	99.28	0.010	bdl	bdl	bdl	bdl
230991 1c	79.33	19.23	0.06	98.62	0.011	bdl	bdl	bdl	bdl
230991 1r	79.23	19.26	0.07	98.56	0.012	0.003	bdl	bdl	bdl
230991 2c	79.58	19.08	bdl	98.66	0.009	bdl	bdl	bdl	bdl
230991 2r	79.82	19.25	bdl	99.06	0.012	bdl	bdl	bdl	bdl
230991 3c	79.21	19.21	bdl	98.45	0.010	0.040	bdl	bdl	bdl
230991 3c1	79.49	19.21	bdl	98.70	0.011	0.012	bdl	bdl	bdl
230991 3r	78.83	19.27	bdl	98.10	0.009	0.007	bdl	0.024	bdl
230991 4c	78.63	19.10	bdl	97.73	0.011	bdl	bdl	bdl	bdl

Scheelite_ spot	WO3 (%)	CaO (%)	MnO (%)	Total (%)	Na (%)	Fe (%)	Mo (%)	Sr (%)	Y (%)
230991 4r	78.19	19.20	bdl	97.39	0.010	bdl	bdl	0.018	bdl
230993 1c	79.51	19.18	bdl	98.68	0.011	0.003	bdl	bdl	bdl
230993 1r	79.44	19.26	bdl	98.69	0.013	bdl	bdl	bdl	bdl
230993 2c	78.43	18.91	bdl	97.37	0.013	bdl	bdl	0.032	bdl
230993 2r	74.11	17.80	bdl	91.91	0.013	bdl	bdl	0.010	bdl
230994 1c	79.15	19.01	0.10	98.26	0.012	0.009	bdl	0.184	bdl
230994 1r	79.37	19.05	bdl	98.45	0.011	0.004	bdl	0.139	bdl
230994 2c	78.86	19.16	bdl	98.01	0.014	bdl	bdl	0.151	bdl
230994 2r	79.02	19.09	bdl	98.12	0.012	bdl	0.056	0.129	bdl
230996 1c	78.65	19.11	bdl	97.76	0.010	bdl	0.131	bdl	bdl
230996 1r	78.53	19.35	bdl	97.88	0.015	bdl	0.135	bdl	bdl
234002 1c	79.13	19.35	bdl	98.48	0.006	0.006	bdl	0.015	bdl
234002 1i	79.55	19.15	bdl	98.69	0.008	0.003	bdl	0.053	bdl
234002 1r	79.89	19.21	bdl	99.10	0.008	bdl	bdl	0.044	bdl
234002 2c	79.99	19.18	bdl	99.17	0.016	bdl	bdl	0.014	bdl
234002 2i	80.24	19.14	bdl	99.38	0.011	bdl	bdl	0.047	bdl
234002 2r	79.22	19.27	bdl	98.49	0.010	bdl	bdl	0.015	bdl
234002 3c	79.41	18.81	bdl	98.23	0.016	0.049	0.020	0.010	bdl
234002 3c1	79.18	19.05	bdl	98.23	0.015	0.016	0.054	bdl	bdl
234005 1c	79.85	19.12	bdl	98.97	0.009	bdl	bdl	0.089	bdl
234005 1r	79.58	19.11	bdl	98.69	0.009	bdl	0.008	0.060	bdl
234005 2c	79.77	18.85	0.06	98.69	0.014	bdl	bdl	0.280	bdl
234005 2r	79.18	18.83	bdl	98.01	0.016	0.005	bdl	0.250	bdl
234005 4c	79.63	19.14	0.07	98.84	0.015	0.043	bdl	bdl	bdl
234005 4r	79.30	19.22	0.11	98.63	0.012	0.003	0.006	bdl	bdl
234005 5c	79.19	19.24	bdl	98.43	0.009	0.003	bdl	0.014	bdl
234005 5r	79.70	19.17	bdl	98.87	0.011	0.004	bdl	bdl	bdl
234009 1c	78.19	18.67	bdl	96.86	0.020	0.009	bdl	0.038	bdl
234009 1r	80.05	19.26	bdl	99.31	0.019	bdl	bdl	0.077	bdl
234009 2c	79.74	19.06	bdl	98.81	0.015	bdl	bdl	0.025	bdl
234009 2r	79.41	19.00	bdl	98.44	0.018	bdl	bdl	0.084	bdl
234010 1c	80.84	19.09	bdl	99.93	0.003	bdl	bdl	bdl	bdl
234010 1r	79.95	19.00	bdl	98.96	0.005	bdl	bdl	0.063	bdl
234011 1c	79.88	19.06	bdl	98.94	0.007	0.003	bdl	bdl	bdl
234011 1r	79.90	19.09	bdl	98.98	0.007	0.007	bdl	bdl	bdl
234011 2c	80.15	19.14	bdl	99.31	0.007	bdl	bdl	0.031	bdl
234011 2c1	79.28	19.16	bdl	98.45	0.009	0.003	bdl	0.075	bdl
234011 2r	78.85	19.17	bdl	98.04	0.007	bdl	bdl	0.017	bdl
234011 3c	79.96	19.14	bdl	99.10	0.007	bdl	0.055	bdl	bdl
234011 3c1	79.52	19.30	bdl	98.82	0.002	0.172	bdl	bdl	bdl
234011 3r	79.57	19.22	0.05	98.84	0.009	0.079	0.017	bdl	bdl

Scheelite_ spot	WO3 (%)	CaO (%)	MnO (%)	Total (%)	Na (%)	Fe (%)	Mo (%)	Sr (%)	Y (%)
234011 3r1	79.20	19.16	bdl	98.36	0.004	0.261	bdl	bdl	bdl
234012 1c	79.54	19.13	bdl	98.68	0.007	bdl	0.276	bdl	bdl
234012 1r	79.38	19.15	bdl	98.53	0.007	0.005	0.290	bdl	bdl
234019 1c	79.37	19.23	bdl	98.60	0.008	bdl	bdl	0.016	bdl
234019 1i	79.86	19.08	bdl	98.97	0.013	bdl	bdl	0.024	bdl
234019 1r	79.30	19.07	bdl	98.37	0.012	0.005	bdl	0.022	bdl
234019 2c	79.37	18.95	bdl	98.32	0.006	0.003	bdl	0.055	bdl
234019 2i	80.39	19.04	bdl	99.43	0.008	bdl	bdl	0.084	bdl
234019 2r	79.67	19.06	bdl	98.73	0.009	bdl	bdl	0.082	bdl
234019 3c	79.52	19.07	bdl	98.59	0.017	0.013	bdl	0.011	bdl
234019 3r	79.03	19.11	0.05	98.19	0.015	0.015	bdl	0.020	bdl
247526 1c	79.14	19.08	bdl	98.22	0.018	bdl	bdl	bdl	bdl
247526 1i	79.51	19.10	bdl	98.62	0.016	bdl	bdl	0.021	bdl
247526 1r	79.42	19.22	bdl	98.68	0.017	0.004	bdl	0.011	bdl
247526 2c	79.76	19.06	bdl	98.82	0.007	0.006	bdl	0.046	bdl
247526 2r	79.46	19.07	bdl	98.52	0.006	bdl	bdl	0.040	bdl
247528 1c	79.43	19.18	bdl	98.61	0.008	bdl	0.230	bdl	bdl
247528 1c1	79.10	19.31	bdl	98.42	0.009	0.005	0.215	bdl	bdl
247528 1r	78.96	19.28	bdl	98.24	0.012	bdl	0.233	bdl	bdl
247529 1c	79.23	19.12	bdl	98.35	0.009	0.006	bdl	0.022	bdl
247529 1r	79.75	19.19	bdl	98.94	0.010	0.006	bdl	0.042	bdl
247532 2c	79.48	19.22	bdl	98.71	0.006	0.451	bdl	bdl	bdl
247532 2r	78.16	19.20	bdl	97.37	0.005	0.467	0.005	bdl	bdl
247532 3c	79.32	19.14	0.06	98.51	0.006	0.194	0.009	0.013	bdl
247532 3c1	79.07	19.19	0.05	98.32	0.011	0.493	bdl	0.012	bdl

247532 2c: 247532: ID Sample 2: ID scheelite grain c:core/r:rim bdl: below detection limit

B.4.2.3 LA-ICP-MS results in scheelite grains

Scheelite grain	Li (ppm)	B (ppm)	Na (ppm)	Mg (ppm)	S (ppm)	K (ppm)	Ti (ppm)	V (ppm)	Cr (ppm)	Mn (ppm)	Fe (ppm)
230985	0.154	0.658	18.691	6.262	280.191	6.143	0.656	0.117	bdl	13.338	24.895
230985_secondline	0.562	1.788	22.098	18.860	223.184	38.357	2.811	0.209	bdl	11.466	109.478
230986-1	bdl	0.919	4.224	2.112	272.898	bdl	bdl	bdl	0.338	29.958	4.927
230986-2	bdl	1.026	14.357	2.396	267.551	1.600	bdl	bdl	bdl	19.340	11.158
230987-1	bdl	0.656	16.068	4.193	263.038	1.730	0.332	0.063	bdl	12.507	9.827
230987-3	0.158	0.708	37.363	3.056	239.272	bdl	bdl	0.093	bdl	5.272	0.964
230988-1	bdl	0.456	2.336	3.531	246.463	bdl	bdl	bdl	bdl	25.666	5.487
230988-2	0.076	0.725	25.365	15.534	264.341	bdl	0.147	0.074	bdl	11.402	18.067
230988-3	bdl	0.557	11.503	6.872	248.547	bdl	bdl	bdl	bdl	64.735	116.882
230988-4	bdl	0.778	32.532	2.296	263.537	2.568	bdl	0.038	bdl	12.341	5.251
230988-5	bdl	0.809	20.695	1.875	231.777	bdl	bdl	bdl	bdl	25.248	4.729
230988-6	bdl	0.838	7.593	2.934	259.958	2.633	0.377	bdl	0.382	8.520	15.579
230988-7	bdl	1.063	33.910	2.165	252.781	bdl	bdl	bdl	bdl	8.543	15.741
230988-8	bdl	0.676	8.816	3.860	265.456	3.780	0.424	bdl	bdl	12.151	10.875
230988-9	bdl	0.981	19.092	1.856	287.619	bdl	bdl	bdl	bdl	13.470	19.200
230989	bdl	0.539	22.594	2.511	266.343	bdl	bdl	bdl	bdl	42.644	7.203
230990-1	bdl	0.887	17.313	77.465	270.925	5.085	0.382	0.115	1.145	15.358	133.654
230990-2	0.084	1.288	16.387	56.795	240.786	4.700	1.438	0.133	0.562	14.746	186.449
230991-1	bdl	0.793	8.719	3.121	225.649	1.365	0.207	bdl	bdl	13.483	9.428
230991-2	0.094	0.721	6.977	43.066	270.101	17.005	1.168	0.223	1.682	13.725	86.505
230991-3	0.597	0.663	32.655	360.756	229.408	60.000	10.360	1.483	13.896	38.259	850.314
230991-4	0.118	0.756	12.898	1.878	172.981	bdl	bdl	bdl	bdl	5.940	4.869
230993-1	bdl	0.858	40.895	2.846	315.135	8.290	bdl	bdl	bdl	13.563	1.229
230993-2	bdl	bdl	7.690	16.966	179.535	13.827	3.061	0.116	bdl	27.444	164.288
230994-1	0.243	1.909	36.202	15.635	262.138	6.765	0.461	bdl	bdl	14.148	75.856

Scheelite grain	Li (ppm)	B (ppm)	Na (ppm)	Mg (ppm)	S (ppm)	K (ppm)	Ti (ppm)	V (ppm)	Cr (ppm)	Mn (ppm)	Fe (ppm)
230994-2	bdl	1.314	32.226	11.580	259.108	11.181	2.815	0.158	bdl	9.280	272.157
234002-1	bdl	0.763	3.592	2.750	233.457	0.993	bdl	bdl	bdl	15.509	7.644
234002-2	bdl	0.711	2.135	3.317	253.773	bdl	bdl	bdl	bdl	20.300	7.046
234005-1	bdl	0.658	5.643	2.206	240.910	bdl	bdl	bdl	bdl	15.093	2.122
234005-2	0.070	0.822	43.395	1.691	206.282	bdl	0.396	0.079	bdl	24.031	3.107
234005-4	bdl	1.481	10.277	23.271	273.120	2.077	0.251	0.054	bdl	14.139	77.918
234005-5	bdl	0.518	5.380	2.158	268.678	1.671	bdl	bdl	bdl	9.060	1.776
234009-1	bdl	2.297	99.299	2.215	238.419	2.025	0.209	0.051	bdl	10.829	6.255
234009-2	bdl	0.498	61.384	3.473	238.771	1.460	0.423	bdl	bdl	30.805	14.063
234010	bdl	0.407	14.749	12.708	235.121	1.421	bdl	0.063	bdl	16.705	5.382
234011-1	0.067	0.564	24.141	17.400	242.421	2.434	bdl	0.227	bdl	26.785	15.173
234011-2	bdl	0.666	12.500	5.157	244.428	10.512	0.662	bdl	bdl	10.354	18.341
234011-3	0.856	1.704	37.064	55.370	260.020	15.492	1.037	0.514	0.295	13.558	140.725
234012	bdl	0.582	13.529	51.530	251.380	bdl	0.330	0.616	bdl	10.781	1.080
234019-1	bdl	0.760	39.328	1.936	274.155	bdl	0.140	0.111	bdl	24.824	4.379
234019-2	bdl	0.587	26.718	2.551	235.267	bdl	bdl	bdl	bdl	14.171	3.248
234019-3	0.319	1.079	154.801	1511.734	289.430	65.187	16.376	3.173	8.191	156.066	3758.089
247526-1	1.599	0.592	109.411	1.828	242.289	bdl	bdl	0.660	bdl	4.013	bdl
247526-2	bdl	0.585	5.207	2.703	244.676	1.467	0.140	0.055	bdl	23.860	5.818
247528	0.130	0.623	41.304	62.905	268.849	bdl	0.366	0.205	bdl	19.421	2.336
247529	0.512	0.729	55.056	2.984	251.250	1.496	bdl	0.218	bdl	6.832	5.448
247532-2	bdl	2.059	13.575	68.930	166.643	121.033	11.636	0.283	bdl	12.702	2302.136
247532-3	0.167	0.919	20.885	60.940	302.581	116.009	6.288	0.268	1.816	13.806	193.313

Scheelite grain	Co (ppm)	Cu (ppm)	Zn (ppm)	As (ppm)	Sr (ppm)	Y (ppm)	Nb (ppm)	Mo (ppm)	Ag (ppm)	Sn (ppm)	Ba (ppm)
230985	bdl	2.175	0.535	1.126	1440.738	27.176	8.246	15.101	bdl	bdl	1.665
230985_secondline	bdl	2.571	0.474	1.676	1348.366	26.145	10.727	109.926	bdl	bdl	2.291
230986-1	bdl	1.871	bdl	bdl	511.963	15.436	4.554	0.365	bdl	bdl	1.738
230986-2	bdl	3.369	0.827	1.703	60.448	32.689	9.154	1134.977	bdl	bdl	bdl
230987-1	bdl	1.946	0.439	bdl	1400.553	38.905	4.607	2.026	bdl	bdl	1.618
230987-3	bdl	2.254	0.355	2.700	908.875	617.475	47.814	34.025	bdl	bdl	bdl
230988-1	bdl	0.959	0.338	bdl	1913.113	8.162	4.612	0.117	bdl	bdl	2.246
230988-2	bdl	2.069	0.500	1.079	753.027	66.311	4.727	1.382	bdl	bdl	0.531
230988-3	bdl	1.958	0.187	bdl	5014.970	24.101	4.595	bdl	bdl	0.138	1.391
230988-4	bdl	3.043	bdl	bdl	440.116	117.001	5.431	38.430	bdl	bdl	5.123
230988-5	bdl	3.505	0.471	bdl	3592.653	31.617	4.656	bdl	bdl	bdl	0.530
230988-6	bdl	3.219	0.328	1.311	728.787	18.842	4.827	2.824	bdl	bdl	7.686
230988-7	bdl	2.296	bdl	bdl	4884.217	57.999	4.820	0.267	bdl	bdl	0.335
230988-8	bdl	2.630	0.628	0.640	469.592	19.646	4.927	49.957	bdl	bdl	3.949
230988-9	bdl	3.823	0.407	0.925	480.583	83.934	5.527	40.490	bdl	bdl	7.575
230989	bdl	0.842	bdl	bdl	2691.250	43.138	5.216	0.150	bdl	bdl	1.345
230990-1	0.042	0.262	0.322	bdl	429.065	35.133	4.843	63.235	bdl	bdl	1.098
230990-2	0.052	0.431	0.687	0.806	466.713	32.088	5.135	63.186	bdl	bdl	1.698
230991-1	bdl	2.486	0.371	bdl	425.870	19.685	5.146	61.612	bdl	bdl	2.296
230991-2	0.047	2.894	0.480	bdl	425.230	14.993	5.087	61.082	bdl	bdl	1.038
230991-3	0.150	2.065	0.996	1.019	535.152	108.274	5.178	61.521	bdl	bdl	1.487
230991-4	bdl	bdl	bdl	bdl	522.205	59.889	5.227	52.818	bdl	bdl	0.578
230993-1	bdl	0.102	bdl	bdl	370.420	8.597	4.622	0.169	bdl	bdl	4.095
230993-2	0.918	0.387	bdl	1.388	533.919	29.350	18.362	5.223	0.054	bdl	1.972
230994-1	bdl	1.474	bdl	1.023	3206.144	18.044	5.773	0.226	bdl	bdl	bdl
230994-2	0.346	1.890	0.526	3.671	2089.451	63.969	6.223	240.847	bdl	bdl	2.455
234002-1	bdl	0.468	0.417	0.677	783.590	7.514	4.581	3.188	bdl	bdl	2.302

Scheelite grain	Co (ppm)	Cu (ppm)	Zn (ppm)	As (ppm)	Sr (ppm)	Y (ppm)	Nb (ppm)	Mo (ppm)	Ag (ppm)	Sn (ppm)	Ba (ppm)
234002-2	bdl	1.876	bdl	0.619	722.798	6.663	4.666	4.318	bdl	bdl	1.350
234005-1	bdl	0.434	bdl	bdl	1405.514	20.380	5.869	38.714	bdl	bdl	1.663
234005-2	bdl	bdl	bdl	0.912	3232.437	71.837	4.295	bdl	bdl	bdl	0.362
234005-4	0.020	1.631	bdl	bdl	301.329	10.913	4.591	33.131	bdl	bdl	2.608
234005-5	bdl	1.783	bdl	bdl	419.579	15.233	4.655	21.535	bdl	bdl	1.766
234009-1	bdl	1.111	0.310	1.359	852.282	402.335	42.505	22.195	bdl	bdl	3.688
234009-2	bdl	1.336	0.418	bdl	839.506	92.940	5.233	bdl	bdl	bdl	0.305
234010	bdl	2.925	bdl	1.036	742.995	24.585	5.032	7.072	bdl	bdl	0.675
234011-1	0.032	2.067	0.310	1.163	631.564	46.920	6.245	40.012	bdl	bdl	0.486
234011-2	bdl	2.366	0.366	bdl	1292.195	8.814	5.034	52.508	bdl	bdl	1.208
234011-3	0.052	2.270	0.573	0.911	180.310	24.600	10.783	549.834	bdl	bdl	1.331
234012	bdl	3.352	0.390	1.296	60.485	33.318	18.334	3688.542	bdl	bdl	bdl
234019-1	bdl	2.609	0.341	2.481	935.515	54.415	6.281	0.502	bdl	bdl	0.728
234019-2	bdl	2.070	bdl	0.812	1152.098	71.043	4.695	0.495	bdl	bdl	2.080
234019-3	3.829	3.387	4.058	4.560	465.742	192.620	4.996	29.977	bdl	bdl	3.022
247526-1	bdl	0.685	0.393	5.142	656.532	417.823	26.066	23.326	bdl	bdl	bdl
247526-2	bdl	1.919	0.419	bdl	1148.289	14.416	4.692	0.116	bdl	bdl	0.558
247528	bdl	3.081	0.344	0.665	79.092	150.249	23.596	2951.672	bdl	bdl	bdl
247529	bdl	3.141	bdl	1.058	758.101	154.288	20.452	60.638	bdl	bdl	0.282
247532-2	0.151	2.118	bdl	4.139	269.365	19.052	35.633	5.970	bdl	bdl	2.083
247532-3	bdl	0.391	bdl	bdl	568.067	22.150	5.682	125.967	bdl	bdl	4.841

Scheelite grain	La (ppm)	Ce (ppm)	Pr (ppm)	Nd (ppm)	Sm (ppm)	Eu (ppm)	Gd (ppm)	Tb (ppm)	Dy (ppm)	Ho (ppm)	Er (ppm)
230985	16.980	33.647	3.738	15.799	3.042	9.793	4.188	0.593	4.409	0.742	2.399
230985_secondline	16.216	32.112	4.072	16.002	4.054	7.678	4.576	0.718	3.903	0.792	2.266
230986-1	4.412	5.299	0.414	1.532	0.301	0.999	0.519	0.139	1.053	0.301	1.011
230986-2	0.836	3.419	0.619	3.157	1.488	0.230	2.941	0.613	5.293	1.397	4.930
230987-1	12.595	19.836	1.994	7.712	1.728	16.134	2.518	0.434	3.163	0.711	2.277
230987-3	41.337	178.966	33.135	190.990	52.800	31.981	72.446	10.648	77.443	21.314	74.342
230988-1	1.252	2.190	0.286	1.390	0.467	0.777	0.684	0.113	0.900	0.212	0.736
230988-2	12.885	22.238	2.898	14.305	3.885	6.006	6.780	1.066	7.514	1.800	5.459
230988-3	0.662	2.524	0.553	3.770	3.885	5.581	5.760	1.021	5.462	0.812	1.966
230988-4	0.625	2.936	0.631	6.335	5.904	2.212	20.210	3.576	26.235	6.109	14.615
230988-5	7.285	14.486	1.957	10.083	3.102	10.004	4.464	0.594	4.135	0.840	2.571
230988-6	5.030	9.398	1.192	5.142	1.453	1.607	1.653	0.222	1.826	0.492	1.599
230988-7	22.331	40.287	4.447	15.389	3.770	7.130	4.380	0.809	6.080	1.338	4.777
230988-8	1.664	7.221	1.417	9.585	3.162	1.472	5.519	0.710	4.553	0.884	2.341
230988-9	1.378	5.365	0.779	5.568	4.526	1.599	14.443	2.662	19.296	4.408	10.312
230989	15.891	43.695	5.781	23.415	6.460	5.407	7.319	1.115	7.026	1.187	3.206
230990-1	0.089	0.588	0.211	2.189	2.102	0.643	5.460	1.120	8.440	1.919	4.614
230990-2	0.506	2.019	0.330	2.284	2.015	0.770	5.250	1.063	7.529	1.694	4.277
230991-1	0.177	1.152	0.177	1.647	1.244	0.511	3.258	0.590	4.686	1.056	2.547
230991-2	0.115	0.402	0.141	1.184	0.937	0.480	2.350	0.456	3.773	0.772	1.871
230991-3	0.397	1.768	0.433	5.596	5.553	1.733	16.319	3.304	24.569	5.515	14.463
230991-4	0.064	0.522	0.322	3.615	2.745	2.751	10.747	2.100	14.622	3.171	7.611
230993-1	1.842	3.010	0.273	1.278	0.288	0.503	0.403	0.055	0.521	0.145	0.721
230993-2	8.032	24.479	2.801	9.133	2.701	0.304	3.853	0.740	5.630	1.041	3.696
230994-1	1.948	7.515	1.668	9.249	4.486	6.314	5.945	0.798	5.185	0.671	1.527
230994-2	12.069	37.105	5.645	28.489	7.848	33.180	11.474	1.718	10.901	2.214	5.550
234002-1	3.108	5.774	0.589	2.108	0.485	2.148	0.464	0.088	0.715	0.158	0.543

Scheelite grain	La (ppm)	Ce (ppm)	Pr (ppm)	Nd (ppm)	Sm (ppm)	Eu (ppm)	Gd (ppm)	Tb (ppm)	Dy (ppm)	Ho (ppm)	Er (ppm)
234002-2	2.682	3.791	0.371	1.301	0.286	2.058	0.543	0.080	0.627	0.137	0.480
234005-1	5.268	10.630	1.181	5.086	1.351	2.455	2.134	0.355	2.294	0.545	1.673
234005-2	35.506	65.239	7.649	34.655	13.042	21.911	15.649	2.179	12.911	2.301	5.718
234005-4	0.527	1.776	0.227	0.533	bdl	0.105	0.389	0.114	1.277	0.494	1.580
234005-5	0.261	0.835	0.111	0.674	0.458	0.415	0.930	0.236	2.205	0.641	2.140
234009-1	0.886	4.585	1.261	10.794	10.596	15.793	37.710	8.994	73.162	17.361	48.464
234009-2	63.053	143.350	15.882	55.405	15.445	8.540	16.194	2.623	15.776	2.974	7.771
234010	19.925	38.846	4.326	16.896	3.492	3.902	3.951	0.628	3.576	0.758	2.169
234011-1	20.199	41.601	5.242	22.971	6.334	3.305	8.249	1.223	8.200	1.614	4.305
234011-2	4.012	6.130	0.658	2.581	0.701	0.819	1.034	0.139	0.926	0.216	0.610
234011-3	3.765	14.408	2.560	17.952	7.485	2.442	10.452	1.441	7.797	1.470	3.601
234012	0.681	4.836	1.626	17.729	10.331	4.310	15.637	1.926	10.897	2.409	6.119
234019-1	42.895	89.474	9.475	30.859	6.368	8.469	6.061	1.113	7.412	1.491	4.620
234019-2	16.598	32.536	3.468	14.383	3.202	5.642	5.273	0.893	7.094	1.737	5.673
234019-3	1.439	4.618	1.092	10.120	10.934	3.694	36.070	6.389	44.000	10.358	23.273
247526-1	21.068	163.148	47.029	373.971	187.768	23.866	263.697	36.782	191.319	27.040	44.785
247526-2	3.206	4.876	0.554	2.253	0.918	3.713	1.044	0.179	1.635	0.293	1.041
247528	1.072	5.907	1.397	10.841	6.041	3.280	13.842	2.409	19.205	4.754	14.574
247529	1.488	7.369	3.391	44.804	39.520	8.961	95.174	12.655	63.531	8.153	10.751
247532-2	2.348	4.919	0.652	3.695	0.987	bdl	1.075	0.666	2.920	1.025	3.020
247532-3	0.882	0.669	0.199	1.071	bdl	0.529	0.570	0.172	2.591	0.960	3.558

Scheelite grain	Tm (ppm)	Yb (ppm)	Lu (ppm)	Ta (ppm)	Pb (ppm)	Th (ppm)	Shape
230985	0.306	1.730	0.191	0.206	14.958	0.077	Line
230985_secondline	0.273	1.465	0.155	0.151	15.510	bdl	Line
230986-1	0.162	1.350	0.199	0.107	14.045	0.042	Line
230986-2	0.726	4.413	0.701	0.126	10.492	bdl	Line
230987-1	0.297	1.774	0.190	0.131	8.878	0.040	Line
230987-3	9.945	57.344	7.682	0.248	13.413	0.134	Line
230988-1	0.122	1.036	0.157	0.134	13.756	bdl	Line
230988-2	0.634	3.702	0.489	0.140	10.718	bdl	Line
230988-3	0.242	1.391	0.168	0.138	17.794	0.446	Line
230988-4	1.200	4.159	0.349	0.136	7.137	0.187	Line
230988-5	0.365	1.972	0.240	0.149	14.830	bdl	Line
230988-6	0.230	1.573	0.218	0.122	10.505	0.005	Line
230988-7	0.752	5.087	0.720	0.137	27.440	0.257	Line
230988-8	0.224	0.992	0.103	0.135	9.560	0.047	Line
230988-9	0.930	3.614	0.290	0.182	10.032	0.549	Line
230989	0.449	2.868	0.431	0.182	19.403	0.532	Line
230990-1	0.455	1.639	0.135	0.148	6.020		Line
230990-2	0.387	1.515	0.122	0.136	7.546	0.091	Line
230991-1	0.261	0.879	0.056	0.132	6.296	bdl	Line
230991-2	0.212	0.707	0.040	0.154	5.407	bdl	Line
230991-3	1.274	4.754	0.345	0.136	8.746	0.059	Line
230991-4	0.836	2.545	0.244	0.158	5.021	bdl	Spot
230993-1	0.132	1.224	0.217	0.197	7.502	0.088	Spot
230993-2	0.512	3.157	0.550	0.614	17.891	2.051	Spot
230994-1	0.160	0.655	0.065	0.102	13.305		Line
230994-2	0.495	2.074	0.186	0.177	16.599	0.225	Line
234002-1	0.073	0.536	0.069	0.146	8.347	0.036	Line

Scheelite grain	Tm (ppm)	Yb (ppm)	Lu (ppm)	Ta (ppm)	Pb (ppm)	Th (ppm)	Shape
234002-2	0.072	0.504	0.066	0.143	8.500	bdl	Line
234005-1	0.194	1.251	0.160	0.177	7.397	0.048	Line
234005-2	0.687	3.663	0.414	0.156	4.954	bdl	Spot
234005-4	0.188	0.947	0.077	0.180	7.128	0.072	Line
234005-5	0.290	1.465	0.158	0.124	10.323	bdl	Line
234009-1	4.858	19.354	2.069	0.674	6.448	0.029	Line
234009-2	1.106	7.410	0.846	0.156	14.780	1.268	Line
234010	0.251	1.546	0.182	0.161	4.996	0.067	Line
234011-1	0.475	2.608	0.296	0.168	3.966	bdl	Line
234011-2	0.083	0.599	0.089	0.198	7.319	0.190	Line
234011-3	0.415	2.186	0.381	0.186	11.502	0.068	Line
234012	0.532	2.172	0.325	0.155	7.248	bdl	Line
234019-1	0.729	5.367	0.748	0.188	22.341	0.155	Line
234019-2	0.752	4.547	0.511	0.142	9.596	bdl	Line
234019-3	1.701	6.941	0.730	0.145	9.425	0.387	Spot
247526-1	2.942	8.084	0.488	0.209	17.510	0.039	Line
247526-2	0.126	0.704	0.089	0.117	16.508	bdl	Line
247528	1.746	8.209	0.983	0.144	7.010	bdl	Line
247529	0.558	1.455	0.062	0.220	9.642	0.076	Line
247532-2	0.613	4.807	0.336	0.166	13.685	0.590	Spot
247532-3	0.566	3.827	0.640	0.072	28.493	0.468	Spot

247532-2: 247532: ID Sample 2: ID scheelite grain bdl: below detection limit

B.4.2 Chalcopyrite analysis

B.4.2.1 Detection limits in chalcopyrite analysis

Element	Detection Limit	Unit	Method
S	258-270	ppm	EPMA
Fe	265-290	ppm	EPMA
Cu	2104-2105	ppm	EPMA
Cd	227-245	ppm	EPMA
Sb	33-34	ppm	EPMA
Zn	1256-1562	ppm	EPMA
Mn	516-711	ppm	EPMA
Co	271-287	ppm	EPMA
Ni	256-285	ppm	EPMA
As	238-265	ppm	EPMA
²⁴ Mg	0.043-0.313	ppm	LA-ICP-MS
²⁸ Si	132.9-267.9	ppm	LA-ICP-MS
⁴⁹ Ti	1.062-14.563	ppm	LA-ICP-MS
⁵¹ V	0.056-0.106	ppm	LA-ICP-MS
⁵² Cr	0.820-1.653	ppm	LA-ICP-MS
⁵⁵ Mn	1.10-1.92	ppm	LA-ICP-MS
⁵⁹ Co	0.006-0.010	ppm	LA-ICP-MS
⁶⁰ Ni	0.129-0.223	ppm	LA-ICP-MS
⁶⁶ Zn	0.138-0.765	ppm	LA-ICP-MS
⁷¹ Ga	0.005-0.012	ppm	LA-ICP-MS
⁷² Ge	0.028-0.059	ppm	LA-ICP-MS
⁷⁵ As	0.152-0.591	ppm	LA-ICP-MS
⁷⁸ Se	5.462-8.762	ppm	LA-ICP-MS
⁹⁵ Mo	0.009-0.021	ppm	LA-ICP-MS
¹⁰¹ Ru	0.001-0.002	ppm	LA-ICP-MS
¹⁰³ Rh	0.001-0.019	ppm	LA-ICP-MS
¹⁰⁵ Pd	0.002-0.008	ppm	LA-ICP-MS
¹⁰⁷ Ag	0.016-0.042	ppm	LA-ICP-MS
¹¹¹ Cd	0.027-0.091	ppm	LA-ICP-MS
¹¹⁵ In	0.004-0.012	ppm	LA-ICP-MS
¹¹⁸ Sn	0.013-0.031	ppm	LA-ICP-MS
¹²¹ Sb	0.030-0.063	ppm	LA-ICP-MS
¹²⁵ Te	0.016-0.036	ppm	LA-ICP-MS

Element	Detection Limit	Unit	Method
¹³⁷ Ba	0.008-0.014	ppm	LA-ICP-MS
¹⁹⁷ Au	0.003-0.009	ppm	LA-ICP-MS
²⁰¹ Hg	0.186-0.421	ppm	LA-ICP-MS
²⁰⁸ Pb	0.003-0.009	ppm	LA-ICP-MS
²⁰⁹ Bi	0.005-0.010	ppm	LA-ICP-MS

B.4.3.2 EPMA results in chalcopyrite grains

Chalcopyrite grain	S (%)	Cd (%)	Sb (%)	Zn(%)	Cu (%)	Mn (%)	Fe (%)	Co (%)	Ni (%)	As (%)	Total (%)
234012-1	35.277	0.014	bdl	bdl	33.900	bdl	30.608	bdl	bdl	0.069	99.868
234012-2	35.588	0.034	0.042	0.018	33.583	bdl	30.537	bdl	bdl	0.047	99.849
234012-3	35.871	0.028	0.006	0.225	34.349	bdl	30.596	bdl	0.036	0.063	101.174
234014-1	35.387	0.048	bdl	bdl	33.577	bdl	30.799	bdl	bdl	0.032	101.285
234014-2	35.795	0.024	0.013	bdl	34.506	0.049	30.866	bdl	bdl	bdl	99.828
234019-1	35.705	0.016	bdl	bdl	33.959	bdl	30.964	bdl	bdl	0.035	100.679
234019-2	35.416	bdl	0.019	0.030	34.349	0.025	30.873	bdl	bdl	0.032	100.744
234019-3	35.622	bdl	0.010	0.113	33.686	0.055	31.104	bdl	bdl	0.047	100.636
234019-4	35.560	bdl	0.007	0.012	33.992	bdl	31.028	bdl	bdl	bdl	100.600
247533-1	35.463	bdl	0.016	0.018	33.857	0.068	30.551	bdl	bdl	0.028	100.007
247533-2	35.430	bdl	0.011	bdl	33.753	bdl	30.819	0.039	bdl	bdl	100.066

bdl: below detection limit

B.4.3.2 EPMA results in chalcopyrite grains

Chalcopyrite grain	Mg (ppm)	Si (ppm)	Ti (ppm)	V (ppm)	Cr (ppm)	Mn (ppm)	Co (ppm)	Ni (ppm)	Zn (ppm)	Ga (ppm)
234012-1	0.135	784.109	4.696	bdl	2.995	bdl	0.037	bdl	696.880	0.061
234012-2	0.128	722.157	5.730	bdl	3.642	bdl	bdl	bdl	309.163	0.068
234012-3	bdl	580.885	5.047	bdl	2.632	bdl	bdl	bdl	209.803	0.061
234013-1	0.078	686.773	3.536	bdl	4.272	bdl	0.028	bdl	543.177	0.050
234014-1	0.092	622.881	3.463	bdl	3.915	bdl	0.210	9.872	334.173	0.016
234014-2	7.881	721.612	3.653	0.087	4.150	1.188	0.398	0.509	675.850	0.012
234019-1	2.676	703.782	15.131	0.050	bdl	bdl	0.078	20.961	607.145	0.019
234019-2	7.216	813.972	12.286	0.131	3.674	6.116	0.124	0.681	8.314	0.035
234019-3	bdl	779.684	9.965	bdl	3.266	bdl	bdl	bdl	58.256	bdl
234019-4	6.235	827.700	bdl	0.302	4.721	7.137	0.062	0.582	402.505	0.086
247533-1	0.847	753.765	5.058	bdl	3.567	bdl	0.176	2.780	25.214	0.008
247533-2	0.214	773.388	3.610	bdl	3.339	bdl	0.058	bdl	134.820	0.095
Chalcopyrite grain	Ge (ppm)	As (ppm)	Se (ppm)	Mo (ppm)	Ru (ppm)	Rh (ppm)	Pd (ppm)	Ag (ppm)	Cd (ppm)	In (ppm)
234012-1	0.312	bdl	395.947	bdl	0.060	28.700	22.140	0.074	29.319	4.250
234012-2	0.306	bdl	398.234	bdl	bdl	28.990	22.533	0.411	15.060	4.422
234012-3	0.304	bdl	395.346	bdl	bdl	28.091	21.667	0.209	10.303	4.325
234013-1	0.325	1.838	414.582	bdl	bdl	28.501	21.518	2.986	22.348	4.291
234014-1	0.289	bdl	15.318	bdl	bdl	28.584	22.224	49.021	2.617	1.286
234014-2	0.284	bdl	15.344	0.014	0.052	29.211	22.137	7.084	67.486	1.763
234019-1	0.316	3.690	42.823	bdl	bdl	28.311	21.427	54.208	79.727	6.926
234019-2	0.306	7.352	21.861	bdl	bdl	28.702	23.102	5.142	bdl	0.103
234019-3	0.319	bdl	8.554	bdl	bdl	28.273	21.598	110.984	0.904	3.746
234019-4	0.333	18.507	68.485	0.039	0.082	27.387	20.749	11.790	45.428	4.230
247533-1	0.325	0.705	139.246	bdl	0.060	28.415	22.172	53.305	3.953	9.693
247533-2	0.337	0.984	26.137	bdl	bdl	27.808	21.621	7.052	2.963	1.100

Chalcopyrite grain	Sn (ppm)	Sb (ppm)	Te (ppm)	Ba (ppm)	Au (ppm)	Hg (ppm)	Pb (ppm)	Bi (ppm)
234012-1	7.325	bdl	0.851	bdl	0.012	1.058	0.961	0.351
234012-2	5.684	bdl	0.458	0.022	0.009	0.462	2.113	1.048
234012-3	6.525	bdl	0.641	bdl	0.006	0.345	1.124	0.515
234013-1	6.261	0.049	0.628	bdl	0.025	0.460	5.640	2.339
234014-1	0.585	0.225	2.105	bdl	0.015	bdl	1.655	0.086
234014-2	4.791	0.443	0.922	bdl	0.006	bdl	2.262	0.088
234019-1	4.084	1.385	1.866	2.112	0.144	bdl	7.130	0.038
234019-2	0.060	bdl	0.068	0.438	7.657	bdl	0.820	0.603
234019-3	0.086	bdl	bdl	bdl	0.008	bdl	1.544	0.034
234019-4	0.422	1.115	0.313	1.018	0.025	bdl	4.339	0.603
247533-1	2.101	1.261	0.120	0.025	0.038	0.649	1.601	0.241
247533-2	2.572	0.102	0.076	0.124	0.020	bdl	2.896	0.382

bdl: below detection limit